The Development of Boron Containing Hydrogels for Sensing and Drug Delivery

Williams, George

Award date:
2020

Awarding institution:
University of Bath

UNIVERSITY OF BATH

The Development of Boron Containing Hydrogels for Sensing and Drug Delivery

George Thomas Williams

A thesis submitted for the degree of Doctor of Philosophy

University of Bath

Department of Chemistry

January 2020

Signed:

Declaration of External Input

Biological testing reported within this thesis was performed in part by L. Gwynne and B. Patenall.

Acknowledgements

First and foremost I must thank my Supervisor Prof Toby Jenkins for his support throughout my Ph.D, and for offering me the opportunity to undertake this project in the first place. Many of my best experiences in the last 3 years have been due to being able to present my work and go to a number of conferences, which without you would have been impossible. I would also like to thank Prof Tony James for his advice and scientific knowledge, particularly in the field of boron chemistry. My meetings with Dr Mark Sutton were also something I will be eternally grateful for, it was often not until down the road did I realise the relevance of what I was being told.

The Jenkins group members both past and current have also been an invaluable source of encouragement, knowledge, support, necessary abuse and great memories. I probably in part owe Dr Adam Sedgwick my Ph.D, as my lab time essentially doubled with his coming into my life. Lauren Gwynne I need to thank for putting up with my constant moaning and generally being one of the best technicians (kidding) and best friends I could have ever hoped for. I also must thank Beth Patenall for her help in teaching me what genes actually are, and to both her and Lauren for helping me with all of the microbiology and proof reading my thesis. From within our group and without it I have had a wealth of other Ph.D students offer me knowledge, support and guidance, so I must thank Dr Liam Stephens, Dr Jordan Gardiner, Dr Holly Hathaway, Dr Scarlet Milo, Dr Thet Nuang Tun, Dr Maria Odyniac, Dr Stephen Flower, Dr Simon Lewis, Rachel Heylen and Lloyd Murfin, not to mention the entire Pantos, Lewis and Carberry groups for adopting me into their labs. I also have to thank my previous Students Anna Mroz, Hugh Wetherly, Ash Parker and Astrid Hafner, you guys taught me more about chemistry than you realise, and how much I enjoyed supervising your projects is one of my major draws to academia.

Outside of my university life I was blessed to have an inspirational family, and without their support I don’t know where I would be. My Mum, Nan and Gramps have always been my biggest fans, and are a constant source of love and encouragement.

My friends have been the keepers of my sanity. Jake Matt and Colby have been the most reliable constants in my life, and I can confidently say Jakes pep talks have had me doing more work

than any other factor. Nothing will ever surpass the Zits! It is a known fact that Polzeath with the Pennocks is the greatest relaxation known to man, so I would like to thank Andy, Jake and Robbie for those adventures. After 8 years or so at Bath I have met some truly fantastic people who have all made living here and doing, what felt like a never-ending task, a pleasure. So I would also like to thank Emily, Liam, Lloyd (again), Matt, Sam, Spoon, and all of the staff at the Stable. We sank just the right number of pints. I am going to miss Bath greatly

I also need to say a huge thankyou to my wonderful girlfriend Kaya. You have put up with me during the writing of my thesis and never once complained about the fact I was unrelentingly grumpy for a good few months. You deserve a medal!

I also would like to thank the University of Bath and Public Health England for the financial support that has allowed me to undertake work that I found truly fascinating.

I dedicate my thesis to Jake Oliver, the greatest human being I have ever had the good fortune of meeting.
Thankyou for everything.

Publication list

A Colorimetric chemosensor based on a Nozoe azulene that detects fluoride in aqueous/alcoholic media

Murfin L, C., Chiang K. X., Williams, G. T., Jenkins, A. T. A., James. T. D., & Lewis S., E. In Frontiers in Chemisty

Boronate ester cross-linked PVA hydrogel for the H_2O_2 triggered delivery of small molecules *Chapter 4*

Williams, G. T., Sedgwick, A. C., Gwynne L., Murfin L, C., Gardiner J. E., Brewster II, J. T., Lewis S., E., Sutton M., James. T. D., Jenkins, A. T. A. & Sessler, J. L., In Chemical communications

Reaction-based indicator (RIA) displacement hydrogel for the development of a triggered release system capable of biofilm inhibition *Chapter 2*

Patenall. B. L.[1], Williams G. T.[1], Gwynne L., Stephens, L. S., Lampard. E, V. L., Hathaway, H. J., Thet N. T., Young, A. E., Sutton, M., Short R. D., Bull S. D., Sedgwick A. C., James T. D. & Jenkins, A. T. A., 02 Dec 2019, In Chemical Communications

Delivery and quantification of hydrogen peroxide generated via cold atmospheric pressure plasma through biological material

Hathaway H. J., Patenall, B. L., Thet N. T., Sedgwick A. C., Williams G. T., Jenkins A. T. A., Allinson S. L. & Short R. D., 17 Sep 2019, In : Journal of Physics D : Applied Physics.

A boronic acid-based fluorescent hydrogel for monosaccharide detection

Xu, S., Sedgwick, A. C., Elfeky, S. A., Chen, W., Jones, A. S., Williams, G. T., Jenkins, A. T. A., Bull, S. D., Fossey, J. S. & James, T. D., 21 May 2019, In : Frontiers of Chemical Science and Engineering.

Long wavelength TCF-based fluorescence probe for the detection of Alkaline Phosphatase in live cells

Gwynne, L., Sedgwick, A. C., Gardiner, J. E., Williams, G. T., Kim, G., Maillard, J. Y., Jenkins, T., Bull, S. D., Sessler, J. L., Yoon, J. & James, T. D., 30 Apr 2019, In : Frontiers in Chemistry.

An ESIPT Probe for the Ratiometric Imaging of Peroxynitrite Facilitated by Binding to Aβ-Aggregates

Sedgwick, A. C., Dou, W. T., Jiao, J. B., Wu, L., Williams, G. T., Jenkins, A. T. A., Bull, S. D., Sessler, J. L., He, X. P. & James, T. D., 31 Oct 2018, In : Journal of the American Chemical Society.

Limiting *Pseudomonas aeruginosa* Biofilm Formation Using Cold Atmospheric Pressure Plasma

Patenall, B, L., Hathaway, H. J., Sedgwick, A. C., Thet, N. T., Williams G. T., Young A. E., Allinson S. L. Short R. D. & Jenkins A. T. A., 26 Sep 2018, in Plasma Medicine

Dye Displacement Assay for Saccharides using Benzoxaborole Hydrogels *Chapter 2*

Lampard, E. V., Sedgwick, A. C., Sombuttan, T., Williams, G. T., Wannalerse, B., Jenkins, A. T. A., Bull, S. D. & James, T. D., 1 Mar 2018, In : ChemistryOpen.

Manuscripts in Appendix

Oral Presentations

BioNano Summer School, Hirschegg Austria 08/2017

VBST, Attendorn, Germany 10/2017

BioNano Summer school, Hirschegg Austria 08/2018

VBST, Hirschegg Austria 02/2019

Advanced Polymers via Molecular Engineering, Stellenbosch, 04/2019

BioNano Summer School, Hisrchegg, Austria 08/2019

Abbreviations

°C	Degrees centigrade
µg	Microgram
µL	Microliter
µM	Micromolar
^{1}H NMR	Hydrogen nuclear magnetic resonance
5-FBPBA	5-fluorouracil bis-phenyl boronic acid
AcOH	Acetic Acid
AF-647	Alexafluor-647
AHL	Acetyl-homoserine lactone
AI	Autoinducer
ARS	Ailizarin Red S
BOB	Benzoxaborole
BODIPY	Boron-dipyrromethene
Bpin	Boronic pinacol ester
Br_2	Bromine
CAMHB	Calcium adjusted mueller hinton broth
CAP	Cold atmospheric plasma
CBPBA	Ciprofloxacin bis-phenyl boronic acid
CCC	Critical colonisation concentration
CDI	Carbonyldiimidazole
Cipro	Ciprofloxacin
CMC	Carboxymethyl cellulose
CMO	Chief medical officer
d	Doublet
Da	Dalton
DCM	Dichloromethane
dd	Doublet of doublets
DI	De-ionised
DLS	Dynamic light scattering
DMF	Dimethyl formamide

DMSO	Dimethyl sulfoxide
DMSO	Dimethyl Sulfoxide
DNA	Deoxyribonucleic acid
E. coli	*Enterococcus coli*
EDTA	Ethylenediaminetetraacetic acid
EPS	Extracellular polymeric substance
ESI	Electrospray ionisation
EtOAc	Ethyl Acetate
FTIR	Fourier transform infra-red
FRET	Förster Resonance Energy Transfer
g	Gram
Gment	Greenment
H_2S	Hydrogen Sulfide
HA	Hyaluronic acid
HAase	Hyaluronidase
HAaz	Hyaluronic acid with azide moieties
HGT	Horizontal Gene transfer
HPLC	High pressure liquid chromatography
HOMO	Highest occupied molecular orbital
HRMS	High Resolution Mass Spectrometry
HWE	Horner-Wadsworth-Emmons
ICT	Internal charge transfer
IR	Infra-red
ISC	Internal system crossing
J	Coupling constant
K_2CO_2	Potassium Carbonate
KDa	KiloDalton
LB	Luria-Bertani broth
LUMO	Lowest unoccupied molecular orbital
M	Molar
M	molar

m	Metre
m/z	Mass to charge ratio
MAA	Methacrylic acid
MBA	Methylene Bisacrylamide
MeCN	Acetonitrile
mg	milligram
$MgSO_4$	Magnesium Sulphate
MH	Mueller-Hinton
MHz	Megahertz
MIC	Minimum inhibition concentration
mL	Millilitre
mM	Millimolar
mm	Millimetre
Mol	moles
Mp	Melting Point
MRSA	Methicillin resistant *S. aureus*
mw	Weight average molecular weight
NaCl	Sodium Chloride
NAG	N-acetyl glucosamine
$NaHCO_3$	Sodium Hydrogen Carbonate
NAM	*N*-acetyl muramic acid
NEt_3	Triethylamine
NHS	N-hydroxysuccinimde
NICE	National institute for health and care excellence
P. aeruginosa	*Pseudomonas aeruginosa*
PAA	Polyacrylic acid
PBA	Phenyl boronic acid
PBP	Penicillin Binding Protein
PCR	Polymerase Chain Reaction
PEG	Polyethylene glycol

PET	Photoinduced electron transfer
Pment	Purplement
PNIPAM	Poly(N-isopropylacrylamide)
PVA	Poly(vinyl alcohol)
q	Quartet
quin	Quintet
RFI	Relative fluorescence intensity
RNS	Reactive nitrogen species
RONS	Reactive Oxygen and Nitrogen Species
ROS	Reactive oxygen species
s	Singlet
SPR	Surface plasmon resonance
t	Triplet
THF	Tetrahydrofuran
TMEDA	Tetramethylethylenediamine
TPE	Tetraphenyl ethylene
TPE	Tetre phenylene ethene
Tric	Triclosan
UV	Ultra-violet
UV-vis	Ultraviolet-visible light
VRSA	Vancomycin resistant *Staphylococcus aureus*
WHO	World Health Organisation

Abstract

The threat of antibiotic resistant bacteria is a global one, with no single cause or cure. One of the many faces of this problem is in wound infection. Certain pathogenic bacteria can prevent wound healing, cause pain, and in extreme cases lead to patient mortality. To administer topical antibiotics, or to assess if a wound is infected, a clinician must remove the wound dressing, exposing the wound to contamination from potentially pathogenic species of bacteria. In this research, novel hydrogel materials have been developed that aim to deliver antibacterial compounds into an infected wound environment, without the need for dressing removal.

The novel smart materials developed in this study utilise the reversible, covalent binding of boronic acids to diols. Boronic acid containing monomers have been developed for the development of boronic acid functionalised polyacrylamide gels, which have been shown to bind and release the dye alizarin Red S (ARS) in a controlled fashion. ARS has inherent anti-biofilm activity, and this system has been shown to prevent the growth of *S. aureus* biofilms. Novel prodrugs and fluorophores have been synthesised featuring boronic acids and esters, to mask the reactivity of the active compounds. These compounds have been used as crosslinkers to form hydrogels using poly(vinyl alcohol) (PVA), and their use as H_2O_2 sensitive drug delivery vehicles has been proved using microbiological assays with clinically relevant bacteria. PVA has been successfully crosslinked using both literature reported and novel boronic ester masked fluorophores to yield collapsible hydrogels that find utility both as potential smart materials for wound care, as well as in the sensing of reactive oxygen species.

Contents

1 Introduction 19
1.1 The Clinical Need for Smart Wound Dressings 19
1.2 Bacteria 19
1.3 Wounds and Wound Infection 19
1.4 Biofilms 20
1.4.1 Biofilm Formation 21
1.4.2 Quorum Sensing 22
1.5 Bacterial Infection 23
1.6 Antibiotics 23
1.6.1 Cell Wall Inhibitors 24
1.6.2 Antibiotics that Target the Bacterial Ribosome 30
1.6.3 Antibiotics that Target DNA Synthesis 31
1.7 Antimicrobial Resistance 32
1.7.1 Intrinsic Resistance 33
1.7.2 Acquired Resistance 33
1.7.3 Specific Resistance Genes 35
1.8 What is Being Done to Combat Antibiotic Resistance? 36
1.8.1 Biofilm Inhibitors and Biofilm Disruptors 37
1.9 Fluorescence 38
1.9.1 Designing a Fluorescent Probe 39
1.9.2 Molecular Mechanisms of Fluorescence 40
1.10 Boron Chemistry 44
1.10.1 Boronic Acids and Esters 45
1.10.2 Applications of Boronic Acids 48
1.11 Hydrogels 49
1.11.1 Hydrogels Based on Naturally Occurring Polymers 49
1.11.2 Synthetic Polymer Hydrogels 51
1.12 Cold Atmospheric Plasma (CAP) 53
1.12.1 CAP; an Overview 53
1.12.2 The Biological Effect of CAP 53
1.13 Bibliography 55
2 Boron Containing Polyacrylamide Hydrogels 64
2.1 Introduction 64

2.1.1 Boronic Acid and Boronic Ester Soft Materials 64
2.1.2 Dye Displacement Assay Saccharide Detector 66
2.1.3 Biofilm Inhibitors 68
2.2 Chapter Aims 69
2.3 Materials and Methods 72
2.3.1 General Information 72
2.3.2 Blank Gel Synthesis 72
2.3.3 PBA/BOB Containing Gel Synthesis 72
2.3.4 Dye Uptake Experiments 73
2.3.5 Dye Washing Experiments 73
2.3.6 Dye Release Experiments with H_2O_2 73
2.3.7 Dye Release Experiments with Plasma Activated Buffer 73
2.3.8 Media, Buffers and Stock Solutions 74
2.3.9 Bacterial Strains and Overnight Cultures 74
2.3.10 Bacterial MICs 74
2.3.11 Bacterial Biofilm Formation 74
2.3.12 Crystal Violet Biofilm Staining 75
2.4 Results and Discussion 76
2.4.1 Synthesis of the Boronic Acid Containing Hydrogels 76
2.4.2 Dye Loading and Washing Studies 76
2.4.3 Triggering the Release of ARS With H_2O_2 80
2.4.4 Using Cold Plasma to Trigger ARS release 84
2.4.5 The Biological Activity of ARS 87
2.4.6 Addition of H_2O_2 to Biofilms at Lag Phase 90
2.4.7 Addition of H_2O_2 to Biofilms at Exponential Phase 91
2.4.8 Addition of H_2O_2 to Biofilms at Stationary Phase 93
2.4.9 Addition of H_2O_2 and ARS to a Biofilm at the Lag Phase 94
2.4.10 Testing the Gel System with Biofilm Inhibition 95
2.5 Conclusions 97
2.6 Future Work 98
2.7 Bibliography 101
3 PBA Functionalised Drugs 103
3.1 Introduction 103
3.1.1 Prodrugs 103
3.1.2 ROS Responsive Prodrugs 104

3.1.3 Antibiotic Prodrugs 105
3.2 Aims 107
3.3 Materials and Methods 108
3.3.1 General Information 108
3.3.2 Blank Gel Synthesis 108
3.3.3 Drug/Dye Loaded Gel Synthesis 108
3.3.4 Dye Release Studies 109
3.3.5 Gel Disc Diffusion Assay 109
3.3.6 Modified Gel Disc Diffusion Assay 109
3.4 Results and Discussion 110
3.4.1 Dye Release Studies with AzuFluor 483-Bpin™ 110
3.4.2 Anchoring Drugs to Hydrogels 112
3.4.3 Synthesis of Triclosan-PBA 114
3.4.4 Crosslinking PVA Doped with Triclosan-PBA 115
3.4.5 Disc Diffusion Assays with Triclosan-PBA 117
3.4.6 Synthesis of Ciprofloxacin-PBA 119
3.4.7 Modified Disc Diffusion Assay 123
3.5 Conclusions 126
3.6 Future work 127
3.7 Bibliography 129
4 Dynamic H_2O_2 sensitive hydrogels 132
4.1 Introduction 132
4.1.1 Hydrogen Peroxide Sensing 132
4.1.2 Detecting ROS/RNS 133
4.1.3 ROS/RNS and Their Uses 134
4.1.4 Hydrogels for Bio-imaging 135
4.2 Aims 136
4.3 Materials and Methods 137
4.3.1 General Information 137
4.3.2 Synthetic Experimental 137
4.3.3 Solution Based UV-vis Studies 137
4.3.4 Solution Based Fluorescence Studies 137
4.3.5 Hydrogel Synthesis 138
4.3.6 Gel Based UV-vis Studies 138
4.3.7 Gel Based Fluorescence Studies 138

4.3.8 Gel Dissolution Study 138
4.3.9 Gel Stability Study in Air 138
4.3.10 Gel Stability in Aqueous Solution 139
4.4 Results and discussion 140
4.4.1 Existing Boronate Ester Fluorophores 140
4.4.2 Synthesis of PF-1 140
4.4.3 PF-1 Testing in Solution 141
4.4.4 PF-1 Crosslinked Hydrogel Development 143
4.4.5 Gment Gels in H_2O_2 Solutions 144
4.4.6 Purplement 147
4.4.7 Purplement Testing in Solution 147
4.4.8 Purplement Crosslinked PVA Hydrogel Development 149
4.4.9 Pment Gels in H_2O_2 Solutions 150
4.4.10 Gel Stability 152
4.4.11 Gel Dissolution 153
4.5 Conclusions 155
4.6 Future Work 156
4.7 Bibliography 157
5 Development of Prodrug Crosslinkers 159
5.1 Introduction 159
5.1.1 Polymeric Drug Delivery Systems 159
5.1.2 Ciprofloxacin 159
5.1.3 Ciprofloxacin Mechanism of Action 160
5.1.4 Structure Activity Relationship of Ciprofloxacin 160
5.1.5 Resistance to Ciprofloxacin 161
5.1.6 Infection and Cancer 162
5.1.7 5-Flourouracil 162
5.2 Aims and Objectives 163
5.3 Materials and methods 164
5.3.1 General Information 164
5.3.2 Gel Synthesis 164
5.3.3 UV-vis Measurements in Solution 164
5.3.4 UV-vis Measurements Using CBPBA Hydrogels 165
5.3.5 Fluorescence Measurements in Solution 165
5.3.6 Initial Fluorescence Measurements Using CBPBA Hydrogels 165

5.3.7 Ciprofloxacin Standard Curve 165
5.3.8 MIC Determination 165
5.3.9 Pseudo-MIC CBPBA Release Studies 166
5.4 Results and Discussion 167
5.4.1 Modification of Ciprofloxacin 167
5.4.2 Solution Testing CBPBA 168
5.4.3 Initial Ciprofloxacin Release From CBPBA Hydrogel 170
5.4.4 UV-vis CBPBA Gel Release Studies 172
5.4.5 Converting Absorbance to Concentration 173
5.4.6 Biological Testing – MICs of Ciprofloxacin and H_2O_2 175
5.4.7 Pseudo MICs to Measure Ciprofloxacin Release from CBPBA Gels 178
5.4.8 CBPBA Biological Activity 180
5.4.9 Expansion of the Methodology 181
5.4.10 Gel Stability 183
5.5 Conclusions 185
5.6 Future Work 186
5.6.1 Increasing Scope 186
5.6.2 Theranostic Development 187
5.7 Bibliography 191
6 Synthetic Experimental 194
6.1 Chapter 2 194
6.2 Chapter 3 196
6.3 Chapter 4 198
6.4 Chapter 5 202
7 Appendix 204
7.1 Chapter 1 204
Appendix 1 204
7.2 Chapter 2 205
Appendix 1 – Acrylamide gel synthesis 205
Appendix 2 205
Appendix 3 205
Appendix 3 206
Appendix 4 207
Appendix 5 207
7.3 Chapter 4 208

Appendix 1 208
Appendix 2 208
7.4 Chapter 5 209
Appendix 1 209
Appendix 2 210
7.5 Published Manuscripts 212
7.6 Unpublished Manuscripts 252

1 Introduction

1.1 The Clinical Need for Smart Wound Dressings

Wounds, subsequent wound infection and thus wound care are a near unavoidable aspect of life. Whilst the majority of wounds will heal normally and without the interference of infection, there is a large clinical burden associated with those that do not. An estimation of the economic cost of wound management to the NHS was studied in 2012-13 and was found to be comparable to obesity at £5 billion.[1] Current diagnostics for wound infection rely on clinical inspection of a wound for symptoms such as redness and swelling.[2] To allow for this inspection, wound dressings must be removed, exposing the wound to the environment, at which time infection or re-infection is likely.[3] The same potential for contamination occurs when there becomes a need for the application of topical antibiotics. There is thus a need for dressings that are able to detect infection and administer topical treatments, without the requirement for clinical infection.

1.2 Bacteria

Bacteria are unicellular, microscopic, prokaryotic organisms, which exist in almost every possible ecological niche. They often exist symbiotically with other organisms, including humans, and aid with such processes as digestion and immunity.[4, 5] These organisms can be broadly categorised into two types, gram positive and gram negative. These are named after the Danish scientist Hans Christian Gram who developed the Gram staining procedure in 1884.[6] Gram-positive bacteria retain the stain appearing a violet colour, owing to their thick peptidoglycan cell walls (discussed in 1.5.1.1). As they have a much less porous lipid bilayer, gram-negative bacteria do not retain the stain as it is washed out with solvent. They can instead be counter stained with safranin.[7] Bacterial cells have a global biomass greater than that of both the animal and plant kingdoms, with over 5 x 10^{30} bacterial cells worldwide.[8]

1.3 Wounds and Wound Infection

The skin is the body's first line of defence against a number of potentially harmful external stimuli, both physical (such as sunlight), and biological, namely microbial pathogens.

A wound is a breaking of this barrier, exposing the body to these risks. Wounds are generally categorised as either acute or chronic. An acute wound is one that will progress normally through

the four stages of healing (haemostasis, inflammation, proliferation and remodelling), and will show evidence of healing in a predictable timeframe.[9] Chronic wounds do not progress through these stages at the normal rate, or can be non-healing entirely. Often influenced by other factors, for example diabetes, these wounds will not heal via the usual path, often stalling at one of the aforementioned stages of healing. This extended healing time causes chronic wounds to be far more susceptible to infection, and greatly increases associated morbidity and mortality. In the UK the national health service (NHS) is estimate to spent £2.3 - £3.1 billion a year on the treatment of such wounds.[10]

The skin is host to vast quantity and variety of micro-organisms including bacteria, fungi and mites.[11] The presence of such species is often beneficial, and many of them work symbiotically to maintain healthy skin.[12] However, amongst the skins microbiome there are a number of opportunistic pathogens that can develop infections within wounds. Opportunistic pathogens are those that are not ordinarily harmful, but when allowed to grow in a certain environments can cause harm.[13] Common bacteria that are found within infected wounds include *Staphylococcus aureus, Pseudonomas aeruginosa* and *Enterococcus. faecalis.* Whilst a wound will always contain bacteria, only at high bacterial concentration is there risk of infection. The critical colonisation concentration (CCC) is the point at which the bacterial density becomes high enough to out-compete the host's immune system. This exact point of this threshold is not fully understood, owing to the myriad of factors that influence it. Not only do the species of bacteria present alter this point, known as the ccc, but also the general health and the immune response of the patient.[14] Despite this lack of clinical consensus of what defines an infection, it is universally acknowledged that bacterial infections prevent normal wound healing, often leading to chronic wounds. In 60% of such wounds the bacteria are in the form of a biofilm.[15]

1.4 Biofilms

Biofilms are surface associated, complex communities of bacteria, surrounded by a three dimensional extra-cellular polymeric substance (EPS).[16] Within these architectures bacteria are intrinsically more resistant to conventional antibiotics, owing in part to their low metabolic rate, as well as the EPS providing another barrier of protection.[17] The EPS consists of approximately 90% a combination of DNA, extracellular proteins, sugars, and allows regulation of nutrients and waste for the bacteria as a community, as opposed to as single cells.[18] Bacteria within this

protective layer have minimum inhibition concentrations (MICs) much higher than their planktonic counterparts. Planktonic bacteria are those that are free floating, unbound to surfaces or larger bacterial aggregations Anderl *et al.* found that *Klebsiella pneumoniae* biofilms treated with ten times their planktonic MIC, of both ciprofloxacin and ampicillin, remained unaffected in terms of the number of remaining viable cells.[19] Other papers have reported the MIC increasing to 100-1000 times that the planktonic MIC when the bacteria is protected within a biofilm.[20, 21] This decrease in susceptibility to antimicrobial agents introduced the development of a new measure of drug efficacy, the minimum biofilm eradication concentration (MBEC).[22] This is a much more useful value when dealing with the harder to treat communities.

1.4.1 Biofilm Formation

Biofilm formation is a multi-step process, beginning with the adhesion of planktonic bacteria to a surface.[23] A number of chemical signals and physiological processes then cause the bacteria to bind to the surface, utilising membrane proteins such as SadB in the case of *P. aeruginosa.*[24] Following this binding, extracellular secondary messengers begin to stimulate the production of EPS. These messengers are dependent on environmental conditions, and their regulation and thus that of the EPS production reflects this.[25] As the biofilm matures it forms micro-colonies, the bacterial cells begin to divide and produce more EPS. Within this enclosed matrix the bacteria are protected and are able to communicate via quorum sensing.[26] The structures of these architectures vary between bacterial species as well as environmental conditions, allowing them to more efficiently make use of nutrients and remove waste products.[27] The biofilm can also act as a reservoir of bacteria, which themselves are then able to leave the relative protection of the biofilm to start new biofilms of their own. This dispersal can be either passive, owing to the shearing force of a flow, or active, with intentional release of bacterial cells from the matrix.[28] The intentional release of bacteria is triggered by environmental changes, including a change in temperature, oxygen levels and the increased concentration of metabolites.[28] This overall process can be seen in figure 1.

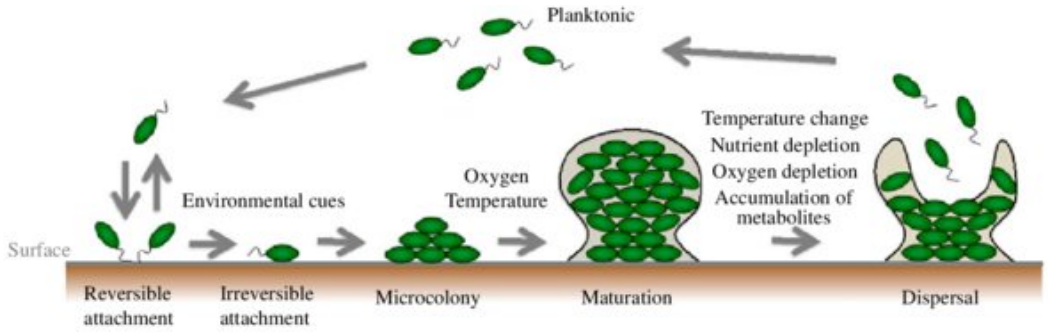

Figure 1 The formation and lifecycle of biofilm formation on a surface, used with permission from[29].

1.4.2 Quorum Sensing

Quorum sensing is the name given to the chemical signalling pathways that allow intercellular communication between bacteria, allowing them to increase their survivability and synchronise their activities when existing in high concentrations, for example in a biofilm.[30] Auto-inducers (AIs) are a class of compounds produced by bacteria, which are released and are able to produce a response based on population density.[31] The number of AIs detected by a bacterium is proportional to the concentration of bacteria that are present around it. The structures of these signalling molecules are varied; different bacterial species produce different AIs, although there is often overlap in the recognition of compounds.[30] Examples of their structures can be seen below in figure 2.

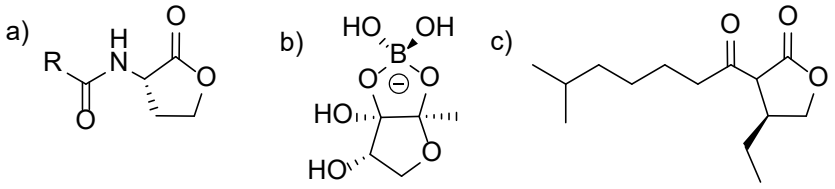

Figure 2 a) Acetyl-homoserine lactones (AHL), an AI with an R chain length that varies between bacterial species. b) AI-2, a family of autoinducers, c) Streptomyces γ-butryolactones

The detection of these species can induce changes in gene expression in individual bacteria to increase the survivability of the biofilm as a whole. The development of a biofilm is not the full extent of quorum sensing's use however; it can also trigger the production of virulence factors.[32] This is done through complex biochemical cascades, and will not be explored in detail within this work.

1.5 Bacterial Infection

Bacterial species that are able to cause harm to the host are known as pathogenic. This pathogenicity will confer an increased level of survivability to the bacteria; this can be through the production of excreted virulence factors.[33] These disease-causing molecules can be either chemical or enzymatic in nature. Within a wound environment one of the most damaging forms of virulence factor are extracellular proteases.[34] Proteases are enzymes that can degrade host tissues, in turn generating both space and nutrients for the invader.[35] These excreted compounds are not restricted to local effects. Non-enzymatic proteins, for example toxic shock syndrome toxin (TSST) produced by *S. aureus,* is a superantigen responsible for a number of disease states. A traditional protein antigen promotes a response only following its ingestion by an antigen presenting cell; super antigens however bind to cells and are not taken up by said cell but rather produce the effect simply by binding. It effects the entire body producing symptoms such as fever, shock and in serious cases death.[36] The bacteria do not however enter the blood stream and produce the toxin, rather they produce the toxin in the local infection site (*i,e, wounds*), and the toxin enters the blood and spreads to receptor sites.[36]

Infections are most commonly treated with antimicrobial chemotherapies, however as previously mentioned, the bacteria become much less susceptible to traditional antimicrobials when they adopt the biofilm phenotype. As a result, novel targets must be found. The term antimicrobial encompasses agents that feature activity against any microbe, including but not limited to fungi, viruses and bacterial. Antibiotics however are specific to bacteria; within this work these terms will be used interchangeably.

1.6 Antibiotics

The discovery and development of antimicrobials was arguably the most important breakthrough in the history of modern medicine. The first antibiotic was discovered by Flemming in 1928 with the introduction of penicillin. This kick started a golden age of antibiotics. Penicillin, being a β-lactam, is ineffective in the treatment of gram negative infections (discussed further in 1.17). This prompted the discovery of a number of other different classes of antibiotics. The WHO's list of 100 essential medicines includes 38 antibiotics for general treatment of bacterial infection.[37] Without the use of antibiotics even minor infections can grow unchecked, causing potential complications with drastic implications for health. This is an even greater danger for

immunocompromised patients, for example those undergoing cancer chemotherapy. Without the prophylactic use of antibiotics, many anti-cancer agents could not be used.[38] The objective of antibacterial drug design is to find a molecule that is toxic to bacterial cells, but does not show activity towards mammalian cells. Common targets include bacterial ribosomes (*e.g.* aminoglycosides and tetracyclines), the cell wall (β-lactams) and the enzymes, including DNA gyrase (fluoroquinolones).[39-41]

1.6.1 Cell Wall Inhibitors

1.6.1.1 β-lactams – Penicillins

The first generation of β-lactams produced were the penicillins. Since the first variation (benzyl-penicillin) was isolated from the *Penicillium* fungi a number of analogues have been produced with varying activity, figure 3.

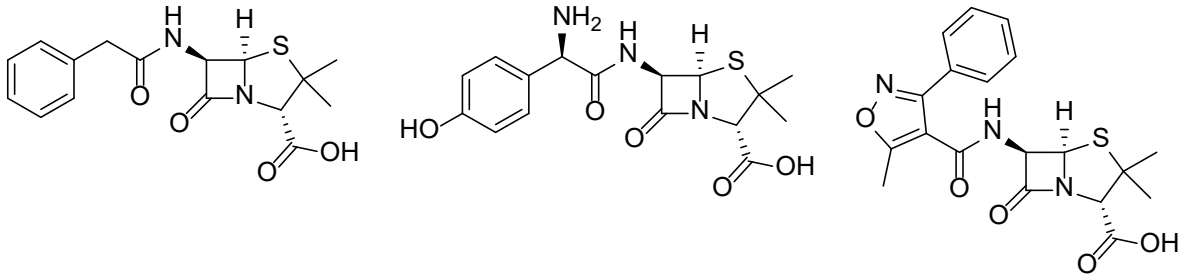

Benzyl Penicillin **Amoxicillin** **Oxacillin**

Figure 3 Three commonly prescribed penicillins, Benzyl Penicillin (also known as penicillin G), Amoxicillin and Oxacillin

Bacterial cell walls are peptidoglycan layers of repeated dimers of N-acetylglucosamine and N-acetylmuramic acid molecules, Figure 4.

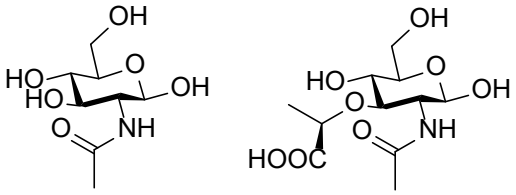

Figure 4 *Left* N-acetylglucosamine *right* N-acetylmuramic acid

. These layers are crosslinked by chains of amino acids, typically with a tetrapeptide.[42] In cell wall synthesis, the step in which the peptidoglycan chains are crosslinked is catalysed by the penicillin binding protein (PBP). The mechanism of action for penicillin is the inhibition of this protein, with the characteristic 4-membered lactam ring inactivating the transpeptidase by binding to its active site.[40] The bacterial cell wall is constantly being formed and destroyed within bacteria, and the PBP is only essential for the formation. This means that with the PBP inhibited, the forward reaction cannot occur whilst cell wall destruction is not affected. This leaves the bacteria with a much weaker cell wall, which is not able to withstand the osmotic pressure changes that the cells regularly experience, 'bursting' the bacteria through osmotic lysis.[43]

This bacterial cell wall is much thicker in gram-positive bacteria (20 – 80 nm) when compared to gram-negative bacteria (<10 nm) which also consists of a far less porous lipopolysaccharides, which is how the previously discussed Gram staining test is able to distinguish the two. Whilst thinner, the lipid bilayer features mechanical strength great enough to withstand the osmotic changes experienced by the bacteria. As a result, the susceptibility of gram-negative bacteria to beta lactams is much lower.[44]

1.6.1.2 β-lactams – Cephalasporins

This lack of ability to treat gram-negative bacteria led to research attempting to create analogues of the drugs with a broader spectrum of activity. Structurally, cephalasporins are very similar compounds to the penicillins, featuring a six membered ring bound to the four membered ring. This class of compounds is slightly less susceptible to the inactivating β-lactamase enzymes (which will be discussed in further detail in chapter 1.7.3.1).

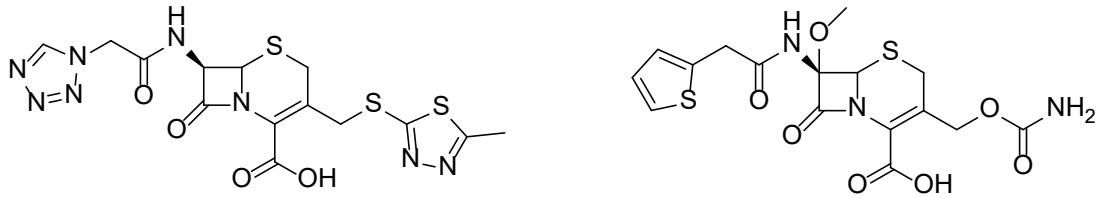

Cefazolin

Cefoxitin

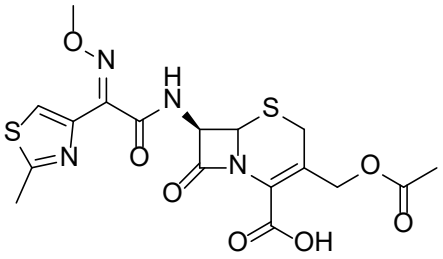

Cefotaxime

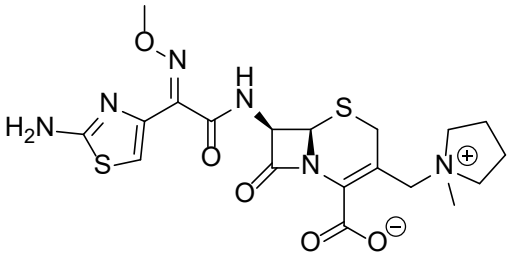

Cefepime

Figure 5 An example of a member of the first four generations of the cephalosporin class of β-lactams. Top left first generation Cefazolin, top right second generation cefoxitin, bottom left third generation cefotaxime and bottom right fourth generation cefepime.

One of the earliest cephalosporins was Cefolazin, figure 5. First reported in 1970, it offers a far greater activity against gram-negative bacteria, including *E. coli* and *Klebsiella pneumoniae.*[45, 46] The second generation cephalasporin Cefoxitin offers a similarly broad spectrum of activity, but has the advantage that it is more resistant to the action of β-lactamase, a drug inactivating enzyme that will be discussed further in 1.6.3.1.[47] The next step in the continuing improvement of this class of antibiotics, was the discovery of the third generation drug Cefotaxime. Cefotaxime was found to have a similar efficacy in the inhibition of gram-positive bacterial growth, however, showed a 50-100 times increase in activity to previously tested cephalosporin sensitive strains, and a 100-1000 times increase in activity against cephalosporin resistant strains.[48] This increased the spectrum of activity of the second generation drugs, which unlike cefotaxime, were not effective against bacterial species such as *Streptococcus faecalis* and *Proteus spp.* Further improvements came with the fourth generation, exemplified by cefepime. Cefepime has a greater activity against both gram positive and gram negative isolates, whilst being more stable to β-lactamase catalysed

hydrolysis. Its increased penetration into gram negative bacteria owes itself to the presence of the N-methylpyrrolidine.

1.6.1.3 β-lactams – Carbapenems

The carbapenems are another class of β-lactam, and tend to offer both a broader spectrum of activity and greater efficacy, combined with a lower likelihood of resistance when compared to the penicillins. This is due to their ability to inhibit the β-lactamase enzymes.[49] As a result of their efficacy, they are currently used as "last resort" antibiotics.[50]

Thienamycin was isolated from *Streptomyces cattleya* in the 1970's, and remains one of the most potent antibiotics discovered. It was faced with the damning disadvantage however that it was unstable not only in the solid state, but also in any aqueous solution, removing any possible medical utility it may have had, figure 6.[51] It was therefore of great interest to develop a compound with a similar activity, but greater stability and pharmokinetic profile. This led to the development of Imipenem. It is degraded by dehydropeptidase enzymes, but can be co-administered with cilastatin, which is an inhibitor of these enzymes. It offers a broad spectrum of activity, being one of the few drugs able to treat *P. aeruginosa* infections, yet is inactive against methicillin resistant *Staphylococcus aureus* (MRSA).[51] A recently released carbapenem is Doripenem, which offers a greater hydrolytic stability versus previously mentioned members of this class. This gives it a better pharmokinetic profile and can make it more effective in the treatment of more persistent infections.

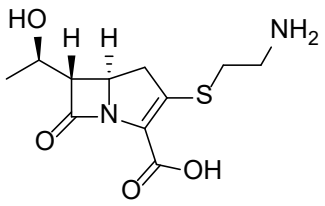

Thienamycin

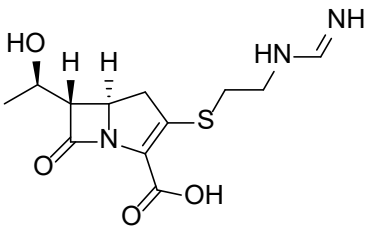

Imipenem

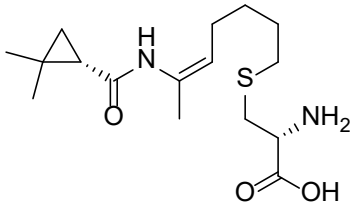

Cilastatin

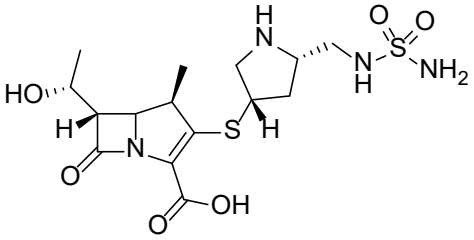

Doripenem

Figure 6 Examples of carbapenems showing the development of treatment. *Top left* initially discovered natural product thienamycin, *top right* first available carbapenem Imipenem, *bottom left* dehydropeptidase inhibitor Cilastatin, *bottom right* recent development in carbapenem treatments Doripenem

1.6.1.4 Glycopeptides

Glycopeptides are another class of antibiotic that affect bacterial cell wall synthesis. As with the penicillins, glycopeptides have a narrow spectrum of activity, chiefly targeting gram-positive bacteria. Unlike β-lactams which bind to PBPs, glycopeptides bind to lipid II, a precursor to peptidoglycan.[52] The first to be isolated and approved for clinical use was vancomycin, figure 7. It has been used as a drug of last resort (not being in regular use owing to its high nephrotoxicity) since the emergence of drug resistant strains of *S. aureus* in the 1980s.[53]

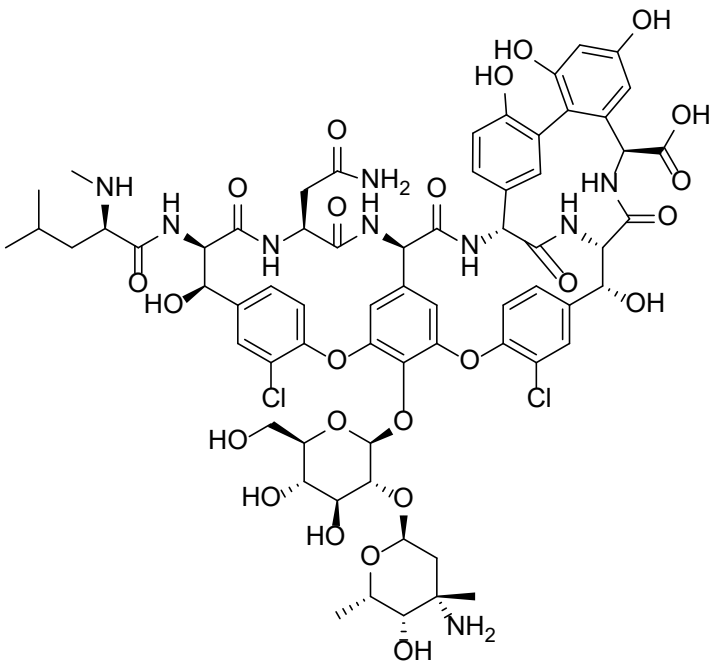

Figure 7 The first glycopeptide to be isolated, vancomyin

Vancomycin remained the drug of choice for a number of multi-drug resistant (MDR) bacteria, however in the 1990s isolates of vancomycin resistant *S. aureus* (VRSA) were discovered.[53] Vancomycin is not the only commercially available glycopeptide however, figure 8 shows the timeline of the discovery and clinical use of a number of important glycopeptides (important structures found in appendix 7.1.1).

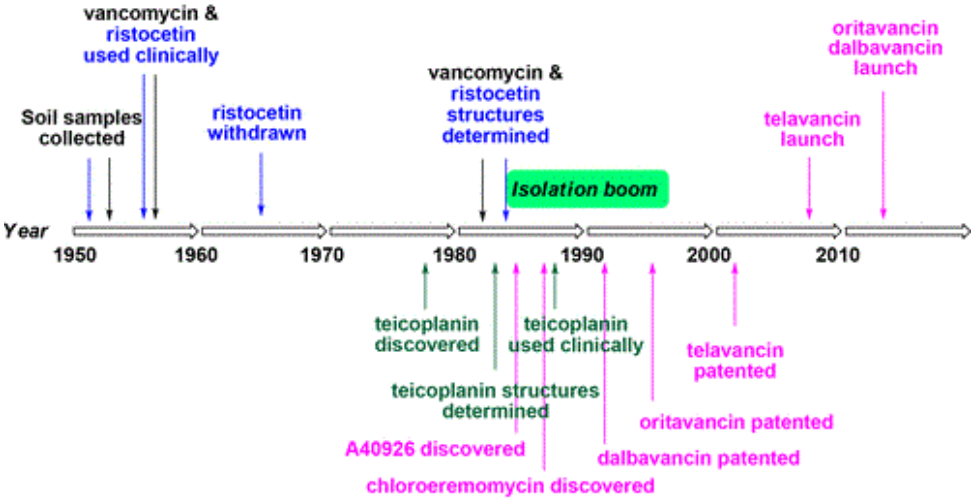

Figure 8 Development and release timeline for the glycopeptide antibiotics, adapted with permission from [54]

1.6.2 Antibiotics that Target the Bacterial Ribosome

A key feature of antibacterials is that they must be as non-toxic towards mammalian cells as possible. As such, the bacterial ribosome is a common target.[55] The ribosome is the organelle within a cell in which protein synthesis occurs – this is true of both prokaryotic and eukaryotic cells. However, whilst exhibiting the same basic functions, the structure of these two organelles differ. Ribosomes are split into sub-units, the larger eukaryotic ribosome is split into 60s and 40s subunit to form an 80s ribosome, whilst the prokaryotic equivalent is split into 50s and 30s subunits forming a 70s whole unit.[56] Preventing these organelles to function can occur through a number of chemical pathways including preventing the subunits splitting, and preventing the binding of DNA. Either of these mechanisms prevents the bacteria from being able to synthesise enzymes and other proteins crucial to their survival, leading to cell death.

1.6.2.1 Aminoglycosides

Aminoglycosides have a wide spectrum of activity against gramnegative bacteria, yet most fall short when attempting to treat gram positive infections.[57] As the name implies they all contain amine functionalised sugars. All of the aminoglycosides are produced from grampositive actinomycetes of two families. Those produced by *Streptomyces* are given the suffix -mycins, (*i.e.* streptomycins) and those produced by *Micromonospora* are given the suffix –micins (*i.e.* gentamicin), figure 9.[57]

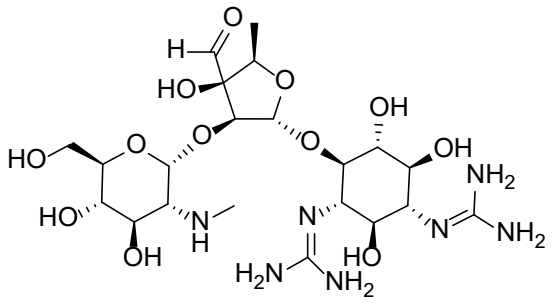

Streptomycin

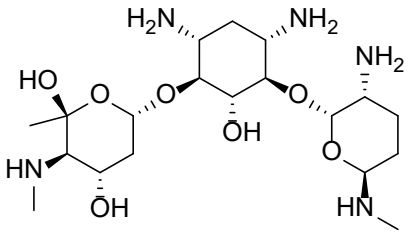

Gentamicin

Figure 9 Two commonly prescribed aminoglycoside antibiotics, *left* Streptomycin, *right* Gentamicin

Despite showing great efficacy in the treatment of *P. aeruginosa* infections, they are only active against *Enterococci* when co-administered with a bacterial cell wall synthesis inhibitor, such as those previously discussed.[58] This, owing to inefficient active transport across the cytoplasmic membrane, leads to sub-inhibitory intracellular drug concentrations.[59]

1.6.2.2 Tetracyclines

The tetracyclines are natural products, or semi-synthetic broad-spectrum antibiotics, which were initially isolated from *Streptomyces spp.* in the 1940's.[60] Despite the nomenclature, the original compound tetracycline was not the first to gain FDA approval (in 1953), and actually both chlortetracycline and oxytetracyline were isolated first, gaining FDA approval in 1948 and 1951, respectively, figure 10.[61] This anomaly in naming comes due to their antibiotic activity being discovered prior to their structures being elucidated.

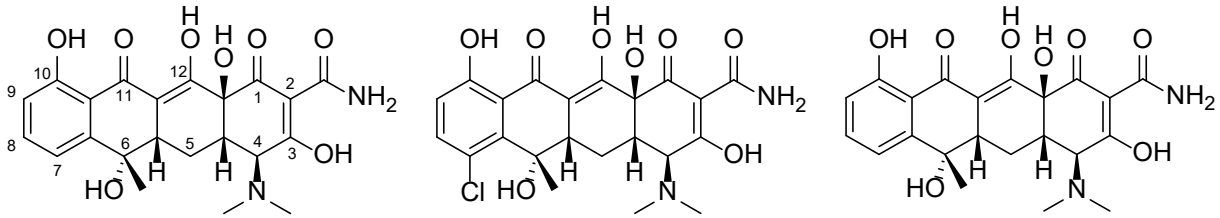

Tetracycline **Chlortetracycline** **Oxytetracycline**

Figure 10 *Left* Tetracycline and the generic numbering system used for all tetracyclines, *Middle* Chlortetracycline, *Right* Oxytetracycline

The tetracylines used to be favoured as treatments for those patients with allergies to β-lactams, however, increasing levels of resistance have reduced their usefulness.[62]

This list of ribosome targeting antibiotics is not exhaustive, and there are a number of other therapies available, *i.e.* the macrolides, but for the purpose of this work they will not be explored.

1.6.3 Antibiotics that Target DNA Synthesis

1.6.3.1 Quinolones

The quinolones are broad-spectrum antibiotics. Fluoroquinolones are a subset of quinolones that feature a fluorine atom. Owing to how commonly the structures feature fluorine these two terms are often used interchangeably. Unlike all previously discussed antibiotic classes, the quinolones are one of the few classes that were synthetically isolated. The original 'quinolone' was not actually a quinolone, but a napthyridone, nalidixic acid, figure 11. Nalidixic acid, first isolated in the 1960s, showed good activity towards a number of bacterial species, but with a relatively high toxicity to mammalian cells.[63] It was over a decade before cinoxacin was approved for use, offering an increase in activity against all bacteria, with no increase in toxicity to mammalian cells.[64] Until the late 1980s there was a developmental boom in the production of quinolones, with over 10,000

quinolones being patented for antimicrobial use by 2003.[63] Many of the antibiotics produced in this period are still used today to treat *P. aeruginosa* infections, for example levofloxacin.

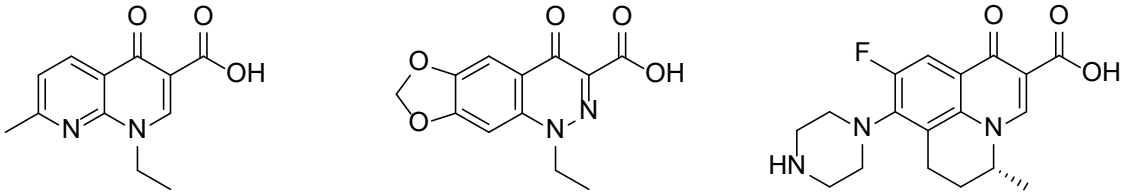

Nalidixic acid **Cinoxacin** **Levofloxacin**

Figure 11 *Left* The first 'quinolone' Nalidixic acid, *Middle* Cinoxacin, *Right* Levofloxacin

As with all of the mentioned classes of antibiotic, resistance has been identified in a number of bacterial strains, but it is not only resistance threatening their use. It has been found that a number of quinolones are causing damage to tendons, joints and the central nervous system with prolonged exposure.[65]

The recurring theme in all of the antibiotic classes mentioned is that they are losing efficacy over time owing to the bacteria that they are designed to treat gaining resistance. The mechanisms by which this resistance occurs are varied, and will be discussed in greater detail.

1.7 Antimicrobial Resistance

The rising resistance of bacteria to current antibiotics is considered to be one of the greatest threats to modern medicine. The speed at which bacteria are able to acquire resistance to new therapeutic compounds has made the development of such drugs less financially viable, leaving pharmaceutical companies unwilling to spend money on the development of a product that may only be on the market for under five years.[66] There are many reasons why antibiotic resistance is becoming such a grave problem, major factors are: the over use of antibiotics in agriculture, over prescription of antibiotics within healthcare and also exposure to ineffective antibiotics (through either misdiagnosis or mis-prescription).[67, 68] Exposing a bacterial population to sub-therapeutic concentrations of an antibiotic will always select for survival, and as such, in the UK the given advice is to finish an antibiotic course, to prevent incomplete eradication of an infection. A recent paper by Llewelyn *et al.* has contradicted this however, indicating that this is not founded in evidence and that it has been shown that prolonged exposure to the antibiotics may in fact be increasing the prevalence of resistance.[69]

1.7.1 Intrinsic Resistance

Certain bacteria have an intrinsic resistance to some drugs; as previously discussed, a number of drugs that are active against the bacterial cell wall are inactive against gram-negative species. These resistances are a result of a spontaneous mutation and Darwinian selection pressures, as opposed to horizontally transferred genes.[70] These resistance genes have often been part of bacterial genomes for millions of years, as exemplified by the resistome of *Paenibacillus spp.* found in the Lecugulia cave in New Mexico, which has resistance to most clinically available antibiotics despite never having been in contact the compounds.[71]

Efflux pumps are ubiquitously present in all bacteria, suggesting that their initial purpose was not for the development of resistance to antibiotics.[72] These are essentially protein channels which actively transport chemical entities across membranes, utilising energy produced from adenosine tri-phosphate (ATP). Efflux pumps can be either specific for certain molecules or can transport a range of compounds.[73] As a result, these efflux pumps can convey resistance to a number of antimicrobial entities (including metal ions like silver, with a known toxicity to bacterial thought to be attributed to their interactions with thiols), and are common to a range of bacterial species.[74, 75] These are known as multi-drug resistant (MDR) efflux pumps.

1.7.2 Acquired Resistance

Bacteria mutate rapidly. This can lead to the spontaneous development of genes coding for proteins that can infer resistance to a particular species.[76] Whilst initially this would yield a negligible percentage of the population that featured this gene, that the bacteria have the ability to transfer genetic material horizontally.

Bacterial genetic material is not histone bound like that of eukaryotic cells, but is free floating. There is a large, single loop of DNA known as the bacterial chromosome, and a number of smaller loops known as plasmids. These plasmids code for a far smaller number of genes than the bacterial chromosome.[77]

1.7.2.1 Horizontal Gene Transfer (HGT)

Bacteria are able to transmit DNA horizontally as well as vertically to offspring. There are three separate mechanisms by which this genetic material can be transferred: transformation, transduction and conjugation.[78]

1.7.2.2 Transformation

Transformation is the process by which bacteria are able to take up DNA from their surrounding environment, figure 12. The presence of such extracellular DNA is normal within typical bacterial growing conditions, but the cells must reach a state of 'competence' before they are able to take on said genetic material; this state is induced by a number of factors such as nutrient access.[79] This genetic material often comes from lysed cells, but is also a component of biofilm EPS.[80]

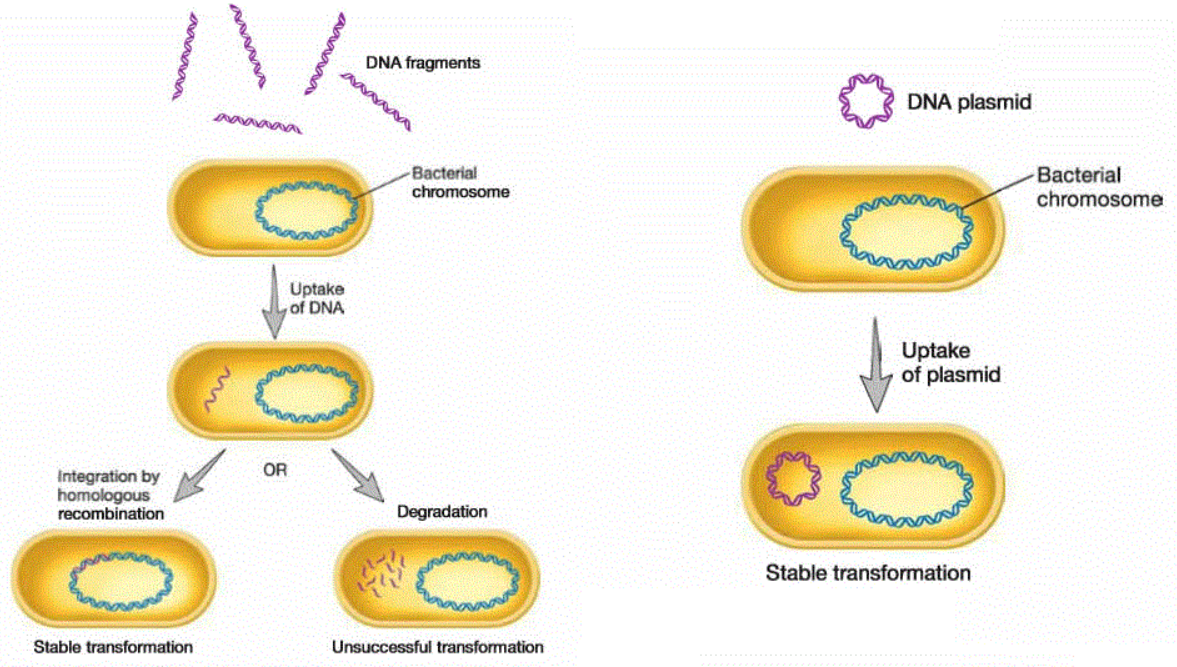

Figure 12 The two types of transformation; *Left* The uptake of fragmented bacterial DNA from a bacterial chromosome *Right* The uptake of a plasmid into a bacteria

1.7.2.3 Transduction

Transduction is another method by which bacteria can acquire new genetic material, however, this mechanism requires a vector to carry the DNA; this vector comes in the form of a bacteriophage.[81] Bacteriophage, or phage, are viruses that are highly specific towards bacteria. Depending on the phage this can be specific for a species of bacteria or even a single strain. Once bound to a bacteria, the phage 'hijack' the DNA replicative abilities of the bacteria and are able to reproduce. This can be either predatory, leading to bacterial cell death, or symbiotic.[82, 83] Within transduction a bacteriophage will infect a bacteria, breaking down the hosts DNA. It will then proceed to replicate. During this replication, some of the newly produced phage will have acquired bacterial DNA. Once the new phage are released, they can infect other bacteria with the genetic material

from the previous bacteria.[84] This requires the phage to be temperate as opposed to virulent. In essence this makes them non-toxic bacteria; these differences are beyond the scope of this work.[85]

1.7.2.4 Conjugation

The most studied and understood mechanism of the three is conjugation. Conjugation requires cell to cell contact of the bacteria. In this method the bacteria dock at recognition sites and form a conjugal pilus, through which they are able to transfer even large strands of DNA.[86]

Regardless of the three methods in which HGT occurs, the end-result is that bacteria are able to transmit genes to other bacteria inferring an increased level of fitness to other bacterial cells.

1.7.3 Specific Resistance Genes

Bacteria can have resistance to antibiotics in a far more specific manner than blocking their entry or ejecting toxic chemicals from their cells. Either the bacteria will inactivate the attacking species (the antibiotic) or it can modify the drugs target site.[87]

1.7.3.1 Antibiotic Destruction and Alteration

Resistance to penicillin was one of the earliest reported, with the mechanism of resistance owing to the bacterial enzyme β-lactamase.[88] These enzymes open the strained four membered ring within the β-lactam antibiotics that is essential to their activity. They do this through either a zinc centre, or more commonly through serine ester formation (via an acyl enzyme intermediate).[89]

Aminoglycoside inactivation through bacterial enzymes has also been widely reported.[90] Acyl-transfer enzymes are able to inactivate the drugs through acylation of the hydroxyl and amine groups, preventing it binding to the bacterial ribosome (hydrogen bonding is essential to a number of drug binding interactions).

Chloramphenicol is an antibiotic that also inhibits protein synthesis, figure 13. Chloramphenicol acetyl transferase (cat) acetylates the hydroxyl groups within the molecule, preventing it binding to its bacterial target ,the 50s subunit, by inhibiting hydrogen bonding.[91]

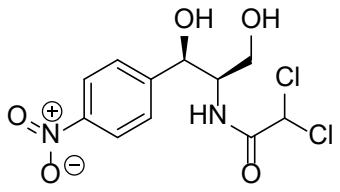

Figure 13 The antibiotic chloramphenicol

This is only a small number of the many compounds that bacteria have evolved enzymatic mechanisms for destroying or altering; Munita *et al.* have a more exhaustive list more in this review.[92]

1.7.3.2 Target Alteration

As well as preventing the action of antibiotics by altering the chemical structure, bacteria are able to alter the target site. This is exemplified in bacteria that are resistant to β-lactams. As the drugs have a very specific binding to the PBP, bacteria such as *Streptococcus pneumoniae* have evolved by altering the structure of the PBP, giving PBP2A.[93] This altered protein no longer features the binding site for penicillin, yet retains the ability to construct the cell wall.

It is not only single proteins like the PBPs that can be altered. Small structural changes to large organelles, such as that of the ribosome, have also been observed.[94] One example is the di-methylation of two amino groups, preventing the antibiotic erythromycin from binding.[95]

It is possible for these genes that code for wide ranges of resistance, *i.e.* efflux pumps, to be transferred horizontally. In areas of higher bacterial density, such as in clinical settings, these genes can spread rapidly, causing widespread resistance. As more is being learned of the global threat that is antibiotic resistance, more action is being taken to slow it and to find new therapies.

1.8 What is Being Done to Combat Antibiotic Resistance?

Antimicrobial or antibiotic stewardship is a term that outlines the practise of avoiding incorrect prescription of antimicrobials. The National Institute for Health and Care Excellence (NICE) have developed a set of guidelines for the decision making processes when considering the correct choice of prescription.[96] Point of care diagnostics for early wound detection can help prevent the prophylactic use of antibiotics following invasive surgeries.[97] Within the agricultural settings the problem and the solution is predominately based in governmental policy; the use of preventative antibiotics in agriculture was banned in the European Union (EU) in October 2018, with an aim to reduce the prevalence of resistance. Therapies that are able to neutralise the pathogenicity in bacteria are also being explored. These are compounds that interfere with the bacteria's quorum sensing, which can prevent it from switching its phenotype to one that produces virulence.

1.8.1 Biofilm Inhibitors and Biofilm Disruptors

The exposure of an organism to an outside selection pressure, in this case an antibiotic, will always select for evolution that overcomes this pressure. This is the fundamental basis of the rise of antibiotic resistance. The inhibition of the quorum sensing that move between bacteria does not directly affect individual bacterial cells. This inhibition will simply prevent the chemical or biological effect of these signalling molecules. These treatments are essentially 'shooting the messenger'. This can mean the prevention of the formation of a biofilm or even preventing virulence factors being produced.[32, 98]

For *P aeruginosa* there are 3 chief quorum sensing pathways, *las*, *rhl* and *PQS.* The *PQS* pathway is regulated by 2-Heptyl-3-hydroxy-4(1*H)*-quinolone (PQS), figure 13.[99] Li *et al.* noted that this regulatory chemical was essential to the formation of the *P. aeruginosa* biofilms, as well as a chelator of iron; bio-available iron can promote the biofilm formation.[100] The group were able to produce a library of pyranone containing compounds, able to inhibit the action of PQS, preventing the formation of *P. aeruginosa* biofilms. Their lead compound can be seen in figure 14, and featured a biofilm inhibition rate of over 50%, with no toxicity to the bacterial cells.[101]

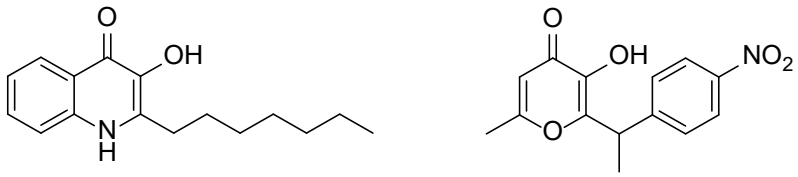

Figure 14 *Left* The PQS signalling molecule 2-Heptyl-3-hydroxy-4(1*H)*-quinolone *Right* PQS inhibitor

Unlike biofilm inhibitors, biofilm disruptors are able to cause the breakdown of an already established biofilm. Böttcher *et al.* used the natural biofilm disruptor norspermidine as a starting point to develop a library of active compounds, figure 14. Norspermidine is a natural part of the bacterial physiological process to collapse existing biofilms in the developmental cycle of *Bacillus subtilis.* The most effective compound they produced, 1-(3-guanidinylpropane-1-yl)-1,1'-(propane-1,3-diyl)-diguanidine, figure 15, was able to disrupt biofilms with an MBIC of 10 μM for *B. subitlis* and at 50 μM could also disrupt *S. aureus* biofilms.[102]

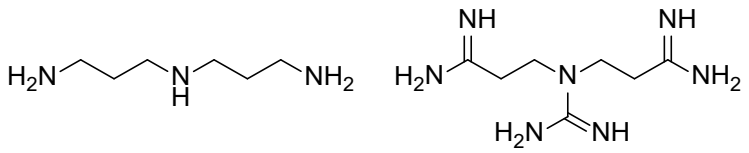

Figure 15 *Left* Natural biofilm disruptor Norspermidine. *Right* Synthesised broader spectrum biofilm disruptor based on spermidine

1.9 Fluorescence

Luminescence is the production of light from an electronically excited substance; this can be broadly split into either fluorescence of phosphorescence. These processes involve the relaxation of an excited electron from either a singlet or triplet excited state respectively.[103] The main difference between these two processes is the rate at which the emission occurs – this is much faster in fluorescence (10^8 s^{-1}) than in phosphorescence (10^3 s^{-1}). The process of fluorescence is most commonly described with the Jablonski diagram, figure 16.

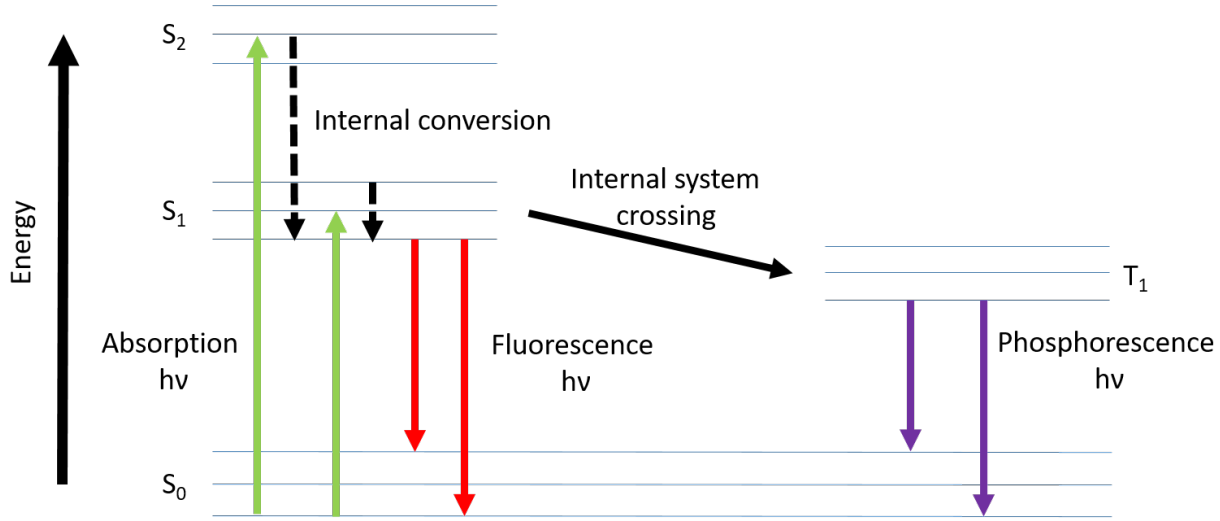

Figure 16 Jablonski diagram showing the potential excitation of an electron to a higher energy level and its subsequent relaxation with the release of a photon

In figure 16 the absorption (arrows in green) indicates the excitation of the electron from its ground state, S_0, to one of its excited states, S_1 or S_2 depending on the energy of the incoming photons. The levels within the electronic states are vibrational, and energy can be dissipated to the surroundings via these non-radiative steps, this is known as internal conversion (IC). The electron

in these states will have a spin opposite to that of the electron in the ground state. This means that the transition to S_0 is allowed, making the emission of the fluorescence photon fast. Should the electron undergo internal system crossing (ISC) this spin flips. This makes the transition between the excited state, T_1, and the ground state S_0 forbidden (purple arrows). This results in in the wavelength of light being emitted increasing and the rate at which it is released decreases. Owing to the speed often being an important factor for diagnostic systems, fluorescence will be focussed on in this thesis.

1.9.1 Designing a Fluorescent Probe

A fluorescent probe is compound, which will give a fluorescent response in the presence of an analyte. Upon interaction they form a host-guest complex. There are two key types of fluorescent probe; chemodosimeters are reaction based sensors, in which the guest irreversibly changes the host to give a response. These tend to give greater selectivity as well as lessened influence by the environment.[104] The other types of probes are chemosensors – these feature non-covalent reversible interactions between the host and the guest.[105] For the purpose of medical diagnostics and fluorescent imaging, these two types of probe offer indistinguishable results, and as such the term fluorescent probe will henceforth be used to describe either of these.

There are two key components to a fluorescent sensor, the reporting fluorophore and the receptor. The receptor, either bound directly to the fluorophore or via a linker, will in some-way change the fluorescence of the compound. The choice of reporter depends on the application. If it is for the imaging of cells then the fluorophore must have an adequate hydrophilicity to be transported to cells, yet still be hydrophobic enough to enter the cells it needs to image. A number of common fluorophores can be seen below, figure 17a. The fluorescence of some these compounds is pH dependent owing to the equilibria illustrated by fluorescein in figure 17b.

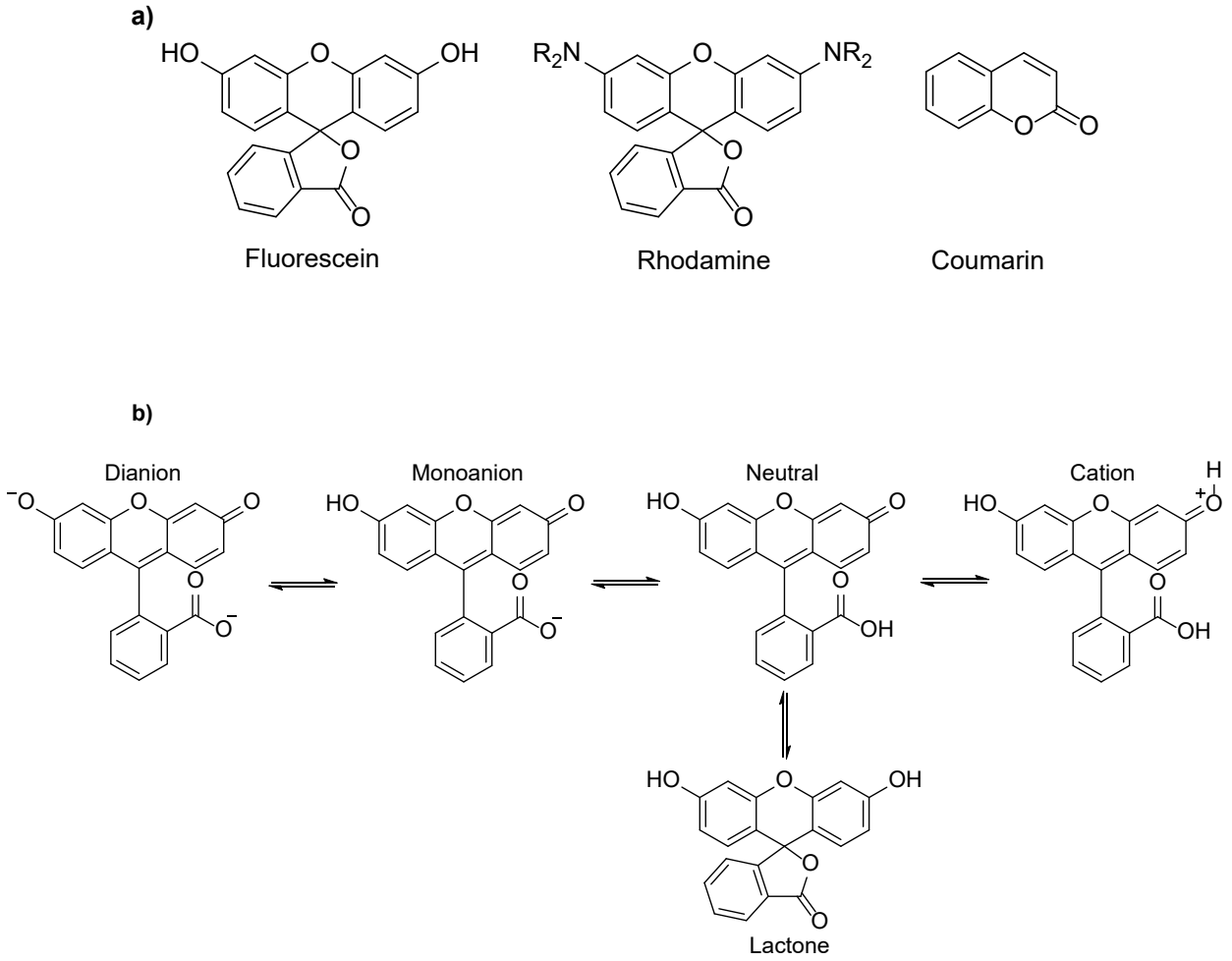

Figure 17 a) Three common fluorophores used for the creation of fluorescent probes b) The pH dependent equilibria illustrated by fluorescein, in which only the anionic forms are fluorescent. It is highly fluorescent with a large quantum yield at pH 5 – 9 (hence its use in physiological systems); with neutral forms exhibiting a much lower quantum yield

These are of great utility as they have all been used in prior cell based studies, and as a result, they are known to be of low toxicity and high optical brightness.[106, 107] High optical brightness is important for good image to background differentiation and low toxicity is essential to not damage mammalian cells. On exposure to light, fluorophores will lose efficacy, a process known as photo-bleaching. Resistance to this process is of great importance in order to maintain activity.

1.9.2 Molecular Mechanisms of Fluorescence

There are three mechanisms of fluorescence at a particle level, photoinduced electron transfer, (PET), Förster resonance energy transfer (FRET) and internal charge transfer (ICT).

1.9.2.1 Photo-induced Electron Transfer

The simplest of the three mechanisms is the PET. This mechanism can be utilised to generate both turn off or, more desirably, turn on fluorescent sensors. Turn on sensors for bio-imaging offer a bright object to analyse against a dark background, which is easier than a dark object against a light background. In PET a fluorophore has a receptor which quenches its fluorescence. Upon the binding of an analyte the HOMO of the receptor is lowered, which stops this quenching effect, giving a fluorescence turn on, figure 18.

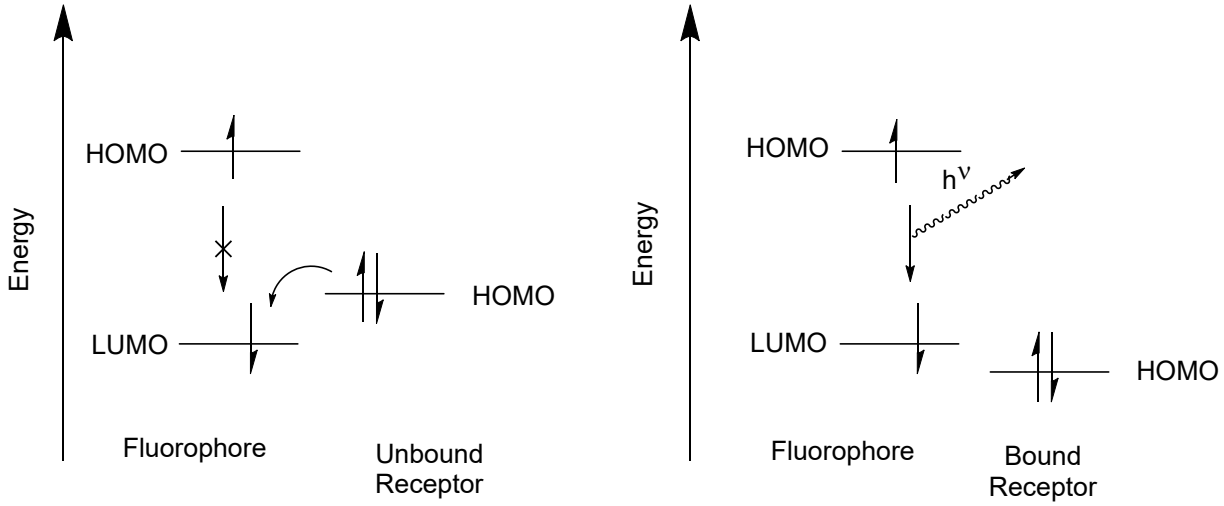

Figure 18 *Left* the quenching of fluorescence by occupation of the fluorophores LUMO with an electron from the receptor. *Right* Electron relaxation from the HOMO to the LUMO of the fluorophore via photon emission. Figure adapted with permission from[108]

On the left of figure 18, there is an electron transfer from the HOMO of the receptor into the LUMO of the fluorophore, as it achieves a lower energy state. This prevents the relaxation of the HOMO into the LUMO or the fluorophore via the emission of a photon. Upon binding to an analyte, the HOMO of the receptor becomes lower in energy than the LUMO of the fluorophore. As a result, it is not energetically favourable for the electron in the HOMO of the receptor to occupy the vacancy in the fluorophore LUMO, allowing the relaxation of the electron from the HOMO to the LUMO of the fluorophore through emission of a photon.[108]

This has been utilised by Burdette *et al.* in the development of a Zn^{2+} sensor. The receptor in this sensor is the pyridine groups, which are able to co-ordinate to the zinc ion, allowing the turn on fluorescence of the reporter, fluorescein, figure 19.[109]

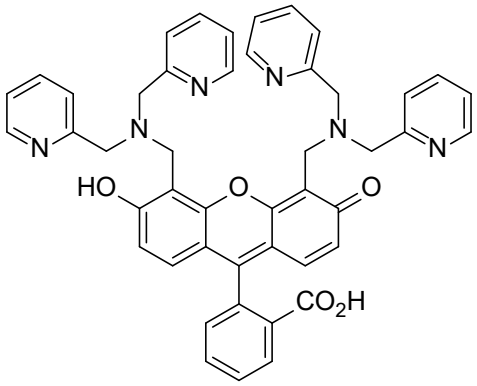

Figure 19 A fluorescent Zn^{2+} sensor synthesised by Burdette *et al.* which uses PET as its fluorescence mechanism

1.9.2.2 Förster Resonance Energy Transfer

FRET requires two molecules of similar excited state energies to be spatially near to each other. One molecule is classed as the donor, the other the acceptor, and the donor transfers energy through a non-radiative process to the acceptor. The donor must have an emission band, and the acceptor an excitation band, that overlap as in figure 20. The energy is transferred from donor to acceptor without the radiation of a photon, and then a photon of the wavelength of the acceptors emission is emitted.[110]

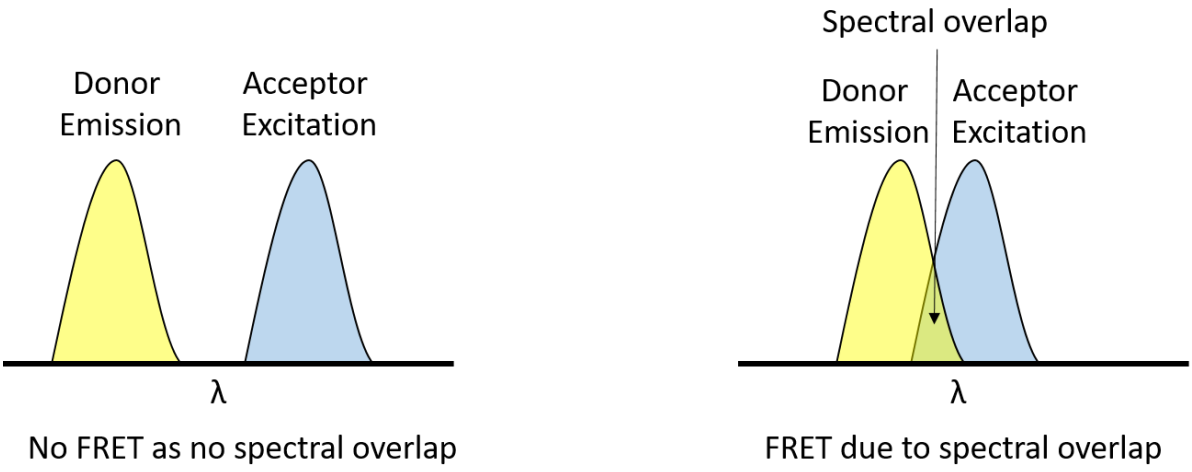

Figure 20 The required overlap of the donor emission and acceptor excitation wavelengths in order to give rise to FRET. Adapted from[111]

The dependence of FRET on the distance between the donor and the acceptor can allow its use in the probing of protein structures, immunoassays and in enzymatic studies. [112-114] If using two distinct dyes (as the process can be done with the same molecules, for example fluorescein), then the process is ratiometric. As one signal decreases, the other increases. The donor signal can be used as an internal calibration when compared to the acceptors emission. This allows more quantitative analysis to be performed.

Zhang *et al.* produced a ratiometric Hg^{2+} sensor utilising a rhodamine derivative (rhodamine B) and BODIPY, figure 21. This offered a large red shifted fluorescence response (100 nm) helped prevent signal interference, and was selective for Hg^{2+} ions vs other common metal ions.[115] The Hg^{2+} ions induced the ring opening shown in figure 21, causing the formation of rhodamine which can act as an energy acceptor. Mercury's toxicity to humans is well known, diagnostic tools such as this sensor can help allow the cellular process by which this damage happens be elucidated.[116]

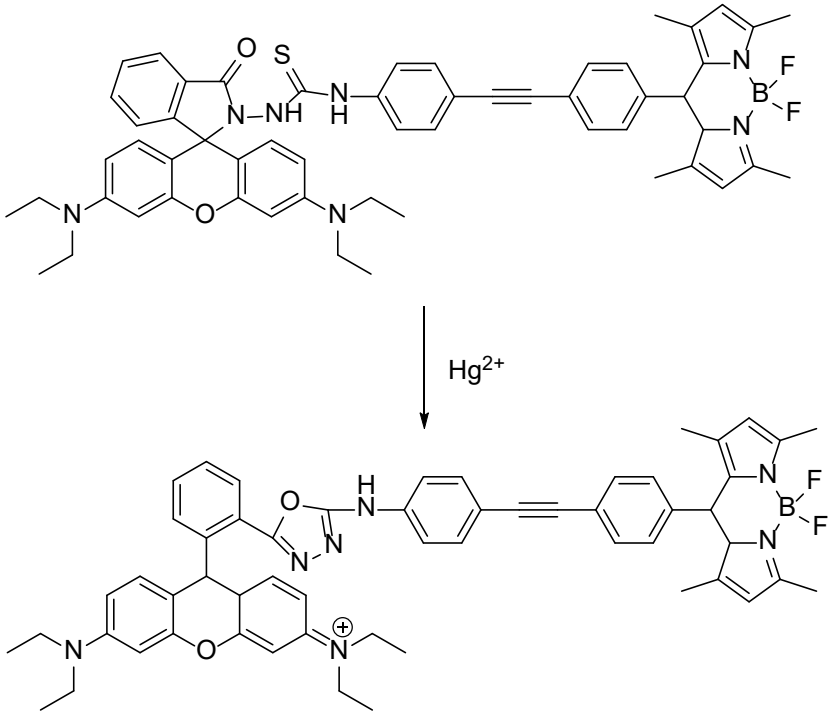

Figure 21 A ratiometric probe for Hg^{2+} utilising a FRET response between a Rhodamine B donor and a BODIPY acceptor

1.9.2.3 Internal Charge Transfer

ICT probes also offer another attractive avenue for the production of ratiometric probes. Within ICT probes there must be an orbital overlap between the receptor and the reporter fluorophore.

There is an electron withdrawing group at one end of the molecule, with an electron donating group at the other; this is often referred to as 'push-pull' system. Upon excitation, there is a dipole formation within the molecule due to the redistribution of electron density. The binding of an analyte to the receptor site shifts the distribution of this electron density, which in turn shifts the excitation and emission wavelengths of the fluorophore. It is this change in fluorescence, rather than a turn on or off response, that often makes these probes ratiometric.

An example of such a system is that developed by Han *et al.* for the visualisation of H_2S within cells dubbed Cy – N_3. H_2S is utilised in a number of processes within cells, but above physiological concentrations can become problematic, contributing diseases such as Alzheimer's.[117] They used a heptamethine cyanine derivatised with an azide, which would react with H_2S forming an amine. This adjusts the electron density within the push pull system in the heptamethine cyanine, figure 22, giving a ratiometric fluorescence change and a blue to green colour change.

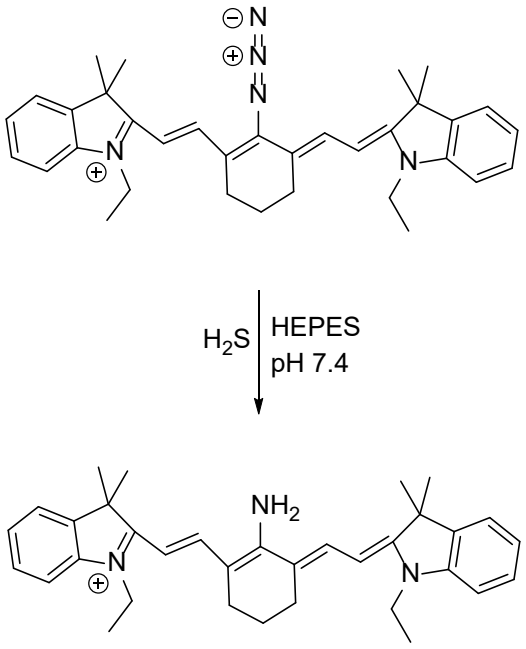

Figure 22 The ICT based H_2S sensor, Cy – N_3 developed by Han *et al.* using heptamethine cyanine.

1.10 Boron Chemistry

All of the novel release systems and hydrogels discussed within this thesis are made possible by the unique chemistry of boron. Boron, the only non-metal group 13 element has a ground state electronic configuration of $1s^2\ 2s^2\ 2p^1$, and as a non-metal forms covalent bonds. The

electronegativity of Boron (χ = 2.0) is comparable to, but crucially lower than, that of both hydrogen and carbon (χ = 2.2 and χ = 2.5 respectively). This means that in organoboron compounds the boron centre will be electron deficient. This boron centre is trivalent and sp^2 hybridised, yielding trigonal planar complexes with an empty P orbital, figure 23.

Figure 23 Common trivalent trigonal planar organo boron compounds include R = H, Me, Et, Cl and Br

This empty p orbital makes the boron centre susceptible to attack from electron rich species. Hard nucleophiles (such as fluoride) add, forming anionic tetrahedral complexes. Lone pairs on Lewis bases (such as pyridine) can also fill the empty p orbital forming dative covalent bonds, yielding neutral tetrahedral complexes, figure 24.

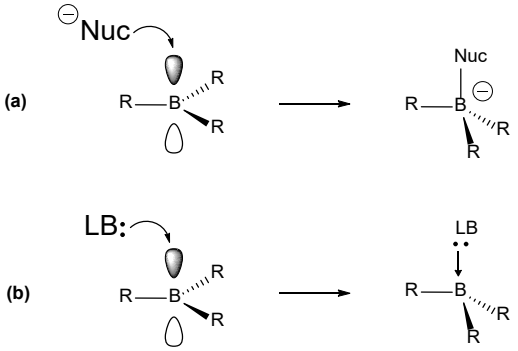

Figure 24 **(a)** Nucleophillic attack on the empty p orbital yielding an sp^3 hybridised anionic tetrahedral boron centre. **(b)** the formation of a dative covalent bond from the lone pairs on a Lewis base to the boron centre yielding a tetrahedral sp^3 complex

1.10.1 Boronic Acids and Esters

Possibly the most widely used organoboron compounds are the boronic acids and esters. These are compounds featuring sp^2 hybridised boron bound to a carbon atom and two oxygen atoms, in the previously shown trigonal planar geometry.[118] They are widely used within synthetic and other chemistries, owing to a combination of their general stability and their properties as a Lewis acid. The Suzuki coupling is a palladium catalysed carbon-carbon bond forming cross coupling reaction, widely utilised in organic synthesis. These reactions require two coupling partners, an aryl halide, as well as an aryl boronic acid. As a result of the huge utility of these reactions, a large number of

boronic acids are now commercially available. The boronic ester equivalents of these compounds are also widely used, as they often offer greater solubility in organic solvents.

1.10.1.1 Boronic Ester Formation

Boronic acids also have a strong and pH dependent affinity for diol containing compounds, forming 5 and 6 membered cyclic ester rings. Studies of these dihydroxyl interactions with boronic acids can be dated to the mid twentieth century with Lorand and Edwards, and have been studied extensively since.[118] The pH dependence of this binding is thought to be due to the steric strain inherent in the trigonal planar complex, binding itself within a 5 membered ring. In more alkaline solutions the hydroxyl anion can bind to the boron centre, changing its hybridisation from sp^2 to sp^3 in order to relieve this strain, yielding a boronate ester, figure 25.

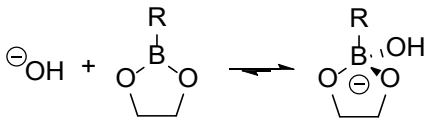

Figure 25 Boronate ester equilibrium with a 1,2 diol bound

The pH at which this occurs is associated to the pKa of the boronic acid. It is at, or above this pKa that the boronate anions are preferentially formed. This pKa can be shifted by using analogous boron containing compounds, such as benzoxaboroles, figure 26.

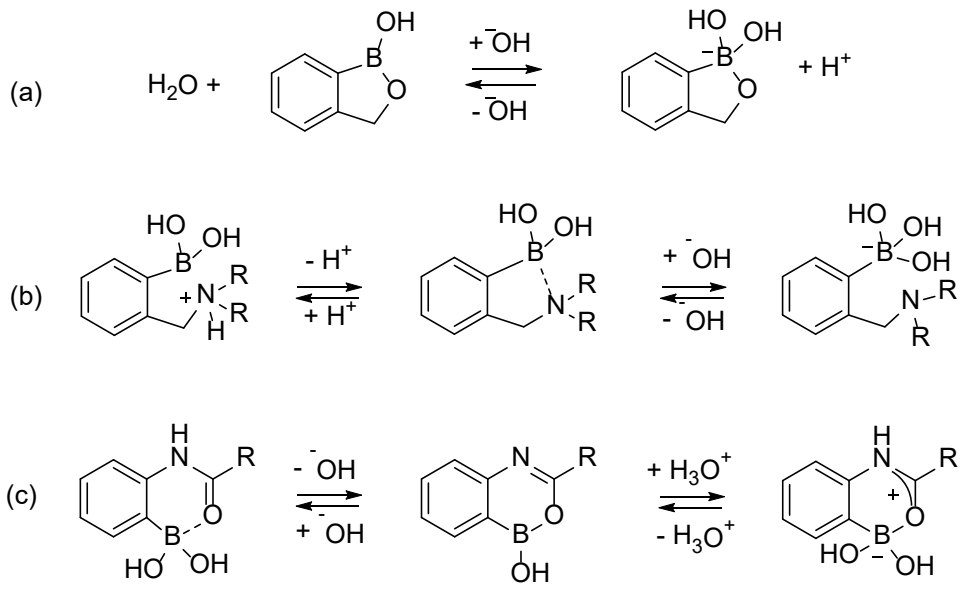

Figure 26 (a) Benzoxaborole and its corresponding boronate anion, (b) Wulff-type boronic acid and its ionisation equilibrium (c) carbonyl co-ordinating boronic acid (adapted from Brooks *et al*.[119])

The pKa of the benzoxaborole compounds is often much lower than that of analogous boronic acids, owing to the ring strain in the heterocycle being released upon the sp^2 to sp^3 transition of the boron centre.[120] Wulff type boronic acids offer a dative bond formation between the lone pair on the nitrogen and the boron, lowering the pKa by increasing the sp^3 nature of the boron centre.[121] Boronic acids with adjacent carbonyls show similar effects, and can facilitate diol binding over an even greater pH range.[122] Alternatively, more simple aryl boronic acids can have their pKa adjusted with electronic effects; compounds featuring electron inductive groups will have an increased pKa, whilst those with electron withdrawing groups will have a decreased pKa.[123] This can be useful for responsive materials dependent on pH.[124]

It is not only the boron substituent that determines the stability of formed esters, but also the interacting diol. When considering the stability of a potential diol complex, geometry is the key characteristic, with cis-diols binding offering the greatest binding affinity as a result of it already being orientated in the conformation required for ester formation. Catechols, (1,2 diols on an aromatic ring), produce the most stable complexes. This is due, not only to their rigid cis diol structures, but also to electronic effects. The inductive nature of the aromatic ring increases the acidity of the diol compared to that of its alkyl alternative.[125]

1.10.2 Applications of Boronic Acids

The reversible covalent bonds seen in these interactions give rise to a number of applications, including sensing, medicine and a number of different smart materials.[126] As carbohydrates are such a biologically relevant class of compounds, the detection and differentiation of monosaccharides is an area that has obtained great interest. This can be achieved using a number of methods with a range of outputs including electrochemical, surface plasmon resonance (spr) and visual (either fluorescent or colour changing).[127-129] For the sake of this thesis only those with optical outputs will be explored in detail.

1.10.2.1 Sugar Sensors

Diabetes mellitus is an incurable disease in which patients are unable to regulate their body's blood glucose levels owing to their inability to produce insulin.[130] Type one diabetes is a genetic disorder whilst type two is an acquired 'life-style disease' associated with lack of exercise and poor diet. There is a rising increase in type two diabetes within the population, with 4.7 million sufferers in 2019. This figure is expected to rise to above 5 million by 2025.[131] Early and rapid diagnosis is important, and as such point-of-care detection devices are of great interest. When haemoglobin in red blood cells comes into contact with glucose in the blood they can covalently bind, forming glycated haemoglobin, haemoglobin A1C (HbA1C). This is representative of ambient blood sugar levels over a number of months, and electrochemical sensors featuring boronic acids have been developed to monitor these.[132] The level of glucose in the blood also must be monitored, and it is in the detection of monosaccharides that boronic acids excel. Selective glucose binding has been achieved with a number of boronic acid containing compounds and a wide array of fluorophores. These include an anthracene based sensor synthesised by James *et al.*, as well as a tetraphenylene ethene (TPE) based sensor developed by Tang *et al.,* figure 27.[133, 134]

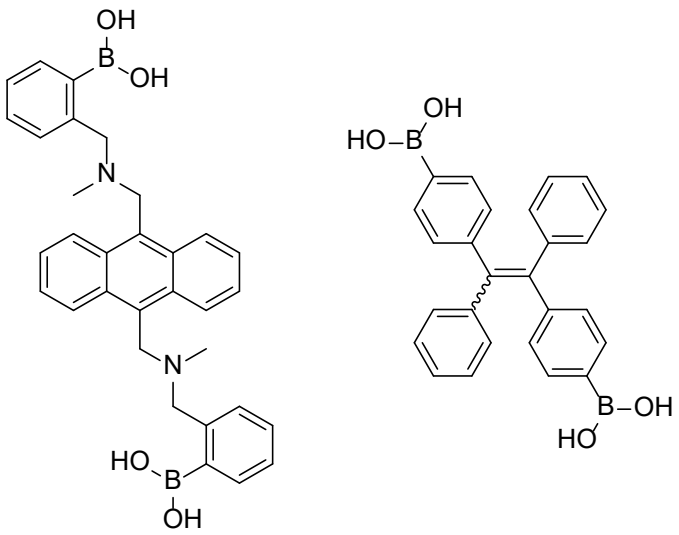

Figure 27 *D*-glucose specific fluorescent turn on sensors based around anthracene (left) and TPE (right)

Self-assembling micelles, based around dimethyl acrylamide and PBA have been developed by Sumerlin *et al.* that are able to collapse at physiologically relevant a pH in response to elevated concentrations of glucose; this offers a promising potential for the release of insulin in response to a diabetes sufferer becoming hyperglycaemic.[135]

1.11 Hydrogels

Hydrogels are three-dimensional, hydrophilic crosslinked polymeric networks. Hydrogels have application spanning a great number of fields including drug delivery, cell culture and sensing.[136-138] These gels can be categorised based on the polymer used within the matrix, as well as their crosslinking methods. The term hydrogel itself is used to describe a range of morphologies, from colloidal suspensions of nano-particles to larger, more rigid structures.[139] The swellability of these materials and their resulting high water contents lends them to being more tissue like, and the ability of molecules to diffuse through this matrix offers an avenue for responsiveness.

Whilst the range of uses of these gels is varied, for the purpose of this work those gels utilised for biological applications will be explored in detail.

1.11.1 Hydrogels Based on Naturally Occurring Polymers

Nature is a source of wide array complex polymers, including but not limited to polypeptides, polysaccharides and polyesters. These polymers are essential to life and have functions varying from the protective shells (chitin, a precursor of chitosan) to the storage of genetic material

(DNA).[140, 141] With the rise in appreciation for the earths limited petro-chemical resources many polymer chemists have turned to such structures to find renewable material sources.

1.11.1.1 Alginate

One such polymer is alginate. Alginate is a biopolymer obtained from seaweed and has found regular use in biomedical applications, particularly in wound healing.[142] Its structure consisists of the sodium salt of repeating units of α-L guluronic acid and β-D mannuronic acid, figure 28.

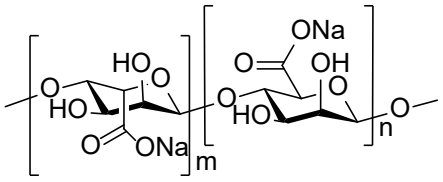

Figure 28 Alginate repeating dimer

Alginate can be crosslinked with divalent cations such as calcium to produce gels over a range of molar mass (32 kDa to 400 kDa), with the molecular weight being a major contributing factor towards its mechanical properties.[143] Shorter gelation times lead to an increase in the order of the crosslinking network, in turn offering greater mechanical stability. The gelation time can be controlled by temperature, hence at lower temperatures the ioninc binding of the divalent cations is much slower, leading to increased order.[144] Alternatively, competitive binding of the cation binding sites with a cationionic buffer solution can also slow the rate of binding.[142] These hydrogels can also be covalently crosslinked with a number of linkers including polyethylene glycol (PEG), owing to the easily accessed functionality present. The different crosslinkers used in this situation can offer different properties depending on the application.[145, 146]

Ionically crosslinked alginate gels are porous, with an average pore size of ~ 5 nm.[147] This allows small molecules to diffuse through them. This is advantageous as most drugs are small molecules. Cerf *et al.* produced Ca^{2+} crosslinked nano-beads with the ability to release theophylline, an adenosine antagonist, in neutral pH.[144]

1.11.1.2 Chitosan

Chitosan is a cationic polysaccharide with repeating units of D-glucosamine and N-acetyl-D-glucosamine figure 29. Chitin is a structural polymer produced by crustaceans in their shells, and as such is the second most abundant biopolymer behind cellulose.[148] It is the deacylation of this natural product, a procedure performed on an industrial scale, that yields chitosan.

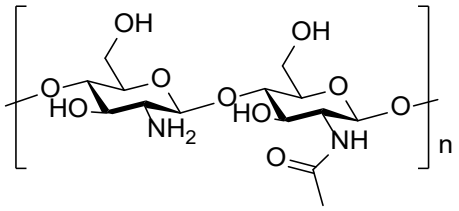

Figure 29 Chitosan

The free amine on the D-glucosamine fragments allows the chitosan to be easily functionalised as well as offering an attractive and reactive binding site for any chemical crosslinkers. Chitosan itself offers antimicrobial properties, however modifications to the structure can begin to introduce properties that make it suitable as a drug delivery vehicle.[149] Modifications to make the polymer more hydrophilic include producing tetra-methyl chitosan, a permanently cationic polymer.[150] This technique was utilised by Jintapattanakit *et al.* for the binding and release of insulin.[151]

1.11.2 Synthetic Polymer Hydrogels

Despite the environmental advantages of having a naturally derived polymer to create the hydrogel, the tailorability of the properties of synthetic polymers often outweighs the environmental factors.

1.11.2.1 Poly(*N*-isoproylacrylamide)

Poly(*N*-isoproylacrylamide) (PNIPAM) is commonly used in responsive hydrogels for biological applications owing to its temperature responsive nature. At low temperatures the amide group, figure 30, is solvated through hydrogen bonding with water, making the polymer soluble. As the temperature increases the amount of hydrogen bonding is lowered, increasing the interactions between the isopropyl groups. This ultimately expels water causing a phase transition and the polymer loses its solubility.[152] Variations in the structure of the polymer, for example branching, can allow for tuning of temperature at which PNIPAM undergoes this transition; .[153]

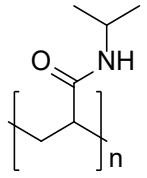

Figure 30 poly(N-Isopropylacrylamide)

PNIPAM has been utilised by Hathaway *et al.* in the release of bacteriophage K. Bacteriophage are viruses that are able to predate on bacteria and have received attention as a potential solution

to the problem of antibiotic resistance. PNIPAM was co-polymerised with allyl amine to produce a material with a trigger point of between 33 and 37 °C, an increase in temperature associated with infection.[154]

1.11.2.2 Poly(vinyl alcohol)

Polyvinyl alcohol (PVA) is a synthetic polymer of repeating diols. It is not directly synthesised via polymerisation of the vinyl alcohol monomer, but is created through the polymerisation and subsequent hydrolysis of poly(vinyl acetate).[155] There exist numerous chemical and physical methods for the crosslinking of PVA. To improve the properties or PVA a number of co-polymers exist, often with saccharides, to improve its hydrophilic character.[156]

1.11.2.3 Chemical Crosslinkers for PVA

The reactivity of the hydroxyl groups on PVA is well documented, and as such a number of bi-functionalised molecules have been used in the crosslinking of such polymers. A commonly used moiety in covalent crosslinking agent are aldehydes, for example glutaraldehyde. These reactions hold the polymer chains together using acetal bonds, figure 31.[157]

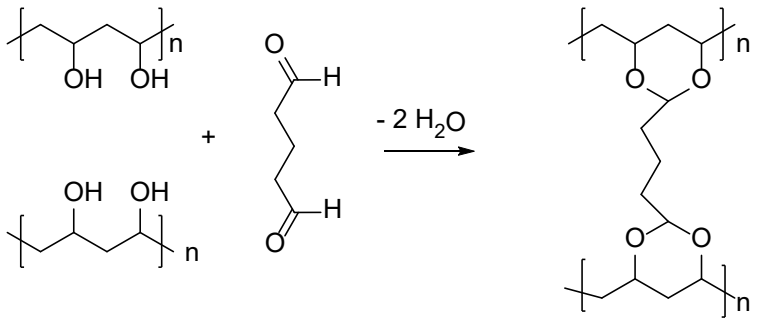

Figure 31 The use of di-aldehyde glutaraldehyde to form acetal bonds with the diols on PVA to crosslink the polymer into a hydrogel

1.11.2.4 Physical Crosslinkers

PVA has found use in a wide array of biomedical applications due to its non-toxic nature. Whilst chemical crosslinking offers an easy avenue to the generation of hydrogels they are often toxic, *i.e.* glutaraldehyde as a result physical crosslinking methods are often preferred for biomedical applications of PVA.

Freeze thawing or cryo-crosslinking is a method of physically crosslinking PVA. In the freezing process, areas of crystallinity are formed within the hydrogel matrix. The number and size of these crystallites determine the mechanical properties of the produced gel, but an increase in the number

of freeze/thaw cycles will increase the mechanical strength of the gel.[158] PVA containing hydrogels prepared in this manner have been utilised in a number of wound dressing and drug delivery systems.[159, 160]

Using such chemistries and techniques as have been discussed throughout this introduction, this thesis will outline attempts that have been made to develop hydrogel systems for the detection of reactive species, and the methods by which these were developed into drug delivery systems.

1.12 Cold Atmospheric Plasma (CAP)

1.12.1 CAP; an Overview

Plasma has a number of forms, the most clinically relevant being cold atmospheric plasma (CAP). Plasma is partially ionised gas containing both charged and non-charged particles including: ions, electrons, photons, atoms and molecules. Thermal plasma features a temperature equilibrium between the heavy particles (*i.e.* atoms and ions) and the lighter particles (*i.e.* electrons), whereas in CAP the lighter particles are at high temperatures, yet the heavy are at room temperature, yielding an overall average temperature of under 40 °C.[161] CAP is generated by passing a high voltage across a flow of gas. This can be achieved with a variety of gases including helium and air, but oxygen, nitrogen air mixes and argon are the most commonly used in clinical settings.[162] There are different forms of plasma generation of which the most frequently used is the di-electric barrier discharge (DBD) system. A DBD system consists of two high voltage electrodes coated in a dielectric material between which gas passes and is ionised. A dielectric material that is an electronic insulator polarisable by the application of an electronic field, between which the gas will pass.[163] One of these electrodes will possess a high voltage, whilst the other is the grounded electrode. Fridman *et al.* have developed a single, or 'floating' electrode. This essentially utilises a second, non-grounded, electrode. As it does not require grounding this electrode can be skin or cell lines, allowing for biological studies to be conducted more easily.[164]

1.12.2 The Biological Effect of CAP

CAP treatment has been shown to induce cell apoptosis, inhibit proliferation in cancer cells and cause bacterial cell death. There have been a number of recent studies seeking to understand these mechanisms.[165] Its efficacy for the prevention of tumour growth was proved *in-vivo* by Tanaka *et al*., where direct plasma treatment of a subcutaneous xenograft tumour in mice was found to

significantly in reduce in size 24 hours after it was treated with plasma for two minutes.[166] It is thought that the overall effect on living tissues is not down to a single factor but is the culmination of a number of elements. The increased concentrations of reactive oxygen and nitrogen species, the toxicity of which have already been discussed, make up a large part of this.[167] DNA damage is one of the main causes of death to the cancer cells, and CAP has been found to be induce double stand breaks (DBS), as well as preventing phosphorylation of p53, an essential gene with many functions towards healthy cancer cell growth.[168] For the inhibition of bacteria it has been shown that gram negative bacteria, in this study *P. aeruginosa,* show an increased membrane permeability following plasma treatment. This not only poses a threat to the cells on their own, but also increases their susceptibility to antibiotics. CAP has also been shown to have the ability to depolarise the bacteria membrane of *S. aureus;* this increases its permeability and changes the cell polarisation though movement of ions, inducing cell death.[169]

The objective of this work is to use boronic acid chemistries in order to combine hydrogels with sensors and antibiotics, yielding novel materials with applications in wound care.

1.13 Bibliography

1. J. F. Guest, N. Ayoub, T. McIlwraith, I. Uchegbu, A. Gerrish, D. Weidlich, K. Vowden and P. Vowden, Bmj Open, 2015, 5, 8.

2. T. Swanson, L. Grothier and G. Schultz, Journal, 2014, https://www.woundsinternational.com/download/resource/6075.

3. V. Jones, J. E. Grey and K. G. Harding, Bmj-British Medical Journal, 2006, 332, 777-780.

4. J. L. Round and S. K. Mazmanian, Nature Reviews Immunology, 2009, 9, 313-323.

5. N. A. Pudlo, K. Urs, S. S. Kumar, J. B. German, D. A. Mills and E. C. Martens, Mbio, 2015, 6, 12.

6. H. C. J. Gram and C. Friedlaender, Ueber die isolirte Färbung der Schizomyceten : in Schnitt-und Trockenpräparaten, Theodor Fischer's medicinischer Buchhandlung, Berlin, 1884.

7. M. J. Wilhelm, J. B. Sheffield, G. M. Sharifian, Y. J. Wu, C. Spahr, G. Gonella, B. L. Xu and H. L. Dai, Acs Chemical Biology, 2015, 10, 1711-1717.

8. W. B. Whitman, D. C. Coleman and W. J. Wiebe, Proceedings of the National Academy of Sciences of the United States of America, 1998, 95, 6578-6583.

9. G. S. Lazarus, D. M. Cooper, D. R. Knighton, D. J. Margolis, R. E. Pecoraro, G. Rodeheaver and M. C. Robson, Archives of Dermatology, 1994, 130, 489-493.

10. T. NT, A. DR, B. JE, B. S, N. J, Y. AE, J. BV and J. AT, ACS Applied materials & interfaces, 2015.

11. E. A. Grice and J. A. Segre, Nature Reviews Microbiology, 2011, 9, 244-253.

12. A. L. Cogen, V. Nizet and R. L. Gallo, British Journal of Dermatology, 2008, 158, 442-455.

13. J. L. Martinez, Frontiers in Microbiology, 2014, 5, 4.

14. R. Edwards and K. G. Harding, Current Opinion in Infectious Diseases, 2004, 17, 91-96.

15. F. Drago, L. Gariazzo, M. Cioni, I. Trave and A. Parodi, European Journal of Dermatology, 2019, 29, 6-13.

16. B. Parrino, D. Schillaci, I. Carnevale, E. Giovannetti, P. Diana, G. Cirrincione and S. Cascioferro, European Journal of Medicinal Chemistry, 2019, 161, 154-178.

17. N. Hoiby, T. Bjarnsholt, M. Givskov, S. Molin and O. Ciofu, International Journal of Antimicrobial Agents, 2010, 35, 322-332.

18. R. M. Donlan, Emerging Infectious Diseases, 2002, 8, 881-890.

19. J. N. Anderl, M. J. Franklin and P. S. Stewart, Antimicrobial Agents and Chemotherapy, 2000, 44, 1818-1824.

20. J. D. Patel, M. Ebert, R. Ward and J. M. Anderson, Journal of Biomedical Materials Research Part A, 2007, 80A, 742-751.

21. K. L. Frank, E. J. Reichert, K. E. Piper and R. Patel, Antimicrobial Agents and Chemotherapy, 2007, 51, 888-895.

22. A. J. Brady, G. Laverty, D. F. Gilpin, P. Kearney and M. Tunney, Journal of Medical Microbiology, 2017, 66, 461-469.

23. J. W. Costerton, P. S. Stewart and E. P. Greenberg, Science, 1999, 284, 1318-1322.

24. N. C. Caiazza and G. A. O'Toole, Journal of Bacteriology, 2004, 186, 4476-4485.

25. K. A. McDonough and A. Rodriguez, Nature Reviews Microbiology, 2012, 10, 27-38.

26. L. Hall-Stoodley, J. W. Costerton and P. Stoodley, Nature Reviews Microbiology, 2004, 2, 95-108.

27. K. Drescher, C. D. Nadell, H. A. Stone, N. S. Wingreen and B. L. Bassler, Current Biology, 2014, 24, 50-55.

28. D. McDougald, S. A. Rice, N. Barraud, P. D. Steinberg and S. Kjelleberg, Nature Reviews Microbiology, 2012, 10, 39-50.

29. M. Toyofuku, T. Inaba, T. Kiyokawa, N. Obana, Y. Yawata and N. Nomura, Bioscience Biotechnology and Biochemistry, 2016, 80, 7-12.

30. C. M. Waters and B. L. Bassler, in Annual Review of Cell and Developmental Biology, Annual Reviews, Palo Alto, 2005, vol. 21, pp. 319-346.

31. S. Swift, J. P. Throup, P. Williams, G. P. C. Salmond and G. Stewart, Trends in Biochemical Sciences, 1996, 21, 214-219.

32. M. Hentzer, H. Wu, J. B. Andersen, K. Riedel, T. B. Rasmussen, N. Bagge, N. Kumar, M. A. Schembri, Z. J. Song, P. Kristoffersen, M. Manefield, J. W. Costerton, S. Molin, L. Eberl, P. Steinberg, S. Kjelleberg, N. Hoiby and M. Givskov, Embo Journal, 2003, 22, 3803-3815.

33. L. Clinton and T. Carter, Labmedicine, 2015, 46, 277-284.

34. I. Lebrun, R. Marques-Porto, A. S. Pereira, A. Pereira and E. A. Perpetuo, Mini-Reviews in Medicinal Chemistry, 2009, 9, 820-828.

35. S. M. McCarty, C. A. Cochrane, P. D. Clegg and S. L. Percival, Wound Repair and Regeneration, 2012, 20, 125-136.

36. M. M. Dinges, P. M. Orwin and P. M. Schlievert, Clinical Microbiology Reviews, 2000, 13, 16-+.

37. W. H. Organization, Journal, 2019.

38. E. M. Trecarichi and M. Tumbarello, Current Opinion in Infectious Diseases, 2014, 27, 200-210.

39. J. Z. Lin, D. J. Zhou, T. A. Steitz, Y. S. Polikanov and M. G. Gagnon, in Annual Review of Biochemistry, Vol 87, ed. R. D. Kornberg, Annual Reviews, Palo Alto, 2018, vol. 87, pp. 451-478.

40. D. J. Waxman and J. L. Strominger, Annual Review of Biochemistry, 1983, 52, 825-869.

41. M. Lebel, R. P. Rapp, G. E. Stein, S. L. Barriere and G. L. Drusano, Pharmacotherapy, 1988, 8, 3-33.

42. M. J. Osborn, Annual Review of Biochemistry, 1969, 38, 501-+.

43. Z. Z. Yao, D. Kahne and R. Kishony, Molecular Cell, 2012, 48, 705-712.

44. A. Mai-Prochnow, M. Clauson, J. M. Hong and A. B. Murphy, Scientific Reports, 2016, 6, 11.

45. L. B. Barradell and H. M. Bryson, Drugs, 1994, 47, 471-505.

46. K. Kariyone, H. Harada, M. Kurita and T. Takano, Journal of Antibiotics, 1970, 23, 131-&.

47. H. R. Onishi, D. R. Daoust, S. B. Zimmerman, D. Hendlin and E. O. Stapley, Antimicrobial Agents and Chemotherapy, 1974, 5, 38-48.

48. J. M. T. Hamiltonmiller, W. Brumfitt and A. V. Reynolds, Journal of Antimicrobial Chemotherapy, 1978, 4, 437-444.

49. K. M. Papp-Wallace, A. Endimiani, M. A. Taracila and R. A. Bonomo, Antimicrobial Agents and Chemotherapy, 2011, 55, 4943-4960.

50. D. L. Paterson, Clinical Microbiology and Infection, 2000, 6, 460-463.

51. F. M. Kahan, H. Kropp, J. G. Sundelof and J. Birnbaum, Journal of Antimicrobial Chemotherapy, 1983, 12, 1-35.

52. M. A. Cooper and D. H. Williams, Chemistry & Biology, 1999, 6, 891-899.

53. T. L. Smith, M. L. Pearson, K. R. Wilcox, C. Cruz, M. V. Lancaster, B. Robinson-Dunn, F. C. Tenover, M. J. Zervos, J. D. Band, E. White, W. R. Jarvis and S. Glycopeptide Intermediate, New England Journal of Medicine, 1999, 340, 493-501.

54. M. A. T. Blaskovich, K. A. Hansford, M. S. Butler, Z. G. Jia, A. E. Mark and M. A. Cooper, Acs Infectious Diseases, 2018, 4, 715-735.

55. D. N. Wilson, Nature Reviews Microbiology, 2014, 12, 35-48.

56. J. Poehlsgaard and S. Douthwaite, Nature Reviews Microbiology, 2005, 3, 870-881.

57. A. Forge and J. Schacht, Audiology and Neuro-Otology, 2000, 5, 3-22.

58. S. B. Vakulenko and S. Mobashery, Clinical Microbiology Reviews, 2003, 16, 430-+.

59. A. Lefort, M. Arthur, L. Garry, C. Carbon, P. Courvalin and B. Fantin, Antimicrobial Agents and Chemotherapy, 2000, 44, 2077-2080.

60. I. Chopra and M. Roberts, Microbiology and Molecular Biology Reviews, 2001, 65, 232-+.

61. M. L. Nelson and S. B. Levy, in Antimicrobial Therapeutics Reviews: Antibiotics That Target the Ribosome, ed. K. Bush, Blackwell Science Publ, Oxford, 2011, vol. 1241, pp. 17-32.

62. F. Nguyen, A. L. Starosta, S. Arenz, D. Sohmen, A. Donhofer and D. N. Wilson, Biological Chemistry, 2014, 395, 559-575.

63. M. I. Andersson and A. P. MacGowan, Journal of Antimicrobial Chemotherapy, 2003, 51, 1-11.

64. A. L. Barry, R. N. Jones, C. Thornsberry, L. W. Ayers, E. H. Gerlach and H. M. Sommers, Antimicrobial Agents and Chemotherapy, 1984, 25, 633-637.

65. P. C. Appelbaum and P. A. Hunter, International Journal of Antimicrobial Agents, 2000, 16, 5-15.

66. C. M. Morel and E. Mossialos, BMJ, 2010, 340, c2115.

67. S. A. McEwen, Animal Biotechnology, 2006, 17, 239-250.

68. A. Alevizos, D. Perimeni, G. Larios, C. Mihas, D. Fanou, M. Papathanasiou, K. Trifynopoulou, K. Stamatiou, K. Kintzoglanakis and A. Mariolis, International Journal of Antimicrobial Agents, 2007, 29, S646-S646.

69. M. J. Llewelyn, J. M. Fitzpatrick, E. Darwin, S. Tonkin-Crine, C. Gorton, J. Paul, T. E. A. Peto, L. Yardley, S. Hopkins and A. S. Walker, Bmj-British Medical Journal, 2017, 358, 5.

70. G. Cox and G. D. Wright, International Journal of Medical Microbiology, 2013, 303, 287-292.

71. A. C. Pawlowski, W. L. Wang, K. Koteva, H. A. Barton, A. G. McArthur and G. D. Wright, Nature Communications, 2016, 7, 10.

72. L. J. V. Piddock, Nature Reviews Microbiology, 2006, 4, 629-636.

73. P. Blanco, S. Hernando-Amado, J. A. Reales-Calderon, F. Corona, F. Lira, M. Alcalde-Rico, A. Bernardini, M. B. Sanchez and J. L. Martinez, Microorganisms, 2016, 4, 19.

74. J. A. Delmar, C. C. Su and E. W. Yu, in Annual Review of Biophysics, Vol 43, ed. K. A. Dill, Annual Reviews, Palo Alto, 2014, vol. 43, pp. 93-117.

75. W. K. Jung, H. C. Koo, K. W. Kim, S. Shin, S. H. Kim and Y. H. Park, Applied and Environmental Microbiology, 2008, 74, 2171-2178.

76. P. K. Lindgren, A. Karlsson and D. Hughes, Antimicrobial Agents and Chemotherapy, 2003, 47, 3222-3232.

77. I. Rychlik, D. Gregorova and H. Hradecka, Veterinary Microbiology, 2006, 112, 1-10.

78. H. Ochman, J. G. Lawrence and E. A. Groisman, Nature, 2000, 405, 299-304.

79. C. M. Thomas and K. M. Nielsen, Nature Reviews Microbiology, 2005, 3, 711-721.

80. H. C. Flemming and J. Wingender, Nature Reviews Microbiology, 2010, 8, 623-633.

81. J. Davison, Plasmid, 1999, 42, 73-91.

82. M. Merabishvili, J. P. Pirnay, G. Verbeken, N. Chanishvili, M. Tediashvili, N. Lashkhi, T. Glonti, V. Krylov, J. Mast, L. Van Parys, R. Lavigne, G. Volckaert, W. Mattheus, G. Verween, P. De Corte, T. Rose, S. Jennes, M. Zizi, D. De Vos and M. Vaneechoutte, Plos One, 2009, 4, 10.

83. B. Koskella and S. Meaden, Viruses-Basel, 2013, 5, 806-823.

84. J. R. Huddleston, Infection and Drug Resistance, 2014, 7, 167-176.

85. C. Howard-Varona, K. R. Hargreaves, S. T. Abedon and M. B. Sullivan, Isme Journal, 2017, 11, 1511-1520.

86. I. Chen, P. J. Christie and D. Dubnau, Science, 2005, 310, 1456-1460.

87. R. Jayaraman, Current Science, 2010, 99, 1008-1010.

88. D. M. Livermore, Clinical Microbiology Reviews, 1995, 8, 557-&.

89. J. Lamottebrasseur, G. Dive, O. Dideberg, P. Charlier, J. M. Frere and J. M. Ghuysen, Biochemical Journal, 1991, 279, 213-221.

90. F. Sanz-Garcia, E. Anoz-Carbonell, E. Perez-Herran, C. Martin, A. Lucia, L. Rodrigues and J. A. Ainsa, Frontiers in Microbiology, 2019, 10, 11.

91. L. C. Sands and W. V. Shaw, Antimicrobial Agents and Chemotherapy, 1973, 3, 299-305.

92. J. M. Munita and C. A. Arias, Microbiology spectrum, 2016, 4, 10.1128/microbiolspec.VMBF-0016-2015.

93. A. M. Smith, C. Feldman, O. Massidda, K. McCarthy, D. Ndiweni and K. P. Klugman, Antimicrobial Agents and Chemotherapy, 2005, 49, 2002-2007.

94. T. J. Foster, Fems Microbiology Reviews, 2017, 41, 430-449.

95. B. Weisblum, Antimicrobial Agents and Chemotherapy, 1995, 39, 577-585.

96. NICE, Antimicrobial stewardship: systems and processes for effective antimicrobial medicine use, 2015.

97. D. W. Bratzler, P. M. Houck and G. Surg Infect Prevention, Clinical Infectious Diseases, 2004, 38, 1706-1715.

98. M. Hentzer, K. Riedel, T. B. Rasmussen, A. Heydorn, J. B. Andersen, M. R. Parsek, S. A. Rice, L. Eberl, S. Molin, N. Hoiby, S. Kjelleberg and M. Givskov, Microbiology-Sgm, 2002, 148, 87-102.

99. H. D. Li, X. Y. Li, Z. L. Wang, Y. K. Fu, Q. Ai, Y. Dong and J. L. Yu, Bmc Microbiology, 2015, 15, 8.

100. B. Tettmann, C. Niewerth, F. Kirschhofer, A. Neidig, A. Dotsch, G. Brenner-Weiss, S. Fetzner and J. Overhage, Frontiers in Microbiology, 2016, 7, 11.

101. Y. B. Li, J. Liu, Z. X. Huang, J. H. Yu, X. F. Xu, P. H. Sun, J. Lin and W. M. Chen, European Journal of Medicinal Chemistry, 2018, 158, 753-766.

102. T. Bottcher, I. Kolodkin-Gal, R. Kolter, R. Losick and J. Clardy, Journal of the American Chemical Society, 2013, 135, 2927-2930.

103. J. R. Lakowicz, Principles of Fluorescence Spectroscopy, New York, NY : Springer US : Imprint: Springer, New York, NY, 3rd ed. edn., 2006.

104. K. Kaur, R. Saini, A. Kumar, V. Luxami, N. Kaur, P. Singh and S. Kumar, Coordination Chemistry Reviews, 2012, 256, 1992-2028.

105. X. Qi, E. J. Jun, L. Xu, S. J. Kim, J. S. J. Hong, Y. J. Yoon and J. Y. Yoon, Journal of Organic Chemistry, 2006, 71, 2881-2884.

106. D. de la Fuente-Herreruela, V. Gonzalez-Charro, V. G. Almendro-Vedia, M. Moran, M. A. Martin, M. P. Lillo, P. Natale and I. Lopez-Montero, Biochimica Et Biophysica Acta-Bioenergetics, 2017, 1858, 999-1006.

107. H. Y. Liu, M. Zhao, Q. L. Qiao, H. J. Lang, J. Z. Xu and Z. C. Xu, Chinese Chemical Letters, 2014, 25, 1060-1064.

108. A. P. de Silva, H. Q. N. Gunaratne, T. Gunnlaugsson, A. J. M. Huxley, C. P. McCoy, J. T. Rademacher and T. E. Rice, Chemical Reviews, 1997, 97, 1515-1566.

109. S. C. Burdette, G. K. Walkup, B. Spingler, R. Y. Tsien and S. J. Lippard, Journal of the American Chemical Society, 2001, 123, 7831-7841.

110. R. P. Haugland, J. Gregory, M. T. Z. Spence and I. D. Johnson, Handbook of fluorescent probes and research products, Molecular Probes, 2002.

111. J. A. Broussard, B. Rappaz, D. J. Webb and C. M. Brown, Nature Protocols, 2013, 8, 265-281.

112. M. Dimura, T. O. Peulen, C. A. Hanke, A. Prakash, H. Gohlke and C. A. M. Seidel, Current Opinion in Structural Biology, 2016, 40, 163-185.

113. B. Y. Wu and X. P. Yan, Chemical Communications, 2015, 51, 3903-3906.

114. Z. H. Mohamed, C. Rhein, E. M. Saied, J. Kornhuber and C. Arenz, Chemistry and Physics of Lipids, 2018, 216, 152-161.

115. X. L. Zhang, Y. Xiao and X. H. Qian, Angewandte Chemie-International Edition, 2008, 47, 8025-8029.

116. M. Valko, H. Morris and M. T. D. Cronin, Current Medicinal Chemistry, 2005, 12, 1161-1208.

117. F. B. A. Yu, P. Li, P. Song, B. S. Wang, J. Z. Zhao and K. L. Han, Chemical Communications, 2012, 48, 2852-2854.

118. J. P. Lorand and J. O. Edwards, Journal of Organic Chemistry, 1959, 24, 769-774.

119. W. L. A. Brooks and B. S. Sumerlin, Chemical Reviews, 2016, 116, 1375-1397.

120. A. Adamczyk-Wozniak, M. K. Cyranski, A. Zubrowska and A. Sporzynski, Journal of Organometallic Chemistry, 2009, 694, 3533-3541.

121. S. L. Wiskur, J. J. Lavigne, H. Ait-Haddou, V. Lynch, Y. H. Chiu, J. W. Canary and E. V. Anslyn, Organic Letters, 2001, 3, 1311-1314.

122. K. L. Bhat, N. J. Howard, H. Rostami, J. H. Lai and C. W. Bock, Journal of Molecular Structure-Theochem, 2005, 723, 147-157.

123. M. A. Martinez-Aguirre, R. Villamil-Ramos, J. A. Guerrero-Alvarez and A. K. Yatsimirsky, Journal of Organic Chemistry, 2013, 78, 4674-4684.

124. A. Mahalingam, J. I. Jay, K. Langheinrich, S. Shukair, M. D. McRaven, L. C. Rohan, B. C. Herold, T. J. Hope and P. F. Kiser, Biomaterials, 2011, 32, 8343-8355.

125. C. Bromba, P. Carrie, J. K. W. Chui and T. M. Fyles, Supramolecular Chemistry, 2009, 21, 81-88.

126. R. Nishiyabu, Y. Kubo, T. D. James and J. S. Fossey, Chemical Communications, 2011, 47, 1106-1123.

127. A. Kikuchi, K. Suzuki, O. Okabayashi, H. Hoshino, K. Kataoka, Y. Sakurai and T. Okano, Analytical Chemistry, 1996, 68, 823-828.

128. R. Gabai, N. Sallacan, V. Chegel, T. Bourenko, E. Katz and I. Willner, Journal of Physical Chemistry B, 2001, 105, 8196-8202.

129. D. Bruen, C. Delaney, L. Florea and D. Diamond, Sensors, 2017, 17, 21.

130. J. R. Gavin, K. Alberti, M. B. Davidson, R. A. DeFronzo, A. Drash, S. G. Gabbe, S. Genuth, M. I. Harris, R. Kahn, H. Keen, W. C. Knowler, H. Lebovitz, N. K. Maclaren, J. P. Palmer, P. Raskin, R. A. Rizza, M. P. Stern and D. Expert Comm Diag Classification, Diabetes Care, 1999, 22, S5-S19.

131. D. UK, Us, diabetes and a lot of facts and stats, (accessed 18/07/19, 2019).

132. J. Anzai, Materials Science & Engineering C-Materials for Biological Applications, 2016, 67, 737-746.

133. T. D. James, K. Sandanayake and S. Shinkai, Angewandte Chemie-International Edition in English, 1994, 33, 2207-2209.

134. B. W. Liu, N. Novikova, M. C. Simpson, M. S. M. Timmer, B. L. Stocker, T. Sohnel, D. C. Ware and P. J. Brothers, Organic & Biomolecular Chemistry, 2016, 14, 5205-5209.

135. D. Roy and B. S. Sumerlin, Acs Macro Letters, 2012, 1, 529-532.

136. A. S. Hoffman, Advanced Drug Delivery Reviews, 2002, 54, 3-12.

137. Y. Qiu and K. Park, Advanced Drug Delivery Reviews, 2001, 53, 321-339.

138. D. Buenger, F. Topuz and J. Groll, Progress in Polymer Science, 2012, 37, 1678-1719.

139. H. Kawaguchi, Progress in Polymer Science, 2000, 25, 1171-1210.

140. J. G. Fernandez and D. E. Ingber, Macromolecular Materials and Engineering, 2014, 299, 932-938.

141. J. Y. Cherng, Journal of Pharmacy and Pharmaceutical Sciences, 2009, 12, 346-356.

142. K. Y. Lee and D. J. Mooney, Progress in Polymer Science, 2012, 37, 106-126.

143. M. George and T. E. Abraham, Journal of Controlled Release, 2006, 114, 1-14.

144. J. L. Drury, R. G. Dennis and D. J. Mooney, Biomaterials, 2004, 25, 3187-3199.

145. X. H. Zhao, N. Huebsch, D. J. Mooney and Z. G. Suo, Journal of Applied Physics, 2010, 107, 5.

146. P. Eiselt, K. Y. Lee and D. J. Mooney, Macromolecules, 1999, 32, 5561-5566.

147. T. Boontheekul, H. J. Kong and D. J. Mooney, Biomaterials, 2005, 26, 2455-2465.

148. R. Hejazi and M. Amiji, Journal of Controlled Release, 2003, 89, 151-165.

149. C. Q. Qin, H. R. Li, Q. Xiao, Y. Liu, J. C. Zhu and Y. M. Du, Carbohydrate Polymers, 2006, 63, 367-374.

150. P. Ledung, M. Milas, M. Rinaudo and J. Desbrieres, Carbohydrate Polymers, 1994, 24, 209-214.

151. A. Jintapattanakit, V. B. Junyaprasert and T. Kissel, Journal of Pharmaceutical Sciences, 2009, 98, 4818-4830.

152. M. A. Haq, Y. L. Su and D. J. Wang, Materials Science & Engineering C-Materials for Biological Applications, 2017, 70, 842-855.

153. A. P. Vogt and B. S. Sumerlin, Macromolecules, 2008, 41, 7368-7373.

154. H. Hathaway, D. R. Alves, J. Bean, P. P. Esteban, K. Ouadi, J. M. Sutton and A. T. A. Jenkins, European Journal of Pharmaceutics and Biopharmaceutics, 2015, 96, 437-441.

155. L. S. Peixoto, F. M. Silva, M. A. L. Niemeyer, G. Espinosa, P. A. Melo, M. Nele and J. C. Pinto, 2006, 243, 190-199.

156. S. Tripathi, G. K. Mehrotra and P. K. Dutta, International Journal of Biological Macromolecules, 2009, 45, 372-376.

157. K. C. S. Figueiredo, T. L. M. Alves and C. P. Borges, Journal of Applied Polymer Science, 2009, 111, 3074-3080.

158. C. M. Hassan and N. A. Peppas, Macromolecules, 2000, 33, 2472-2479.

159. J. H. Sung, M. R. Hwang, J. O. Kim, J. H. Lee, Y. Il Kim, J. H. Kim, S. W. Chang, S. G. Jin, J. A. Kim, W. S. Lyoo, S. S. Han, S. K. Ku, C. S. Yong and H. G. Choi, International Journal of Pharmaceutics, 2010, 392, 232-240.

160. X. M. Yang, Q. Liu, X. L. Chen, F. Yu and Z. Y. Zhu, Carbohydrate Polymers, 2008, 73, 401-408.

161. C. Hoffmann, C. Berganza and J. Zhang, Medical Gas Research, 2013, 3, 15.

162. G. Isbary, T. Shimizu, Y. F. Li, W. Stolz, H. M. Thomas, G. E. Morfill and J. L. Zimmermann, Expert Review of Medical Devices, 2013, 10, 367-377.

163. K. D. Weltmann and T. von Woedtke, Plasma Physics and Controlled Fusion, 2017, 59, 11.

164. A. Fridman, A. Chirokov and A. Gutsol, Journal of Physics D-Applied Physics, 2005, 38, R1-R24.

165. D. Y. Yan, J. H. Sherman and M. Keidar, Oncotarget, 2017, 8, 15977-15995.

166. H. Tanaka, M. Mizuno, K. Ishikawa, K. Takeda, K. Nakamura, F. Utsumi, H. Kajiyama, H. Kano, Y. Okazaki, S. Toyokuni, S. Maruyama, F. Kikkawa and M. Hori, Ieee Transactions on Plasma Science, 2014, 42, 3760-3764.

167. D. Y. Yan, A. Talbot, N. Nourmohammadi, J. H. Sherman, X. Q. Cheng and M. Keidar, Biointerphases, 2015, 10, 13.

168. M. Weiss, D. Gumbel, E. M. Hanschmann, R. Mandelkow, N. Gelbrich, U. Zimmermann, R. Walther, A. Ekkernkamp, A. Sckell, A. Kramer, M. Burchardt, C. H. Lillig and M. B. Stope, Plos One, 2015, 10, 17.

169. P. Brun, G. Bernabe, C. Marchiori, M. Scarpa, M. Zuin, R. Cavazzana, B. Zaniol and E. Martines, Journal of Applied Microbiology, 2018, 125, 398-408.

2 Boron Containing Polyacrylamide Hydrogels

2.1 Introduction

2.1.1 Boronic Acid and Boronic Ester Soft Materials

Boronic acid containing hydrogels combine the previously discussed reactivity of boronic acids with a biocompatible, hydrophilic matrix, capable of being formed into a variety of macrostructures. These boronic acid macromolecules have been effective in sensors, nano-materials, and in the delivery of insulin and other therapeutics.[1] Whilst many polymeric systems for topical drug delivery tend to be plastic and rigid in their mechanical properties, the dynamic nature of the boronic ester bonds offers a route to the development of more ductile and responsive materials. In many cases these materials exhibit interesting properties, such as being self-healing (the ability to be cut, and be reformed without external influence).[2, 3] Whilst for structural implants such as bone supports, rigidity is of the utmost importance,[4] for medical devices such as wound dressings, less stiff materials can be advantageous.[5] Boronic ester soft materials tend to offer much greater biocompatibility, as well as being able to act as a reservoir for drug release, an ability utilised heavily in the delivery of contraceptive drugs.[6]

Of the number of forms of boronic esters possible, the most widely used in such materials is phenyl boronic acid (PBA). This is due to its availability, stability and well-documented reactivity. The incorporation of PBA moieties into polymeric systems can be achieved in numerous ways, figure 1. Existing polymers containing pendant groups that offer reactivity, including polyesters and amides, can have PBA groups coupled to them using the wide range of available coupling chemistries available. Commonly used coupling methods include carbodiimide (CDI) and EDC/NHS couplings. Chen *et al.* used such chemistry to functionalise hyaluronic acid with either maltose or PBA, to produce a dynamic covalently crosslinked hydrogel of hyaluronic acid. Hyaluronic acid is ubiquitous within tissues and as such is highly biocompatible, offering a glucose responsive polymer with potential biomedical application in drug release or sensing.[7]

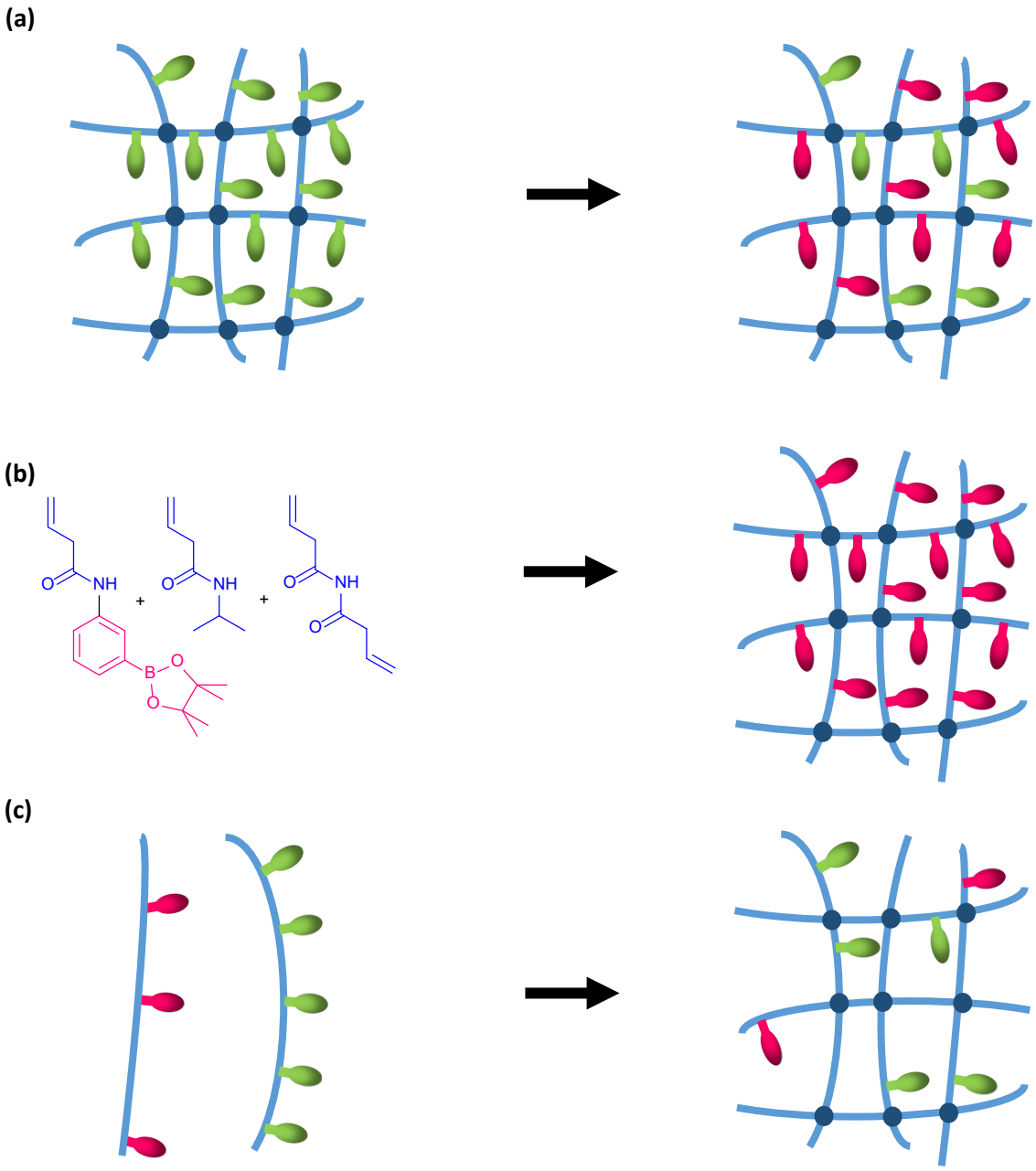

Figure 1 Different ways of forming boronic acid functionalised polymers; **(a)** Formation of a PBA functionalised polymer by reacting pendant groups with a PBA containing compound, **(b)** PBA functionalised polymer synthesis using a PBA containing monomer, **(c)** crosslinking of a PBA containing polymer chain and a diol containing polymer chain. Adapted with permission from [8] Green ovals represent pendant reactive groups. Pink ovals represent phenyl boronic acids units. Blue lines represent polymer chains.

2.1.2 Dye Displacement Assay Saccharide Detector

Alternatively, a monomer can be synthesised containing PBA, which can then be polymerised forming polymeric chains featuring the boronic acid reactivity, which are then able to be crosslinked forming hydrogels. Utilising a similarly created hydrogel and the chromophore Alizarin Red S (ARS), Lampard *et al.* developed a hydrogel saccharide sensor.[9] ARS is a deep red colour, appendix 7.2.1 and features a 1,2 diol in the form of a catechol, thus can form boronic esters. Upon binding, ARS exhibits a clear colour change from red to orange. Performing conventional UV-vis experiments on gels is difficult, owing to the light scattering nature of different gel morphologies. To navigate this issue, the gel was placed in solutions of different concentrations of glucose, fructose, mannose and galactose. The competitive binding of the sugars displaced the bound ARS, reverting its colour from orange back to red. The released ARS then dissolved in the surrounding solution, which was subsequently and UV-vis spectroscopy was performed on this solution at the absorbance max (513 nm) allowing the concentration of free ARS to be determined. From this, the concentration of saccharide bound could be back calculated.

The different forms of boronic esters have different affinities for certain compounds. As such Lampard *et al.* produced not only the PBA containing hydrogel but also a benzoxaborole (BOB) containing gel.[9] The analogous monomer was synthesised as per figure 2.

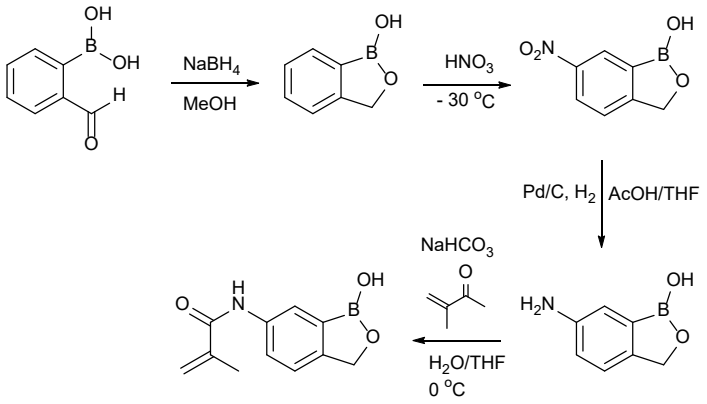

Figure 2 The overall synthetic route towards the BOB acrylamide monomer

The gels were synthesised utilising radical initiated polymerisation (mechanism in appendix 2.1), yielding hydrogels containing water (60% w/w), acrylamide (38% w/w), methylene bisacrylamide (1% w/w) and the boronic acid containing monomer (1% w/w). The gels used as controls, the 'blank' gels, contained 39 % w/w acrylamide. To maintain a constant gel size the activated

monomer solution was taken into a 3 mL syringe. Upon polymerisation and gel formation, the end of the syringe was cut off, allowing a cylinder to be formed with consistent volumes. These boron containing gels were found to be able to bind to ARS as shown in figure 3.

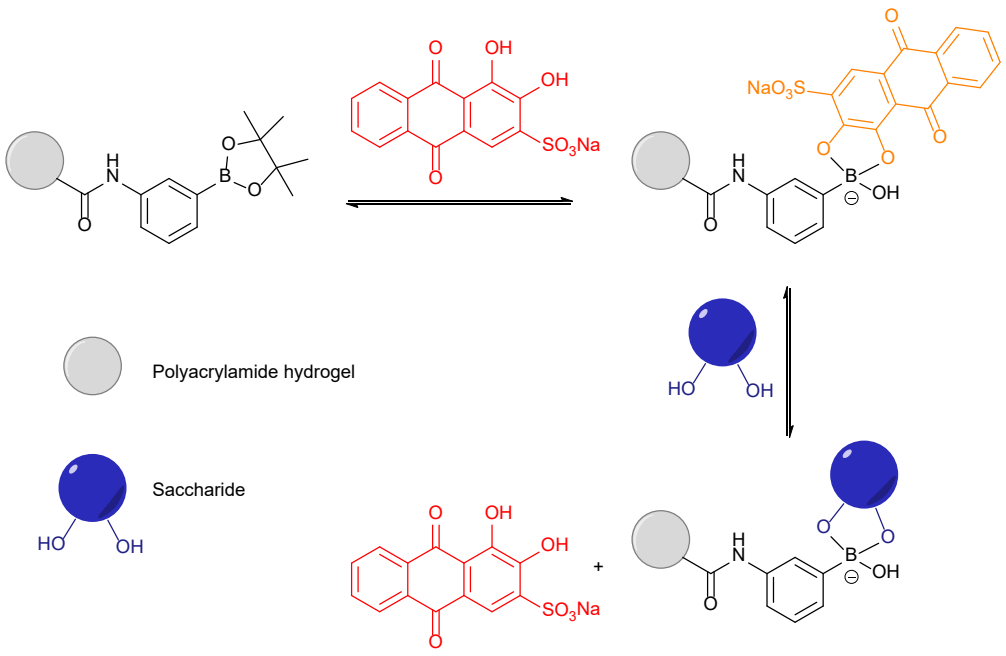

Figure 3 Displacement of ARS from PBA containing hydrogel matric due to competitive binding of saccharide

As the above figure shows, there is an equilibrium reached between saccharide and unbound ARS. To observe the difference in binding between the BOB and PBA gels, a cylinder of each gel was loaded with ARS. Upon placing these gels into a solution of saccharide, the increase in concentration of ARS was measured.

The ARS concentration was measured via its absorbance and the results for each saccharide were compared in the table below, table 1. It is important to note here that for each of the monomeric sugars the BOB containing gels showed a greater displacement of ARS, and thus binding to the sugars.

Table 1 The amount of ARS released from each boronic ester functionalised polyacrylamide gel as abs g^{-1} at 513 nm^{-1}.Reporduced with permission from [9]

	FRUCTOSE	GALACTOSE	MANNOSE	GLUCOSE
BOB	0.94	0.53	0.59	0.53
PBA	0.82	0.40	0.41	0.34
BLANK	0.23	0.21	0.22	0.19

2.1.3 Biofilm Inhibitors

Small chemical biofilm inhibitors prevent the formation of a bacterial biofilm via the inhibition of intercellular signalling, or through the binding of crucial ions, *i.e.* Ca^{2+}.[10, 11] Ca^{2+} ions are crucial for biofilm formation of *S. aureus* at μM concentrations, yet the ions are inhibitory at mM concentrations. Lee *et al.* have found that the use of Alizarin and a number of other similarly structure compounds reduces the concentration at which Ca^{2+} is inhibitory to the formation of biofilms. This inhibition has been proved to not be electrostatic in nature by Shukla and Rao, and it is thought that the complexation of the alizarin related chemicals was the reason for the increased activity.[12] There is also evidence for the anti-hemolytic activity of the Alizarin compounds.[11] Alpha toxin, a haemolytic protein, secreted by *S. aureus* is essential for its biofilm formation and the inhibition of this is another method by which the Alizarins are able to inhibit biofilm formation.[13]

Whilst it is not clear the exact mechanism or mechanisms by which the Alizarin compounds are able to inhibit the formation of biofilms, it was assumed that ARS, whilst not tested in by Lee *et al.,* would act in a similar manner, with the advantage of being more water-soluble owing to the sulfonate group.

2.2 Chapter Aims

Following from work done previously, we theorised that we would be able to bind a diol-containing compound to these gels, and then be able to release this compound on addition of H_2O_2. Where the binding and subsequent release of the ARS in response to the presence of sugars was in equilibrium, addition of H_2O_2 prevents the backwards reaction pathway. This is owing to the oxidation of the boron-carbon bond to a boron-oxygen bond, removing the binding site for the ARS' catechol.

While previously ARS was used as a colourimetric test compound to model the potential release of drug molecules, studies have shown it has the potential to act as a biofilm inhibitor. Using ARS the drug uptake and release can be measured using UV-vis, preventing the need for extensive microbiological experiments. As described in the previous work, PBA and BOB gels offer different binding affinities for different diols, which could allow for tailorable release concentrations.

The ARS binding and release should occur in a similar fashion to that of the carbohydrate, with the oxidation of the boronic ester causing the release of the bound dye as opposed to displacement with the saccharide. The end result should be the same, with diffusion of the free (thus red) ARS out of the gel and into the surrounding solution, figures 4 and 5.

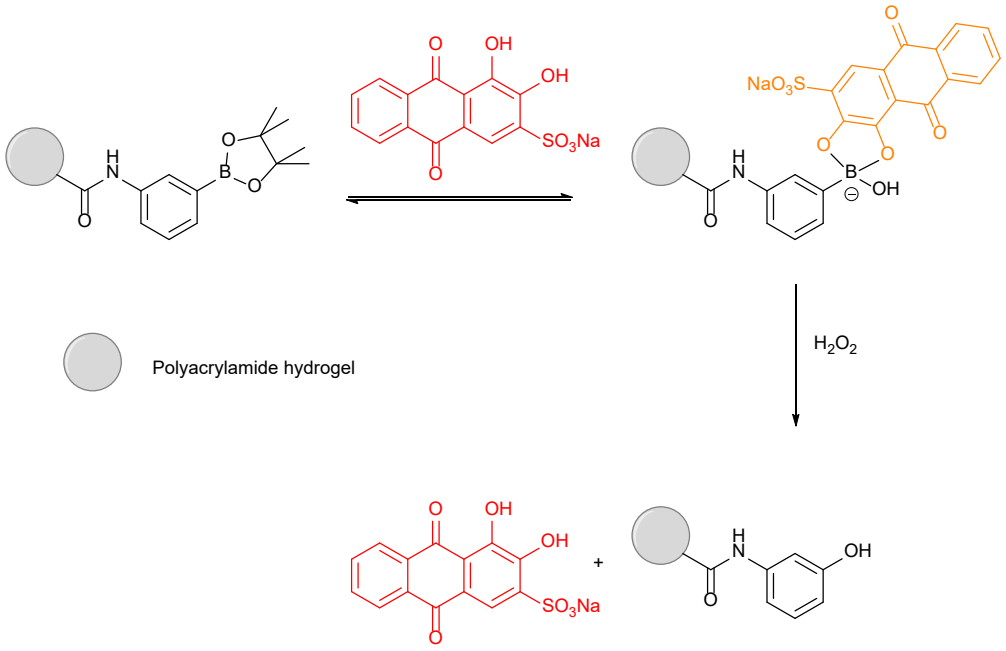

Figure 4 The binding of ARS to a PBA monomer within a polyacrylamide hydrogel, indicated by the red to orange colour change of ARS, with the oxidative release of the ARS indicated by the reverse colour change on addition of H_2O_2

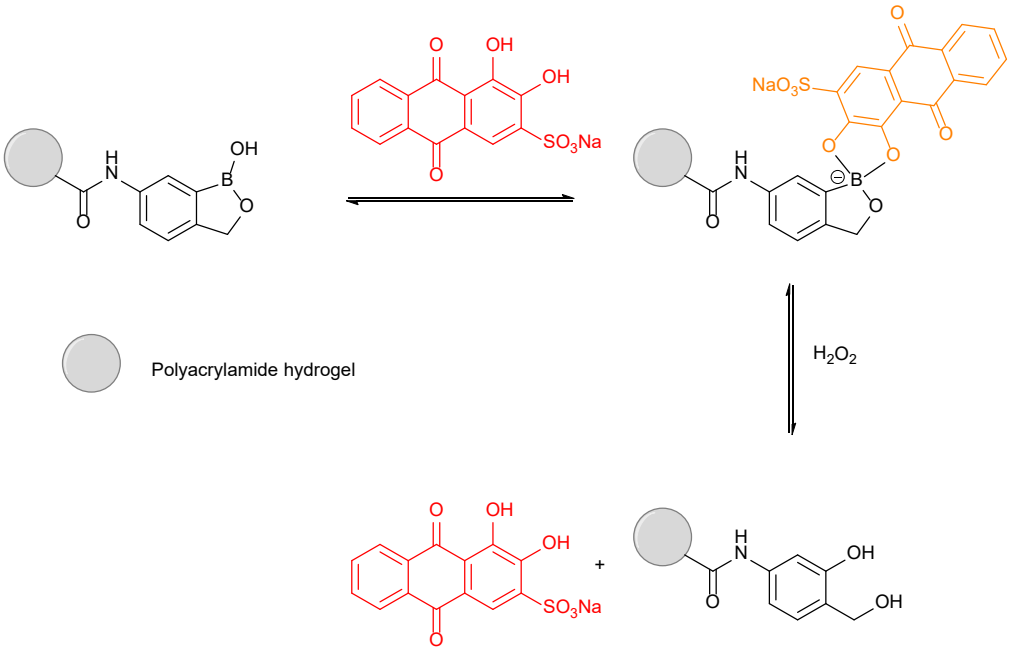

Figure 5 The binding of ARS to a BOB monomer within a polyacrylamide hydrogel, indicated by the red to orange colour change of ARS, with the oxidative release of the ARS indicated by the reverse colour change on addition of H_2O_2

There are a range of diol containing antimicrobial compounds, a large class of which are the aminoglycosides, for example streptomycin, figure 6. As these contain sugars, it is predicted that they will bind to both the PBA and BOB gels, but with a greater affinity to the PBA, as has been previously reported.[9] Other small molecular antibiotics such as chloramphenicol, figure 6, also contain diols which will bind to the boronic acid gels and be released with H_2O_2.

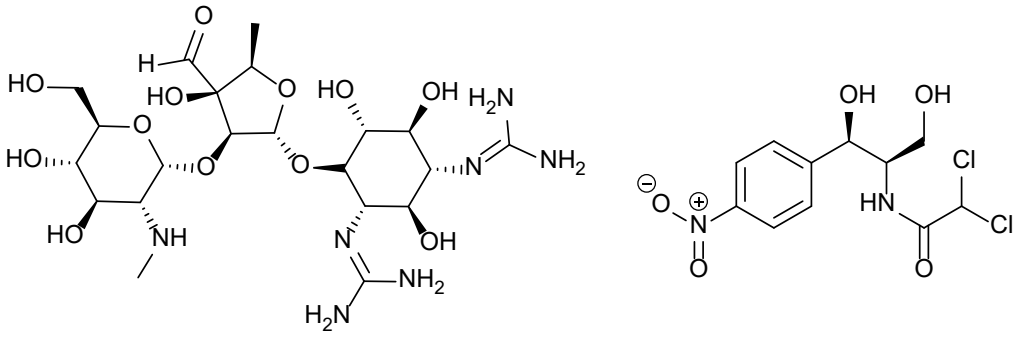

Figure 6 *Left* Streptomycin, *Right* Chloramphenicol

2.3 Materials and Methods

2.3.1 General Information

All solvents and reagents were purchased from commercial suppliers and used without further purification unless otherwise specified. Thin-layer chromatography (TLC) was performed using commercial precoated silica gel plates containing a fluorescent indicator. Column chromatography was carried out using silica gel (0.040 - 0.063 mm). Proton and carbon NMR were recorded using a Bruker Advance 500. Chemical shifts are reported in ppm using TMS or solvent residual signals as internal reference standards. High-resolution mass spectrometry (HRMS) were performed on an Agilent 6545 LC/Q-TOF. UV-vis were performed on a BMG Labtech CLARIOstar using costar u bottom 96 well microplates. Data was collected via the BMG Labtech CLARIOstar data analysis software package MARS.

Synthetic experimental information can be found in chapter 6.1.

2.3.2 Blank Gel Synthesis

Hydrogels were formed by the dissolution of acrylamide (3.9 g) and methylene bisacrylamide (0.1 g) in distilled water (20 mL). Tetramethylethylenediamine (50 μL) and an aliquot of freshly prepared ammonium persulphate solution (10% w/v, 150 μL) were added. The solution was taken up into 1 mL syringes, which were then inverted and placed in a test tube rack. After the gel had set, as determined by a visual inspection (30 – 45 mins), the end of the syringe was removed with a pair of scissors and 0.1 mL pieces of gel were cut using a scalpel.

2.3.3 PBA/BOB Containing Gel Synthesis

Hydrogels were formed by the dissolution of acrylamide (3.8 g), PBA/BOB monomer (0.1 g) and methylene bisacrylamide (0.1 g) in distilled water (20 mL). Tetramethylethylenediamine (50 μL) and an aliquot of freshly prepared ammonium persulphate solution (10% w/v, 150 μL) were added. The solution was taken up into 1 mL syringes, which were then inverted and placed in a test tube rack. After the gel had set, as determined by a visual inspection (45 – 60 mins), the end of the syringe was cut off with a pair of scissors and 0.1 mL pieces of gel were cut using a scalpel.

2.3.4 Dye Uptake Experiments

To measure the binding of the dye to the gel, a cylinder of gel with a volume of 0.1 mL was weighed and placed into the well of a 24 well microtitre plate. 1 mL of 2.5 x 10^{-4} M ARS solution in PBS was then added to the well. The initial absorbance of this solution was measured by taking a 100 µL aliquot in a 96 well microplate and measuring using its absorbance at 513 nm using a Spectrostar Omega plate reader from BMG Labtech. The aliquot was then returned to the well containing the gel in order to maintain its volume. Aliquots were then taken over time and the decrease in absorbance was plotted as a function of the mas of the individual gel used.

2.3.5 Dye Washing Experiments

To measure the release of non-covalently bound dye from the gel, a cylinder of ARS loaded gel with a volume of 0.1 mL was weighed and placed into the well of a 24 well microtitre plate. 1 mL PBS was then added to the well. The initial absorbance of this solution was measured by taking a 100 µL aliquot in a 96 well microplate and measuring using its absorbance at 513 nm using a Spectrostar Omega plate reader from BMG Labtech. The aliquot was then returned to the well containing the loaded gel in order to maintain its volume. Aliquots were then taken over time and the increase in absorbance was plotted as a function of the mas of the individual gel used.

2.3.6 Dye Release Experiments with H_2O_2

To measure the release of dye upon exposure to H_2O_2, solutions of H_2O_2 were prepared in PBS, with concentrations ranging from 0 to 4 mM. ARS loaded gel cylinders with a volume of 0.1 mL were weighed and placed into the wells of a 24 well microtitre plate. 1 mL of either PBS of H_2O_2 solution was added to the well and experiment aliquots were removed and their UV-vis was measured every 10 minutes for 60 minutes then hourly for 2 hours was repeated. Aliquots were returned to the experimental solution to maintain sink conditions.

2.3.7 Dye Release Experiments with Plasma Activated Buffer

In order to generate a ROS/RNS solution using cold plasma, PBS (1 mL) was treated with the cold plasma jet for set period of time (0 – 30 mins). The plasma conditions used were: 10 kV, 25 A, 0.6 slp with a distance of 15 mm. Once the plasma activated solutions were generated, they were used in the same manner as the H_2O_2 solutions in 2.3.6.

2.3.8 Media, Buffers and Stock Solutions

Medium or buffer	Reagents
Luria-Bertani (LB)	ThermoFisher Scientific U.K
Luria-Bertani agar (LBA)	ThermoFisher Scientific U.K
Tryptic soya broth (TSB)	ThermoFisher Scientific U.K
Tryptic soya agar (TSA)	ThermoFisher Scientific U.K
Phosphate buffered saline (PBS)	Sigma Aldrich U.K

*All media was sterilised using an autoclave prior to use

2.3.9 Bacterial Strains and Overnight Cultures

P. aeruginosa PAO1, *S. aureus* H560 and *S. aureus* MRSA252 were obtained from a strain collection belonging to the Biophysical Chemistry Research Group at the University of Bath. *E. coli* NCTC 10418 was obtained from Professor Maillard's group at Cardiff University. All strains were stored in a 30% (v/v) glycerol solution at -80 °C. Overnight cultures of bacterial strains were routinely grown in 10 mL of LB medium for *P. aeruginosa* PAO1 and *E. coli* NCTC 10418, and TSB medium for *S. aureus* MRSA252 and H560 at 37 °C with shaking (225 rpm) for 24 hours.

2.3.10 Bacterial MICs

Antimicrobial susceptibility testing was carried out in a 96-well microtiter plate using a standard two-fold broth microdilution method as recommended by the Clinical Laboratory Standards Institute (CLSI). 100 µL of an antimicrobial agent of known concentration was serially diluted two-fold across the 96 well plate in 1% (w/v) D-(+)-glucose for TSB and 50% (w/v) D-(+)-glucose for LB. Re-suspended bacterial cultures were diluted in TSB/LB, and added in equal volume, so that each well contained approximated 5 x 10^5 Colony Forming Units per mL CFU/mL (range 2 – 8 x 10^5 CFU/mL). The Minimum Inhibitory Concentration (MIC) was defined as the lowest concentration of antimicrobial agent required to inhibit the visible growth of bacterial strains after 18 h incubation at 37 °C.

2.3.11 Bacterial Biofilm Formation

Bacterial biofilms were formed in 96 well microplates (Nunc, UK). Overnight bacterial cultures were sub-cultured into fresh medium, supplemented with 1% (w/v) D-(+)-glucose for TSB and 50% (w/v) D-(+)-glucose for LB, to a starting bacterial concentration of 10^6 CFU/mL. An aliquot of 100 µL of subculture was added to selected wells, before an equal volume of known drug (or

drug combination) concentration was added at desired stage of growth. Plates were then incubated statically at 37 °C for 24 hours. Supplemented TSB or LB was used as a negative control.

2.3.12 Crystal Violet Biofilm Staining

After incubation, planktonic bacteria were removed from the microtiter plate, and the remaining biofilm was washed three times with PBS. Next, 250 µL of 0.1% (w/v) Crystal Violet (CV) was added to each well and left to incubate at room temperature for 15 min. After staining, the wells were rinsed three times in PBS and left to dry at room temperature for 3 – 4 hours. To quantify the biofilm biomass, 250 µL of 33% (v/v) acetic acid (AcOH) was added to each well to elute the CV stain, and left to incubate at room temperature for 15 min. Note – AcOH measured with pipette calibrated to water ergo uncertainty in measurement. Finally, 125 µL of eluted dye solution was transferred into a fresh 96 well microtiter plate and absorbance was measured at 570 nm (Spectrostar Omega plate reader, BMG Labtech).

2.4 Results and Discussion

2.4.1 Synthesis of the Boronic Acid Containing Hydrogels

The two boronic acid containing monomers were prepared according to the synthesis previously reported by Lampard *et al,* as shown above in figure 7.

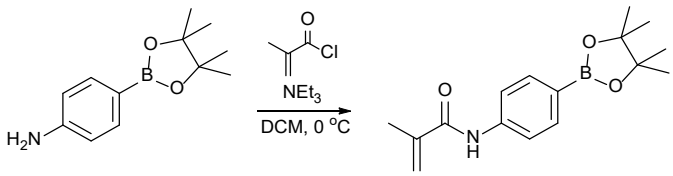

Figure 7 The binding of the PBA to an acrylamide monomer

To create the hydrogel, acrylamide, methylene bisacrylamide and the chosen boronic ester containing monomer were dissolved in distilled water. TMEDA and ammonium persulphate solution were added into the flask using a syringe to initiate the polymerization, and the solution was taken up into 1 mL syringes. After 40 minutes the gelation was complete and the end of the syringe could be cut off, allowing cylinders with a measurable volume of 0.1 mL to be cut. The produced gels were very pale in colour, meaning they were able take on the colour of the dye, figure 8.

Figure 8 Clear poly acrylamide gels doped with *left* PBA and *right* BOB monomers. Slight yellow tint due to TEMED impurities.

2.4.2 Dye Loading and Washing Studies

To bind the ARS to the boronic ester moieties within the hydrogel, the gels were placed in a solution of 2.5 x 10^{-4} M of ARS in PBS buffer for 5 hours. As the concentration of free ARS in the solution decreases, so does its absorbance in accordance to the beer lambert law.[14]

$$A = \varepsilon C l$$

Aliquots were therefore taken and measured at different intervals to discover the minimum time required to soak the gels to allow them to obtain their maximum loading. The larger the gel, the more boronic acid binding sites would be available to bind the ARS. Therefore, to allow for potential differences in gel swelling and size, the absorbance was plotted as a function of the masses of the individual gels used, figures 9 and 10.

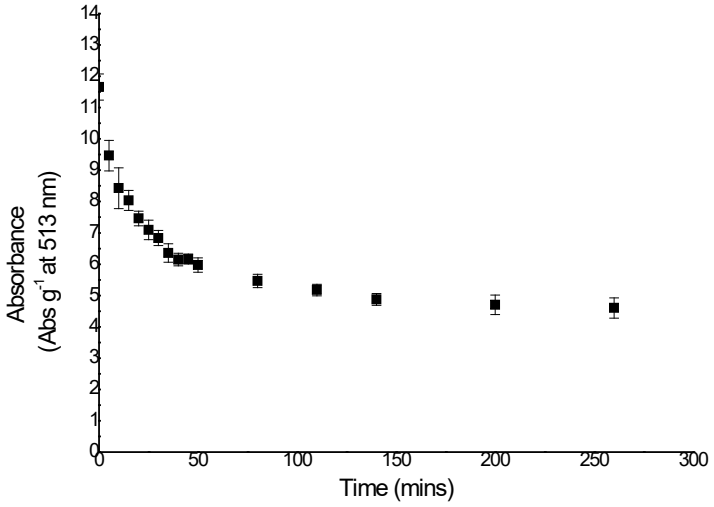

Figure 9 The decreasing absorbance at 513 nm of a solution of ARS (in PBS) as it binds to the PBA containing gel. The assay was conducted three times and results plotted as mean ± standard deviation

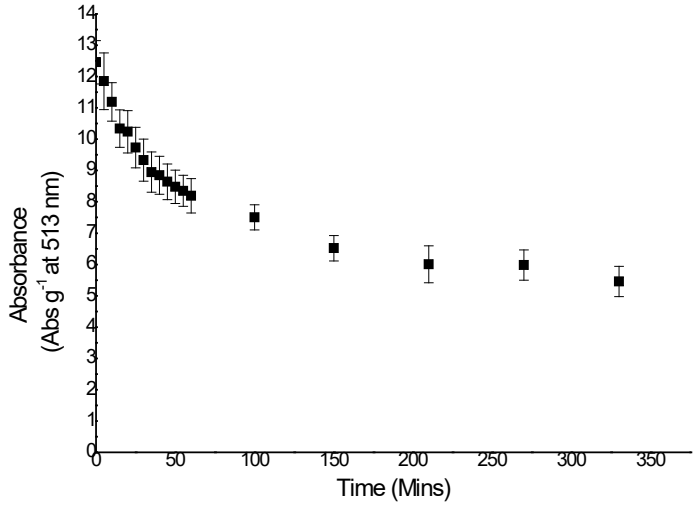

Figure 10 The decreasing absorbance at 513 nm of a solution of ARS (in PBS) as it binds to the BOB containing gel. The assay was conducted three times and results plotted as mean ± standard deviation

It can be seen from the loading graphs, figures 9 and 10, that the final ARS concentration is greater in the solution containing PBA gel than in the solution containing the BOB gel. This is indicative of a higher binding affinity between the ARS and the PBA compared to the BOB boronic esters.

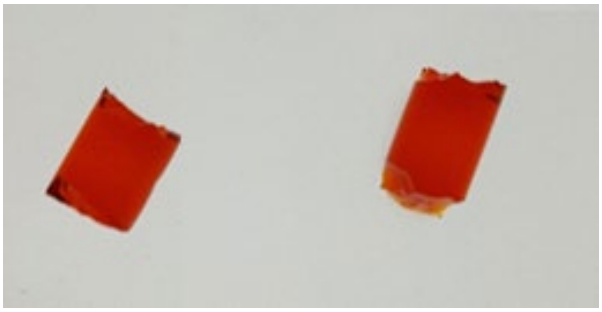

Figure 11 ARS loaded *left* PBA containing and *right* BOB containing hydrogels pre-washing

Following loading, it had to be ensured that all the non-specifically bound ARS was removed from within the gels. Gels with unbound ARS within the hydrogel matrix have a deep red colour, figure 11. This shows that there is free ARS that requires removal. This simply involved washing the loaded pieces of gel in PBS (pH 7.4). To monitor the washing of un-bound ARS from the gels, aliquots of washings were removed periodically, and the concentration of ARS was measured. Once the absorbance stopped increasing, it was deemed that the washing process was complete

and the remaining ARS was covalently bound to the gel, figures 12 and 13. However, the surrounding solution would reach equilibrium with the internal gel matrix, ergo fresh PBS should have been used to gain a more true zero value.

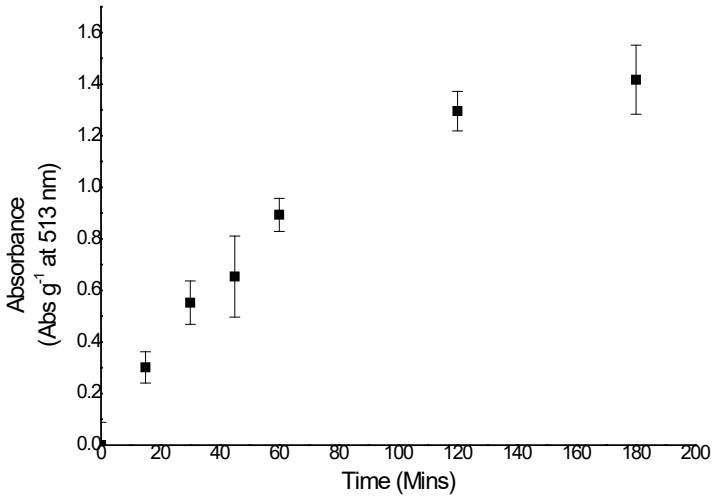

Figure 12 Absorbance of ARS at 513 nm upon washing the ARS-containing PBA gel in PBS over time. Increased absorbance indicates release of non-bound ARS. The assay was conducted three times and results plotted as mean ± standard deviation

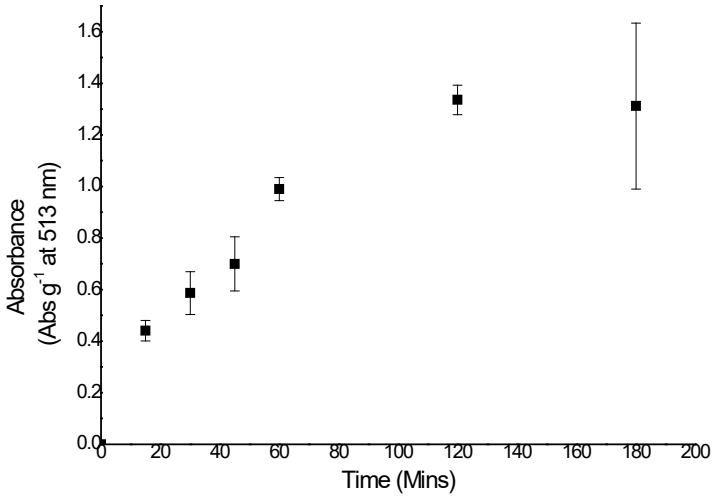

Figure 13 Absorbance of ARS at 513 nm upon washing the ARS-containing BOB gel in PBS over time. Increased absorbance indicates release of non-bound ARS. The assay was conducted three times and results plotted as mean ± standard deviation

As can be seen in figure 14 the unbound red free ARS has been removed, yielding gels that are the orange colour of ARS bound to boron.

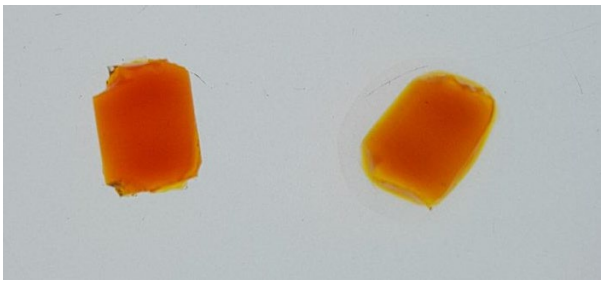

Figure 14 ARS loaded *left* PBA containing and *right* BOB containing hydrogels post washing

Beyond 180 minutes there was a plateau in the absorbance, indicating the removal of all of the unbound ARS. To ensure complete removal each gel was washed for 5 hours.

2.4.3 Triggering the Release of ARS With H_2O_2

Following these washing steps the ARS loaded gels were exposed to differing concentrations of H_2O_2 in PBS. As any unbound dye had already been removed, the increase in absorbance was proportional to the amount of bonds oxidised by H_2O_2, which itself was proportional to the concentration of H_2O_2 used. Figures 15 and 16 shows the release of ARS from the hydrogel

matrixes containing PBA or BOB monomers, with increasing absorbance at 513 nm found upon increasing H_2O_2 concentration.

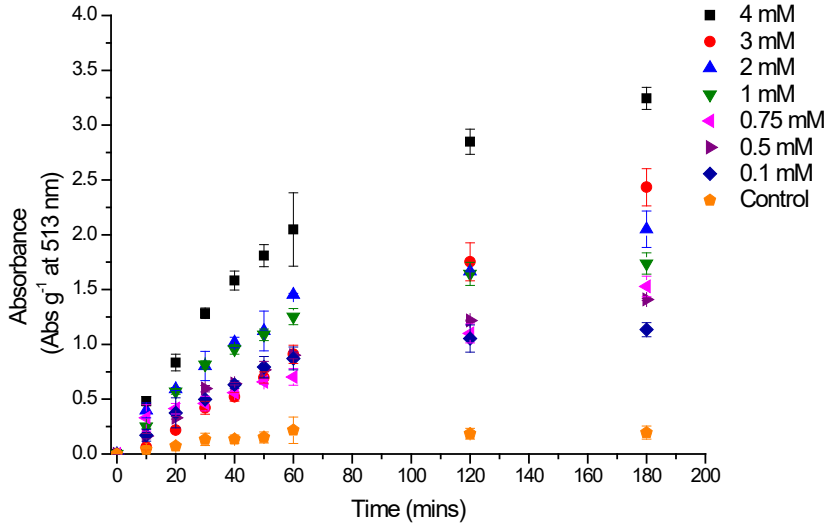

Figure 15 Absorbance at 513 nm of ARS released over time from PBA gels upon differing concentrations (0 – 4 mM) of H_2O_2 in PBS. The assay was conducted three times and results plotted as mean ± standard deviation

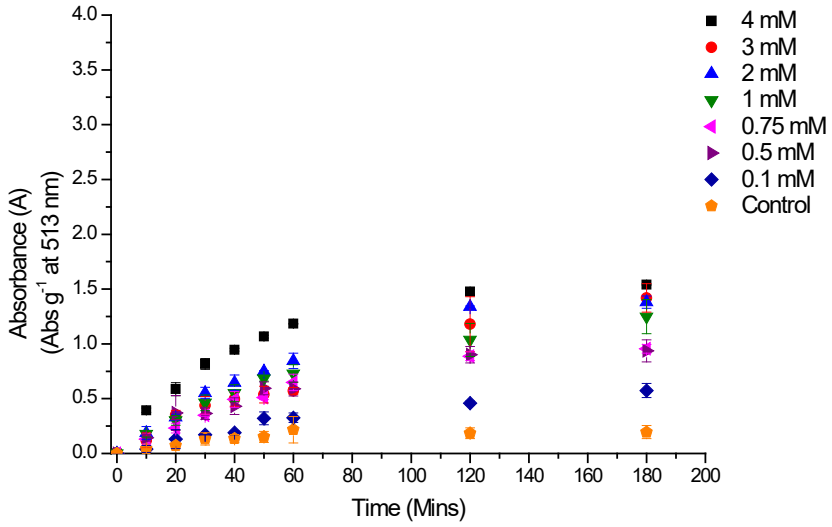

Figure 16 Absorbance at 513 nm of ARS released over time from BOB gels upon differing concentrations (0 – 4 mM) of H_2O_2 in PBS. The assay was conducted three times and results plotted as mean ± standard deviation

Exposure of ARS loaded hydrogels to concentrations of H_2O_2 ranging from 100 µM to 4 mM gave a dose dependent release of ARS from the hydrogel matrix for both the PBA and the BOB containing gels. Likely owing to the increased loading efficency of the ARS into the PBA gel, the maximum absorbance for ARS release upon addition of 4 mM H_2O_2 was much higher. The maximum release after 3 hours can be seen in figures 17 and 18.

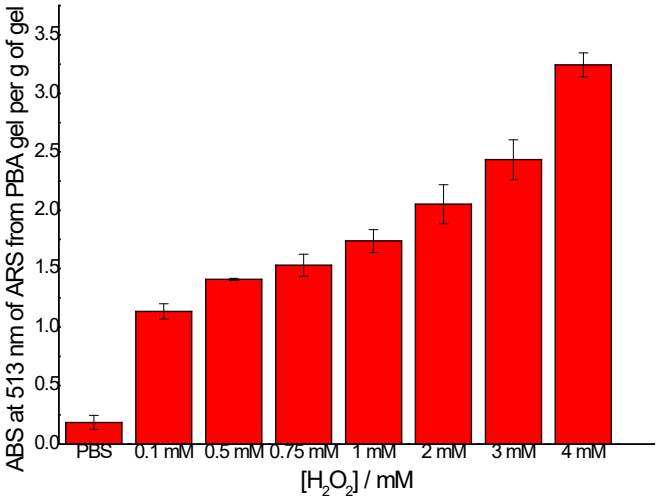

Figure 17 Absorbance of released ARS from PBA gels in solution at 513 nm after 3 hours incubation with increasing concentrations (0 – 4 mM) of H_2O_2 in PBS. The assay was conducted three times and results plotted as mean ± standard deviation

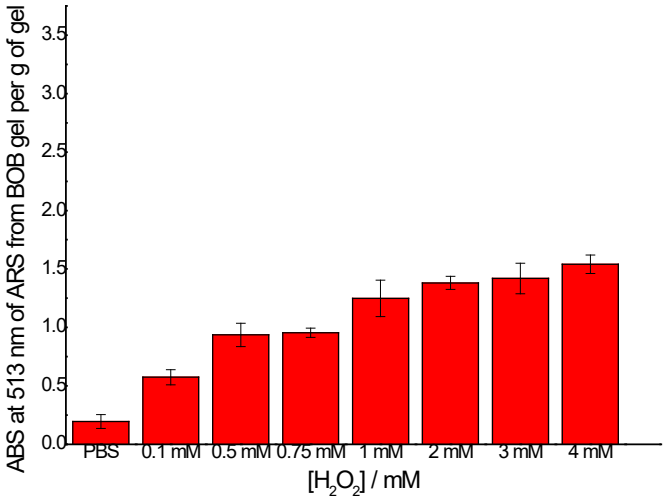

Figure 18 Absorbance of released ARS from BOB gels in solution at 513 nm after 3 hours incubation with increasing concentrations (0 – 4 mM) of H_2O_2 in PBS. The assay was conducted three times and results plotted as mean ± standard deviation

As can been seen above in figures 17 and 18, after the 3 hours of release there was more than a two-fold increase in the release of the ARS when using the highest concentration of H_2O_2 (4 mM), regardless of the form of boronic ester used. However, in both the PBA and BOB gels there was still some non-specific release of the ARS. This could be due to the washing steps being incomplete, or the fact that the boronic ester-ARS bond is a dynamic covalant bond, hence an equiliburm with the surrounding solution was reached.

The diameter of cyclinders of both gel were measured upon exposure to H_2O_2 to ensure that there was no degradation of the overall gel structure, but it was found to be stable under such conditions. Loaded gel cylinders of both the PBA and BOB gels were submerged in 5 mM H_2O_2 for 24 hours with only a slight swelling observed in both, figure 19.

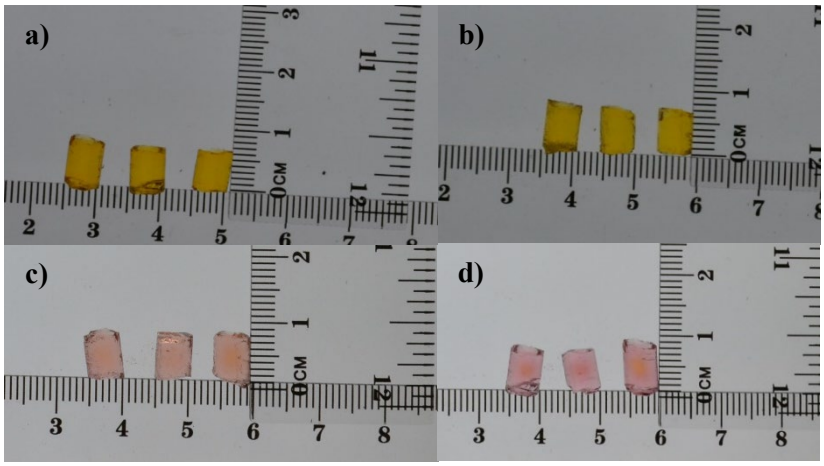

Figure 19 **a)** PBA containing gels loaded with ARS, **b)** BOB containing gels loaded with ARS, **c)** PBA containing gels loaded with ARS following 24 hour incubation with 5 mM H_2O_2, ***d)*** BOB containing gels loaded with ARS following 24 hour incubation with 5 mM H_2O_2

2.4.4 Using Cold Plasma to Trigger ARS release

While the proof-of-concept model of utilising H_2O_2 to trigger the release of a diol containing small molecule from the hydrogel matrix was achieved, the overall intended use was to trigger the release using Cold Atmospheric Plasma (CAP). Initial experiments were conducted using plasma treated PBS buffer. Briefly, 1 mL of PBS in a 24 well plate was treated with CAP for differing amounts of time to produce ROS/RNS solutions of differing concentrations. Whilst the produced ROS/RNS solution has yet to be fully quantified in terms of the concentrations of its indivdual components, it is known that H_2O_2 is the predominent species.[15] As such, increasing the duration of treatment of PBS with the CAP jet was found to increase the concentration of H_2O_2 in solution, figures 20 and 21.

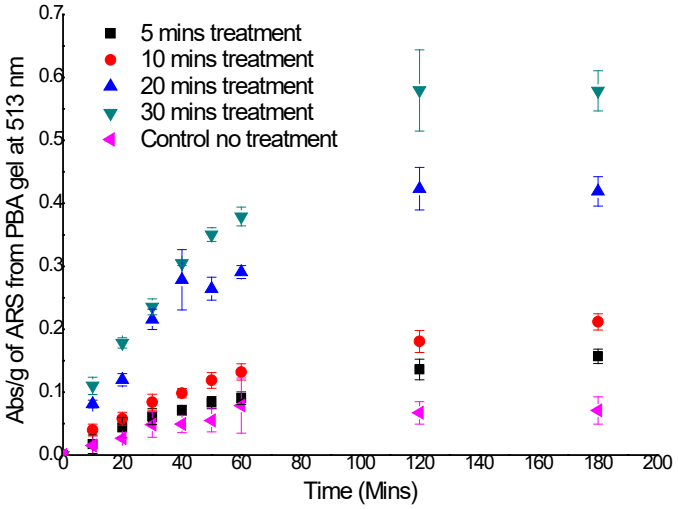

Figure 20 Absorbance at 513 nm of released ARS in solution over time from a PBA hydrogel after incubation with solutions of ROS/RNS in PBS generated by plasma for different lengths of time (0 – 30 mins). The assay was conducted three times and results plotted as mean ± standard deviation

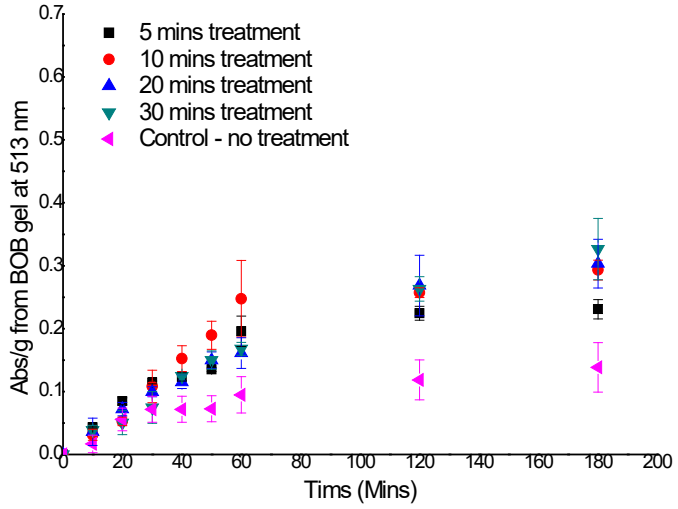

Figure 21 Absorbance at 513 nm of released ARS in solution over time from a BOB hydrogel after incubation with solutions of ROS/RNS in PBS generated by plasma for different lengths of time (0 – 30 mins). The assay was conducted three times and results plotted as mean ± standard deviation

The longer the treatment of PBS with CAP, the greater the concentration of H_2O_2 (and other ROS/RNS) produced.[16] This is exemplified in figures 20 and 21. The ARS release follows the

same dose dependent response on increased treatment time with CAP as it did with increasing concentrations of H_2O_2. There is little differentiation between the 10, 20 and 30 minute treatment times when investigating the release of the ARS form the BOB gel. This could indicate that the shorter lived species, *i.e.* peroxynitrite, within the plasma treated buffer offering a greater rate of reactivity with the BOB functionality than the longer lived species like hydrogen peroxide.

The overarching aim of the project was to develop a system that would be able to release a molecule, or molecules, on contact with direct plasma treatment. This proved problematic, as it was found that the direct plasma onto the gel surface caused dehydration and as a result the gel burned. These initial experiments were conducted using small discs of gel. However, it was theorised that if larger pieces were used, the increased volume of hydrogel could act as a resevoir, allowing movement of water and decreasing the rate of burning. This was found not to be the case, and instead after only 5 minutes of direct application the centre of the gel would dry, causing the entire gel to deform, figure 22.

Figure 22 The burnt hole within a sheet of PBA gel surrounded by a ring of dehydrated hydrogel caused by direct plasma treatment. The edges of the gel were taped down to avoid folding

From this, numerous blank hydrogel gels were synthesised and exposed to CAP treatment, to screen for a gel that could withstand a greater degree of plasma contact. These gels include agarose, carboxymethyl cellulose (CMC) and PVA. Owing to the ease in which it can be cryocrosslinked (and bound to the polyacrylamide) PVA was chosen, and a bi-layered film of the two gels was produced.

These gels provided a more robust layer for direct plasma treatment – the theory was that upon plasma treatment this could generate a resevoir of reactive species that could then diffuse through the hydrogel matrix, into the polyacrylamide layer. Upon reaching the acrylamide layer, the

ROS/RNS produced in the PVA layer would oxidise the boronic ester, releasing the ARS through the base of the gel. Unfortunately, it was found that the reactive species reacted with the boronic acids closest to the reservoir, forming a concentration gradient in the wrong direction, hence the ARS diffused upwards, figure 23. Pre-soaking the PVA gels in ARS may have been a way to combat this.

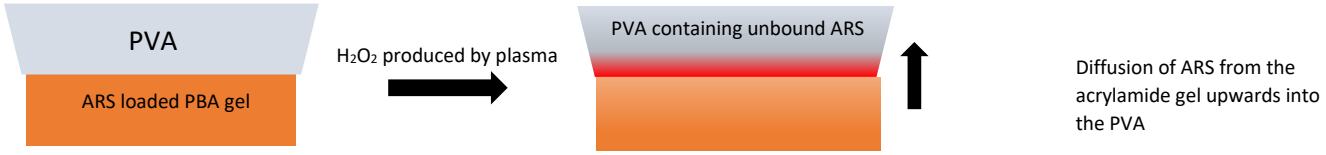

Figure 23 The dual layer PVA and poly acrylamide system which was able to withstand direct plasma treatment

In terms of its application this diffusion is in the wrong direction (*i.e.* away from the wound) and thus the rest of the testing was performed using the loaded acylamide gels without any other gel layers. As such the biological testing was performed with only H_2O_2 solutions and solutions of plasma activated buffer, not direct plasma treatment.

2.4.5 The Biological Activity of ARS

During normal bacterial growth there are three key stages, lag, exponential and stationary phase. The growth of a bacterial population is exponential, owing to their reproduction via division. The initial lag phase is owing to bacterial using the nutrients within the broth to grow, preparing for division by synthesising crucial proteins. During the exponential phase the bacteria divide, the population doubling in size with each division. Following this growth the bacteria will reach stationary phase in which the number of cells platues and remains relatively consistent. Cells will still continue to replicate but others will die. At this stage their growth is limited by either lack of nutrients or the accumlation of toxic by products of growth. The length of each of these phases depends on the bacteria, figure 24.

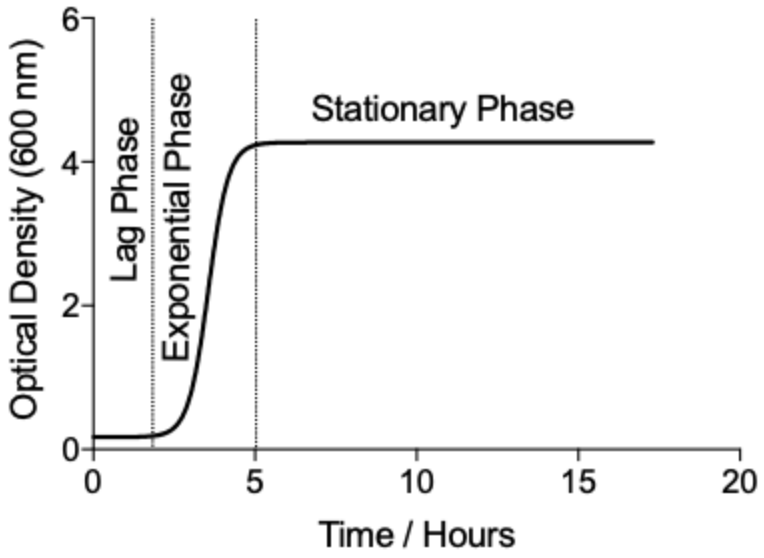

Figure 24 A bacterial growth curve showing the optical density change over 18 hours due to growth at the three key phases; lag exponential and stationary. This is generally measured at 37 °C. Reproduced with permission from[17]

The antibacterial actvity of ARS was tested using MIC measurements against isolates of *S. aureus* H560 and MRSA 252*, P. aeruginosa* PA01 and *E. coli* NCTC 10418, but was found to be non-inhibitory for all strains of bacteria tested, even at its maximum concentration in aqueous solution, appendix 7.2.2. An MIC is the measure of the minimum concentration of an antibiotic required to prevent the growth of bacteria. It has however been previously demonstrated by Lee *et al* that certain alizarins and other calcium chelators, have the ability to prevent the formation of biofilms in *S. aureus*.[11] As ARS can also chelate to Ca^{2+} we assumed it to, would be able to inhibit biofilms. In order to measure biofilm formation, biofilms were grown and biomass was assessed by adding crystal violet stain. This dye bound to biological material, giving an indication of the amount of biofilm formed through absorpstion measurments.[18] The ability of ARS to inhibit the formation of biofilms in the lag phase be seen in figure 25.

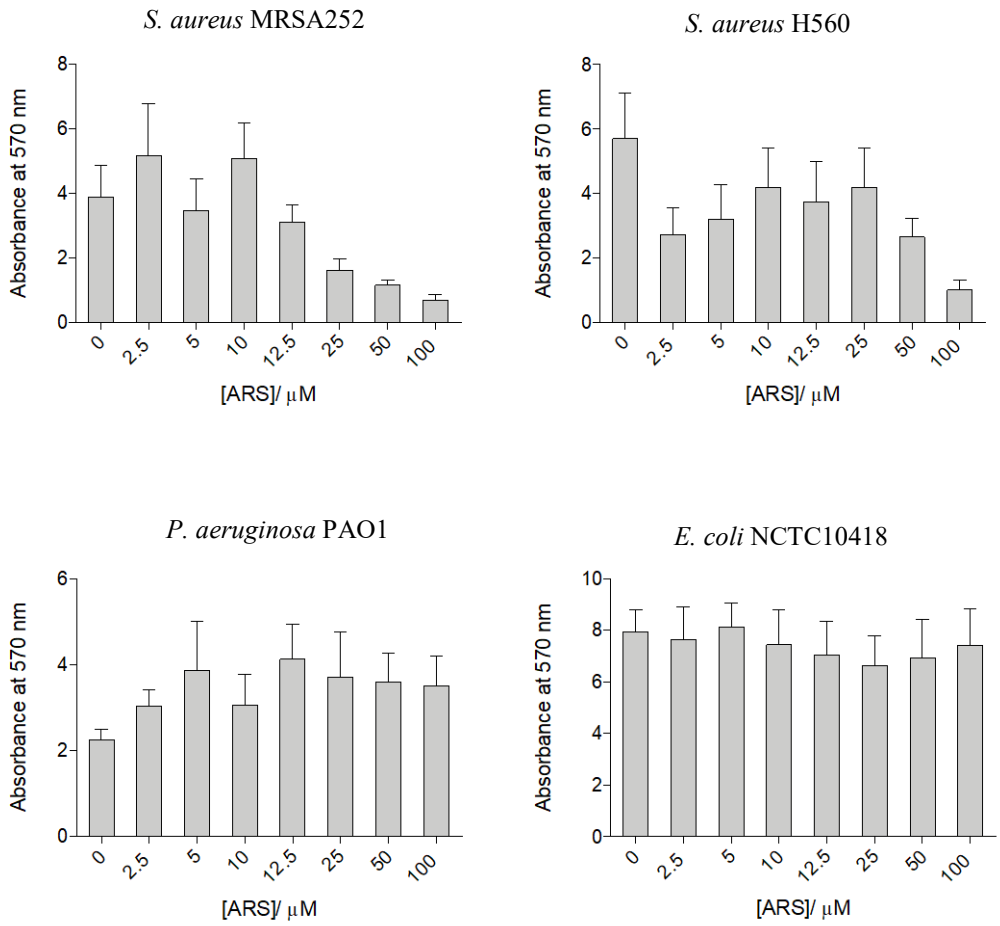

Figure 25 Absorbance at 570 nm of crystal violet, correlating to the amount of biological material present (and thus amount of biofilm formation), with the addition of ARS (0 – 100 μM) at the lag phase. Data plotted as the mean, n = 3. Error bars indicate standard deviation

As can be seen in figure 25 there is no decrease in the biofilm forming ability of the two gram negative strains, however there is a pronounced decrease in biomass measured for both *S. auerus* strains at 100 μM, less than half of the amount of ARS loaded in the gels. One of possibility as to why this would have a greater effect on the gram positive strains, is that the ARS can to the quorum sensing molecules that instigate biofilm formation, blocking the signals. As ARS is a known chelator of Ca^{2+}, it is also possible that during this lag stage there are calcium dependant pathways for the formation of essential proteins for biofilm formation, and these unable to be created due to Ca^{2+} capture. Ca^{2+} is essential to the growth of extracellular DNA, which is a crucial component of the biofilm EPS, and it is during the lag phase that this synthesis occurs.[19] As expected this

inhibitory effect was not seen for the addition of ARS to any other stage of the bacterial growth, appendix 7.2.3 and 7.2.4.

In order to ensure that the cause of the systems reduction in biofilm was the ARS and not due to the trigger, H_2O_2 was also assessed for biofilm inhibiton. Differing concentrations of H_2O_2 (0 – 100 mM in PBS) were added to growing cultures of *S. aureus* H560, *S. aureus* MRSA252, *E. coli* NCTC 10418 and *P. aeruginosa* PAO1 at the lag phase, figure 26, the exponential phase, figure 27, and at the stationary phase, figure 28. The different bacterial species grow in the same general pattern of stages, but with different timings at each stage. As such the growth curves of these bacteria were first obtained, appendix 7.2.5.

2.4.6 Addition of H_2O_2 to Biofilms at Lag Phase

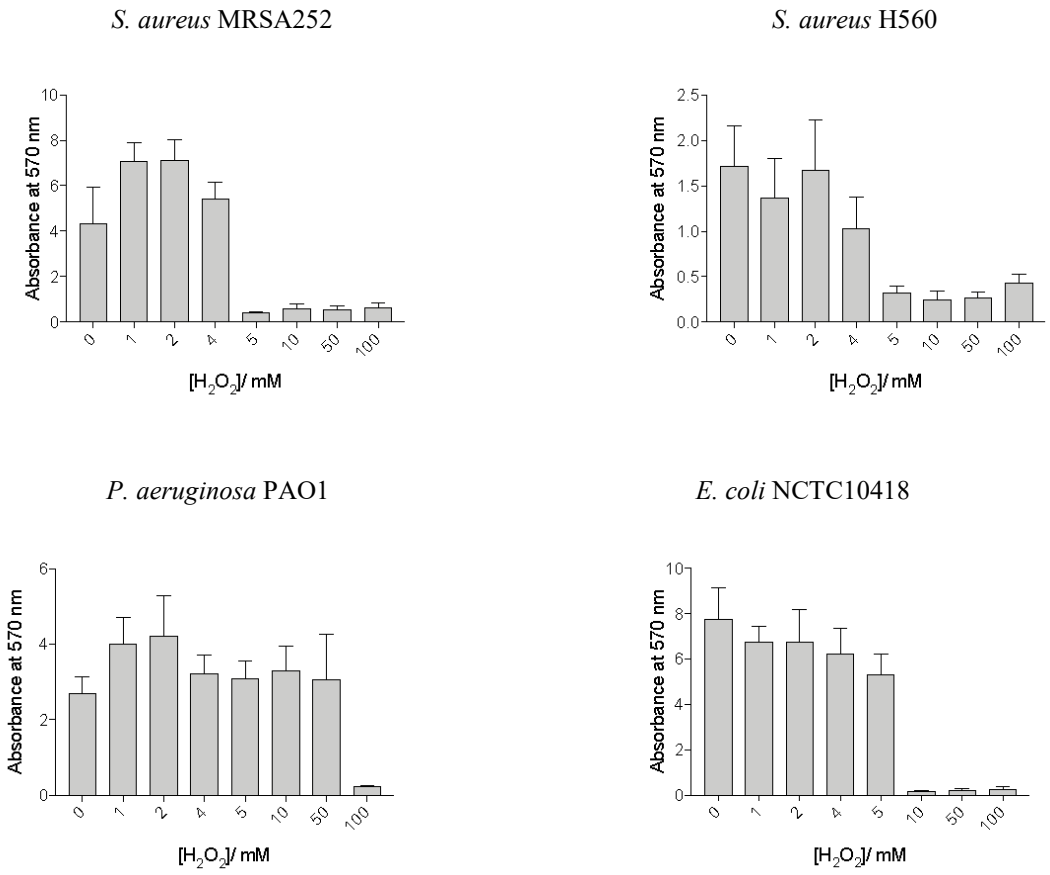

Figure 26 Absorbance at 570 nm of crystal violet, correlating to the amount of biological material present (and thus amount of biofilm formation), with the addition of H_2O_2 (0 – 100 mM) at the lag phase. Data plotted as the mean, n = 3. Error bars indicate standard deviation

As is to be expected from differening species, each bacteria reacted differently to the addition of the H_2O_2. During lag phase, the addition of H_2O_2 to the gram positive *S. aureus* strains at concentrations as low as 5 mM caused a large reduction in biomass. There was a comparitive increase in resistance to the effects of H_2O_2 seen in both gram negative strains, with the *P. aeruginosa* and *E. coli* strains requiring the addition of 100 mM and 10 mM of H_2O_2 respectively to see a significant decrease in biomass. That the H_2O_2 had a greater effect on the gram negative strains could be due to cell wall effects, or possibly due to a difference in the biofilm forming signalling molecules produced by the gram negative species having a greater reactivity with the H_2O_2.

2.4.7 Addition of H_2O_2 to Biofilms at Exponential Phase

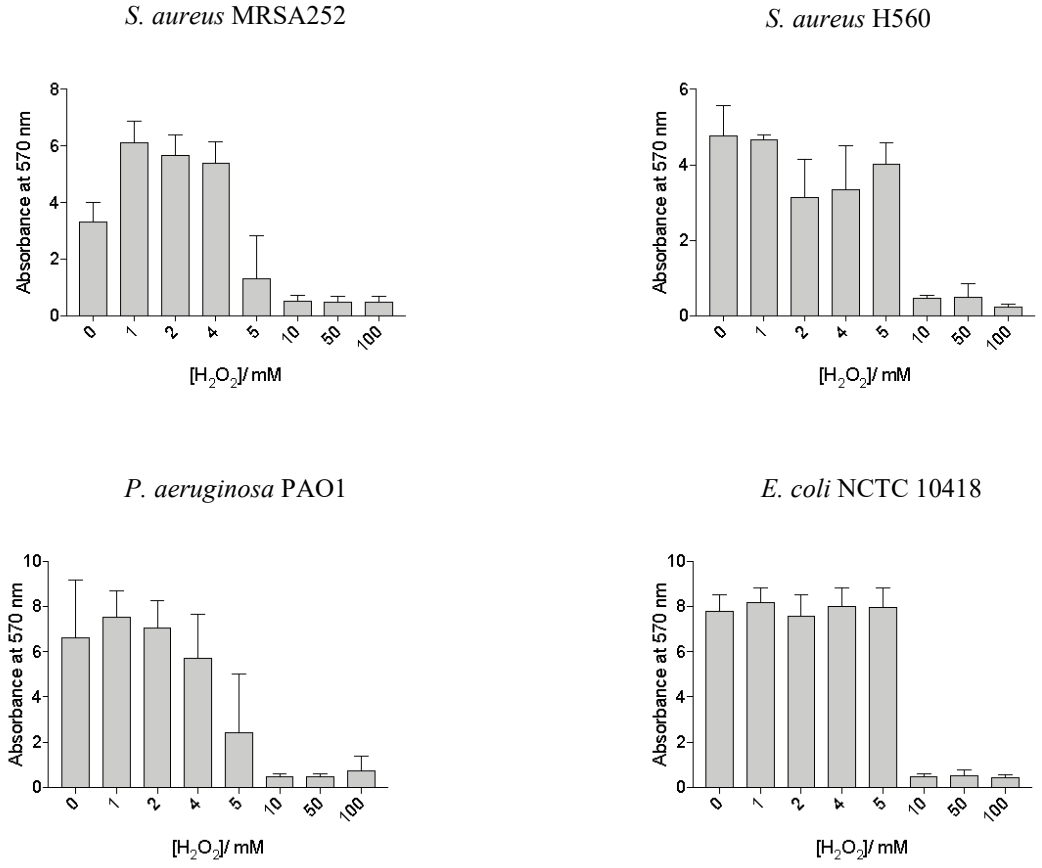

Figure 27 Absorbance at 570 nm of crystal violet, correlating to the amount of biological material present (and thus amount of biofilm formation), with the addition of H_2O_2 (0 – 100 mM) at the exponential phase. Data plotted as the mean, n = 3. Error bars indicate standard deviation

There is a slightly increased resistance to the antibiofilm formation effects of H_2O_2 in both of the *S. aureus* strains during the exponential phase when compared to the lag phase. The lag phase is the stage in which the bacteria are synthesising the enzymes and other factors that they require for division. It could be that the nutrients that are uptaken during this stage are broken down by the presence of the H_2O_2, and that once they have been synthesised the division can occur without interference. For the gram-negative bacteria the *E. coli* strain features no change in its biofilm forming ability, however there is a huge drop in the bioforming ability of *P. aeruginosa.* During this growth stage the concentration of the bacteria will become great enough that the bacteria will begin producing more autoinducers. That the *P. aeruginosa* is effected more strongly is likely due to the structure of one of its chief autoincudcers, autoinducer-2, a furanoysl sugar containing a borate diester.[20] This would be oxidised by the presence of H_2O_2, preventing the signalling molecules from reaching their bacterial targets.

2.4.8 Addition of H_2O_2 to Biofilms at Stationary Phase

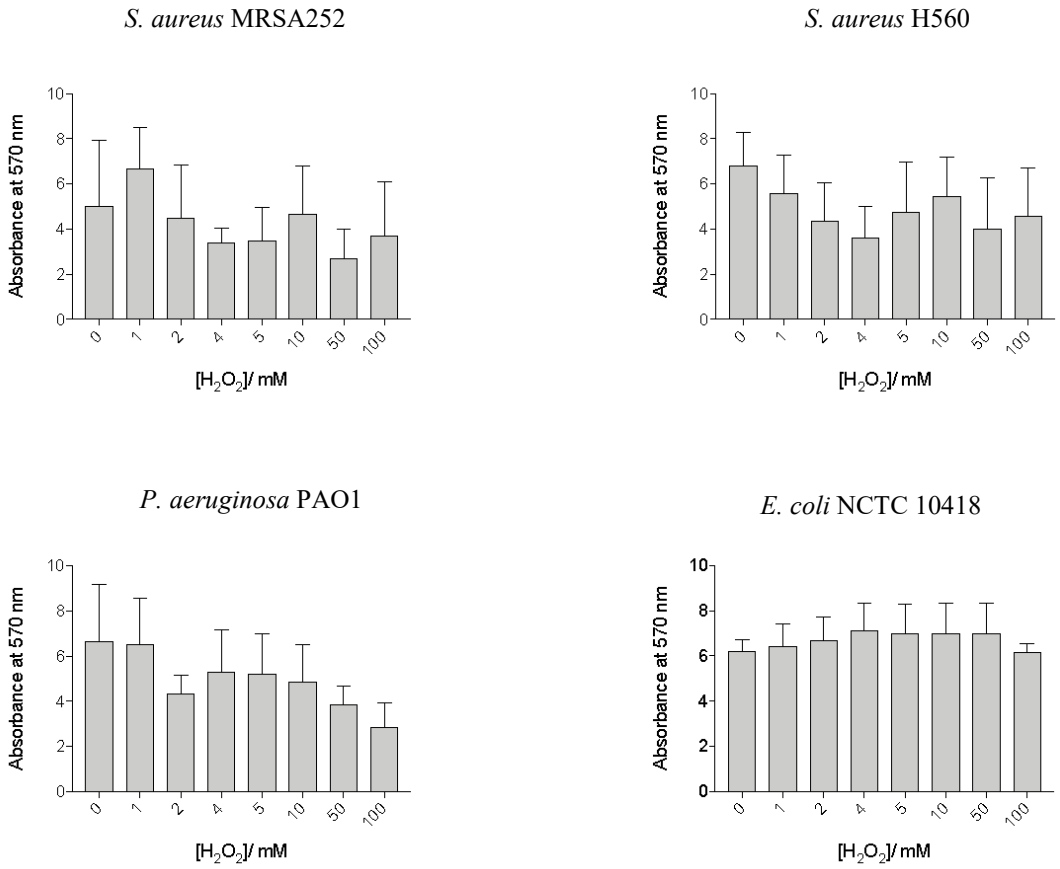

Figure 28 Absorbance at 570 nm of crystal violet, correlating to the amount of biological material present (and thus amount of biofilm formation), with the addition of H_2O_2 (0 – 100 mM) at the stationary phase. Data plotted as the mean, n = 3. Error bars indicate standard deviation

For stationary phase bacteria, no significant differences were observed for the addition of all concentrations of H_2O_2 compared to that of the controls. Though 100 mM is a large excess when considering triggered release, clinical topical use of hydrogen peroxide is 3%, which equates to 980 mM. This is why there is bacterial survivabilty and biofilm formation at what appear to be high H_2O_2 concentrations. There is a large increase in tolerance to H_2O_2 for all of the bacteria at this phase. This is likely owing to the decrease in metabolic activity of the bacteria that they achieve in stationary phase. As well as their metabolic activity decreasing, the concentrations of bacteria has been high for a period of hours (depending on the bacteria). This therefore means that the interference of the H_2O_2 with intracellular signalling will have a lessened effect.

Following these experiments it was deduced that regardless of the bacterial species or strain used, or the stage of growth at which the H_2O_2 was addd, the addition of 2 mM of H_2O_2 would not inhibit the formation of biofilms on its own, and thus the ihibition of biofilm formation would be due to the addition of ARS.

2.4.9 Addition of H_2O_2 and ARS to a Biofilm at the Lag Phase

Next, the combination therapy of 2 mM H_2O_2 with two different concentrations of ARS (50 and 100 μM) was tested at each stage of growth.

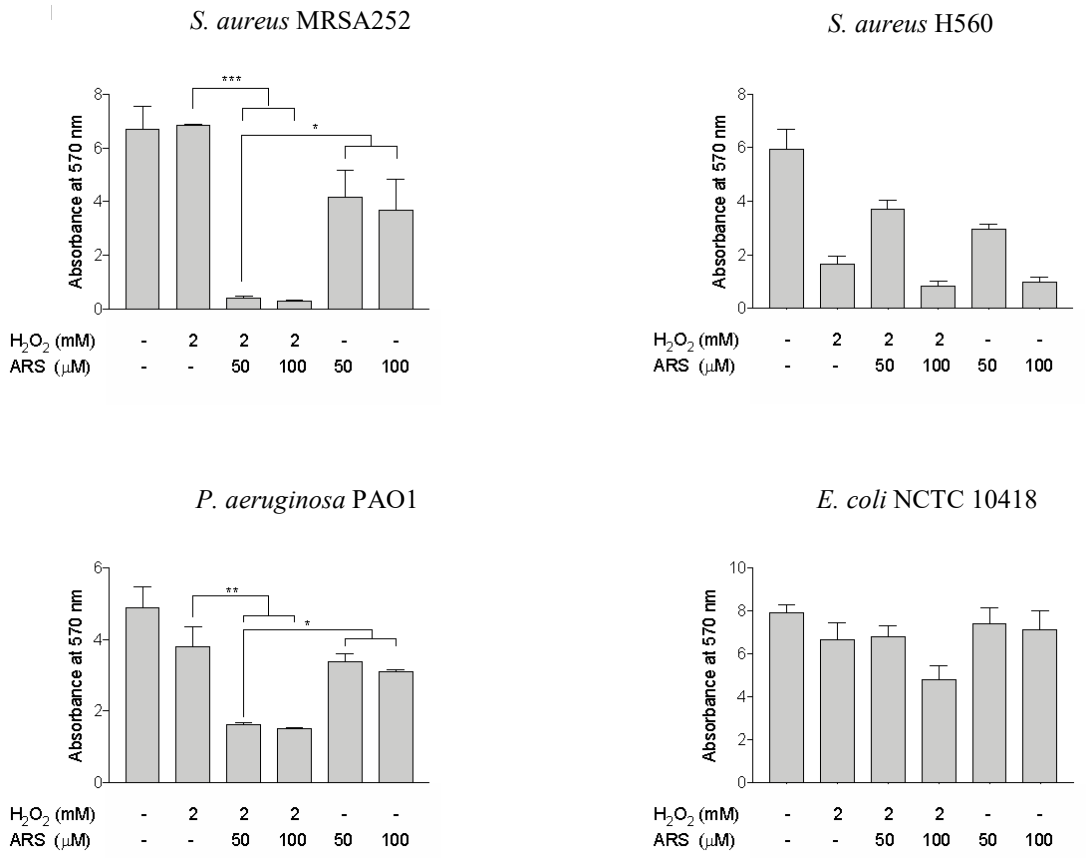

Figure 29 Absorbance at 570 nm of crystal violet, correlating to the amount of biological material present (and thus amount of biofilm formation), with the addition of H_2O_2 (2 mM) and ARS (0 – 100 μM) at the lag phase. Data plotted as the mean, n = 3. Error bars indicate standard deviation.Statistical significance calculated using a one way anova

The lag phase was the only phase at which the addition of ARS caused a statistically significant decrease in biomass for any of the bacteria, compared to using the 2 mM H_2O_2 on its own. This

indicates that the ARS is having an effect on the bacteria; either preventing the uptake of nutrients, or interfereing with the production of metabolites that are essential to the formation of biofilms. Its lack of effect on the rapidly dividing exponential phase is indicative that it is not interfering with any intercellular signalling pathways. Similarly to H_2O_2 having no effect on the biofilm forming ability of the bacteria at the stationary phase due to them already having formed the biofilm, it is unsurprising that the ARS follows this trend.

As can be seen from figure 29 there was a significant decrease in the biofilm formation of both *S. aureus* MRSA252 and *P. aeruginosa* PAO1. Why this did not effect the other two bacteria is unknown, however it is possible that it is due to differences in the signalling molecules produced by each strain that triggers the biofilm formation between the species. Whilst this seems to not explain why the two *S. aureus* strains would be different, the mechanisms by which MRSA 252 resists antibiotics may offer protection from the H_2O_2 in some manner, increasing its biofilm fitness.

2.4.10 Testing the Gel System with Biofilm Inhibition

Whilst the ARS had initially only been intended as a model system for a drug release, the above data shows it's potential utility as a stand alone, triggered anti-biofilm agent release system. To prove this, the biofilm inhibition experiment was repeated using lag phase *S. aureus* MRSA252, but using gel excudate as opposed to a solution of ARS. A PBA gel loaded with 0.25 mM ARS was incubated with 2 mM of H_2O_2 for 3 hours, and the resultant this solution was used to assess biofilm inhibition, figure 30.

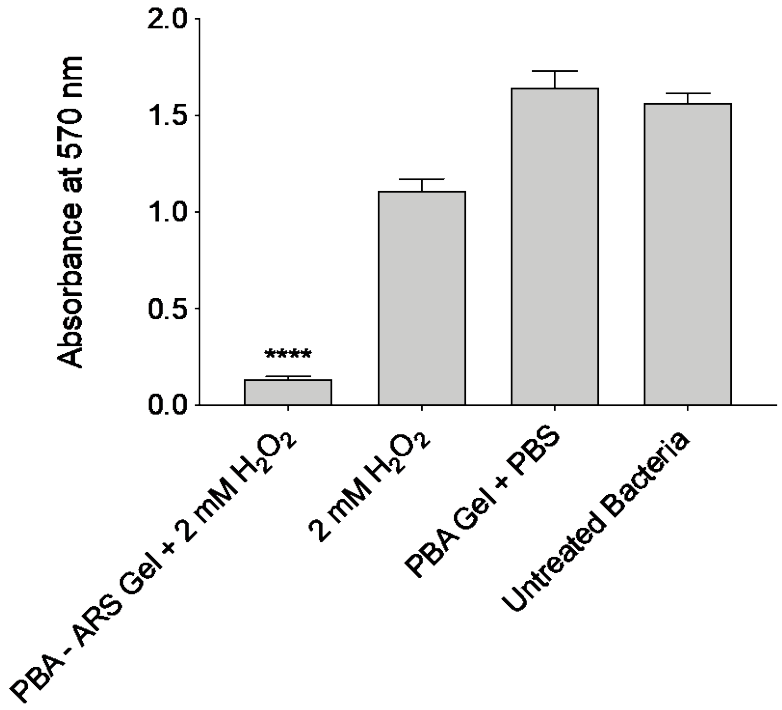

Figure 30 The statistically significant decrease in absorbance at 570 nm (correlating to biofilm formation) by addition of excudate from an ARS loaded gel incubating in 2 mM H_2O_2 when compared to controls of H_2O_2 and a blank PBA gel in H_2O_2. Data plotted as the mean, n = 3. Error bars indicate standard deviation.Statistical significance calculated using a one way anova

As can be seen above there is a large reduction in absorbance, correlating with reduced biofilm biomass, when the bacteria are exposed to the gel excudate triggered by 2 mM of H_2O_2 when compared to 2 mM of H_2O_2 as a single treatment. This shows that ARS is effective as a biofilm inhibitor.

2.5 Conclusions

Two different boronic ester containing acrylamide monomers have been synthesised, and subsequently polymerised into boronic ester functionalised polyacrylamide hydrogels. Both PBA and BOB gels have been shown to be able to bind to a diol containing dye (ARS), and then release it in response to the addition of hydrogen peroxide in a dose dependent manner. It was also shown that the release of ARS could be similarly triggered with the use of plasma treated buffer, the amount of the release again correlating to the duration of the plasma treatment. If this is to be translated into a working direct plasma treatable system, then a new gel layering system must be found. This offers immediate use as a solid state reaction based indicator of hydrogen peroxide concentration, but also as a model for a drug release system. Additionally, Alizarin Red S has been found to have biofilm inhibitive activity, which was independent of its co-administration with H_2O_2.

2.6 Future Work

Aminoglycosides are a large class of antibiotics, with varying solubilites and efficacies. One such antibiotic is kanamycin, figure 31.

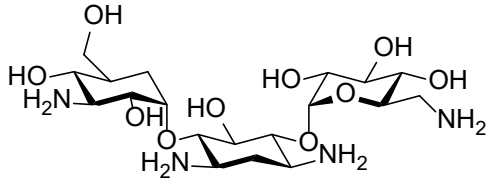

Figure 31 The Aminoglycoside Kanamycin

Kanamycin is an antibiotic that is prescribed for a number of infections, historically it was used to treat tuberculosis, however *Mycobacterium tuberculosis* strains are gaining resistance.[21] The sugars that make up the aminoglycosides offer a number of 1,2 and 1,3 diols, which are attractive sites for the binding of boronic acids. Whilst the catechol featured in ARS offers a higher affinity of binding to the PBA moiety, simple sugars have already been shown to preferentially bind to benzoxaboroles. This could mean that the BOB containing gels could offer a triggered release system mirroring the ARS release from PBA, but with the release of an antibiotic. Kanamycin is a convenient drug to begin testing with owing to its high solubility in water. Much like ARS being used as model system to monitor release, it would be convenient to be able to do the same with this follow up work. A dye that could be used was developed by Maria Odyniac of the James group at the University of Bath. It is fluorescein derived and features a boronic acid functionality as well as a glucose bound via an ether on the other hydroxyl group, figure 32.

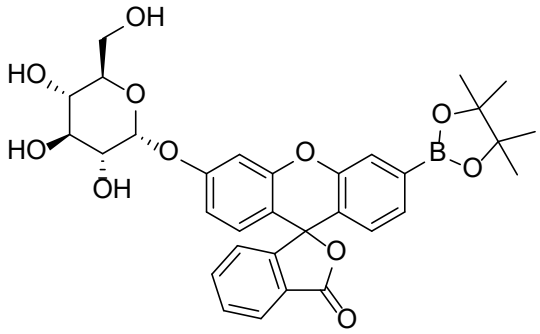

Figure 32 Fluorescein functionalised by glucose and BPin

Originally designed as an and/or logic gate sensor for glucosidase enzymes and hydrogen peroxide, this probe will mimic the binding of the sugars of the aminoglycoside to the boronic acid

containing gels. The compound is colourless and non-fluorescent. On exposure to either the enzyme or H_2O_2 it exhibits a colour change and an increase in fluorescence, with increased fluorescence and colour intensity upon exposure to both external stimuli.

Initial experiments using PBA (owing to material constraints) containing gels showed the ability of the dye to bind to the gels, with subsequent release and activation of fluorescence when exposed to H_2O_2 figure 33 This was performed following the methods used for ARS; however, a lower loading concentration (0.1 mM) of dye was used owing to its large fluorescence intensity.

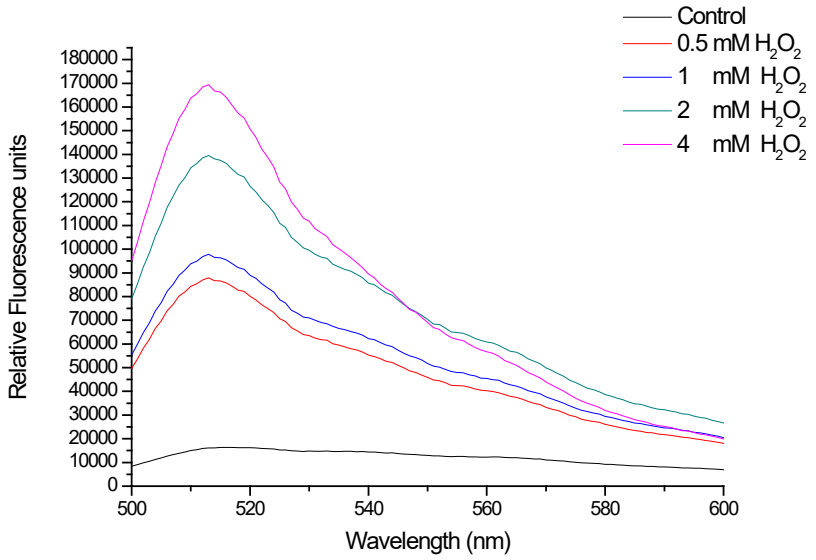

Figure 33 A dose dependent increase of fluorescence due to addition of H_2O_2 (0.5 – 4 mM) to Glucose-Fluorescein-BPin bound PBA gel

Following this, to ensure that there would be binding of the kanamycin a simple dye displacement assay performed with ARS. Briefly, ARS loaded PBA gels were made and then subsequently exposed to differing concentrations of kanamycin. This shown that the drug will bind to the PBA gel figure 34. Whilst the binding is only slightly increased compared with the blank, this is owing to the equilibrium nature of the binding. In a purely kanamycin loaded gel there will be no competition from the ARS; the ARS due to its catechol will likely bind to the PBA more strongly than the kanamycin.

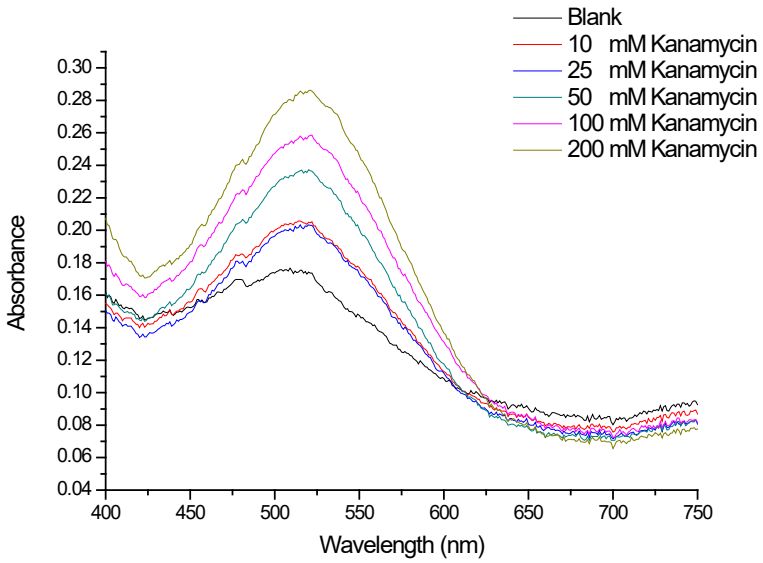

Figure 34 Increasing absorbance at 525 nm due to the increasing concentration of ARS in solution due to displacement from the addition of different concentrations of kanamacyin (0 – 200 mM)

As the concepts of the release of the drug from this system have been proved to work, the next step is to measure the difference in preference of binding of the kanamycin to either the PBA or the BOB gels, and to then look at testing the system with live bacteria to see if kill can be achieved. If sufficient concentrations of drug can be released on application of H_2O_2, then the dual release of the kanamycin and ARS should be investigated.

2.7 Bibliography

1. W. L. A. Brooks and B. S. Sumerlin, Chemical Reviews, 2016, 116, 1375-1397.

2. B. Marco-Dufort and M. W. Tibbitt, Materials Today Chemistry, 2019, 12, 16-33.

3. Y. N. Wang, L. Li, Y. Kotsuchibashi, S. Vshyvenko, Y. Liu, D. Hall, H. B. Zeng and R. Narain, Acs Biomaterials Science & Engineering, 2016, 2, 2315-2323.

4. N. Argarate, B. Olalde, G. Atorrasagasti, J. Valero, S. C. Cifuentes, R. Benavente, M. Lieblich and J. L. Gonzalez-Carrasco, Materials Letters, 2014, 132, 193-195.

5. E. Calo and V. V. Khutoryanskiy, European Polymer Journal, 2015, 65, 252-267.

6. X. Chen, F. Li, L. L. Feng, L. Yu and J. D. Ding, Journal of Biomedical Nanotechnology, 2017, 13, 1357-1368.

7. D. Tarus, E. Hachet, L. Messager, B. Catargi, V. Ravaine and R. Auzely-Velty, Macromolecular Rapid Communications, 2014, 35, 2089-2095.

8. Y. Guan and Y. J. Zhang, Chemical Society Reviews, 2013, 42, 8106-8121.

9. V. Lampard Emma, C. Sedgwick Adam, T. Sombuttan, T. Williams George, B. Wannalerse, A. T. A. Jenkins, D. Bull Steven and D. James Tony, ChemistryOpen, 2018, 7, 266-268.

10. N. Rabin, Y. Zheng, C. Opoku-Temeng, Y. X. Du, E. Bonsu and H. O. Sintim, Future Medicinal Chemistry, 2015, 7, 647-671.

11. J. H. Lee, Y. G. Kim, S. Y. Ryu and J. Lee, Scientific Reports, 2016, 6, 11.

12. S. K. Shukla and T. S. Rao, Colloids and Surfaces B-Biointerfaces, 2013, 103, 448-454.

13. N. C. Caiazza and G. A. O'Toole, Journal of Bacteriology, 2003, 185, 3214-3217.

14. D. Calloway, Journal of Chemical Education, 1997, 74, 744-744.

15. K. Anzai, T. Aoki, S. Koshimizu, R. Takaya, K. Tsuchida and T. Takajo, Journal of Clinical Biochemistry and Nutrition, 2019, 64, 187-193.

16. A. Khlyustova, C. Labay, Z. Machala, M. P. Ginebra and C. Canal, Frontiers of Chemical Science and Engineering, 2019, 13, 238-252.

17. B. L. Patenall, G. T. Williams, L. Gwynne, L. J. Stephens, E. V. Lampard, H. J. Hathaway, N. T. Thet, A. E. Young, M. J. Sutton, R. D. Short, S. D. Bull, T. D. James, A. C. Sedgwick and A. T. A. Jenkins, Chemical Communications, 2019, 55, 15129-15132.

18. G. A. O'Toole, Jove-Journal of Visualized Experiments, 2011, 3.

19. T. Das, S. Sehar, L. Koop, Y. K. Wong, S. Ahmed, K. S. Siddiqui and M. Manefield, Plos One, 2014, 9, 11.

20. H. Li, X. Li, C. Song, Y. Zhang, Z. Wang, Z. Liu, H. Wei and J. Yu, Frontiers in Microbiology, 2017, 8, 9.

21. G. J. Alangaden, B. N. Kreiswirth, A. Aouad, M. Khetarpal, F. R. Igno, S. L. Moghazeh, E. K. Manavathu and S. A. Lerner, Antimicrobial Agents and Chemotherapy, 1998, 42, 1295-1297.

3 PBA Functionalised Drugs

3.1 Introduction

3.1.1 Prodrugs

The term "prodrugs" refers to drugs that are inactivated or masked and become re-activated in-situ.[1] This can be either through a chemical or an enzymatic (biochemical) reaction, which for compounds with poor pharmacokinetic properties can increase their bio-availability.[2] For drugs with inherently poor aqueous solubility this is of particular use; addition of polar groups such as phosphate esters can increase in water solubility, well exemplified by the antibiotic Clindamycin phosphate, figure 1. Clindamycin has poor solubility in water, but the highly charged phosphate group makes the molecule more hydrophilic, and is then removed *in vivo.* Approximately 20% of all drugs approved between 2000 and 2008 were prodrugs, demonstrating the utility of this method.

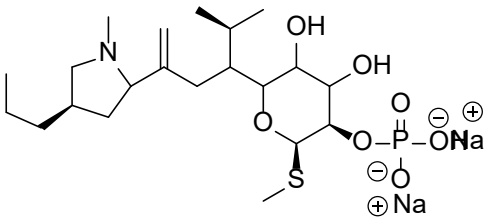

Figure 1 Clindamycin Phosphate

The design of a prodrug should include a promoiety. This component of the prodrug prevents its activity, and is subsequently removed *in vivo*. Prodrugs of even common drugs such have aspirin have been synthesised in attempts to improve their pharmacokinetic profile.[3]

Upon the co-administration of two or more drugs, and the subsequent drug-drug interactions, the drugs can inactivate eachother. They are acting as promoieties to each other. These are known as codrugs.[4] An example of a co-drug is Ro 23-9424 produced by Jones *et al*., a combination of fleroxacin and desacetylcefotaxime, figure 2. It displays greater efficacy than it's individual components, displaying activity against hard to treat fluoroquinolone and beta-lactam resistant bacteria strains.[5]

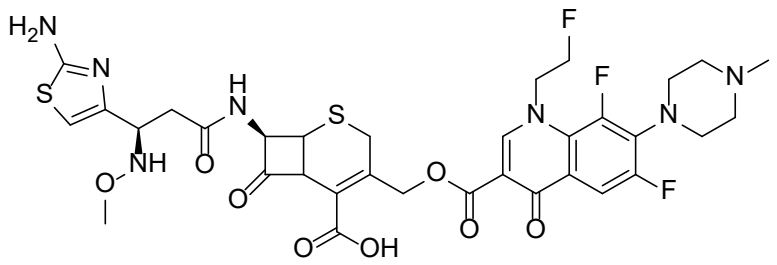

Figure 2 Ro 23-9424, a codrug formed from Fleroxacin and Desacetylcefotaxime

It is the through action of bacterial esterases and lipases that the drugs reactivate, with hydrolysis of the ester between the two drug molecules.

3.1.2 ROS Responsive Prodrugs

Prodrugs and polymer-drug conjugates have been used extensively in cancer chemotherapies.[6, 7] Owing to the increased concentrations of ROS in tumours, ROS sensitive pro-drugs have been developed. This drive in creating prodrugs is due to the fact that several current cancer therapies are equally as damaging to healthy cells as they are to cancer cells, leading to a myriad of side effects and ill health associated with these treatments. ROS dependent prodrugs attempt to mask the toxicity of the active compound, only activating on exposure to the high oxidative stress within tumours. In simplistic terms cellular oxidative stress can be considered an increased ROS concentration. A number of these prodrug are boronic or boronate ester based.[8] One such drug is a mustard gas derivative developed by Kuang *et al.* Mustard gas agents are able to crosslink strands of DNA causing cell death, but are not specific to cancer cells.[9] With the addition of a phenyl boronate ester on the nitrogen of mechlorethamine, a large reduction in toxicity to mammalian cell lines was achieved; upon addition of H_2O_2, as per a tumour environment, the activity of the drug was restored and with it, its toxicity to cells, figure 3.

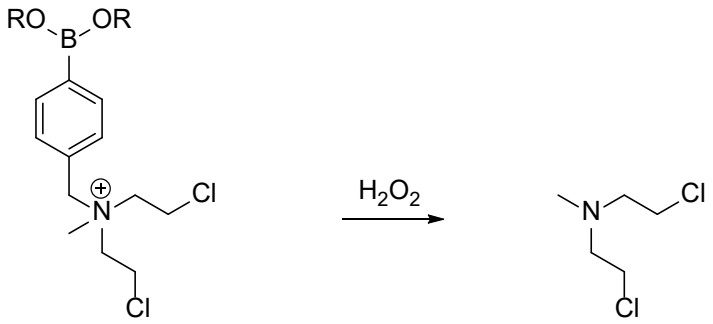

Figure 3 The re-activation of a phenyl boronic ester masked mustard gas prodrug by hydrogen peroxide

These drugs serve a two-fold effect; not only do they provide a method by which to only activate in proximity to tumour environments, they are also able to 'mop-up' some of the excess ROS which can cause oxidative stress, and thus reduce damage to healthy cells.

3.1.3 Antibiotic Prodrugs

With the increasing costs associated with the development of novel therapies, the ability to mask toxicity, or increase cell permeability of previously discarded drugs is a huge advantage, especially within antimicrobial therapy.[10] Commonly used activating groups in the design of antibiotic pro-drugs are ester groups. Bacteria specific esterase enzymes can be used as a target; a drug will have its polar ester group converted into a non-polar ester, increasing penetration through the bacterial membrane, before being activated by intracellular enzymes back into the active form of the drug.[11] An example of such a strategy is shown in figure 4. Clayton *et al.* used the addition of tertiary butyl esters to ampicillin, yielding the pro-drug pivampicillin. Now used in clinic, pivampicillin features increased lipophilicity, and thus crosses cell membranes more readily.[12]

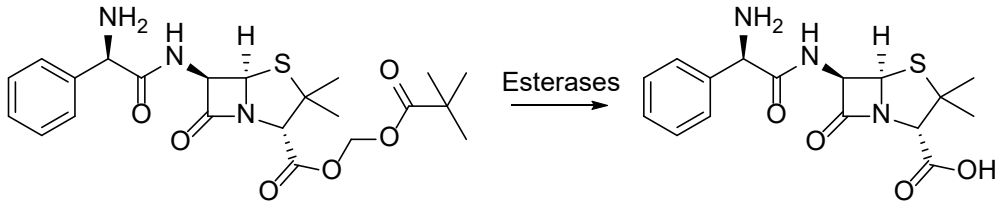

Figure 4 The esterase catalysed removal of a tertiary butyl ester to form ampicillin from pivampicillin

This chapter aimed to develop a hydrogen peroxide activated prodrug, and utilise boronic acid/diol binding to develop a drug that could be inactivated while bound to a PVA gel, with activation via topical application of H_2O_2. Whilst such work has been done for the treatment of tumours, to the

best of the authors knowledge, this is the first example of either an antimicrobial drug being used in this manner, or topical application of H_2O_2 being used as a trigger for drug release.

3.2 Aims

This project aimed to develop synthetic methodologies in order to functionalise existing antimicrobial compounds with a boronic acid or a boronic ester, which will subsequently be bound to PVA via a cyclic boronic ester. This formed boronate ester could be bound either directly to the molecule to yield a phenol upon oxidation, or through a linker such as PBA. Upon exposure to H_2O_2, the boronic acid/ester 'anchor' gets oxidised, releasing and simultaneously activating the drug, figure 5. It was hoped that these drugs would be released from the gel and restored to their active form in high enough concentrations to inhibit the growth of bacteria, with minimal non-triggered bacterial killing.

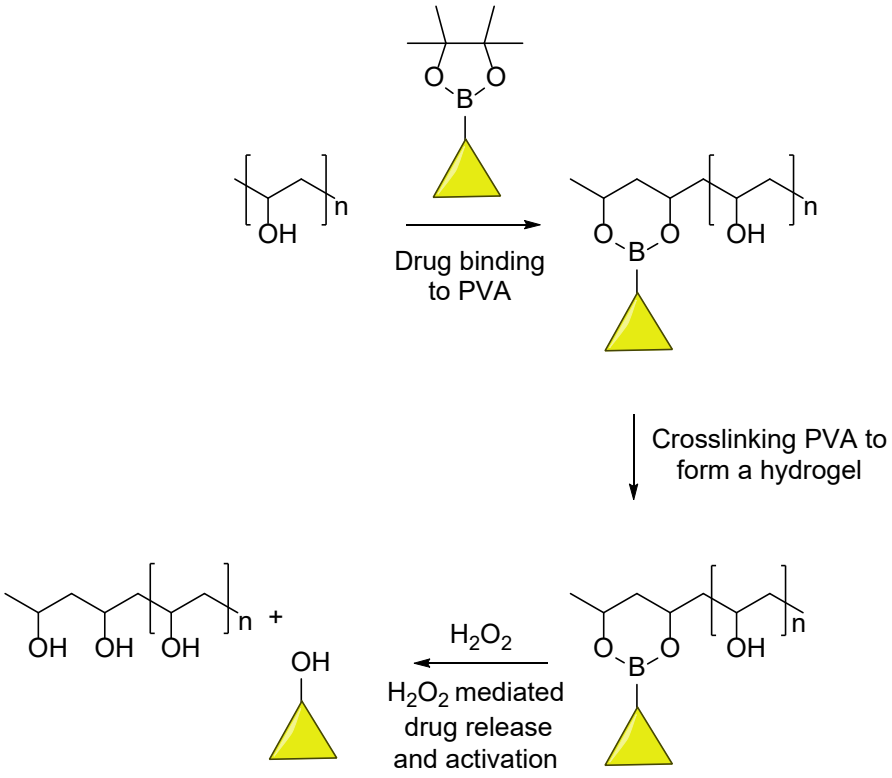

Figure 5 A general representation the release and oxidative activation a boronic ester masked prodrug

3.3 Materials and Methods

3.3.1 General Information

All solvents and reagents were purchased from commercial suppliers and used without further purification unless otherwise noted. Analytical thin-layer chromatography (TLC) was performed using commercial precoated silica gel plates containing a fluorescent indicator. Column chromatography was carried out using silica gel (0.040 - 0.063 mm). Analytical thin-layer chromatography (TLC) was performed using commercial precoated silica gel plates. Proton and carbon NMR were recorded using a Bruker Advance 500. Chemical shifts are reported in ppm using TMS or solvent residual signals as internal reference standards. High-resolution mass spectrometry (HRMS) were performed on an Agilent 6545 LC/Q-TOF. UV-Vis and fluorescence measurements were performed on a BMG Labtech CLARIOstar using costar u bottom 96 well microplates or Greiner Bio-One microplates (96-well, PS, f-bottom (chimney well), black-walled) respectiely. Data was collected via the BMG Labtech Clariostar data analysis software package MARS. AzuFluor 483-Bpin™ was prepared by L C Murfin of the Lewis group in the University of Bath.

Synthetic experimental information can be found in Chapter 6.2.

3.3.2 Blank Gel Synthesis

PVA (mw 13,000 – 23,000 kDa) was dissolved in DMSO to form a 10% w/v solution. Solutions of the crosslinker, 1,4 benzene bis-boronic acid, were prepared to achieve a final concentration of 100 mM in DMSO. Aliquots of the PVA solution (0.5 mL) were combined with the crosslinker solution (0.5 mL), and spontaneous gelation occurred at room temperature. The resultant hydrogels were washed in PBS (3 mL overnight) and then stored in PBS until used.

3.3.3 Drug/Dye Loaded Gel Synthesis

Drug loaded gels were synthesised as outlined in Chapter 3 1.3.2 with one modification. Drug-PBA conjugates were dissolved in the 10% w/v PVA solution (in DMSO) at the desired concentration before mixing with the crosslinker using a pipette tip.

3.3.4 Dye Release Studies

Azufluor 483-Bpin™ loaded gels were synthesised as in 3.3.3. Gel pieces of mass 200 mg ± 10 mg were cut with a scalpel, and incubated in either PBS, 0.5 mM H_2O_2 or 1 mM H_2O_2. The fluorescence of the resulting solutions was measured, Ex 350 – 20 nm, Em 450 – 550 nm.

3.3.5 Gel Disc Diffusion Assay

Gel discs (both with and without the addition of a pro-drug) with a diameter of 9 mm (±1 mm) were prepared as described in the above methods 3.3.3 and 3.3.4, lawns were prepared by spreading 500 µL of bacterial culture (grown in accordance with 2.3.9), using a sterile plastic spreader. Drug-loaded gel discs was subsequently placed in the centre of the plates. Next, 100 µL of H_2O_2 (1 mM) or PBS (serving as a triggered-release control) were added to the surface of the gels before incubation at 37 °C for 18 hours. Further control experiments were conducted using blank gels exposed to either the test condition (H_2O_2) or control condition (PBS) to ensure the gel and H_2O_2 had no effect on bacterial growth. Each condition was repeated using three biological replicates. After incubation, the diameter of the zone of inhibition was then measured in millimetres and plotted as the mean ± SD.

3.3.6 Modified Gel Disc Diffusion Assay

Drug loaded gels were incubated with either a 2 mL solution of H_2O_2 (1 mM) or PBS for 3 hours. Subsequently, sterile paper discs were loaded with 100 µL of gel exudate and placed onto bacterial lawns as prepared in 3.3.5. The plates were then incubated at 37 °C for 18 hours, and measured as outlined above in 3.35. Each condition was repeated using three biological replicates.

3.4 Results and Discussion

3.4.1 Dye Release Studies with AzuFluor 483-Bpin™

The use of a dye as a model system for drug release can avoid the use of labour intensive microbiological experiments. To be representative of the drugs binding, the dye had to contain a single Bpin group which would enable it to be bound into a PVA hydrogel, and subsequently released with the addition of H_2O_2. The chosen dye was an azulene based sensor produced by the Lewis group in Bath named AzuFluor 483-Bpin™, figure 6.[13]

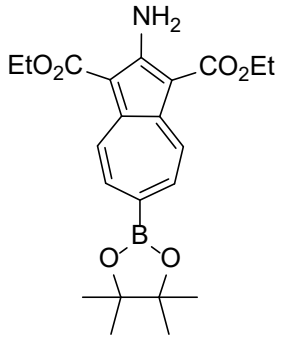

Figure 6 The azulene based fluorescent sensor, AzuFluor 483-Bpin™, produced by the Lewis group at the university of Bath

Azulene compounds are bicyclic isomers of naphthalene featuring a 5 and a 7 membered ring as opposed to two six membered rings. Unfunctionalised, they are a dark blue colour, yet by adding functionality and changing electron density in certain positions, a number of different coloured compounds can be formed.[14] These have found use in a number of sensing applications, as perturbation of the electronic system can lead to large chromic shifts in its absorbance spectrum.

AzuFluor 438-Bpin™ shown above in figure 6 is oxidised to the corresponding phenol on exposure to H_2O_2. This results in a shift in its absorbance maximum and a large increase in fluorescence, figure 7.

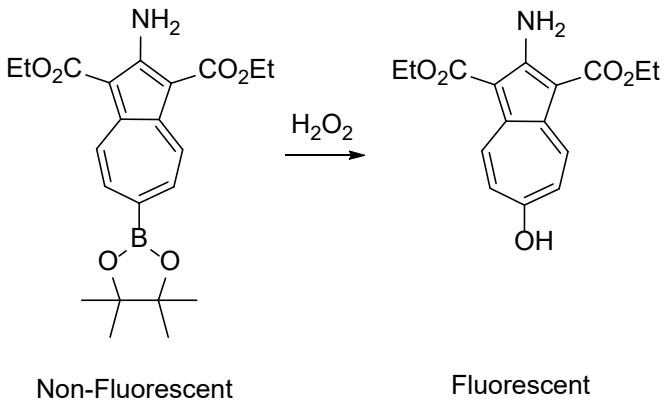

Figure 7 The oxidation of the boronic ester on AzuFluor 438-Bpin™ to its corresponding phenol generating the highly fluorescent active species

The fluorescent dye can bind to the diols within the PVA hydrogel through the formation of a 6-membered cyclic boronic ester. On addition of H_2O_2 to these gels the boronic ester bond should oxidise, turning on fluorescence, figure 8.

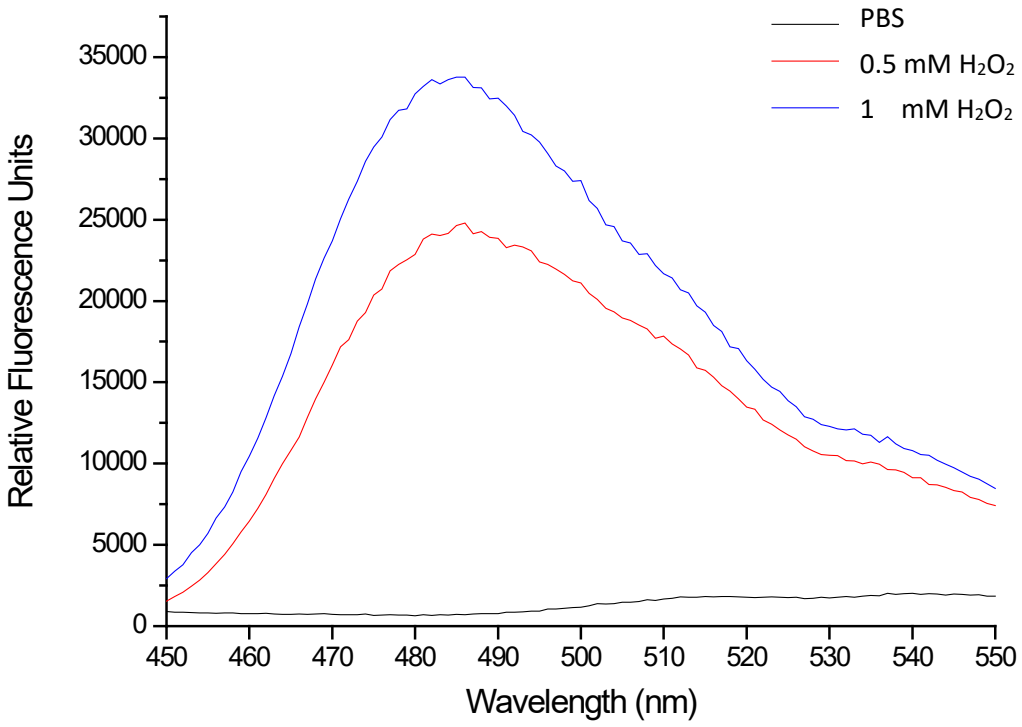

Figure 8 An increase in fluorescence at 485 nm due to the oxidation of the Azufluor 438-Bpin™ bound to PVA into it fluorescent form due to exposure to H_2O_2 Ex 350 – 20 nm, Em 450 – 550 nm

As can be seen from the above data, figure 8, there is a H_2O_2 concentration dependent fluorescence increase of the AzuFluor 438-Bpin™ doped PVA hydrogel. This indicates that there has been oxidative release of the dye and activation of the fluorophore; this shows the potential for the gel as a drug delivery system.

3.4.2 Anchoring Drugs to Hydrogels

A number antimicrobial compounds that can be found on the World Health Organisation's (WHO's) list of essential medicines contain phenols, including amoxicillin and chlortetracycline, figure 9.[15] If boronic ester containing analogues of a phenol containing antibiotic were to be synthesised it would produce a pro-drug activated by ROS/RNS.

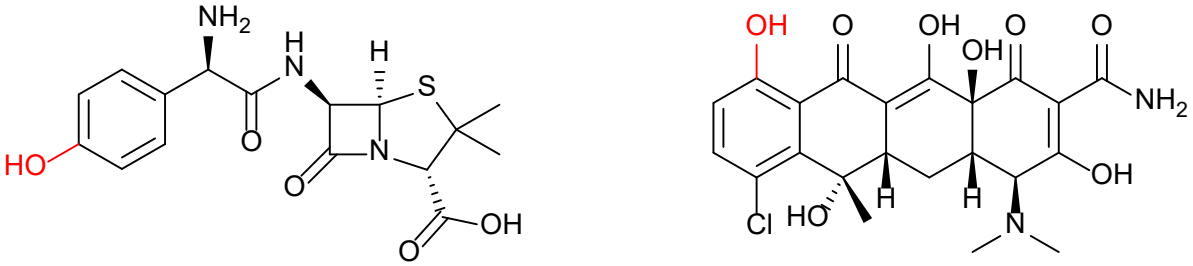

Figure 9 *Left* Amoxicillin, *Right* chlortetracycline

The selective transformations required to make the boronic acid containing analogues could be synthetically very challenging, owing to a number of potential groups that could be functionalised, for example the carboxylic acid on the amoxicillin or the numerous hydroxyl groups on the tetracyclines. Although precursors such as bromo-amoxicillin are commercially available, which would only require a single Miyuara borylation, they come at a vast expense (~ \$5000 g^{-1}).

In order to navigate these synthetic hurdles, a PBA linker can be used. As shown in figure 10 upon oxidation to the phenol, the linker will undergo a 1,4 elimination, yielding the original drug product, boric acid and paraquinone methide. This is hugely advantageous as it increases the number of the therapeutic agents that can be used, as synthetically the only requirement is that the drug has a functional group of either an acid, an alcohol or an amine.

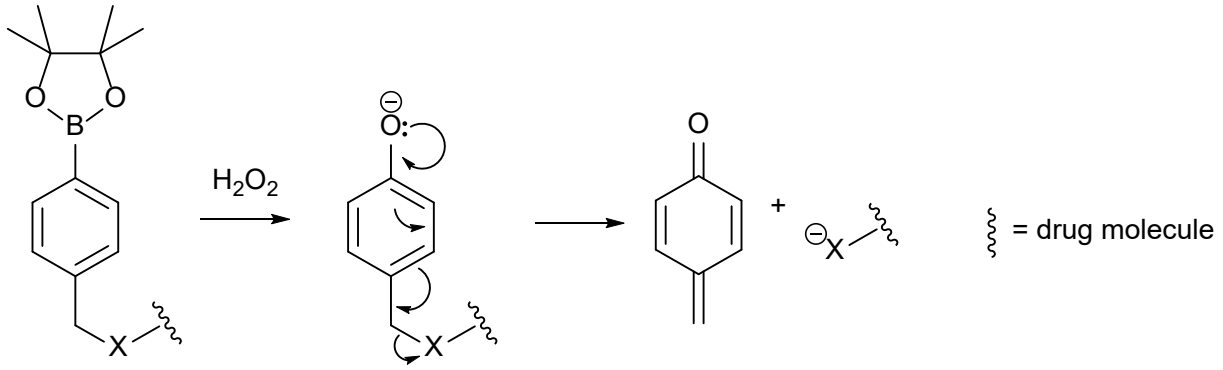

Figure 10 The initial oxidation of the boronic pinnacol ester to the phenolic anion, and the subsequent 1,4 elimination of paraquinone methide with the reformation of a drug. X = O or N

The quinone methides are conjugated non-aromatic analogues to quinones, but with an oxygen atom replaced with a carbon atom. The para,1,4 quinone methide offers the greatest stability owing to the zwitterionic resonance form featuring an electron donating para O^-,[16] as shown in figure 11.

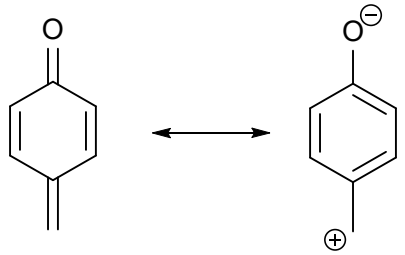

Figure 11 The resonance stabilised zwitterionic form of para quinone methide

These simple quinone methides tend to be short lived, as they are highly reactive under a wide variety of conditions. They are very susceptible to nucleophilic attack as well as reduction, which is driven by the fact that on reduction, re-aromatisation can occur. The biological effects of these molecules have been studied in detail, due to their prevalence as intermediate metabolites in various biological pathways. Their presence has been linked to toxicity through a number of pathways, and are the central active core to a number of anti-cancer drugs. Testing on endothelia cell lines would thus need to proceed this linkers use as part of a topical system.[17, 18]

The initial task was to produce a drug molecule bearing this H_2O_2 sensitive phenyl boronic acid linker. Phenol containing antibiotics were the first to be considered; a commonly prescribed antibiotic with this functional group was amoxicillin, figure 12.

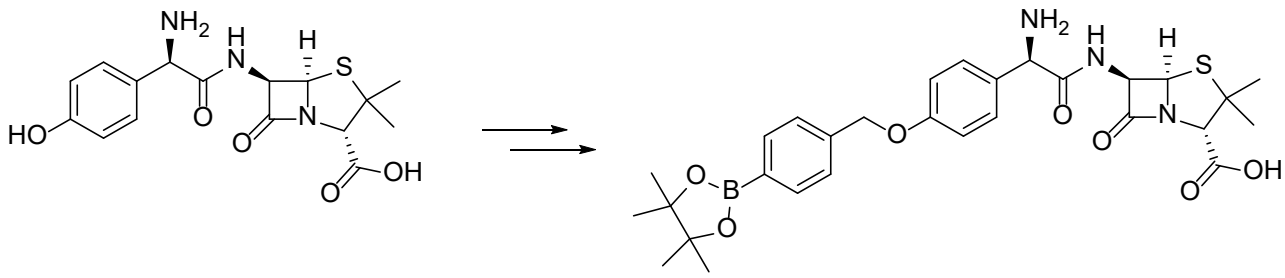

Figure 12 Amoxicillin and its proposed PBA derivative

Initially an ether synthesis was attempted, however resulting NMR spectra showed a large number of peaks indicative of a compound degrading. Following literature searches, the alkylation at the phenolic hydroxyl group would have been problematic owing to the instability of the lactam ring to hydrolysis; as a result, industrial synthesis utilises enzymatic processes.[19]

3.4.3 Synthesis of Triclosan-PBA

As functionalising clinically relevant antibiotics were found to be synthetically challenging, attention was turned to finding a relevant active molecule that would be easy to functionalise as a proof of concept.

Triclosan, figure 13, is an antimicrobial, used in antiseptics and in toiletries (*i.e.* toothpaste, soaps) owing to its activity towards *S. aureus* as well as a number of other bacterial species. This has led to concerns over it developing resistance, culminating in the banning of its use in the USA. However, as this was a proof of concept study, triclosan was deemed suitable for use, with the aim to expand to more clinically relevant antibiotics in the future.[20]

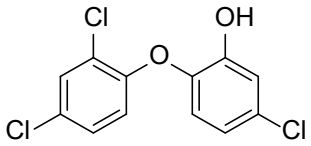

Figure 13 The antiseptic triclosan

As can be seen in figure 13 triclosan features a phenolic hydroxyl group and no other overtly reactive groups. Therefore, there is no need to introduce any protecting steps, or any complex chemistries.

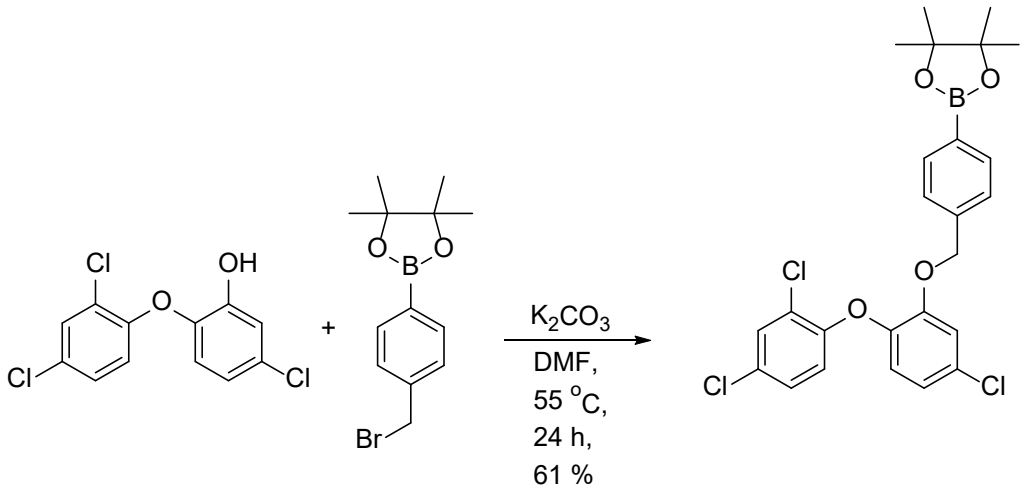

Figure 14 The reaction of the bromo-benzyl phenyl boronic acid linker (PBA-Br) with base and triclosan to yield triclosan ether bound to the benzyl linker with boronic acid functionality

The reaction shown in figure 14 gave yields of over 80%, with no discernible loss in yield or in crude purity when the reaction as scaled up to over a gram.

To ensure that the addition of H_2O_2 decomposes the compound as expected, and the active antimicrobial is released, two solutions of the compound (50 μM in MeOH) were made, to one of which 1 mM of H_2O_2 in PBS was added, and to the other PBS was added. After one hour HRMS was performed on both compounds, confirming the release of the active triclosan in the solution of H_2O_2, but not in that of the PBS.

3.4.4 Crosslinking PVA Doped with Triclosan-PBA

Once the drug-PBA conjugate had been synthesised, the next step was to develop a gel system in which to bind it. The affinity of boronic acids and esters to 1,2 and 1,3 diols has been discussed previously in detail (1.9.1). Owing to this affinity, an obvious choice of polymer to use in this study was PVA due to the abundance of repeating 1,3 diols, as well as its proven biocompatibility.[21]

Previous work performed by the Sessler group utilised bis-boronic acid containing compounds for the crosslinking of PVA.[22] Whilst the aim of this work was for the preparation of an ^{-}OH anion capture gel, the chemistry behind the crosslinking was convenient for the applications of sensing and drug delivery. Most of the prior work within our group regarding the use of PVA has involved physical crosslinking using freeze thaw cycles. This, whilst possible in DMSO/water mixes,

requires extremely low temperatures (< -50 °C) and yields less stable gels. The triclosan-PBA conjugate has little solubility in aqueous solutions and will not stay in solution for mixes including even with 95% DMSO. However, both 1,4 benzene bis-boronic acid and PVA are soluble in DMSO, allowing for efficient gelation without the need for water. Following this, the PBA-drug conjugate could be mixed with the PVA solution in DMSO at the required concentration, with gelation achieved upon mixing both solutions, figure 15.

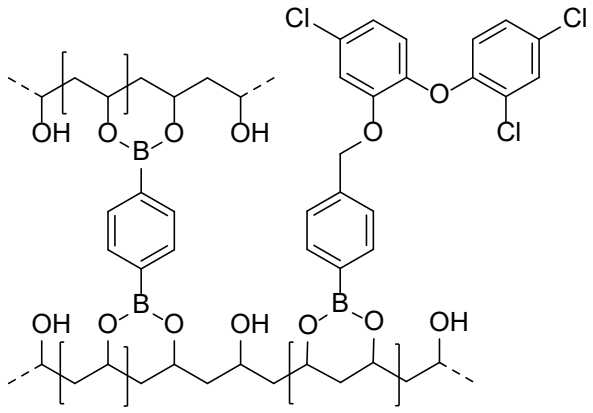

Figure 15 A schematic representation of a triclosan-PBA doped 1,4 benzene bis-boronic acid crosslinked PVA hydrogel

It was a considered that the large triclosan molecule between the polymer chains could interfere with the crosslinking, however despite this steric hindrance, a stable gel was able to be formed, as shown in figure 16.

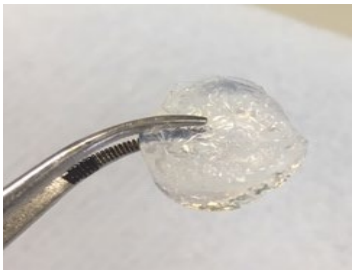

Figure 16 A 1,4 benzene bis boronic acid crosslinked PVA gel , doped with 1 $mgml^{-1}$ of the triclosan conjugate

Triclosan was loaded into the gel at concentrations up to 20 mg ml^{-1}, far above the reported MIC values.[23] This was to ensure that clear zones of inhibition could be seen in preliminary studies as it was unknown if the gel density would inhibit diffusion of the drug out of the gel once the boronic

acid had been oxidised. Additionally, at all concentrations of triclosan tested, the gels formed near instantaneously and with adequate mechanical strength.

3.4.5 Disc Diffusion Assays with Triclosan-PBA

The re-activation and subsequent release of the triclosan from the gel matrix was tested using a modified disc diffusion assay. While a standard disc diffusion assay involves the use of a sterile paper disc inoculated with an antimicrobial solution, in this modified version a gel disc of 9 mm (± 1 mm) was placed in the centre of an inoculated agar plate. To determine the triggered release, triclosan doped gels (1 mg mL^{-1}) were either treated with H_2O_2 (100 µL, 1 mM), or PBS and left to incubate for 18 hours. The zones of inhibition produced by both conditions were compared with themselves, and to that of further controls (blank gels with and without treatment of 1 mM H_2O_2). These controls were to ensure that the zones of inhibition were due to the release of triclosan, and not due to the addition of H_2O_2 or the gels themselves. The experiment was performed using three separate bacterial species: *P. aeruginosa* PA01*, S. aureus* H560 and *E. coli* NCTC 10418. They were chosen as the efficacy of triclosan against these species was known, and are all relevant pathogens in wound care.[24]

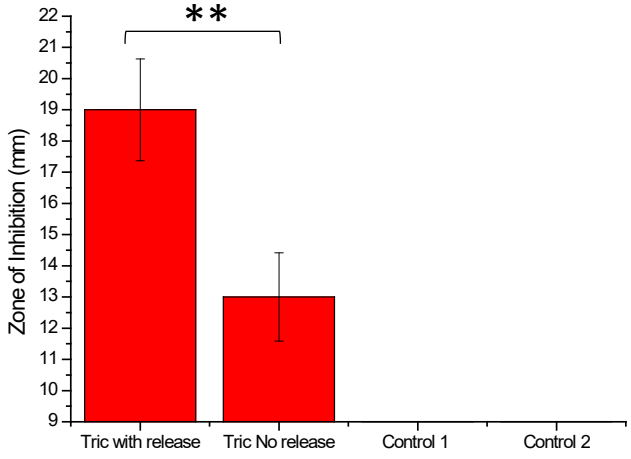

Figure 17 Calculated zones of inhibition (mm) for: triclosan loaded gels with H_2O_2 (100 µL, 1 mM), triclosan loaded gels with PBS (100 µL), blank gels with H_2O_2 (100 µL, 1 mM; control 1), and blank gels with PBS (100 µL; control 2) on a lawn of *S. aureus* H560. Data was plotted starting at 9 mm as this was the average diameter of the gel disc. Assays were performed three times, with results expressed as mean ± standard deviation. Statistical significance was determined by an unpaired t-test with ** $p < 0.01$

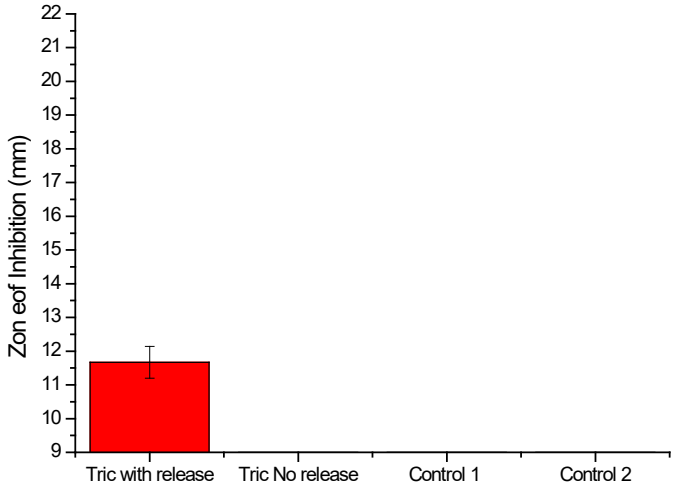

Figure 18 Calculated zones of inhibition (mm) for: triclosan loaded gels with H_2O_2 (100 µL, 1 mM), triclosan loaded gels with PBS (100 µL), blank gels with H_2O_2 (100 µL, 1 mM; control 1), and blank gels with PBS (100 µL; control 2) on a lawn of *E. coli* NCTC 10478. Data was plotted starting at 9 mm as this was the average diameter of the gel disc. Assays were performed three times, with results expressed as mean ± standard deviation

As expected, for both *S. aureus* H560 and *E. coli* NCTC 10418, there was a large zone of inhibition for triclosan loaded gels incubated with H_2O_2, and no noticeable inhibition attributed to the blank gels (both with and without treatment). Hence it can be inferred that any inhibition was due to the release of triclosan from the gels.

However, for *S. aureus* H560 it was noted that triclosan was also released when incubated with PBS, indicating the possibility of either passive release of triclosan, or the anchored triclosan retained some antimicrobial activity. The definitive way to test for such activity would be to do an MIC test of the conjugated triclosan. Unfortunately, the molecule itself is insoluble under aqueous conditions, solubility is only achieved in a DMSO/Water mix of over 20% DMSO, or 40% ethanol in an ethanol/water mix. This unfortunately prevents an MIC being undertaken as these solvent concentrations inhibit bacterial growth. Whilst it was tested, there was no inhibition of growth in any of the conditions with the bacteria *P. aeruginosa* PAO1. This is likely due to the widespread resistance to triclosan found in *P. aeruginosa* strains.[25]

3.4.6 Synthesis of Ciprofloxacin-PBA

Once the triggered release of the triclosan had been confirmed using microbiology, the next step was to synthesise a new drug, one that was of more clinical relevance and had a greater spectrum of activity; namely one that could treat both gram-positive and gram-negative bacteria. Previous searches for drugs had been aimed towards finding a phenolic alcohol group. It was realised at this stage that this was a needlessly limiting option, and that the same chemistries could be one applied to carboxylic acids and amines. This resulted in a large new source of potential drug candidates.

One of the most commonly prescribed antibiotics is the fluoroquinolone ciprofloxacin.[26] This is largely due to its wide spectrum activity, making it any easy drug choice for infections of which the cause may not be specifically known. Ciprofloxacin offers either a secondary amine or a carboxylic acid that can be functionalised with the PBA linker. It was decided that the acid would be the target of choice, owing to the ease in which amines can be protected and de-protected at near quantitate yields. Figure 19 shows the intended product and its oxidation by H_2O_2 into the active antibiotic.

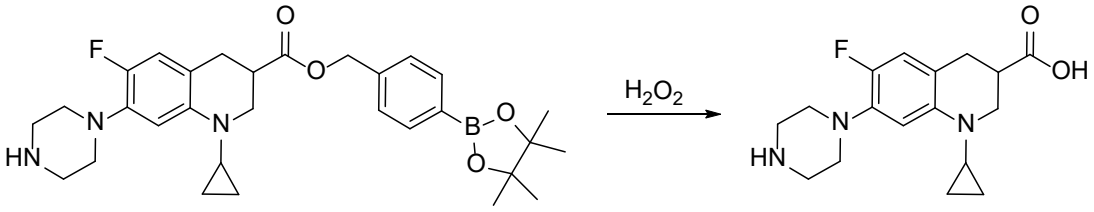

Figure 19 Ciprofloxacin-PBA conjugate and its subsequent oxidation into the original drug ciprofloxacin

The synthesis mimicked the conditions of a benzyl protection performed by Fardeau *et al.* in their work investigating the effects of binding catechol containing substituents to the amino group of ciprofloxacin.[27] The reaction itself was simple and featured acceptable yields. Both the starting material and product were of very similar polarity, and weren't highly soluble in common solvents used for column chromatography. Instead, a Soxhlet extraction was used using Et_2O.

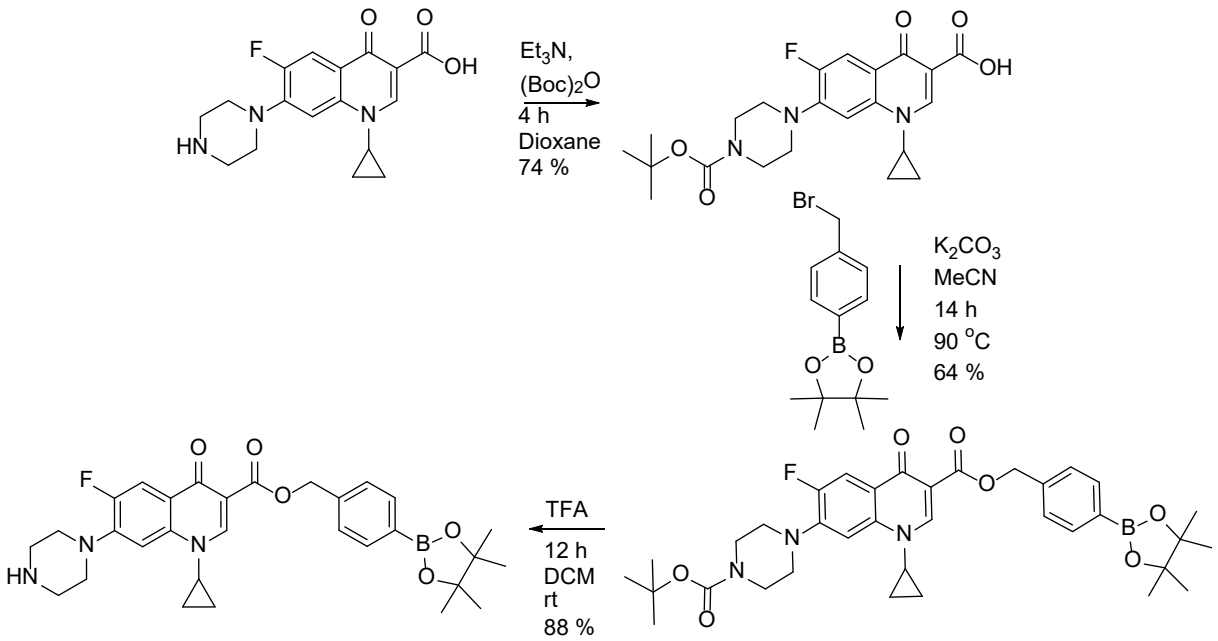

Figure 20 The overall synthesis of Ciprofloxacin-PBA

That ciprofloxacin contains both an amine and an acid means that it required protection steps within the synthesis. There was also concern that its larger size had the potential to impede the crosslinking utilising the 1,4 dibenzene crosslinker, but as with the triclosan and the AzuFluo 483-Bpin™ we were still able to form a solid gel. This offered evidence that this crosslinking method is tolerant to a range of molecules.

As with triclosan, the ciprofloxacin containing gel was exposed to 1 mM H_2O_2 in PBS and the exudate was analysed by HRMS. This confirmed the presence of the reformed ciprofloxacin.

Ciprofloxacin has an inherent fluorescence, and as a result concentration dependent fluorescence assays were performed to monitor release, figure 21. Ciprofloxacin's excitation is 270 nm with an emission max of 445 nm in water.[28] Owing to instrumental restrictions, the excitation wavelength used was 315 – 325 nm and an emission wavelength of 415-5 nm. Fluorescence could be observed at these wavelengths for a pure ciprofloxacin solution.

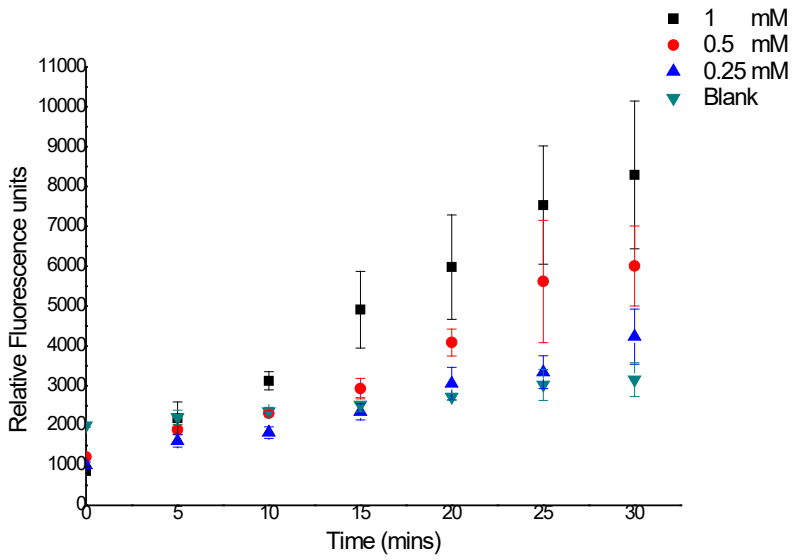

Figure 21 Dose dependent release of ciprofloxacin from a ciprofloxacin doped, 1,4 benzene bis-boronic acid crosslinked PVA hydrogel on exposure to different concentrations of H_2O_2 (0 -1 mM). Ex 315 – 325 nm, em 415-5 nm. Assays were performed three times, with results expressed as mean ± standard deviation

This preliminary data indicated that there was triggered release of ciprofloxacin, due to the rise in fluorescence intensity being 3-fold greater than that of the blank. However, the increase in fluorescence of the blank showed that a fluorescent compound was also being released by simple passive diffusion. Owing to the dynamic nature of the boronic ester diol bond, it is thought that some of ciprofloxacin was diffusing out, and that the drug-PBA conjugate also retained some of its fluorescence intensity.

Once this evidence had been obtained, the same modified disc diffusion methodology used to evaluate the triclosan loaded gels was employed. The same three bacterial species were used in this assay, and the results obtained are shown in figures 22, 23 and 24.

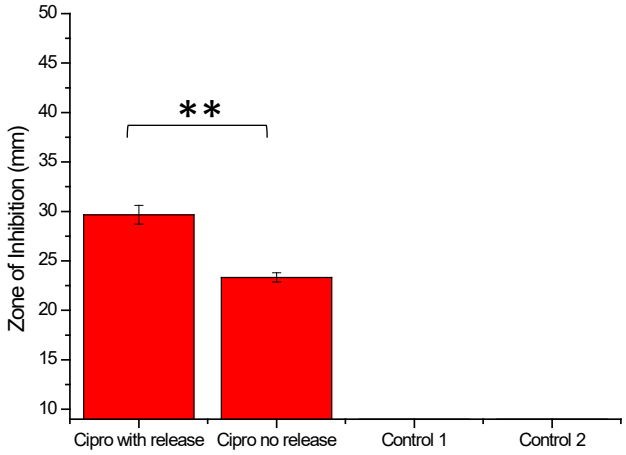

Figure 22 Calculated zones of inhibition (mm) for: ciprofloxacin loaded gels with H_2O_2 (100 µL, 1 mM), ciprofloxacin loaded gels with PBS (100 µL), blank gels with H_2O_2 (100 µL, 1 mM; control 1), and blank gels with PBS (100 µL; control 2) on a lawn of *S. aureus* H560. Data was plotted starting at 9 mm as this was the average diameter of the gel disc. Assays were performed three times, with results expressed as mean ± standard deviation. Statistical significance was determined by an unpaired t-test with ** $p < 0.01$

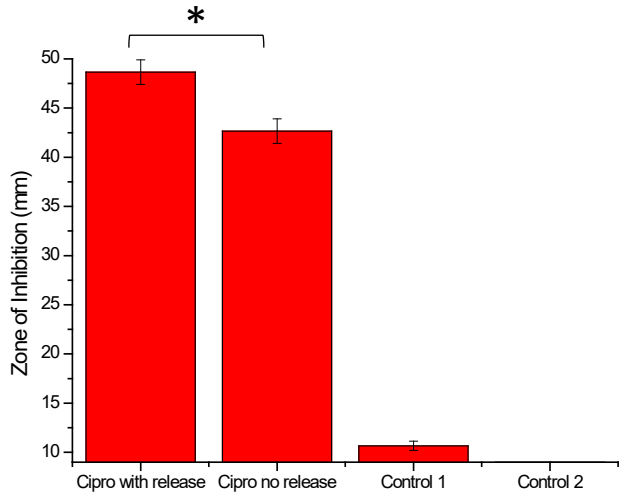

Figure 23 Calculated zones of inhibition (mm) for: ciprofloxacin loaded gels with H_2O_2 (100 µL, 1 mM), ciprofloxacin loaded gels with PBS (100 µL), blank gels with H_2O_2 (100 µL, 1 mM; control 1), and blank gels with PBS (100 µL; control 2) on a lawn of *E. coli* NCTC 10478. Data was plotted starting at 9 mm as this was the average diameter of the gel disc. Assays were performed three times, with results expressed as mean ± standard deviation. Statistical significance was determined by an unpaired t-test with ** $p < 0.05$

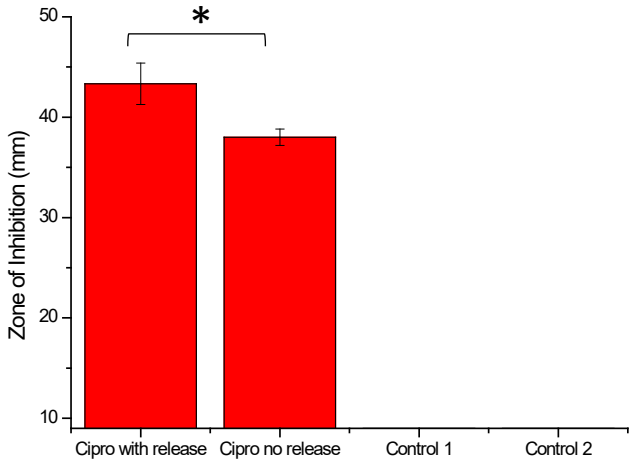

Figure 24 Calculated zones of inhibition (mm) for: ciprofloxacin loaded gels with H_2O_2 (100 µL, 1 mM), ciprofloxacin loaded gels with PBS (100 µL), blank gels with H_2O_2 (100 µL, 1 mM; control 1), and blank gels with PBS (100 µL; control 2) on a lawn of *P. aeruginosa* PA01. Data was plotted starting at 9 mm as this was the average diameter of the gel disc. Assays were performed three times, with results expressed as mean ± standard deviation. Statistical significance was determined by an unpaired t-test with ** $p < 0.05$

Whilst the controls in every case (a blank gel and a blank gel with added H_2O_2) showed no inhibition of growth, there was a large amount of non-triggered inhibition from the gels. This showed that not only was there leaching of the ciprofloxacin-PBA conjugate, but that this PBA bound drug was still active against bacteria. The dynamic nature of the bond between boron and diols was thought to be a potential reason for this leaching. A major component of bacterial agar is agarose, which could be binding the drug-PBA conjugate. It is also a possibility that there is endogenous production of ROS by the bacteria. Whilst this has not been studied specifically for the bacterial strains used, it is a known occurrence in a number of pathogenic bacteria.[29] [30] This would release and activate the bound drugs in the same manner as the addition of H_2O_2 and could explain the non-triggered kill that was seen.

3.4.7 Modified Disc Diffusion Assay

The assay was modified to prevent the potential interference of the agarose. The assay was modified by incubating the gels in a solution of either H_2O_2 (1 mL, 1 mM) or PBS for three hours, after which the exudate was added onto sterile discs, following more traditional disc diffusion assay methodologies, figures 25, 26 and 27.

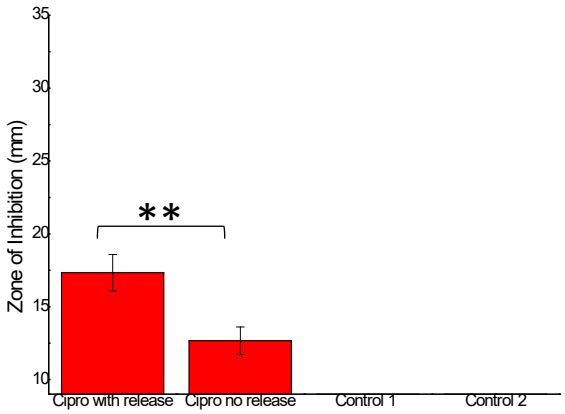

Figure 25 Calculated zones of inhibition (mm) for: the exudate of ciprofloxacin loaded gels incubated with H_2O_2 (2 mL, 1 mM), ciprofloxacin loaded gels incubated with PBS (2 mL), blank gels with H_2O_2 (2 mL, 1 mM; control 1), and blank gels with PBS (2 mL; control 2) on a lawn of *S. aureus* H560. All gels were incubated in their corresponding solution for 3 hours. Assays were performed three times, with results expressed as mean ± standard deviation. Statistical significance was determined by an unpaired t-test with ** $p < 0.01$

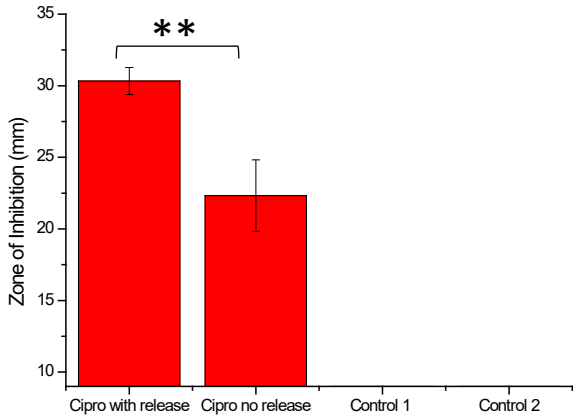

Figure 26 Calculated zones of inhibition (mm) for: the exudate of ciprofloxacin loaded gels incubated with H_2O_2 (2 mL, 1 mM), ciprofloxacin loaded gels incubated with PBS (2 mL), blank gels with H_2O_2 (2 mL, 1 mM; control 1), and blank gels with PBS (2 mL; control 2) on a lawn of *E. coli* NCTC 10418. All gels were incubated in their corresponding solution for 3 hours. Assays were performed three times, with results expressed as mean ± standard deviation. Statistical significance was determined by an unpaired t-test with ** $p < 0.01$

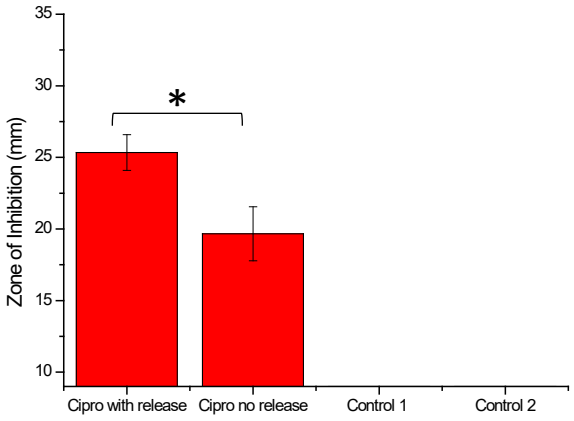

Figure 27 Calculated zones of inhibition (mm) for: the exudate of ciprofloxacin loaded gels incubated with H_2O_2 (2 mL, 1 mM), ciprofloxacin loaded gels incubated with PBS (2 mL), blank gels with H_2O_2 (2 mL, 1 mM; control 1), and blank gels with PBS (2 mL; control 2) on a lawn of *P. aeruginosa* PA01. All gels were incubated in their corresponding solution for 3 hours. Assays were performed three times, with results expressed as mean ± standard deviation. Statistical significance was determined by an unpaired t-test with ** $p < 0.05$

There was a statistically significant increase in the zones of inhibition caused by the ciprofloxacin-loaded gels that were incubated in H_2O_2, compared to ciprofloxacin-loaded gels incubated with PBS. Owing to ciprofloxacin's broad spectrum of activity it was able to inhibit the growth of both gram-negative and gram-positive bacteria. However, much like the triclosan gels, the non-specific release and kill is still present. As a result of the insolubility of the ciprofloxacin-PBA conjugate, it was impossible to dissolve in useable solvent mixes for microbiology, and thus we were unable to determine its MIC.

3.5 Conclusions

Two compounds with antibiotic activity, triclosan and ciprofloxacin, were functionalised with a PBA group yielding antibiotics with the ability to bind to diols featured in a PVA. This drug bound PVA could then be crosslinked using 1,4 benzene bis-boronic acid, with the bound drugs not affecting the hydrogel formation. Following addition of these gels to H_2O_2 solutions HRMS confirmed that the native drugs had been released into the surrounding solutions. The biological effect of these hydrogels were tested against three bacterial species relevant to wound infection, *S. aureus* H560, *P. aeruginosa* PAO1 and *E. coli* NCTC 10418. It was found that there was a small amount of slow, passive release of the bound drug-PBA conjugates, likely due to the dynamic nature of the boronic ester bonds. These released compounds displayed a small amount of biological activity indicating either that the PBA bound drugs are active against the bacteria, or that the bacteria are producing enough endogenous RONS that they are causing oxidation of the PBA. However, the release of these molecules could be triggered by the addition of H_2O_2. Under these conditions, it was found that the drugs were released in high enough quantities to inhibit the growth of the bacteria towards which they were active significantly more than the passive release. It can be concluded that a H_2O_2 triggered release system has been has been successfully produced and its function tested, however, it requires further work to prevent passive diffusion in order for it to find any potential use in a clinical setting.

3.6 Future work

Moving forward, one crucial aim is to develop analogues of the mentioned compounds which are more soluble in water. This will enable conclusions to be drawn about whether endogenous RONS produced by the bacteria themselves could be triggering the release of the active compounds, or if the PBA conjugated antimicrobials also feature antibiotic activity. In the case of ciprofloxacin, instead of using ciprofloxacin in its neutral form, the hydrochloride salt could be used. This ionic compound offers greater solubility in aqueous solutions. Another option for future use is to conduct the synthesis with the boronic acid analogue of the ester PBA linker compound used, exemplified by ciprofloxacin in figure 28. This boronic acid will increase the hydrophilicity of the molecules making them more soluble in water.

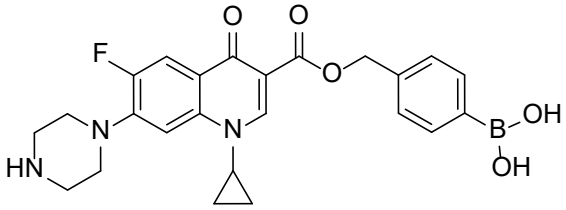

Figure 28 Ciprofloxacin bound to a phenyl boronic acid linker

As the PBA linker can be bound to several functional groups, and the crosslinking system is tolerant to a range of molecules, there is potential to use other antimicrobials. As seen with the lack of antimicrobial activity of triclosan against *P. aeruginosa*, often a single compound is unable to treat all infections. An advantage of this system is that there is a high number of binding sites for the boronic acid cross linker, making it possible to load drugs in a higher concentration, or use numerous antimicrobials at clinically relevant concentrations. This allows for the development of a combination therapy; preliminary HRMS data of a ciprofloxacin-PBA and triclosan-PBA both bound within a gel that was subsequently exposed to H_2O_2 supports this.

Other sources of ROS as a trigger are also an area to be considered. Pyroelectric particles are particles that over a specific transition temperature undergo a phase change. This phase change causes spontaneous polarisation, able to generate enough potential difference to generate OH radicals, which can cause to development of other, longer lived ROS.[31] In collaboration with other departments at the University of Bath, we are beginning to look at the incorporation of these particles into polymer matrices. The pyroelectric point of Strontium/Barium particles can be tuned,

and particles have been developed that produce low levels of ROS at 35 °C. As a normal wound is between 32 and 34 °C and an infected wound is often above 37 °C, they may be an avenue for an automatically triggered release theranostic wound dressing when combined with PBA-drug conjugates.[32]

3.7 Bibliography

1. J. Rautio, H. Kumpulainen, T. Heimbach, R. Oliyai, D. Oh, T. Jarvinen and J. Savolainen, Nature Reviews Drug Discovery, 2008, 7, 255-270.

2. K. M. Huttunen, H. Raunio and J. Rautio, Pharmacological Reviews, 2011, 63, 750-771.

3. S. Sehajpal, D. N. Prasad and R. K. Singh, Mini-Reviews in Medicinal Chemistry, 2018, 18, 1199-1219.

4. W. M. Lau, A. W. White, S. J. Gallagher, M. Donaldson, G. McNaughton and C. M. Heard, Current Pharmaceutical Design, 2008, 14, 794-802.

5. R. N. Jones, A. L. Barry and C. Thornsberry, Antimicrobial Agents and Chemotherapy, 1989, 33, 944-950.

6. F. Kratz, Journal of Controlled Release, 2008, 132, 171-183.

7. R. Duncan, Nature Reviews Cancer, 2006, 6, 688-701.

8. X. H. Peng and V. Gandhi, Therapeutic Delivery, 2012, 3, 823-833.

9. Y. Y. Kuang, K. Baakrishnan, V. Gandhi and X. H. Peng, Journal of the American Chemical Society, 2011, 133, 19278-19281.

10. D. B. Tiz, D. Kikelj and N. Zidar, Expert Opinion on Drug Discovery, 2018, 13, 497-507.

11. E. M. Larsen and R. J. Johnson, Drug Development Research, 2019, 80, 33-47.

12. J. P. Clayton, M. Cole, S. W. Elson, H. Ferres, J. C. Hanson, L. W. Mizen and R. Sutherland, Journal of Medicinal Chemistry, 1976, 19, 1385-1391.

13. L. C. Murfin, M. Weber, S. J. Park, W. T. Kim, C. M. Lopez-Alled, C. L. McMullin, F. Pradaux-Caggiano, C. L. Lyall, G. Kociok-Köhn, J. Wenk, S. D. Bull, J. Yoon, H. M. Kim, T. D. James and S. E. Lewis, Journal of the American Chemical Society, 2019, 141, 19389-19396.

14. C. M. Lopez-Alled, A. Sanchez-Fernandez, K. J. Edler, A. C. Sedgwick, S. D. Bull, C. L. McMullin, G. Kociok-Kohn, T. D. James, J. Wenk and S. E. Lewis, Chemical Communications, 2017, 53, 12580-12583.

15. World Health Organisations List of Essential Medicines, (accessed 06/09/19, 2019).

16. M. M. Toteva and J. P. Richard, in Advances in Physical Organic Chemistry, Vol 45, ed. J. P. Richard, Academic Press Ltd-Elsevier Science Ltd, London, 2011, vol. 45, pp. 39-91.

17. D. C. Thompson, K. Perera and R. London, Chemical Research in Toxicology, 1995, 8, 55-60.

18. F. Dufrasne, M. Gelbcke, J. Neve, R. Kiss and J. L. Kraus, Current Medicinal Chemistry, 2011, 18, 3995-4011.

19. A. Bruggink, E. C. Roos and E. de Vroom, Organic Process Research & Development, 1998, 2, 128-133.

20. C. A. Giuliano and M. J. Rybak, Pharmacotherapy, 2015, 35, 328-336.

21. G. Paradossi, F. Cavalieri, E. Chiessi, C. Spagnoli and M. K. Cowman, Journal of Materials Science-Materials in Medicine, 2003, 14, 687-691.

22. G. M. Peters, X. D. Chi, C. Brockman and J. L. Sessler, Chemical Communications, 2018, 54, 5407-5409.

23. M. T. E. Suller and A. D. Russell, Journal of Antimicrobial Chemotherapy, 2000, 46, 11-18.

24. H. N. Bhargava and P. A. Leonard, American Journal of Infection Control, 1996, 24, 209-218.

25. T. T. Welsch and E. T. Gillock, Journal of Environmental Science and Health Part a-Toxic/Hazardous Substances & Environmental Engineering, 2011, 46, 436-440.

26. M. J. Durkin, S. R. Jafarzadeh, K. Hsueh, Y. H. Sallah, K. D. Munshi, R. R. Henderson, V. J. Fraser and C. D. C. P. Epictr, Infection Control and Hospital Epidemiology, 2018, 39, 584-589.

27. S. Fardeau, A. Dassonville-Klimpt, N. Audic, A. Sasaki, M. Pillon, E. Baudrin, C. Mullie and P. Sonnet, Bioorganic & Medicinal Chemistry, 2014, 22, 4049-4060.

28. B. P. Kamat, Journal of Pharmaceutical and Biomedical Analysis, 2005, 39, 1046-1050.

29. B. Gonzalezflecha and B. Demple, Journal of Biological Chemistry, 1995, 270, 13681-13687.

30. R. Hertzberger, J. Arents, H. L. Dekker, R. D. Pridmore, C. Gysler, M. Kleerebezem and M. J. T. de Mattos, Applied and Environmental Microbiology, 2014, 80, 2229-2239.

31. A. Benke, E. Mehner, M. Rosenkranz, E. Dmitrieva, T. Leisegang, H. Stocker, W. Pompe and D. C. Meyer, Journal of Physical Chemistry C, 2015, 119, 18278-18286.

32. A. Chanmugam, D. Langemo, K. Thomason, J. Haan, E. A. Altenburger, A. Tippett, L. Henderson and T. A. Zortman, Advances in Skin & Wound Care, 2017, 30, 406-414.

4 Dynamic H_2O_2 sensitive hydrogels

4.1 Introduction

4.1.1 Hydrogen Peroxide Sensing

Reactive oxygen species (ROS) and reactive nitrogen species (RNS) regulate a number of important biological processes, including cell apoptosis and a variety of signalling pathways.[1, 2] The cellular production of ROS/RNS is balanced by the production of antioxidants, which serve to 'mop-up' excessive ROS/RNS to prevent damage. The over-production of these reactive species is known as oxidative stress and is a well-documented disease state with links to chronic illness including diabetes, Alzheimer's, and even the natural processes of aging.[3]

There are two main types of reactive oxygen species, the radical compounds and the non-radicals. The radical compounds contain an unpaired electron in their valence shells, and include superoxide, nitric oxide, hydroxyl and peroxyl radicals. These radical species are shorter lived than the non-radicals owing to their greater reactivity. These non-radical compounds include hydrogen peroxide, peroxynitrite, singlet oxygen and hypochlorite, table 1.

Table 1 Common ROS/RNS and their molecular formula

Radical	**Non Radical**
Superoxide	Hydrogen Peroxide
$^{-}O_2$	**H_2O_2**
Hydroxyl	Peroxy nitrite
HO·	**$ONOO^-$**
Nitric Oxide	O_3
NO·	**Ozone**
Peroxyl radical	Hypochlorite
ROO·	**ClO^-**
	Singlet Oxygen
	$^1O_2$

4.1.2 Detecting ROS/RNS

As well as being of biological importance, many industrial processes utilise the reactivity of ROS/RNS for applications such as disinfectants, but often these reactive species are an unwanted by-product. This is particularly the case in facilities utilising high temperature processes and those involved with metal production.[4, 5] Hydrogen peroxide has found common use in decolourising hair and bleaching paper.[6] As a result of both their biological relevance, and the need to ensure safe levels of these compounds for both health and environmental safety, the sensing of ROS/RNS is a field of research that has attracted much attention. A number of commercial detectors for potentially hazardous workplaces are available, with the ability to detect both gaseous and aqueous levels of H_2O_2 in industry, and a number of chemical sensors have been developed to detect them for medical purposes.

Detection of biological ROS/RNS is achievable using fluorescent probes. Near infra-red/long wavelength probes are of particular interest due to their ability to visualise cells *in vivo* without damaging the host, whilst also maintaining good penetration through tissue and good visibility.[7]

One such probe was developed by Sedgwick *et al* for the detection of peroxynitrite. The development of sensors for specific reactive oxygen species can be difficult owing to their often similar reactivity. The lifetime of peroxynitrite is low (in the millisecond range), however, as shown by Sikora *et al* its reaction with aromatic boronate compounds is around 10^6 times faster than that of hydrogen peroxide. It is this difference in the rates of reaction, which give such compounds their selectivity, figure 1.[8]

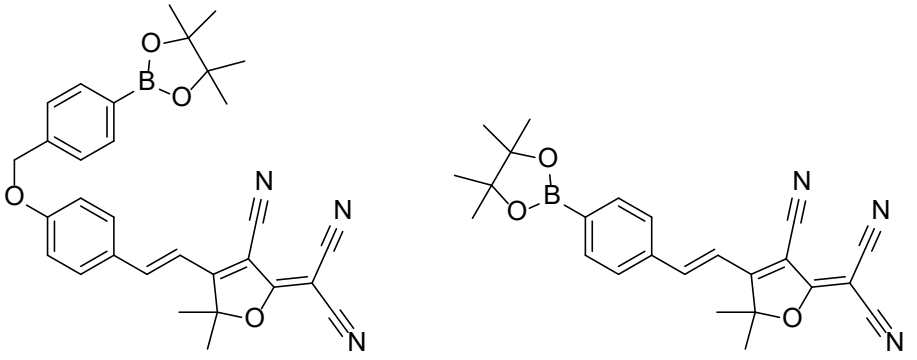

Figure 1 *Left* TCFB1 *Right* TCFB2, two fluorescent peroxynitrite probes developed by Sedgwick *et al.*[7]

Detection of cellular H_2O_2 *in vivo* is particularly important for the monitoring of cellular messaging processes. Owing to the low rate reactivity of H_2O_2 compared to a number of the other reactive species, as well as the rapid degradation in cells (through enzymatic activity) it has been historically difficult to detect with a large degree of specificity.[9] However, a number of small molecular fluorescent probes have now been developed for *in vivo* imaging, many with the ability to target individual organelles within the cells, figure 2.

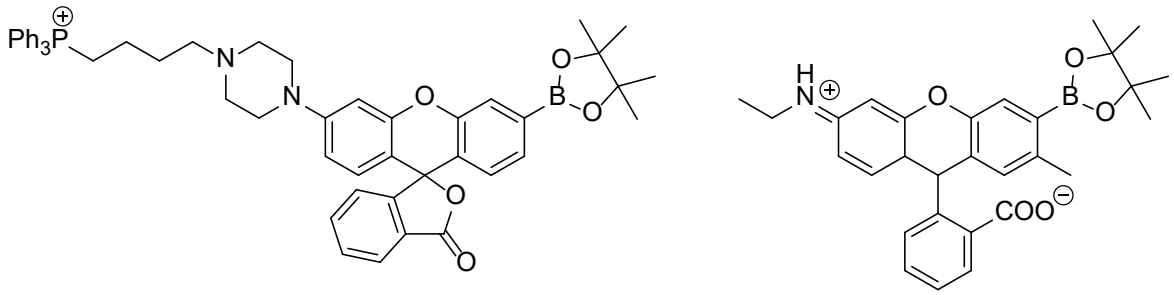

Figure 2 *Left* MitoPY1, a H_2O_2 sensor which targets the mitochondria *Right* NucPE1 a H_2O_2 sensor that targets cellular nuclei

Both of the probes in the above figure are able to detect H_2O_2 at biologically relevant concentrations. Being able to track the formation of H_2O_2 within regions of cells has allowed for the study of the contribution to disease that comes from the presence of these species in cells.[10, 11] This greater understanding of the sub-cellular processes and causes of disease allows for more targeted drug design.

4.1.3 ROS/RNS and Their Uses

Environmentally ROS/RNS are produced by UV radiation as well as high levels of man-made oxidants.[12] Whilst these have an effect on those cells that they come into contact with, it is the biologically produced ROS/RNS that are more closely examined with chemical probes and will therefore be the focus of this section.

Production of ROS within cells is by-product of anaerobic processes. Super oxide and hydrogen peroxide can be formed within the mitochondria; they are produced as part of respiratory chain complexes, in which a sufficient negative potential is generate to reduce molecular oxygen to superoxide.[13] There are a number of other enzymatic processes that can occur at a cellular level to produce such ROS, for example fumarate reductase, succinate dehydrogenase and aspartate oxidase.[14]

There are a number of biochemical methods that the ROS are used for signalling. Healthy signalling and oxidative stress will often be caused by the same molecules, but in different concentrations. One well-documented example of this is the reversible oxidation of thiols and thiolate anions on cysteine residues, catalysed by the redox potential of different ROS.[15] In doing this cells can promote or prevent certain biosynthetic pathways, leading to a change in phenotypic expression.

4.1.4 Hydrogels for Bio-imaging

Supermolecular hydrogels for use as bio-imaging probes is an emerging area of research.[16] These hydrogels have found utility in MRI imaging as well as the visualising of important polyanions polyamines and bacteria.[17, 18] One area that to our knowledge is yet to be explored is the use of such a hydrogel in the detection of high levels of ROS, which can indicate cancer within the body.

4.2 Aims

The aim of the work in this chapter is to utilise the binding between boronic esters and diols to develop a novel crosslinker for the synthesis of intelligent PVA hydrogels. The aim was to design a crosslinker that consists of a masked fluorophore featuring two boronic esters. Following the formation of the PVA hydrogels, the aim is to measure the reactivity and release of the crosslinking molecules ROS solutions and the activation of the fluorophores through UV-vis and fluorescence measurements, figure 3.

The aim is to develop not only a stand-alone hydrogel H_2O_2 senor with potential for *in vivo* imaging, but a model system for the release of similarly functionalised and bound molecules for potential drug release in response to high ROS concentrations.

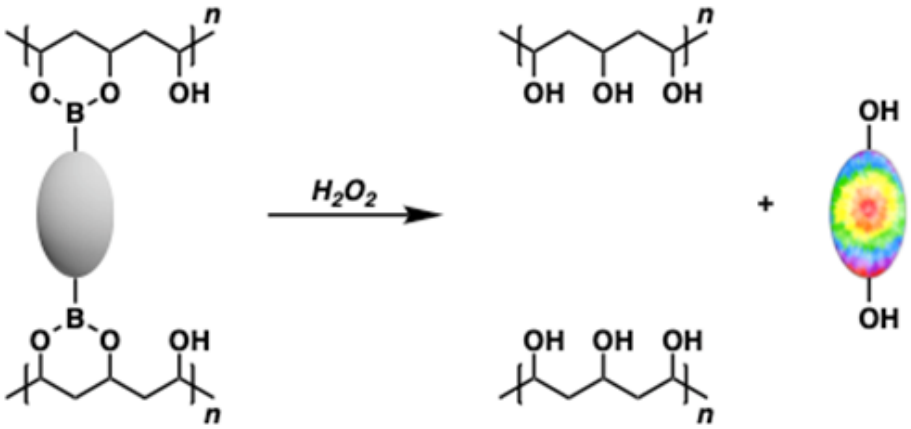

Figure 3 The activation and release of boronic ester masked fluorophores from a boronate ester crosslinked hydrogel of PVA

4.3 Materials and Methods

4.3.1 General Information

All solvents and reagents were purchased from commercial suppliers and used without further purification unless otherwise noted. Analytical thin-layer chromatography (TLC) was performed using commercial pre-coated silica gel plates containing a fluorescent indicator. Column chromatography was carried out using silica gel (0.040 - 0.063 mm). Proton and carbon NMR were recorded using a Bruker Advance 500. Chemical shifts are reported in ppm using TMS or solvent residual signals as internal reference standards. High-resolution mass spectrometry (HRMS) were performed on an Agilent 6545 LC/Q-TOF. UV-vis and fluorescence measurements were performed on a BMG Labtech CLARIOstar using costar u bottom 96 well microplates or Greiner Bio-One microplates (96-well, PS, f-bottom (chimney well), black-walled) respectiely. Data was collected via the BMG Labtech Clariostar data analysis software package MARS. All UV-vis and fluorescence measurements were performed in triplicate and plotted as an average.

4.3.2 Synthetic Experimental

The synthetic experimental procedures and data can be found in chapter 6.3.

4.3.3 Solution Based UV-vis Studies

20 μM solutions of PF-1 or Pment were made in 1% DMSO PBS v/v. 100 μL of these solutions were combined with 100 μL of H_2O_2 (1 mM) in PBS giving final solution concentrations of 10 μM of the probe solution and 500 μM H_2O_2. A control experiment was performed replacing the H_2O_2 with PBS. The UV-vis spectra of the two solutions was then measured after 1 hour of incubating at room temperature.

4.3.4 Solution Based Fluorescence Studies

20 μM solutions of PF-1 or Pment were made in 1% DMSO PBS v/v. 100 μL of these solutions were combined with 100 μL of H_2O_2 (1 mM) in PBS giving final solution concentrations of 10 μM of the probe solution and 500 μM H_2O_2. A control experiment was performed replacing the H_2O_2 with PBS. The fluorescence was measured every 10 minutes for one hour at room temperature, Ex = 472 – 16 nm, Em = 500 – 600 nm for PF-1, Ex = 570 – 16 nm, Em = 600 – 700 nm for Pment.

4.3.5 Hydrogel Synthesis

PVA (mw 13,000 – 23,000 kDa) was dissolved in DMSO to form a 10% w/v solution. Solutions of PF-1 and Pment were prepared to achieve a final concentration of 100 mM in DMSO. Aliquots of the PVA solution (0.5 mL) were combined with either PF-1 or Pment solutions (0.5 mL), and while stirring were heated to induce gelation within 30 s. The resultant hydrogels were left overnight at 60 °C in an oven, before being washed twice with petroleum ether (5 mL) and PBS (5 mL, 10 mM, pH 7.4). The hydrogels were stored in PBS until required.

4.3.6 Gel Based UV-vis Studies

After the gels had been formed they were cut with a scalpel into pieces with a mass of 200 mg ± 10 mg. These gel pieces were submerged in 2 mL of 1 mM H_2O_2 in PBS. Aliquots of 200 µL of the resulting solution were removed and a UV-vis spectrum measured at 30 minute intervals for 90 minutes at room temperature.

4.3.7 Gel Based Fluorescence Studies

After the gels had been formed they were cut with a scalpel into pieces with a mass of 200 mg ± 10 mg. These gel pieces were submerged in 2 mL of H_2O_2 in PBS, at a concentration of either 0, 125, 500, 750 or 1000 µM. Aliquots of 200 µL were removed from the solution and transferred to a black walled micro-plate and the fluorescence was measured. After the measurement the aliquot was returned to the experimental solution. Ex = 472 – 16 nm, Em = 500 – 600 nm for Gment, Ex = 570 – 16 nm, Em = 600 – 700 nm for Pment.

4.3.8 Gel Dissolution Study

Gment and Pment hydrogels were prepared with a mass of 1000 mg ± 50 mg. These pieces of gel were placed in H_2O_2 (10 mL, 100 mM) and shaken in an incubator at 37 °C for 1.5 hours. A control of PBS was used as a comparison.

4.3.9 Gel Stability Study in Air

Gment and Pment hydrogels were prepared with a mass of 500 mg ± 50 mg. They were exposed to air at room temperature and photographed at 24 hour intervals for 48 hours, then 48 hour intervals for 10 days.

4.3.10 Gel Stability in Aqueous Solution

Gment and Pment hydrogels were prepared with a mass of 500 mg ± 50 mg. The gels were submerged in PBS (5 mL) at room temperature. 200 μL aliquots of this solution were transferred to a clear micro-plate and the UV-vis spectrum was measured at 24 hour intervals for the first 48 hours, and then at 48 hour intervals for 10 days.

4.4 Results and discussion

4.4.1 Existing Boronate Ester Fluorophores

Boronic acid masked fluorophores have already been widely utilized in ROS sensing, and as a result there are a number of well documented compounds that could have been utilised as crosslinkers. The main criteria was that there had to be more than one boronate ester on the molecule, to act as a crosslinker. Chang *et al.* at the University of Berkley developed three compounds: PR-1, PF-1 and PX1, that feature the bis-boronic acid moiety required, and are fluorescence in response to H_2O_2, emitting red, green and blue light respectively, figure 4.[19]

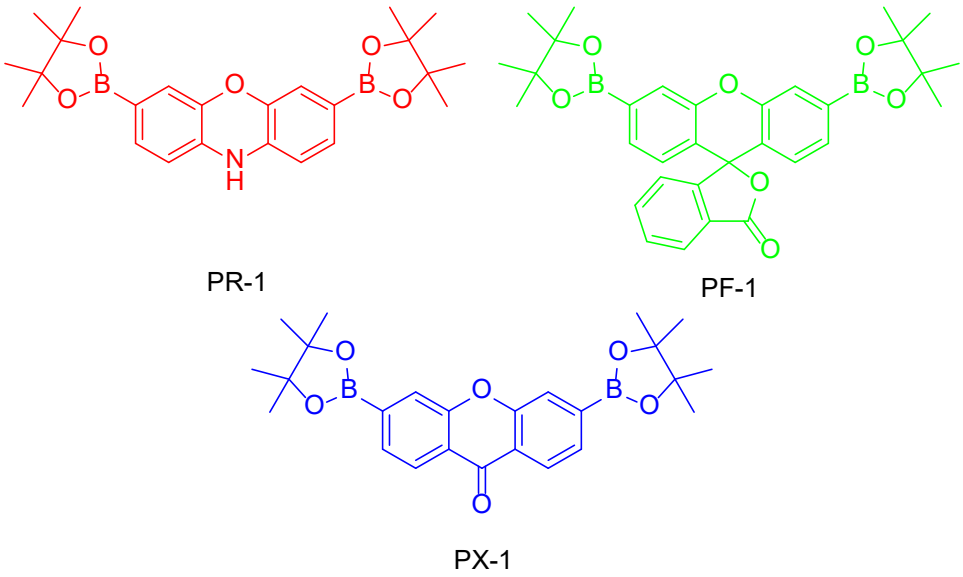

Figure 4 Chang *et al.*'s boronate based fluorescent sensors based on resorufin (PR-1), fluorescein (PF-1) and xanthone (PX-1)

4.4.2 Synthesis of PF-1

The compound PF-1 was prepared according to the procedure seen in figure 5.

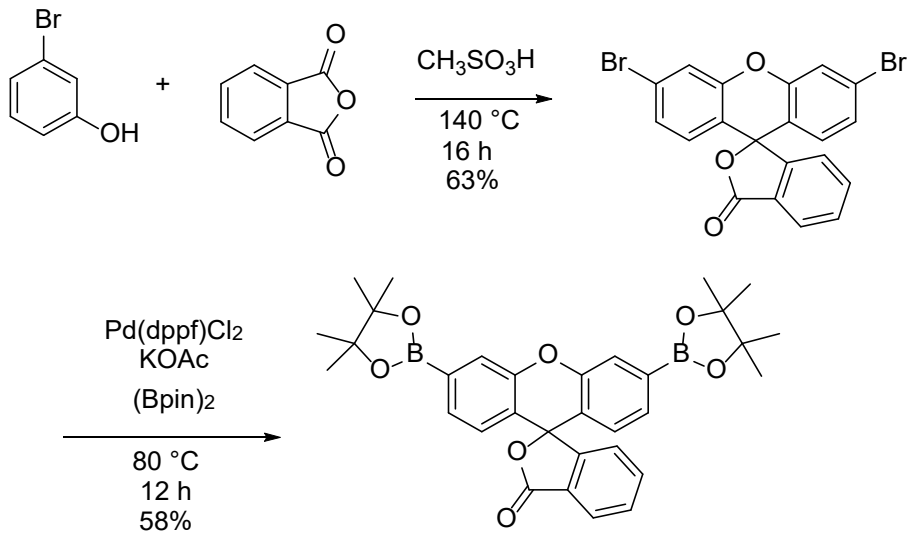

Figure 5 The synthetic route for the production of PF-1

PF-1 will be oxidised as in scheme figure 5 to form the fluorophore which is also strongly coloured. UV-vis and fluorescence measurements were performed to ensure the PF-1 reacted as according to literature, despite already having confirmation through NMR and HRMS that the compound had been synthesised; this was to give further confirmation that the synthesised probe would act as reported.

4.4.3 PF-1 Testing in Solution

PF-1 should oxidise to the green fluorescent fluorescein as according to figure 6.

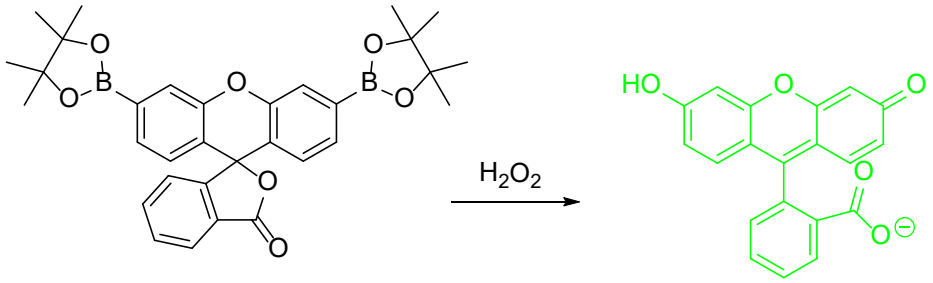

Figure 6 The oxidative activation of PF-1 to the green florescent fluorescein, fluorescent over pH 5-9 (encompassing most biological systems).

4.4.3.1 PF-1 Testing in Solution UV-vis

The initial test to ensure that the synthesised compound acted as expected was to obtain its UV-vis spectrum. Figure 7 shows the increase in absorbance of a solution of PF-1 after 1 hour with a defined peak at 494 nm, characteristic of fluorescein, indicating oxidation of the Bpin groups.

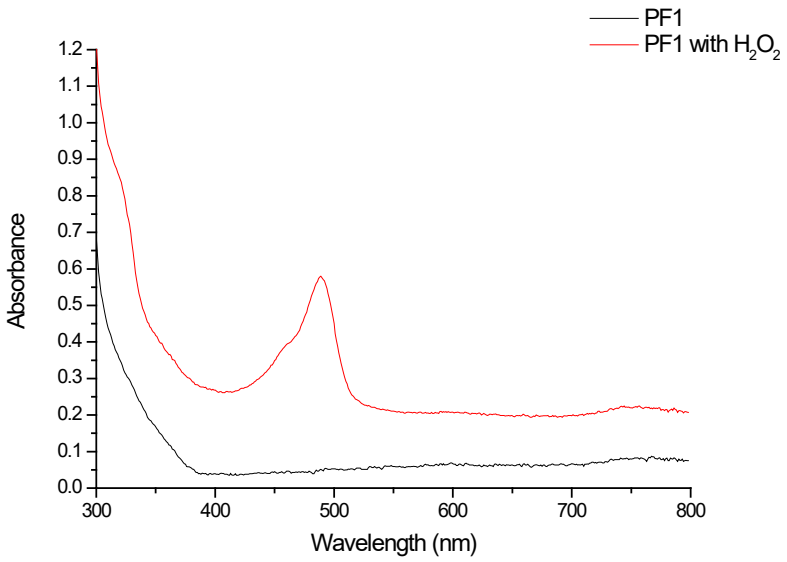

Figure 7 The increase in absorbance of 10 µM PF-1 on addition of H_2O_2 500 µM after 1 hour, indicating the activation of the compound by oxidation of the boronate esters after 60 minutes at 25 °C in 1% DMSO 99% PBS buffer

4.4.3.2 PF-1 Testing in Solution Fluorescence

Confirmation of successful synthesis was further investigated through the use of more sensitive fluorescence measurements, to gain an understanding of the timescale at which the gel may activate, figure 8.

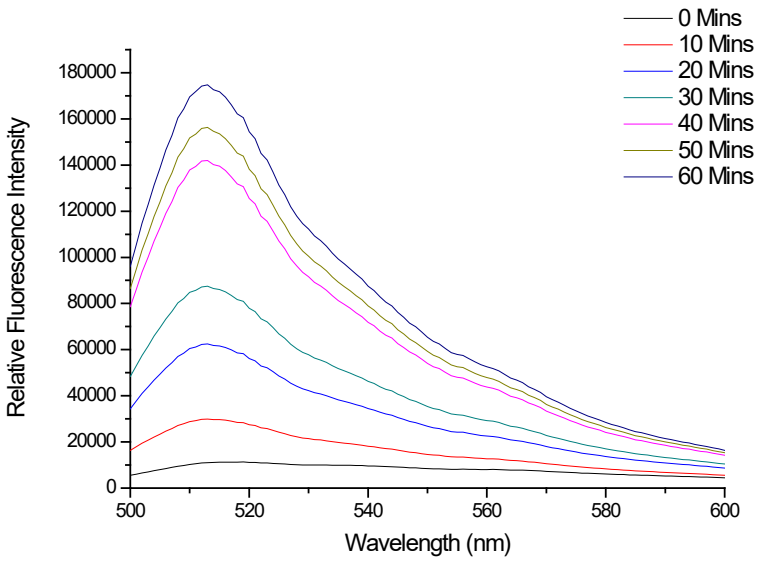

Figure 8 Fluorescence spectra of 10 µmol PF-1 in PBS, on addition of 0.5 mM H_2O_2 in PBS. Measurements were taken over the course of 1 h at room temperature in 1% DMSO 99% PBS buffer Ex = 472 – 16 nm, Em = 500 – 600 nm

Both the degree of fluorescence increase and the change in absorbance values indicated that the PF-1 would be suitable for use as a fluorescent and colourimetric ROS sensitive crosslinker, both with regards to its activity, its rate of activation and its sensitivity. It is known from making the blank PVA gels in chapter 3 that the bis-boronic acid crosslinker concentration required to form stable hydrogels is 1000 times higher than that used in this experiment. The timescale of activation is suitable for its intended use, as a clear activation, with a 5-fold increase in fluorescence, can be observed within 10 minutes.

4.4.4 PF-1 Crosslinked Hydrogel Development

As with the gels produced in chapter 3 solutions of 10% PVA in DMSO and 100 mM PF-1 in DMSO were made. However, whereas the 1,4 benzene bis-boronic acid solution gelled immediately upon mixing with the PVA, it was found that this mixing caused the formation of a viscous liquid. Upon heating with a heat gun for around 30 seconds this viscous liquid would begin to gel, however, upon standing overnight at room temperature a large portion of the gel would revert back to this liquid form. It is thought that the increased temperature is to aid in the removal of the free displaced pinacol through evaporation, preventing re-binding to the diols. The would reduce the binding sites available for the crosslinker in the PVA. The fact that overnight the gel would revert back to liquid was thought to be due to this displacement of crosslinker with free

pinacol, that as itself displaced when the crosslinker bound to the diols. As such, the two solutions were combined and the vial placed in a 70 °C oven for 12 hours, figure 9. This gel will be known from here onwards as greenment (Gment).

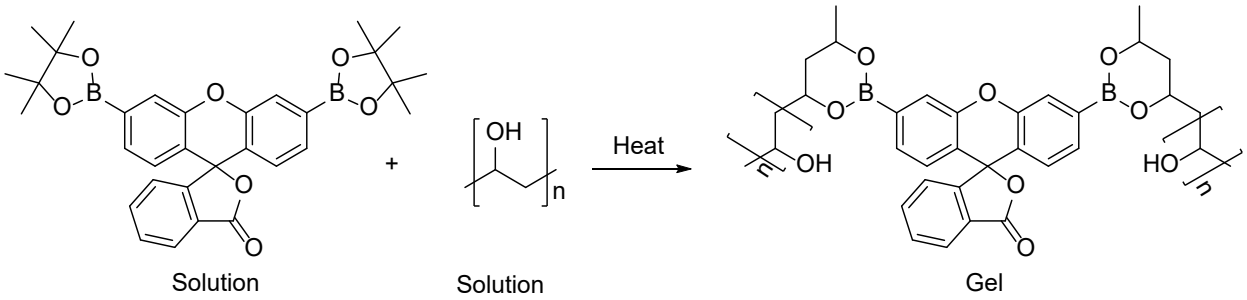

Figure 9 Crosslinking PVA with PF-1 to form a stable Gment hydrogel

To remove the DMSO and any unbound pinacol, the gels were washed with PBS buffer and petroleum ether before being rewashed and stored in PBS buffer to prevent dehydration.

4.4.5 Gment Gels in H_2O_2 Solutions

The gels are intended to react with H_2O_2 in two separate manners; not only will the fluorophore be activated but the gel, losing its crosslinker, will degrade as in figure 10.

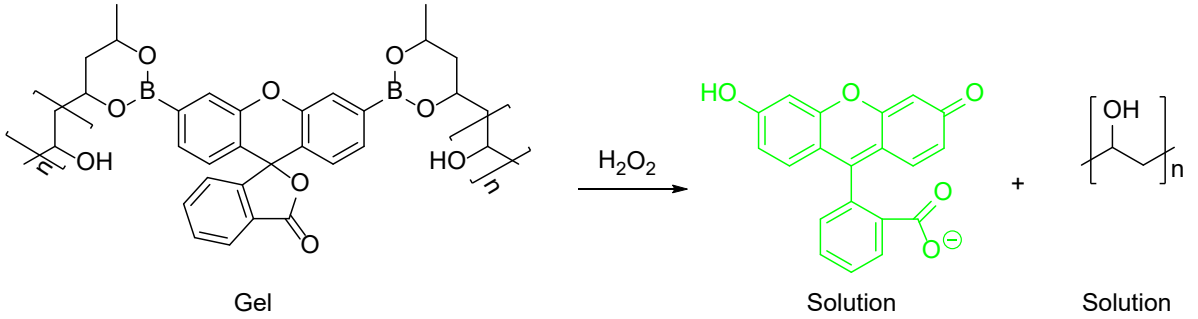

Figure 10 The degredation of GMent gel into the green fluorescent fluorescein and a solution of PVA

This dehydration back into solution would be accompanied by the release of water trapped within the hydrogel matrix, which would serve to aid in the rehydration of a wound. When considering this material as an *in vivo* imaging system, its degradation into only PVA and fluorescein, both non-toxic compounds, is crucial.[20]

4.4.5.1 Gment Gels in H_2O_2 Solutions – UV-vis

To test the reactivity of the washed Gment gels, pieces of gel were cut into 200 mg ± 10 mg and placed in 2 mL of H_2O_2 solution in PBS at a concentration of 1 mM, and aliquots of this solution

were removed every 30 minutes. The UV-VIS spectrum of each aliquot was recorded and the aliquot replaced. This took place every 30 minutes for 90 minutes, figure 11.

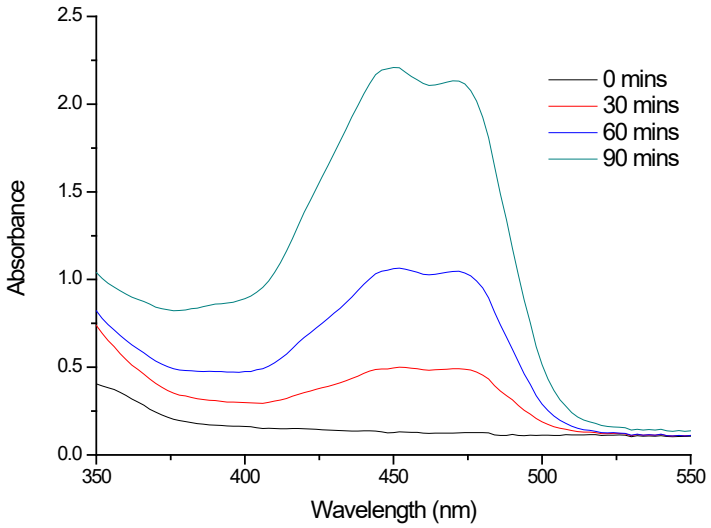

Figure 11 The increasing absorbance of solution of Gment as the gel is degraded by H_2O_2 back into fluorescein over time in PBS

As can be seen in figure 11 there is an increase in the absorbance of the solution containing the gel over time, due to the release of the activated chromophore. This colour change can be seen visually in figure 12. Within the first time period of 30 minutes there is a large increase in the colour, showings its potential utility in point of care diagnostics. The broadness of the peak and the presence of a second peak in this spectrum is tentatively assigned to the monoboronate species. It is assumed that this would be lost at higher concentrations of H_2O_2.

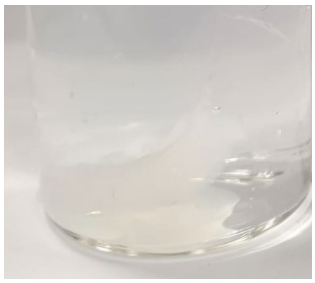

Before addition of H_2O_2

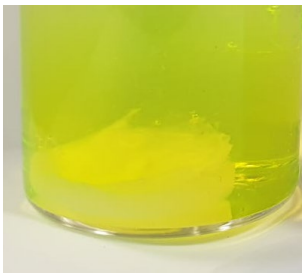

After addition of H_2O_2

Figure 12 *Left* photo showing the Gment gel in PBS, *Right* photo showing the Gment gel in 1 mM of H_2O_2 in PBS after 90 mins

As can be seen in these photos there is a clear increase in colour, but the gel is still solid, and has not noticeably degraded from exposure to the low concentration of H_2O_2.

4.4.5.2 Gment in H_2O_2 Solutions – Fluorescence

To test the sensitivity of the Gment gels to H_2O_2 the gels were placed in solutions of varying concentrations of H_2O_2, from 0 – 1 mM. The fluorescence of the resulting solutions was measured after 1 hour, figure 13.

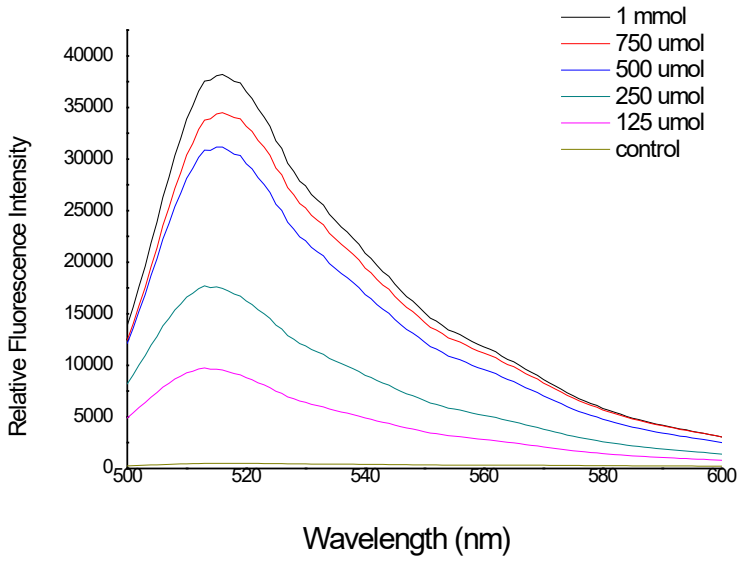

Figure 13 The dose dependent increase of fluorescence from the addition of Gment gels to solutions of increasing H_2O_2 concentration in PBS. Readings taken after 1 hour 25 °C. Ex = 472 – 16 nm, Em = 500 – 600 nm

As can be seen above the sensitivity of the Gment hydrogel is similar to that of the free PF-1, with a clear increase in fluorescence after one hour. This is to be expected from a reaction-based indicator.

This data gave us confidence that the use of a boronate ester masked fluorescent and colour changing dye as a crosslinker could yield a H_2O_2 sensitive PVA hydrogel. As such, we aimed to expand the work beyond that of Chang *et al.* and develop a new molecule, which shall be hence forth referred to as purplement (Pment).

4.4.6 Purplement

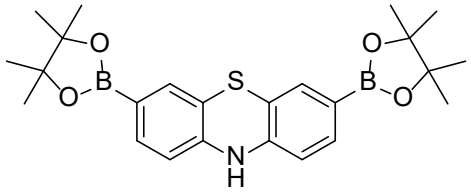

Figure 14 The Phenothiazene derived H_2O_2 sensitive compound, Pment

Purplement, figure 14, has not been previously published in literature for the purpose of sensing. The only online reference to the structure is within a patent, in which it is used as a reagent for the synthesis of dyes.[21] Whilst it has been assigned a CAS number it is not available from commercial sources, but was synthesised according to figure 15.

4.4.6.1 Purplement Synthesis

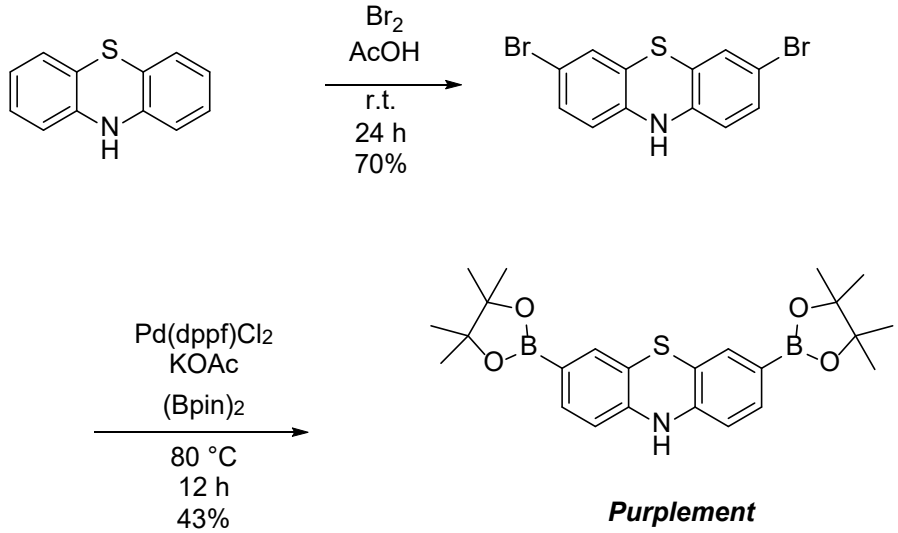

Figure 15 The synthetic route for Pment

4.4.7 Purplement Testing in Solution

Upon exposure of Pment to H_2O_2, it should oxidise to the purple fluorescent compound thionol, accompanied by a colour change to purple, according to figure 16

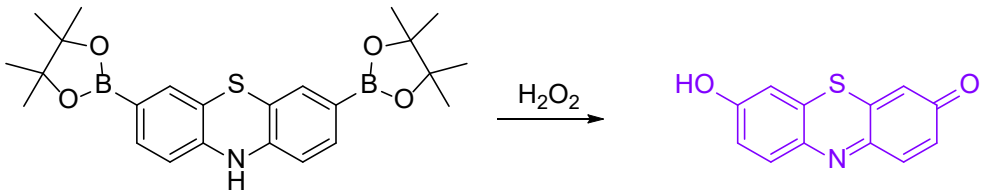

Figure 16 The oxidation of the boronate esters by H_2O_2, converting Pment into the purple fluorescent compound thionol

4.4.7.1 Purplement Testing in Solution – UV-vis

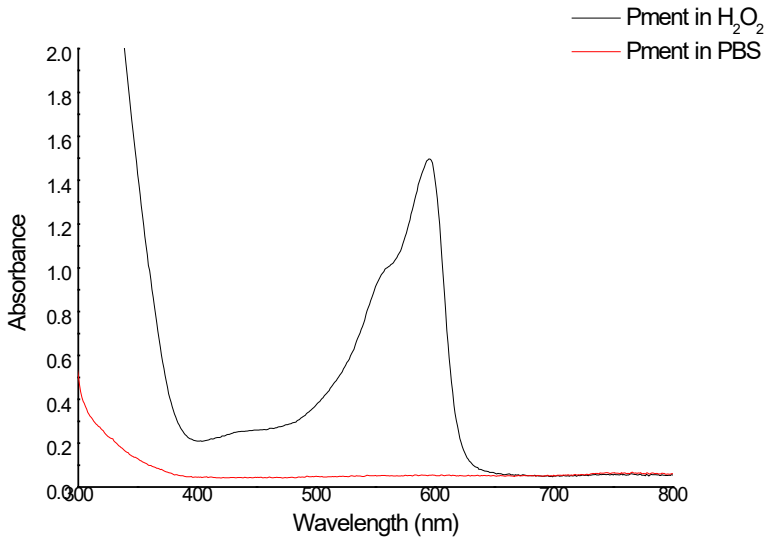

Figure 17 The increase in absorbance of 10 µM Pment on addition of H_2O_2 500 µM after 1 h indicating the activation of the compound by oxidation of the boronate esters in 1% DMSO 99% PBS buffer

In an analogous experiment to that performed with PF-1, a solution of Pment was exposed to a 500 µM H_2O_2 solution, resulting in a colour change with an absorbance increase at 595 nm, characteristic of the absorption of thionol.

4.4.7.2 Purplement Testing in Solution – Fluorescence

As done with the PF-1 solution, the increase in fluorescence of a solution of Pment upon reaction with a solution of H_2O_2 was measured over the course of an hour, figure 18.

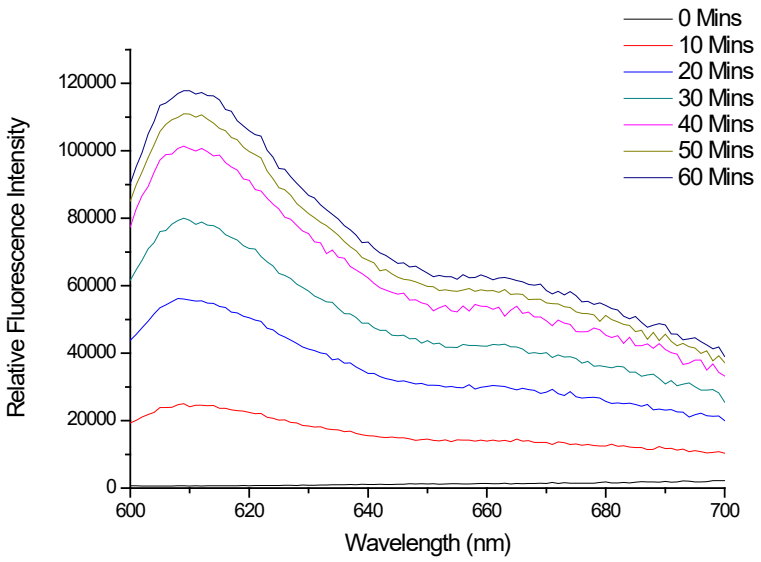

Figure 18 Fluorescence spectra of 10 µmol PF-1 in PBS; 0.1 mM, on addition of 500 µM H_2O_2 in PBS. Measurements were taken over the course of 1 h at 25 °C. in 1% DMSO 99% PBS buffer Ex = 570 – 16 nm, Em = 600 – 700 nm

Pment shows the same general increase in fluorescence over time, with a nearly 20000-fold increase in fluorescence after only 10 minutes. This indicates that much like PF-1 it would offer a rapid enough response to be considered for use in a diagnostic or drug delivery system.

4.4.8 Purplement Crosslinked PVA Hydrogel Development

As the Pment molecule features the same reactivity as the PF-1 when crosslinking, we used the same conditions as were found to be successful in making the Gment gels. A 100 mM solution of Pment in DMSO was mixed in a 1:1 ratio with 10% w/v PVA in DMSO, in a vial, and the vial was placed in a 70 °C oven overnight. As expected this yielded hydrogels similar in properties to the Gment hydrogels, with the structure shown in figure 19.

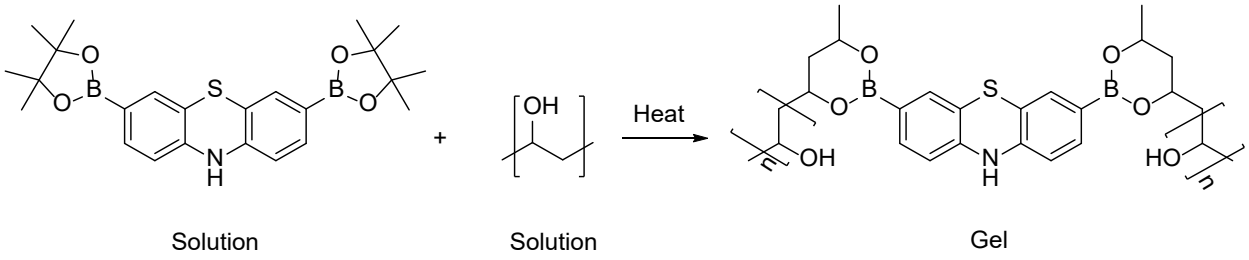

Figure 19 Crrosslinking a PVA solution into a stable hydrogel using Pment as the crosslinker

4.4.9 Pment Gels in H_2O_2 Solutions

As with the Gment gels we wanted to ensure that the activity of the Pment compound would not be hindered in its activity by the binding of the PVA. Just as fluorescein is produced by the oxidation of the Gment gel by H_2O_2 thionol should be produced by the Pment gels, thus there should therefore be a colour change to purple and a large increase in fluorescence of the surrounding solutions, figure 20.

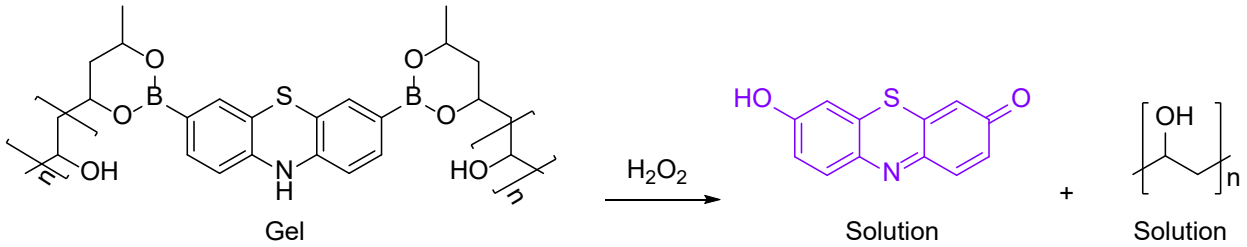

Figure 20 The degredation of the Pment gel into purple fluorescent thionol due to exposure to H_2O_2

4.4.9.1 Pment Gels in H_2O_2 Solutions – UV-vis

To test the gels, the same procedures were followed as with the Gment gels, and the UV-vis spectrum was measured of a H_2O_2 solution with a piece of gel, figure 21.

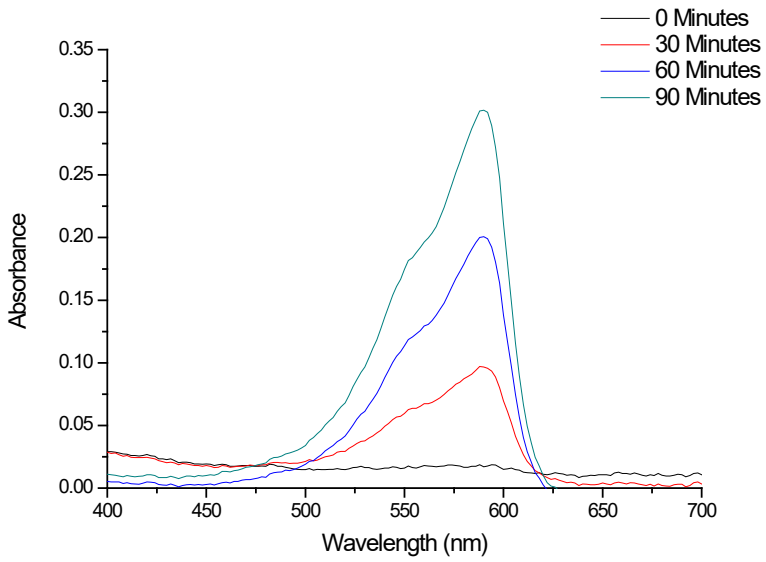

Figure 21 The increasing absorbance of solution of Pment as the gel is degraded by 1 mM H_2O_2 into thionol over 90 minutes in PBS

Once again this change in the colour is obvious by visual inspection, figure 22, and the time scale-on which the activation occurs is suitable for the development of a point of care diagnostic device.

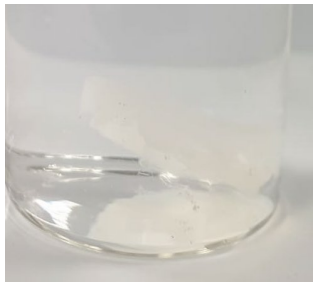

Before the additon of H_2O_2

After the addition of H_2O_2

Figure 22 *Left* photo showing the Pment gel in PBS, *Right* photo showing the Pment gel in 1 mM of H_2O_2 in PBS after 90 mins

4.4.9.2 PMent Gels in H_2O_2 Solutions – Fluorescence

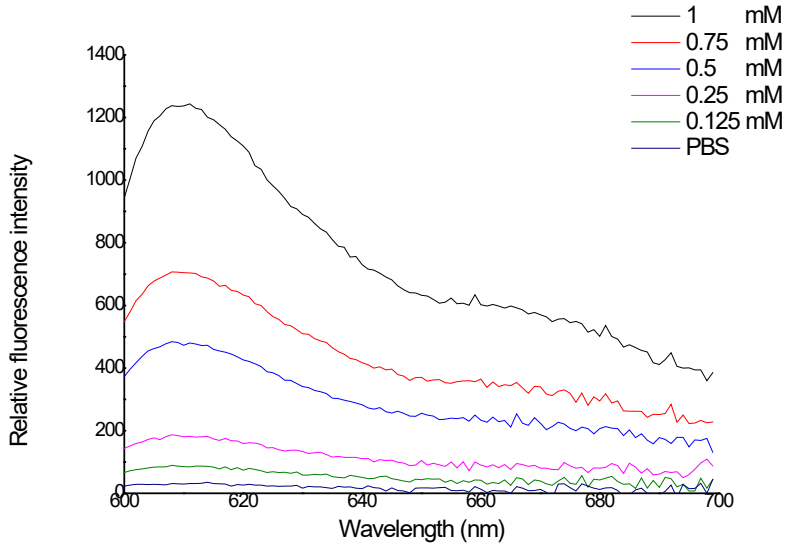

Figure 23 The dose dependent increase of fluorescence from the addition of Pment gels to solutions of increasing H_2O_2 concentration in PBS. Readings taken after 1 hour 25 °C in PBS Ex = 570 – 16 nm, Em = 600 – 700 nm

As in solution the Pment gels offered a similar reactivity to that of the Gment, giving an increase in fluorescence with increasing concentrations of H_2O_2, figure 23. When directly comparing the relative fluorescence increase of the two gels, it can be seen that the Pment does require a greater concentration of peroxide for the same increase of intensity. However, an 8 fold increase in intensity can be seen at with only 125 µM H_2O_2, which for the use as a topical drug delivery vehicle is well below clinically approved concentrations of H_2O_2 for wound care.

4.4.10 Gel Stability

Once the activity of the gels had been confirmed, the stability of the gels in both aqueous environments and to the air was investigated. Gels were synthesised of both Gment and Pment and the gels were placed either in 10 mL of PBS buffer or exposed to air. The gels were initially photographed, and then photographed every 24 hours for 48 hours and then every 48 hours for another 8 days. As can be seen in figure 24 the gels exposed to air dehydrated but remained stable.

Day 10

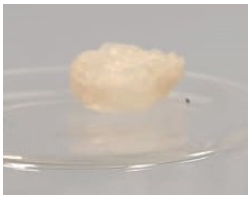

Figure 24 Photographs of gels of Gment and Pment exposed to air for 10 days

To demonstrated their stability in aqueous solution an aliquot of the solution they had been placed in was taken every time a photo of the gels in air was taken, and the UV-VIS spectrum was measured. There was no discernable increase in the absorbance spectra of either fluorescein or thionol in either spectra appendix 7.4.1. For application in either wound care or sensing it is important that the structural integrity of the gel is maintained over periods of time, to maintain both the shelf life of a potential product and retain activity.

4.4.11 Gel Dissolution

As previously discussed the H_2O_2 triggered oxidation of the crosslinker should cause the eventual collapse of the hydrogel. At the concentrations and timescales used for the fluorescence and UV-vis studies this was not observed. To ensure that the gels would dissolve as assumed, both Gment and Pment gels were exposed to 100 mM H_2O_2 and placed in a shaking incubator at 37 °C for 1.5 hours, figure 25.

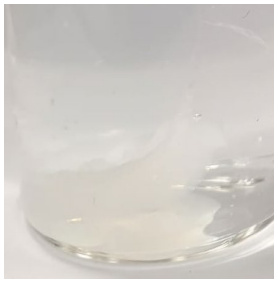

Gment in PBS

Solution of fluorescein and PVA due to decomposition of Gment gel by H_2O_2

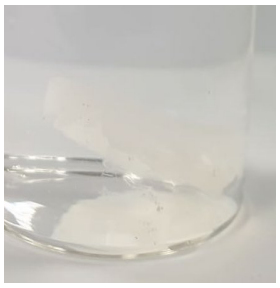

Pment in PBS

Solution of thionol and PVA due to decomposition of Pment gel by H_2O_2

Figure 25 The decomposition of clear Gment and Pment gels into highly coloured solutions of fluorescein and thionol respectively

Whilst it is less clear in the photo of the Pment due to the opacity of the coloured solution, these conditions proved sufficient to fully dissolve the PVA, compared to the solid, insoluble PVA gels in PBS. In wound care, particularly in the treatment of burn wounds, maintaining a moist wound environment is crucial to wound healing.[22] The collapse of the gel is associated with the release of water trapped in the hydrogel matrix, which may be of use as a wound rehydration method.

4.5 Conclusions

A literature reported H_2O_2 responsive green fluorescent and colourimetric dye, PF-1, has been successfully synthesised and repurposed as a ROS activated crosslinker for the preparation of PVA hydrogels. A novel, analogous dye has been designed and synthesised, offering similar reactivity in solution at different excitation and emission wavelengths, giving a deep purple coloured response to H_2O_2. This was also able to crosslink PVA forming stable hydrogels.

This novel smart material has been proved to give a fluorescent and colourimetric response to H_2O_2 concentrations of as low as 125 μM in aqueous solution. This material can also collapse, redissolving into solution in response to excess amounts of H_2O_2, with the crosslinker oxidizing into its fluorescein (Gment) or thionol (Pment). This hydrogel offers a potential as a smart wound dressing material due to being formed of materials and compounds already proven biocompatible, and its ability to release molecules in response to a stimulus. Should different crosslinking densities be investigated, it is likely that these soft materials also potentially have application in the field of injectable hydrogel based bio-sensing.

4.6 Future Work

With the utility of the binding method shown, the use of a number of different fluorophores could be used in order to gain different colours, for example PR-1 and PX-1 produced by Chang *et al*.[23] Having different coloured probes can aid in biological imaging, when more than one substrate is being investigated, as there is the opportunity to increase the contrast.[24] Red and green probes find great utility due to their contrast, for example in the LIVE/DEAD® stain.[25]

The PVA hydrogels that have been synthesised are rigid and therefore not injectable. Whilst these properties are desirable hydrogels that will be applied topically, this restricts their use. The delivery of drugs through injectable PVA hydrogels has been achieved, and as such investigating new polymers or simply adjusting the molecular weight of the PVA used and the crosslinking density could lead to new applications of these gels for imaging.[26] There are a number of injectable polymers utilising boronate esters that have been formed including derivatised hyaluronic acid and PEG, both of which are known for their low toxicity.[27, 28] This is also relevant for the use of these materials in bio-imaging.

The concept of using boronate ester masked active molecules as responsive crosslinker has been proved; the dyes work well as a model system in this respect. More interesting would be to start to develop masked forms of active pharmaceuticals that can be released in response to H_2O_2. These would essentially be dual functional pro-drugs and crosslinkers.

4.7 Bibliography

1. M. L. Circu and T. Y. Aw, Free Radical Biology and Medicine, 2010, 48, 749-762.

2. V. J. Thannickal and B. L. Fanburg, American Journal of Physiology-Lung Cellular and Molecular Physiology, 2000, 279, L1005-L1028.

3. M. Valko, D. Leibfritz, J. Moncol, M. T. D. Cronin, M. Mazur and J. Telser, International Journal of Biochemistry & Cell Biology, 2007, 39, 44-84.

4. J. A. Malvestiti and R. F. Dantas, Journal of Environmental Chemical Engineering, 2018, 6, 560-567.

5. M. A. Badding, A. B. Stefaniak, N. R. Fix, K. J. Cummings and S. S. Leonard, Journal of Toxicology and Environmental Health-Part a-Current Issues, 2014, 77, 1193-1209.

6. J. Chen, Journal of Pulp and Paper Science, 2001, 27, 429-432.

7. A. C. Sedgwick, H. H. Han, J. E. Gardiner, S. D. Bull, X. P. He and T. D. James, Chemical Communications, 2017, 53, 12822-12825.

8. A. Sikora, J. Zielonka, M. Lopez, J. Joseph and B. Kalyanaraman, Free Radical Biology and Medicine, 2009, 47, 1401-1407.

9. H. C. Guo, H. Aleyasin, B. C. Dickinson, R. E. Haskew-Layton and R. R. Ratan, Cell and Bioscience, 2014, 4, 10.

10. B. C. Dickinson, Y. Tang, Z. Y. Chang and C. J. Chang, Chemistry & Biology, 2011, 18, 943-948.

11. E. W. Miller, B. C. Dickinson and C. J. Chang, Proceedings of the National Academy of Sciences of the United States of America, 2010, 107, 15681-15686.

12. R. W. Gracy, J. M. Talent, Y. Kong and C. C. Conrad, Mutation Research-Fundamental and Molecular Mechanisms of Mutagenesis, 1999, 428, 17-22.

13. S. Dröse and U. Brandt, Springer New York, 2012, pp. 145-169.

14. K. R. Messner and J. A. Imlay, Journal of Biological Chemistry, 2002, 277, 42563-42571.

15. H. Kamata and H. Hirata, Cellular Signalling, 1999, 11, 1-14.

16. N. Mehwish, X. Q. Dou, Y. Zhao and C. L. Feng, Materials Horizons, 2019, 6, 14-44.

17. K. J. Chen, S. M. Wolahan, H. Wang, C. H. Hsu, H. W. Chang, A. Durazo, L. P. Hwang, M. A. Garcia, Z. K. Jiang, L. Wu, Y. Y. Lin and H. R. Tseng, Biomaterials, 2011, 32, 2160-2165.

18. Y. Gao, J. F. Shi, D. Yuan and B. Xu, Nature Communications, 2012, 3, 8.

19. E. W. Miller, A. E. Albers, A. Pralle, E. Y. Isacoff and C. J. Chang, Journal of the American Chemical Society, 2005, 127, 16652-16659.

20. R. Alford, H. M. Simpson, J. Duberman, G. C. Hill, M. Ogawa, C. Regino, H. Kobayashi and P. L. Choyke, Molecular Imaging, 2009, 8, 341-354.

21. China Pat., 2015.

22. L. Wei, Open Medicine, 2015, 10, 452-456.

23. M. C. Y. Chang, A. Pralle, E. Y. Isacoff and C. J. Chang, Journal of the American Chemical Society, 2004, 126, 15392-15393.

24. E. Oliveira, E. Bertolo, C. Nunez, V. Pilla, H. M. Santos, J. Fernandez-Lodeiro, A. Fernandez-Lodeiro, J. Djafari, J. L. Capelo and C. Lodeiro, Chemistryopen, 2018, 7, 9-52.

25. L. Boulos, M. Prevost, B. Barbeau, J. Coallier and R. Desjardins, Journal of Microbiological Methods, 1999, 37, 77-86.

26. M. Norouzi, B. Nazari and D. W. Miller, Drug Discovery Today, 2016, 21, 1835-1849.

27. Z. J. Huang, P. Delparastan, P. Burch, J. Cheng, Y. Cao and P. B. Messersmith, Biomaterials Science, 2018, 6, 2487-2495.

28. T. Figueiredo, J. Jing, I. Jeacomine, J. Olsson, T. Gerfaud, J.-G. Boiteau, C. Rome, C. Harris and R. Auzély-Velty, Biomacromolecules, 2019.

5 Development of Prodrug Crosslinkers

5.1 Introduction

5.1.1 Polymeric Drug Delivery Systems

Polymeric drug release systems can take many forms, both on the macro and nano-scales, often depending on the drugs' target site. Those systems designed to cross the blood brain barrier or deliver cargo to specific cells will often be nano-particles. Whereas, hydrogels prepared for topical use will be macro-sized polymers.[1, 2] Polymer systems are utilized for a range of purposes including targeted drug delivery, improvement of the drugs half-life and as drugs themselves.[3] This work will focus on systems that are targeted, and more specifically those that are stimuli responsive.

Owing to the toxicity of numerous anti-cancer chemotherapeutics, there has been great interest into the development of polymer systems that only release drugs within tumour environments, minimising the exposure of healthy cells to the drug. This behaviours is similar to that of a pro-drug, just on a much larger scale.[4] The stimuli that many of these polymeric release systems respond to is the increased levels of ROS that are present within cancer cells.[5] An example of such a system reported by Shim *et al.* utilized the ROS sensitive thioketal bond as a trigger. They synthesised a cationic poly(amino thioketal) polymer, onto which were grafted cancer targeting proteins; these could deliver genes directly to cancer cells, only breaking down to release the genetic material on ROS triggered degradation of the thioketal.[6]

5.1.2 Ciprofloxacin

Ciprofloxacin figure 1 is a second-generation fluoroquinolone antibiotic. It is one of the most highly prescribed antibiotics, with over 7 million prescriptions being filled in the USA in 2016.[7] This is owing to its broad spectrum of activity, particularly its ability to treat *P. aeruginosa,* which very few antibiotics can.[8] It is known to treat nearly all common causes of burn wound infection, as it also offers activity against a number of *S. aureus* strains as well as *E. faecallis*. The three mentioned bacteria are responsible for more than 80% of bacterial burn wound infections.[9]

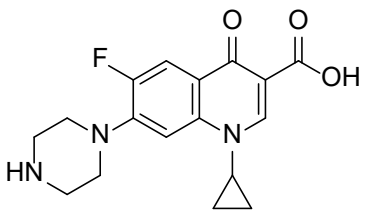

Figure 1 Ciprofloxacin

5.1.3 Ciprofloxacin Mechanism of Action

The mechanism by which ciprofloxacin and other quinolones kill bacteria has been studied in detail. In brief, they inhibit DNA gyrase, an enzyme belonging to type II topoisomerases which induce supercoiling within the bacterial chromosome. This is essential to bacterial survival as the bacterial chromosome is thought to be around 1300 μm in length, and must be super coiled in order to fit spatially within a bacterial cell that is only 1 μm^2. [10] The inhibition of DNA gyrase by ciprofloxacin increases the size of the chromosome to the point that the cell can no longer replicate. At concentrations that are higher than those required to inhibit DNA gyrase, ciprofloxacin has also been seen to inhibit the action of topoisomerase I in *E. coli*, which is thought to be a potential explanation for its broader spectrum of activity when compared with other fluoroquinolones.[11] Studies utilising a different fluoroquinolone, norfloxacin, have shown that the fluoroquinolones antibiotics do not bind directly to the enzymes initially, but instead bind to the DNA before forming the complex with the DNA gyrase prior to the super-coiling.[11]

5.1.4 Structure Activity Relationship of Ciprofloxacin

The structures of ciprofloxacin and the other quinolones have varied greatly since the initial drug, nalidixic acid, was first discovered. The different constituent parts of the drug each convey different reactivity, with respect to different binding modes, as can be seen in figure 2.

As can be seen below in figure 2 the acid at position 3 is essential for the binding of the drug molecule to the DNA gyrase as well as for transport into the bacteria. This would thus make a convenient modification site when considering the creation of a ciprofloxacin pro-drug, as this should inactivate the drug.[12] The alkylation of position 7 with differing amines can direct the spectrum of activity towards different bacterial species. Previously synthesised analogues of ciprofloxacin have used this position to bind groups such as catechols in order to improve cellular uptake, with only slightly reduced efficacies.[13]

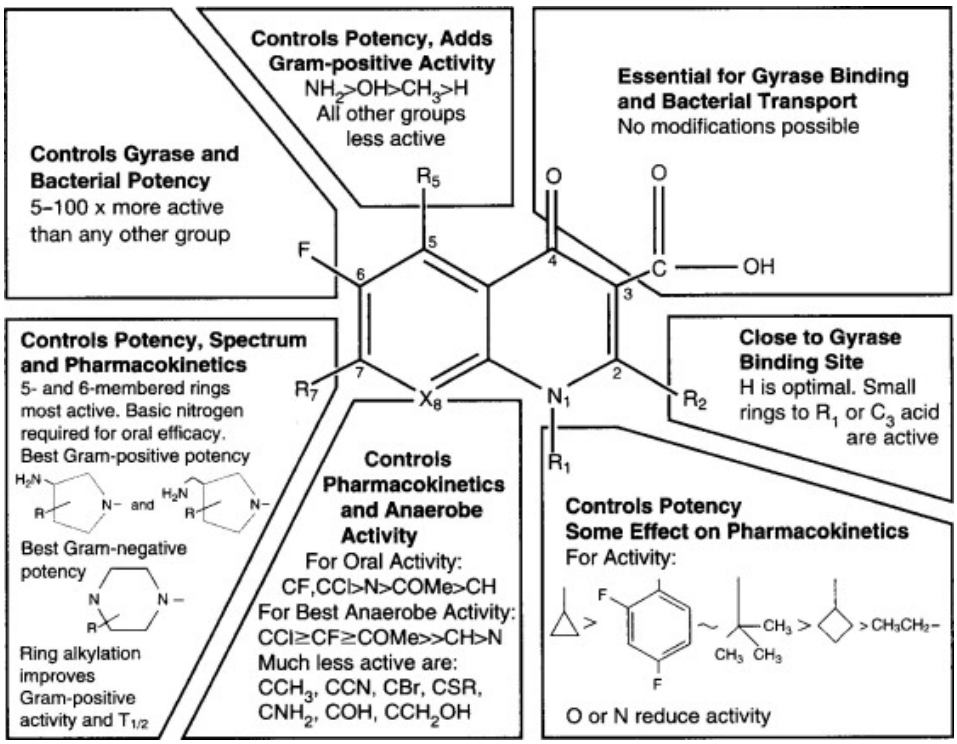

Figure 2 The different domains of the fluoroquinolones and differing the groups at various sites effects the activity and efficacy of the antibiotics versus different bacteria. Reproduced with permission from [12]

5.1.5 Resistance to Ciprofloxacin

As with most modern antibiotics, a number of bacterial strains and species are developing resistance to ciprofloxacin. Aboshanab *et al.* investigated the prevalence of ciprofloxacin resistance in a study using 169 gram-negative isolates taken from cancer patients suffering from infection.[14] Using the broth micro-dilution method, it was found that 89.3% of these isolates showed increased levels of ciprofloxacin resistance. Following the investigation of selected isolates using polymerase chain reaction (PCR) and DNA sequencing, the cause was found to be a combination of factors. These include: the upregulation of the CCCP efflux pump, which removes the antibiotics from the cell, a mutation in the *gyr*A gene, which determines the structure of the DNA gyrase enzymes, as well as an increase in the production of a mutant aminoglycoside modifying enzyme (AAC(6')-Ib-cr) which is able to acetylate ciprofloxacin, thereby deactivating it.[15-17]

5.1.6 Infection and Cancer

Over 15% of malignancies across the globe have been shown to have an infectious cause, including viruses, bacteria, fungi and trematodes (parasitic flat worms).[18] Cancer development through infection is most commonly attributed to viral infections, being responsible for the formation of a variety of different cancers including: T-cell leukemia and lymphoma attributed to HTLV-1, Merkel cell carcinoma attributed to MCV and Kaposi sarcoma that is attributed to HIV.[19] Owing to viruses being such prevalent infectious causes of cancer formation, bacterial causes have been widely overlooked, despite being associated with a number of malignancies. Examples of this include *Helicobacter pylori,* a bacteria with the proven ability to induce the growth of non-cardia gastric carcinoma in humans.[20, 21] *Salmonella trachomatis* is also another bacterial initiator of cancer growth, aiding the development of carcinoma in the cervix and ovaries. The exact cause-and-effect relationship between skin cancer and *S. aureus* infections remains unknown, but there is greatly increased incidence of squamous cell carcinoma of the skin (a type of tumour) and these bacterial skin infections.[22]

5.1.7 5-Flourouracil

5-fluorouracil, figure 3, is an anticancer chemotherapeutic used to treat a number of cancers including breast, colon, and importantly, skin cancers.[23] The fluoropyrimidine molecule is uptaken in cells in the same manner as uracil, an RNA base, and acts as both an antimetabolite drug as well as affecting DNA synthesis.

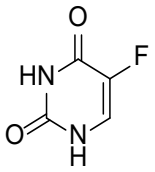

Figure 3 5-Fluorouracil

There is clearly a clinical need that is yet to be addressed for the co-treatment of both of these disease states. Whilst it is unknown on the direction of the cause-and-effect relationship between *S. aureus* infections and skin cancers, controlled topical release of two separate drugs from a wound dressing could provide an answer.

5.2 Aims and Objectives

The aim of this chapter is to combine the two concepts introduced in chapters 3 and 4. Utilising the concept of prodrugs, antibiotic molecules masked with two boronic acids will be synthesised. These will act as crosslinkers to create PVA hydrogels and will activate in response to H_2O_2 due to oxidation of the boronic acid groups. The initial application of this is to develop a topical anti-bacterial hydrogel for the purpose of wound dressings. Beyond this we wish to use other active compounds to show the utility of this method for a number of different drug classes and treatments, and to show the ease in which a responsive, multi-drug release system could be generated, figure 4.

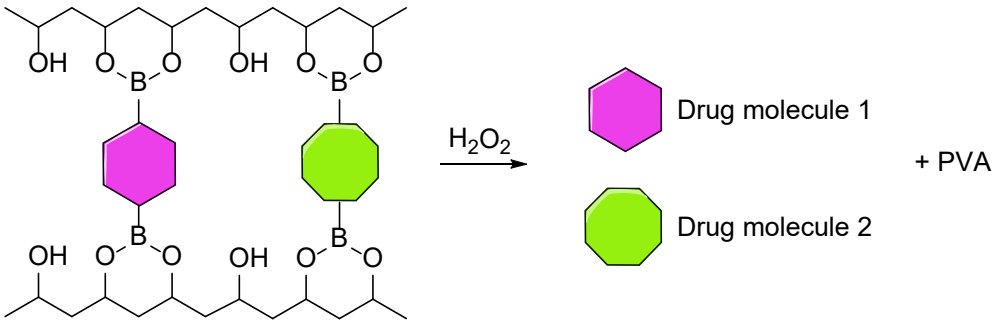

Figure 4 A schematic representation of a PVA hydrogel crosslinked with boronic acid functionalised drugs that on addition of topical H_2O_2 can release and activate drug molecules

5.3 Materials and methods

5.3.1 General Information

All solvents and reagents were purchased from commercial suppliers and used without further purification unless otherwise noted. Analytical thin-layer chromatography (TLC) was performed using commercial pre-coated silica gel plates containing a fluorescent indicator. Column chromatography was carried out using silica gel (0.040 - 0.063 mm). Analytical thin-layer chromatography (TLC) was performed using commercial pre-coated silica gel plates. Proton and carbon NMR were recorded using a Bruker Advance 500. Chemical shifts are reported in ppm using TMS or solvent residual signals as internal reference standards. High-resolution mass spectrometry (HRMS) experiments were performed on an Agilent 6545 LC/Q-TOF. UV-vis measurements were performed using either a BMG Labtech Clariostar in Co-star 96 well plates of variable pathlength, or a Shimadzu UV-1800 UV spectrometer at room temperature in a quartz cuvette, path length 10 mm. Fluorescence measurements were performed on a BMG Labtech CLARIOstar using Greiner Bio-One microplates (96-well, PS, f-bottom (chimney well), black-walled). Data was collected via the BMG Labtech Clariostar data analysis software package MARS.

Synthetic experimental information can be found in chapter 6.

5.3.2 Gel Synthesis

PVA hydrogels were prepared as in chapter 4 A 100 mM solution of ciprofloxacin bisphenylboronic acid (CBPBA) or 5-fluorouracil bisphenylboronic acid (5-FBPBA) in DMSO was mixed with a 10% w/v solution of PVA in DMSO. These were then placed in a 70 °C oven overnight, before washing with PBS, petroleum ether and PBS again. The gels were stored in PBS until needed.

5.3.3 UV-vis Measurements in Solution

UV-vis spectra of the conversion from CBPBA to ciprofloxacin were obtained by addition of H_2O_2 (0.5 mL, 100 μM) in PBS to a solution of CBPBA (0.5 mL, 100 μM) in PBS (1% v/v DMSO). The solution was allowed to react for 30 minutes and was measured against a blank of PBS (1% v/v DMSO) with a control of CBPBA solution (50 μM) in PBS (1% v/v DMSO).

5.3.4 UV-vis Measurements Using CBPBA Hydrogels

CBPBA hydrogels (200 mg ± 10 mg) were incubated in varying concentrations of H_2O_2 in PBS (0 – 50 mM, 1 mL) for 60 minutes at 25 °C. This solution was transferred to a quartz cuvette with a path length of 10 mm.

Alternatively, for the measurements against time the solutions were measured at intervals of 5 minutes, and then returned to the vial containing the CBPBA hydrogel.

5.3.5 Fluorescence Measurements in Solution

Fluorescence spectra of the conversion from CBPBA to ciprofloxacin were obtained by addition of H_2O_2 (0.5 mL, 100 μM) in PBS to a solution of CBPBA (0.5 mL, 100 μM) in PBS (1% v/v DMSO). The solution was allowed to react for 30 minutes and an aliquot of 100 μL was transferred to a micro-plate. This was measured against a control of CBPBA solution (50 μM) in PBS (1% v/v DMSO). Excitation 317 – 14 nm, Emission 330 nm - 600 nm.

5.3.6 Initial Fluorescence Measurements Using CBPBA Hydrogels

CBPBA hydrogels (200 mg ± 10 mg) were incubated in varying concentrations of H_2O_2 in PBS (0 – 980 mM, 1 mL) for 60 minutes at 25 °C. At 10 minute intervals 100 μL of each solution was removed and transferred to a microplate, the fluorescence intensity was measured, and the aliquot was returned to the original solution to maintain sink conditions. Excitation 327 – 14 nm, Emission 415 – 20 nm.

5.3.7 Ciprofloxacin Standard Curve

Solutions of ciprofloxacin in PBS (1% v/v DMSO) at concentrations ranging from 1 – 40 μM were measured by UV-Vis at their absorbance max (275 nm). This data was then plotted as a straight line ($R^2 = 0.9998$) and the Beer Lambert law re-arranged to yield the extinction coefficient of ciprofloxacin (49443 M^{-1} cm^{-1}).

5.3.8 MIC Determination

Antimicrobial susceptibility testing was carried out in a 96-well microtiter plate using a standard two-fold broth microdilution method as recommended by the Clinical Laboratory Standards Institute (CLSI).[24] Briefly, 100 μL of an antimicrobial agent of known concentration was serially diluted two-fold across the 96 well plate in calcium adjusted Mueller Hinton Broth (CAMHB).

Re-suspended bacterial cultures were diluted in CAMHB, and added in equal volume, so that each well contained approximated 5 x 10^5 CFU/mL (range 2 – 8 x 10^5 CFU/mL). The Minimum Inhibitory Concentration (MIC) was defined as the lowest concentration of antimicrobial agent required to inhibit the visible growth of bacterial strains after 18 h incubation at 37 °C.

5.3.9 Pseudo-MIC CBPBA Release Studies

The pseudo-MIC experiment follows the same procedure as a standard MIC determination (outlined above), however the starting solution is not an antimicrobial of known concentration. Instead it is a solution of gel exudate, generated by the incubation of CBPBA hydrogel (1 g) in H_2O_2 (3 mL, 50 mM in PBS) for 3 hours. Instead of being able to plot the concentration of the drug against the optical density of the bacteria, the data must be plotted as a function of the number of dilutions required to allow for bacterial growth (as measured by optical density).

5.4 Results and Discussion

5.4.1 Modification of Ciprofloxacin

In chapter 4 it was shown that masking the hydroxyl groups on fluorescein and thionol with boronic acids was able to quench the fluorescence of the fluorophores, and that these boronic acids could crosslink PVA solutions into hydrogels. A number of studies have investigated the structure activity relationships of the antibiotic ciprofloxacin, and all have agreed that the presence of the acid group and two carbonyls (red, figure 5) in fluoroquinolones are essential for activity, as well as bacterial transport.[12, 25] Substituents in the other commonly modified position (blue, figure 5) are less essential, and the adjustment of the moiety bound can affect the activity of the drug both as well as its spectrum of activity.[26]

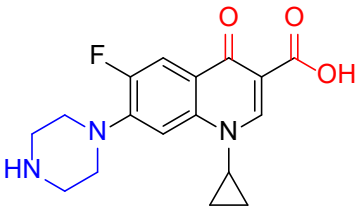

Figure 5 Ciprofloxacin and potential boronic acid linker binding sites

As the intention was to inactivate the drug to form a pro-drug crosslinker, the aim was to use the acid as the anchoring point, as according to literature it would prevent the activity of the drug should there be any crosslinker left unbound within the PVA matrix. Theoretically, the drugs binding to the PVA should prevent any uptake into cells, but as previously discussed, the nature of the boronic acid/diol binding is dynamic, ergo there is the potential for the diffusion of the pro-drug crosslinker out of the system.

As we no longer wished to target a single reactive part of the molecule as in chapter 3, the synthetic procedure became simpler as the need for protection chemistry had been removed. Now a simple one-pot synthesis could be performed, producing a crude product that could be recrystallized as opposed to purified through column chromatography, figure 6.

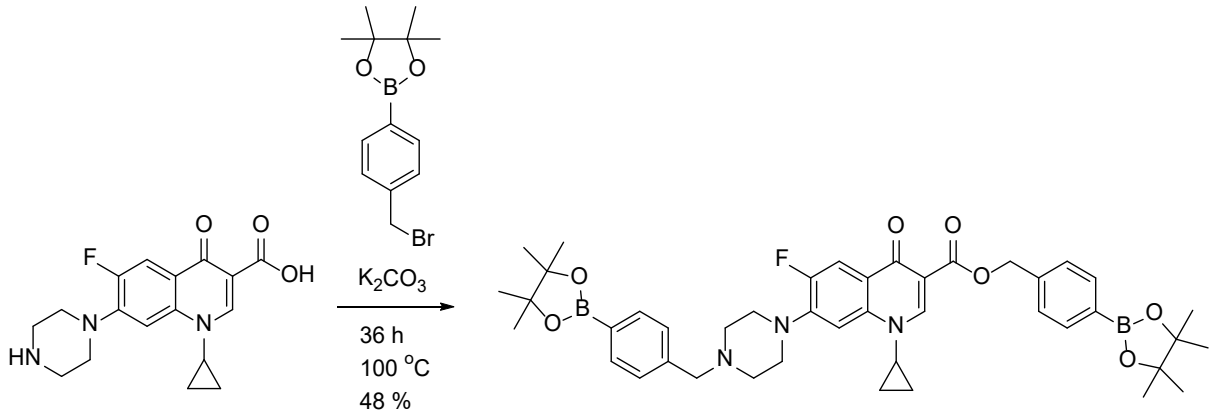

Figure 6 The one pot synthesis towards Ciprofloxacin bis-phenylboronic acid (CBPBA)

The first experiment performed was to ensure that the compound would be able to crosslink PVA in the manner of PF-1 and Purplement. As outlined previously, a 100 mM solution of the crosslinker was stirred with a 10% w/v PVA solution and heated at 70 °C overnight. This produced hydrogels that were stable and pale green in colour, figure 7.

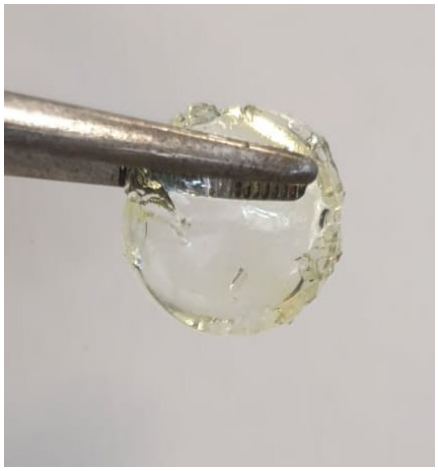

Figure 7 PVA hydrogel crosslinked with CBPBA

5.4.2 Solution Testing CBPBA

The oxidative degradation of CBPBA to native ciprofloxacin using H_2O_2 was confirmed by HRMS. This was then further confirmed using UV-vis, figure 8.

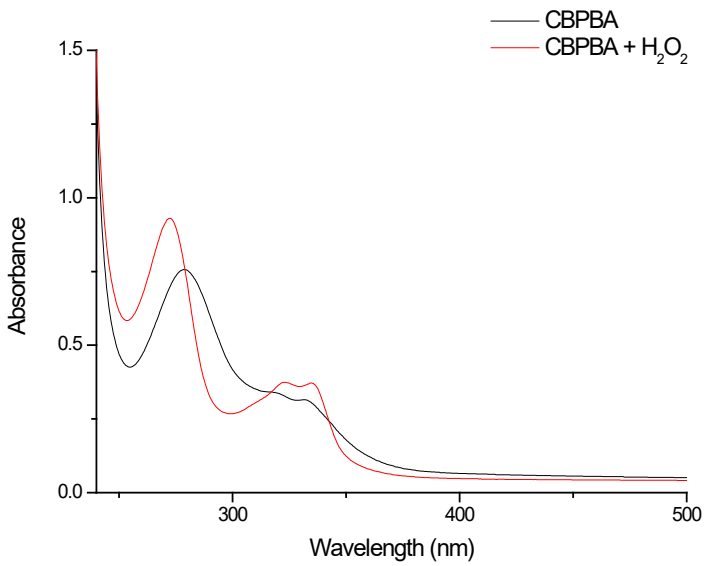

Figure 8 The shift in UV-vis spectra of CBPBA (50 μM) as it is oxidized into ciprofloxacin after 30 minutes after the addition of H_2O_2 (50 μM) in 10% DMSO 90% PBS buffer at 25 °C

The double peak at around 330 nm is characteristic of ciprofloxacin in free solution, as is the absorbance max at 278 nm (in 10% v/v DMSO), indicating the release of the free, active drug. Ciprofloxacin has inherent fluorescence. However, it was unknown whether binding the phenyl bpin linkers would affect the fluorescence, hence the fluorescence before and after the addition of H_2O_2 was measured, figure 9.

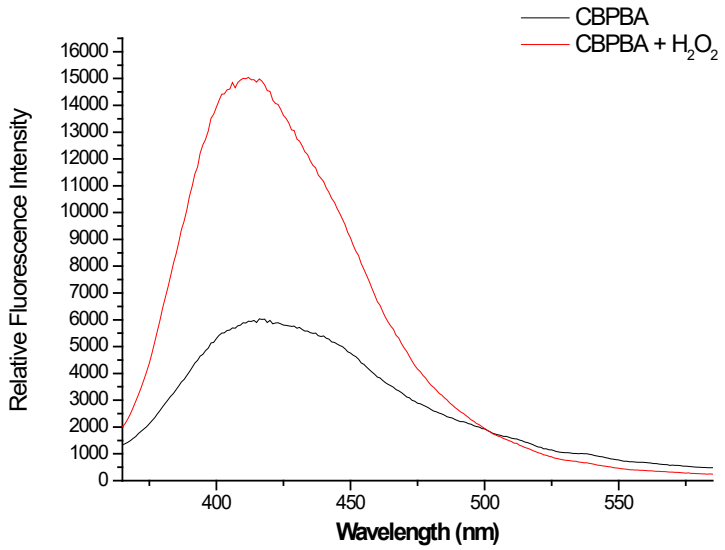

Figure 9 The fluorescence increase of CBPBA (50 µM) as it is oxidized into ciprofloxacin after 30 minutes following the addition of H_2O_2 (50 µM) in 10% DMSO 90% PBS buffer at 25 °C Ex 327 Split width: 14 nm

There is a clear increase of fluorescence on addition of H_2O_2, however, the emission maxima wavelength remains stationary. This indicates that the fluorescence of ciprofloxacin is owing to the bicyclic core and the quinolone, and that the binding of non-conjugated moieties to this (in this example through the acid and the amine), only serves to partially quench this fluorescence.

5.4.3 Initial Ciprofloxacin Release From CBPBA Hydrogel

Before starting detailed release studies, preliminary testing was performed to determine the concentration range of H_2O_2 which would elicit a response via release of the active compound from the hydrogel. To do this, hydrogels (each measuring 200 ± 10 mg) were incubated in solutions of differing concentrations of H_2O_2, and the fluorescence of the solutions were measured. Additionally, topical use of H_2O_2 as a wound disinfectant uses 3% w/v H_2O_2 solution, which equates to 980 mM.[27] This was tested alongside lower concentrations, figure 10.

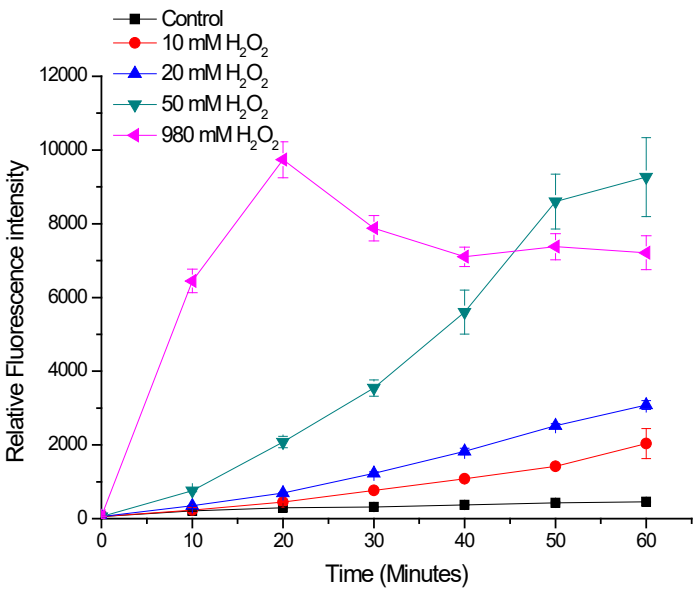

Figure 10 The increase in fluorescence intensity of CBPBA gel (200 ± 10 mg) exudate on exposure to increasing concentrations of H_2O_2 (0 – 980 mM) after 60 mins at 25 °C. Ex 327 – 14 nm, Em 415 – 20 nm. Error bars indicate standard deviation (n = 3)

Over time the fluorescence intensity was found to increase, higher concentrations of H_2O_2were found to achieve the fluorescence maximum at a quicker rate. However, this trend was not followed by the 980 mM solution. This reaches a maximum fluorescence intensity after only 20 minutes, before falling and plateauing at around 60% of its maximum fluorescence. The reason for this is made apparent when the solutions are inspected visually, figure 11, with the solution to the far left being clearly more turbid.

Figure 11 Five pieces of CBPBA gel incubated in H_2O_2 of concentrations (*left to right*) of 0, 10, 20 50 and 980 mM in PBS after 60 minutes

The solubility of unbound ciprofloxacin in aqueous solutions is very low.[28] Due to the high drug content of the gels, exposure to 980 mM H_2O_2 cause the solution to quickly become saturated with

ciprofloxacin. As the gels continue to break down the ciprofloxacin molecules begin to aggregate and become solid – it is suspected that this is quenching the fluorescence of the molecules. It may not be a complex chemical quenching however, and it may simply be that the turbidity of the solution is preventing the transmittance of the emitted light.

5.4.4 UV-vis CBPBA Gel Release Studies

Fluorescence was used to confirm that the rate of ciprofloxacin release was dependent on H_2O_2 concentration, UV-vis spectra was then used to investigate this phenomenon in a quantitative manner, figure 12.

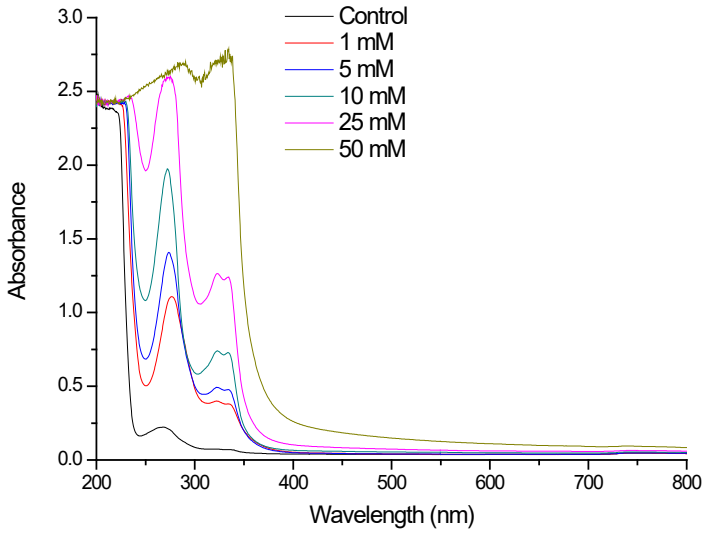

Figure 12 UV-vis spectra of gel exudate from CBPBA gels (200 mg ± 10 mg) incubated in H_2O_2 of varying concentrations (0 – 50 mM) in PBS at 25 °C after 60 minutes. Measurement at 50 mM above instrument maximum.

As can be seen in figure 12, an increase in the absorbance of due to the presence of ciprofloxacin can be seen at concentrations of H_2O_2 as low as 1 mM. The concentration of ciprofloxacin begins to reach the maximum that can be detected by the spectrometer when using 50 mM of H_2O_2, and begins to reach its maximum after one hour on exposure to at 25 mM, figure 13.

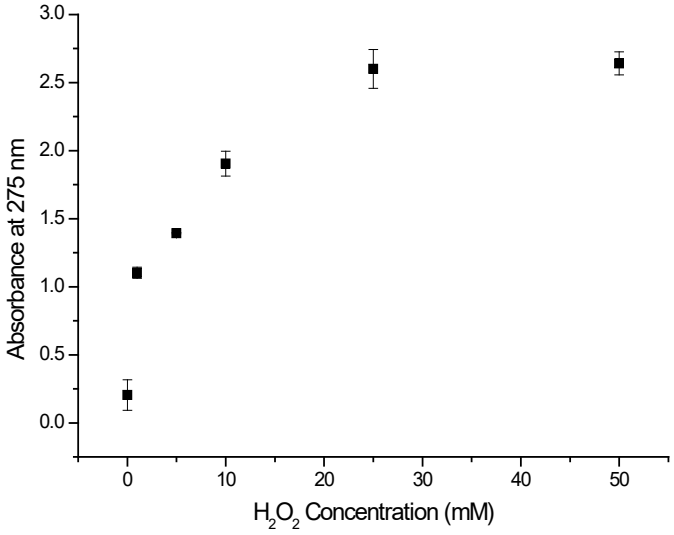

Figure 13 The increase in absorbance at 275 mM of CBPBA gel (200 mg ± 10 mg) exudate after incubation with H_2O_2 solutions (0 – 50 mM) in PBS at 25 °C for 60 minutes. Error bars indicate standard deviation, (n = 3)

Whilst a response could be gained at lower concentrations, the experiments proceeded with 50 mM of H_2O_2, to ensure maximum release of the ciprofloxacin from the gels. This is still a H_2O_2 concentration nearly 20 fold lower than that approved for topical use in healthcare.[29]

5.4.5 Converting Absorbance to Concentration

To gain an understanding of the rate at which the CBPBA gels would decompose with H_2O_2, the UV-vis spectra were measured every five minutes for gels that had been incubated with and without 50 mM of H_2O_2 (in PBS). From figure 13 it was found that after an hour of exposure the solution becomes saturated to the point that further increases of ciprofloxacin concentration could not be detected. As such, the experiment was given a maximum time limit of 45 minutes, Appendix 7.5.1.

Whilst the absorbance values can show that the drug is being released and in concentrations relative to other absorbance experiments, exact concentrations are important for determining if enough drug is being released above the MIC. A standard curve, figure 14, of ciprofloxacin was produced in order to convert the data from absorbance units to concentration.

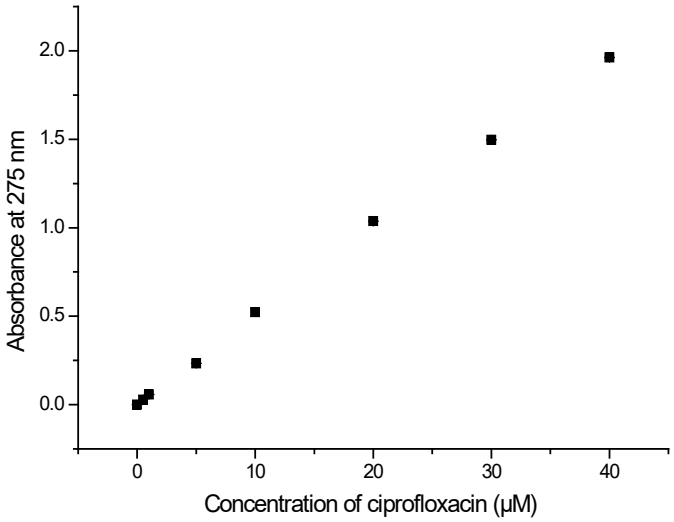

Figure 14 A standard curve of ciprofloxacin in PBS (with 1% DMSO). R^2 = 0.9998, Error bars indicate standard deviation (n = 3)

By rearranging the Beer-Lambert law, this standard curve gives an extinction coefficient for ciprofloxacin of 49443 M^{-1} cm^{-1}, agreeing with the literature values. Using this extinction coefficient appendix 7.5.1 can be replotted as a concentration, figure 15.

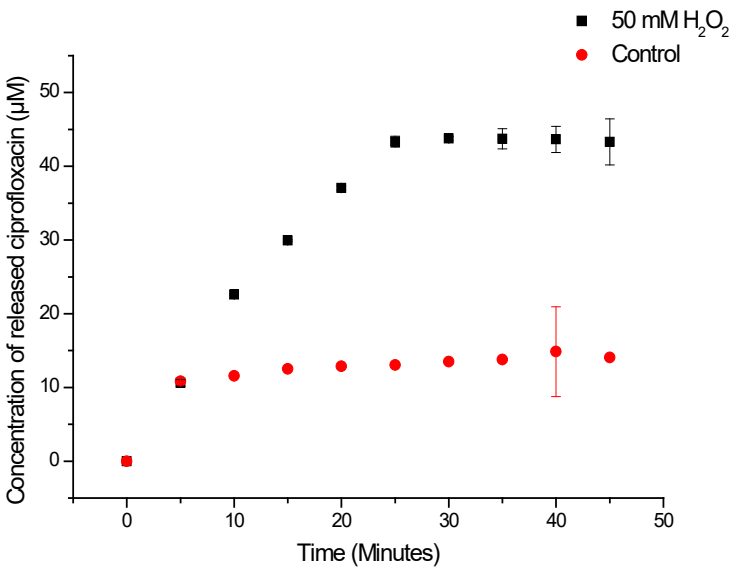

Figure 15 The increasing concentration of ciprofloxacin from CBPBA gel (200 mg ± 10 mg) on exposure to H_2O_2 (50 mM) in PBS at 25 °C over time (45 minutes). Error bars indicate standard deviation (n = 3)

As can be seen in figure 15 there is a near linear increase in concentration until 25 minutes, at which time the value begins to plateau. In contrast, the PBS control shows an initial release, assumed to be due to unbound crosslinker being removed, and then no further increase in ciprofloxacin concentration.

When considering MIC values in microbiology, concentrations are most often reported in $mgmL^{-1}$; after only 25 minutes of exposure to 50 mM of H_2O_2, 200 mg of CBPBA gel is able to produce a ciprofloxacin concentration of 0.014 $mgmL^{-1}$. Despite this being the maximum concentration that could be detected by UV-vis, it was not the maximum concentration that would likely be released, owing to the loading concentration of 100 mM. As per methodology 5.3.9 gels with a volume of 1 mL were submerged in 3 mL of solution, giving a potential final volume of 8.2 $mgmL^{-1}$. The practical value is likely to be lower than this owing to washing steps and incomplete reaction of the H_2O_2 with all of the crosslinker molecules.

5.4.6 Biological Testing – MICs of Ciprofloxacin and H_2O_2

Once it had been established that the gel system would release a therapeutic amount of ciprofloxacin it needed to be tested on an *in-vivo* bacteria model. The MIC's of ciprofloxacin were determined against the bacteria that were going to be tested, which were: gram-positive *S. aureus* H560, and gram-negative *P. aeruginosa* PAO1 and *E. coli* NCTC 10418, figure 16.

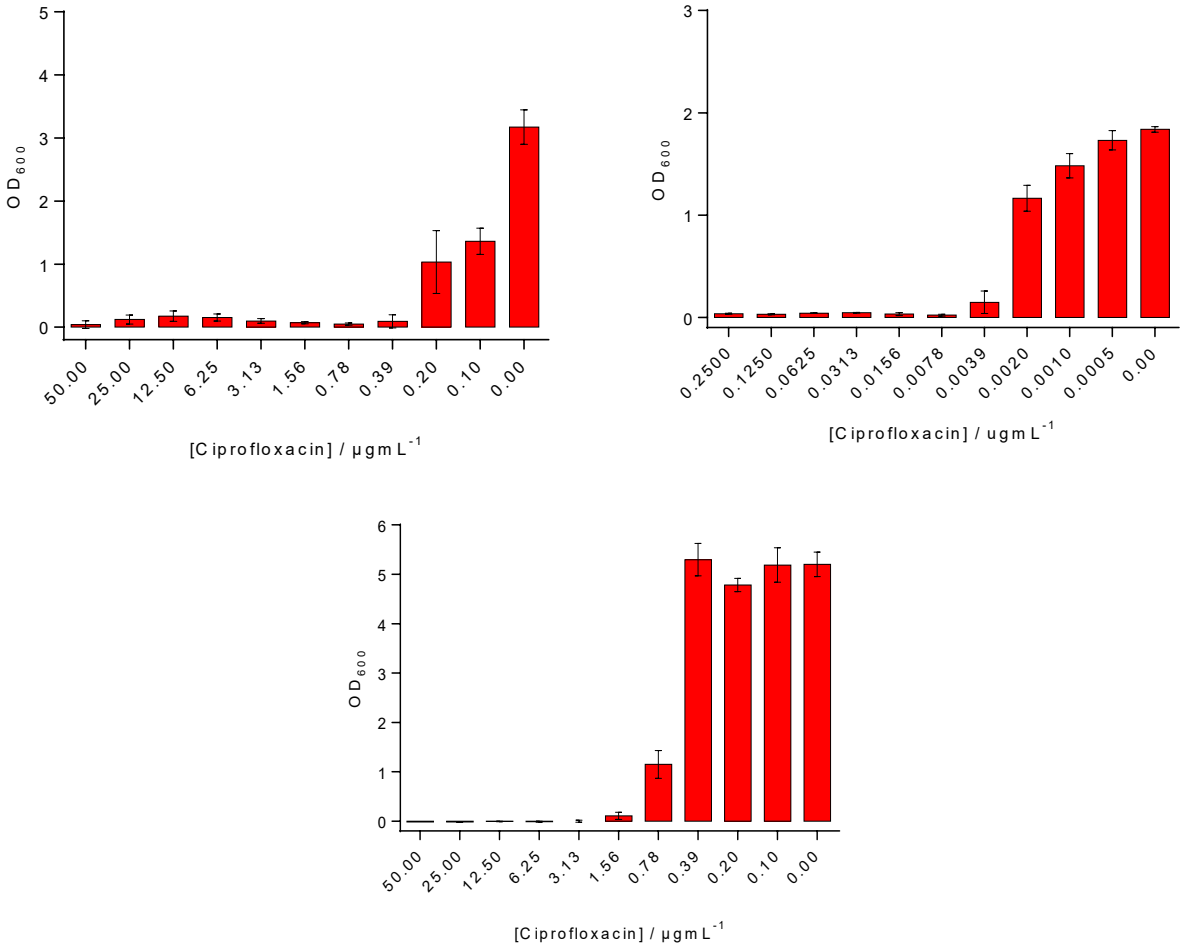

Figure 16 Minimum Inhibitory Concentration (MIC) of Ciprofloxacin for *S. aureus* H560 (*top left) E. coli* NCTC 10418 (*top right*) and *P. aeruginosa* PAO1 (bottom). Optical density was measured at 600 nm after 18 h incubation at 37 °C. Error bars indicate standard deviation (n = 3)

As can be seen in the MIC data, the amount of ciprofloxacin measurable would inhibit the growth of *E. coli* but not the other two bacteria. The calculated MICs were 0.20 – 0.39 µgmL^{-1} for *S. aureus* H560, 0.0039 – 0.0078 µgmL^{-1} for *E. coli* NCTC 10418 and 0.78 – 1.56 µgmL^{-1} for *P. aeruginosa* PAO1. To ensure that there was enough drug released to inhibit the bacterial growth when performing the CBPBA gel experiments, the gels were allowed to incubate in the H_2O_2 solutions for 3 hours.

As when measuring the efficacy of ARS as a biofilm inhibitor in chapter 2, the effect of the trigger H_2O_2 had to be considered. The MICs of H_2O_2 versus the same bacteria were measured, figure 17.

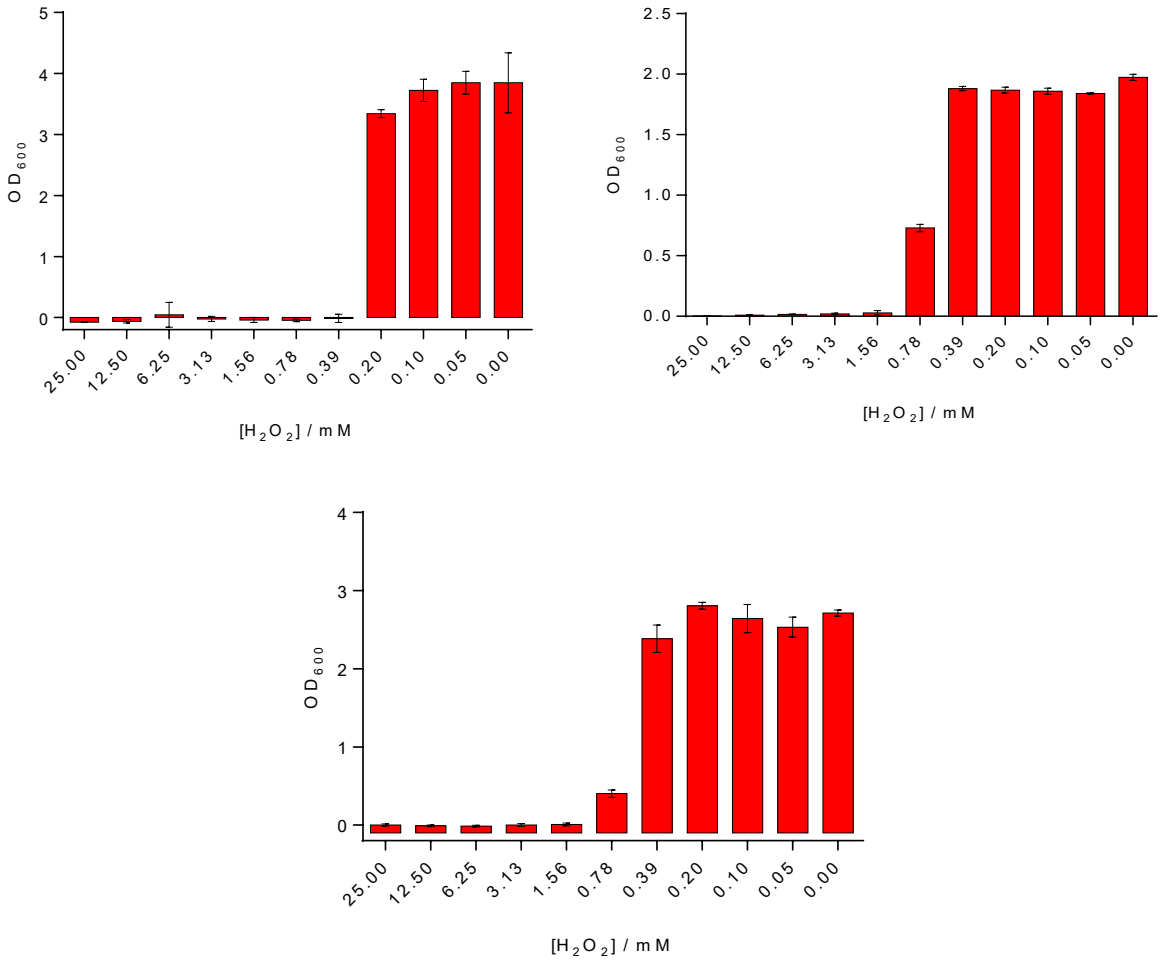

Figure 17 MIC of H_2O_2 for *S. aureus* H560 (*top left) E. coli* NCTC 10418 (*top right*) and *P. aeruginosa* PAO1 (bottom). Optical density was measured at 600 nm after 18 h incubation at 37 °C. Error bars indicate standard deviation (n = 3)

As can be seen from figure 17 the concentration of H_2O_2 required to inhibit the growth of all three species of bacteria is far lower than the 50 mM solution that we are using to trigger the release of ciprofloxacin from CBPBA. The calculated MICs were 0.20 – 0.39 mM for *S. aureus* H560, 0.0039 – 0.0078 mM for *E. coli* NCTC 10418 and 0.78 – 1.56 mM for *P. aeruginosa* PAO1. As a result of these values being lower than the H_2O_2 concentrations being used for the release conditions, both H_2O_2 and the gels in PBS were required as controls. The experiment was designed as a pseudo MIC. It was clear from the bacterial testing above that the large concentration of H_2O_2 would kill the bacteria, masking any effect the released ciprofloxacin may have had. To overcome this a control solution of 50 mM H_2O_2, a control of the CBPBA gel in PBS, as well as the test solution of the CBPBA gel in H_2O_2 were treated as a solution of antimicrobial. These were then diluted

across a microtitre plate, with a two-fold dilution in each well. This allowed a comparison to be made between the H_2O_2 on its own and the solution of H_2O_2 with ciprofloxacin. Each piece of gel was left in the solution for 3 hours to ensure maximum ciprofloxacin release.

5.4.7 Pseudo MICs to Measure Ciprofloxacin Release from CBPBA Gels

The optical density at 600 nm was used as a measure of bacterial growth and was plotted against two fold dilutions. This number, whilst arbitrary as the initial concentration was not known, allowed comparison between our release condition and our control experiments, yielding values shown in table 1 for the number of dilutions required to allow the bacteria grow. Full data can be seen in appendix 5.2.

Table 1 A comparison of the number of two fold dilutions required until the inhibition of growth of bacteria was no longer observed. An increase in the number of diltuions required is indicative of a solution with increased ability to inhibit bacterial growth

Bacterial Species	**Experimental condition**		
	Number of 2-fold dilutions until growth		
	H_2O_2 50 mM	**CBPBA + PBS**	**CBPBA + 50 mM H_2O_2**
***S. aureus* H560**	8	7	13
***E. coli* NCTC 10418**	7	7	15
***P. aeruginosa* PAO1**	7	3	9

This 'pseudo-MIC' data indicates high levels of killing from both of the controls, across all three bacteria. This was expected for H_2O_2, as the MICs had been calculated to be lower than 50 mM. What was surprising, however, was that the CBPBA in PBS induced a large inhibition of growth. Owing to the previously discussed structure activity relationships of ciprofloxacin, it was assumed that CBPBA would be inactive against all strains. However, despite the change in structure at the acid group there is a clear and obvious bactericidal effect on all the strains tested. This could potentially be due to the large excess of CBBPA that is present within the gel. However, despite this non-specific killing, there is a clear decrease in bacterial growth, thus triggered release, from gel exudate exposed to H_2O_2. The black line, indicating the solution under release conditions, clearly shows that bacterial growth was presented after 8, 2-fold dilutions (a total dilution of 512-fold). This is better displayed as a bar chart and can be seen in figures 21, 22 and 23.

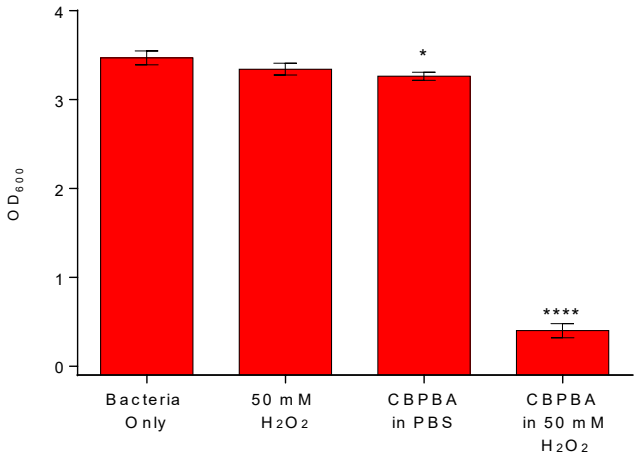

Figure 21 Optical density of *S. aureus* H560 upon exposure to 512-fold diluted: 50 mM H_2O_2, exudate from CBPBA hydrogels in PBS and exudate CBPBA hydrogels in 50 mM H_2O_2. CBPBA hydrogels were incubated for 3 h at 25 °C before subsequent use. Optical density was measured at 600 nm after 18 h incubation at 37 °C. Error bars indicate standard deviation (n = 3). Statistical significance was determined using a one way anova when compared to bacteria only control

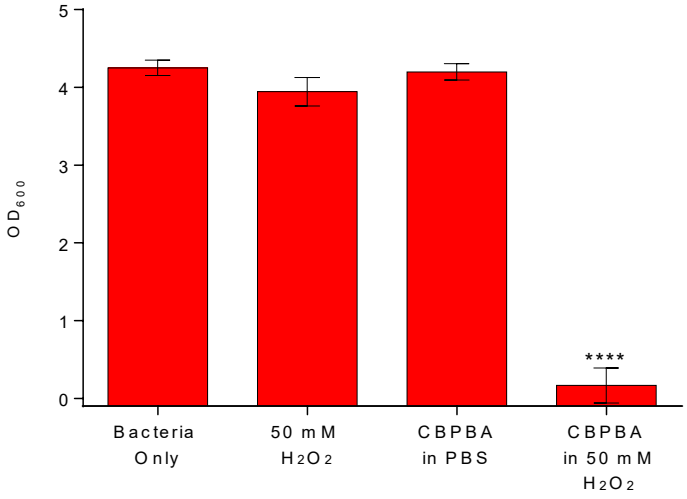

Figure 22 Optical density of *E. coli* NCTC 10418 upon exposure to 512-fold diluted: 50 mM H_2O_2, exudate from CBPBA hydrogels in PBS and exudate CBPBA hydrogels in 50 mM H_2O_2. CBPBA hydrogels were incubated for 3 h at 25 °C before subsequent use. Optical density was measured at 600 nm after 18 h incubation at 37 °C. Error bars indicate standard deviation (n = 3). Statistical significance was determined using a one way anova when compared to bacteria only control

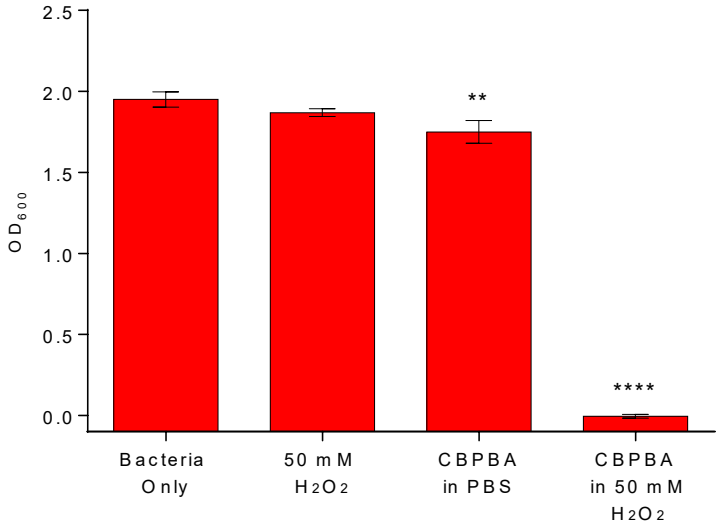

Figure 23 Optical density of *P. aeruginosa* PAO1 upon exposure to 512-fold diluted: 50 mM H_2O_2, exudate from CBPBA hydrogels in PBS and exudate CBPBA hydrogels in 50 mM H_2O_2. CBPBA hydrogels were incubated for 3 h at 25 °C before subsequent use. Optical density was measured at 600 nm after 18 h incubation at 37 °C. Error bars indicate standard deviation (n = 3). Statistical significance was determined using a one way anova compared to bacteria only control

5.4.8 CBPBA Biological Activity

This proved that the methodology of synthesising bis-PBA compounds was able to make active crosslinkers that could be reactivated, with release of the drug from the PVA matrix following the addition of H_2O_2. It was assumed that there would be a measure of non-specific release of the crosslinker over the period of incubation (3 hours) owing to the dynamic nature of the bonds, however it was not expected to produce such a great inhibition of bacterial growth. The obvious experiment to check this would be to perform the MIC of this compound against the three bacteria used. This normally would require making up a solution of 1 $mgmL^{-1}$ in PBS and then perform serial dilutions, testing each dilution to determine if it prevented bacterial growth. For antibiotics with low solubility, co-solvents of DMSO or EtOH can be used up to 10% v/v, however beyond this there can be significant effects on the bacterial growth, invalidating results.[30, 31] To prevent this solvent interference the initial solution could only be made at an initial concentration of 50 μgmL^{-1} (0.64 mM) meaning when incubated with the bacteria the first measurable concentration was 25 μgmL^{-1} (0.32 mM), table 2.

Table 2 MIC value of CBPBA

	Minimum Inhibitory Concentration / μgmL^{-1}
***S. aureus* H560**	> 25.00
***E. coli* NCTC 10418**	12.50 – 25.00
***P. aeruginosa* PAO1**	> 25.00

After 1 hour the gel exudate from 200 mg of CBPBA gel had given a solution concentration of over 10 mM when measured by UV-vis. It is assumed that due to the increased mass of CBPBA gel used (1 g), as well as the increased time of incubation (3 hours), that the concentration would be above that of the MIC, hence the non-specific kill. It is unknown if the CBPBA itself is active, or if endogenous ROS species produced by the bacteria are activating it and producing ciprofloxacin in-situ.

5.4.9 Expansion of the Methodology

Once a working hydrogel system had been designed for the release of an antibiotic, we aimed to prove the more universal utility of this approach for other classes of drug, for other disease states. 5-Fluorouracil is an anti-cancer chemotherapeutic, used in the treatment of a number of conditions, including skin cancers.[32] A topical anti-cancer drug that can treat carcinomas was chosen due to the potential for dual release of the drug with ciprofloxacin, which would be a potential avenue for treatment for the *S. aureus* infections commonly associated with Squamous cell carcinoma patients.[22]

Similarly to the development of CBPBA, the synthesis of 5-fluorouracil bis-phenyl boronic acid (5-FBPBA) could be performed in a single step with commonly used reagents and moderate reaction conditions, figure 24.

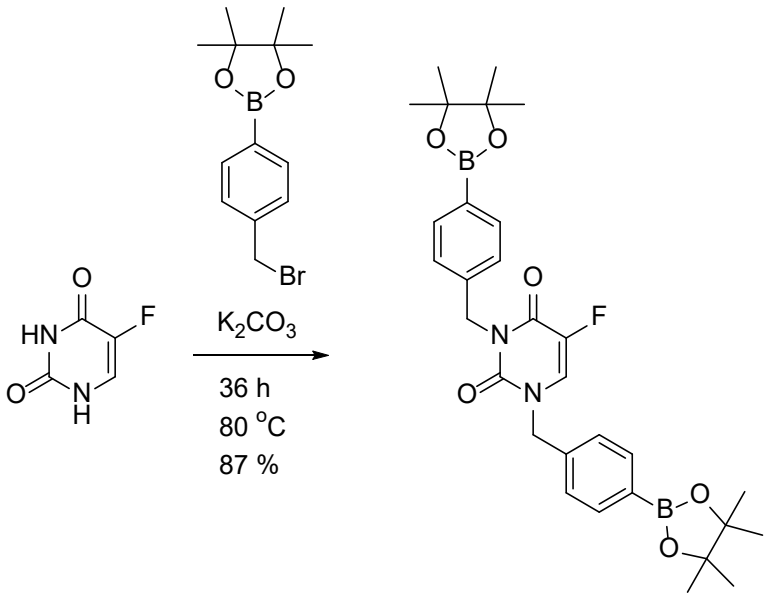

Figure 24 The one pot synthesis for the crosslinking molecule 5-FBPBA

A 100 mM solution of 5-FBPBA in DSMSO was mixed with a 10 % w/v PVA in DMSO solution in the same manner that the previous gels were synthesised, forming a solid hydrogel with PVA that had a faint orange colour, figure 25. These were then washed in the same manner, resulting in gels with similar characteristics.

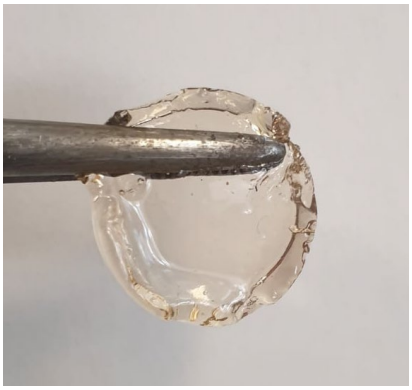

Figure 25 5-FBPBA crosslinked PVA hydrogel

It was shown by HRMS that the native 5-fluorouracil was released from the PVA hydrogel upon exposure to the H_2O_2. Due to not having the facilities within our group to conduct cancer cell line testing, this and further study will be conducted by our collaborators at the University of Austin.

5.4.10 Gel Stability

As in the previous chapter using masked fluorophores, the hydrogels were tested for their stability in both air and aqueous solvent. Figure 26 shows the stability of the gels exposed to air over the course of ten day

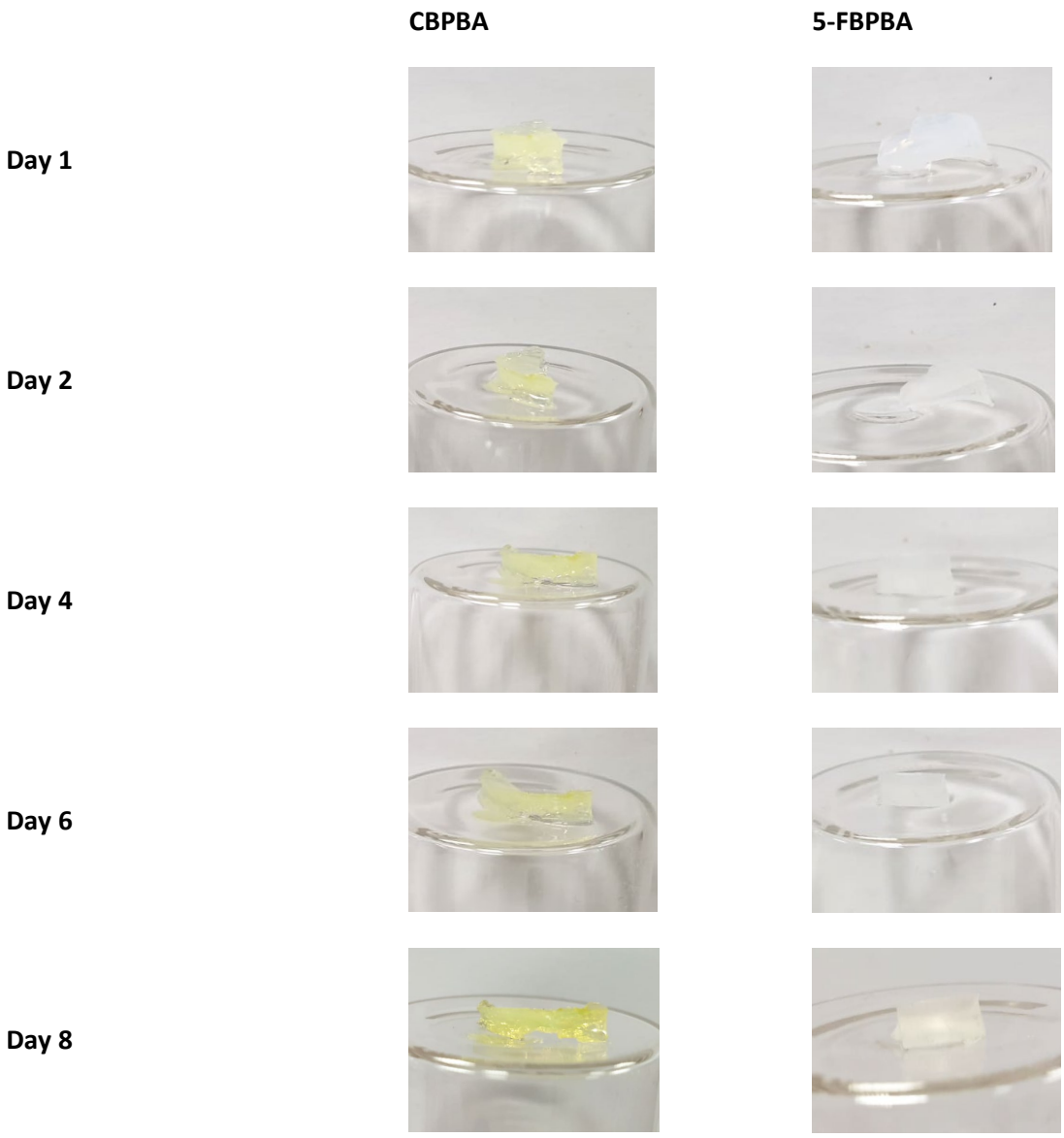

Day 10

Figure 26 The stability of the CBPBA and 5-FBPBA crosslinked PVA hydrogels on exposure to air over the course of 10 days

As can be seen above, the gels began to dehydrate over time, however they remain solid and gelatinous. This could be problematic in the future, as a fully hydrated gel is essential for the application of wound dressings, as the shelf life of such products are of utmost importance to their final use. Whilst rehydration is possible, it could potentially provide a barrier to clinical use.

5.5 Conclusions

We have developed a novel system for the release of drugs in response to H_2O_2 using PVA hydrogels, which have been crosslinked using PBA functionalised drugs. Through simple synthetic modifications, any drug with two carboxylic acids, amines or hydroxyl groups can be functionalised to form a similar crosslinker. It has been shown that ciprofloxacin can be released at concentration that are inhibitory to bacterial growth, to a greater extent than that of control conditions. The CBPBA however, has shown to be effective against bacteria, and thus further study is needed to determine its mode of action, and if this activity is due to the oxidation of the drug by endogenous H_2O_2 produced by bacteria, or if it is simply active in its full form.

The scope for the expansion of this methodology has been shown with the use of the anticancer drug 5-fluorouracil. Identical chemistry was employed to synthesise a derivative of this compound with phenyl-boronic ester, allowing it to act as a crosslinker. This was shown to also form stable PVA hydrogels and release the native anti-cancer drug. This offers the potential for the triggered release of these to drugs in the treatment of skin cancer associated infections.

As a drug delivery mechanism this methodology also shows great promise for use in the triggered release of nearly any drug that requires topical application, due to the broad range of tolerated functionalities.

5.6 Future Work

5.6.1 Increasing Scope

Following the development of a release system able to individually release ciprofloxacin and 5-fluorouracil, it would be an advantage to release the two simultaneously. Theoretically, as long as the total crosslinker concentration used was the same, the composition of that solution could be formed of any number of functionalised drugs. This could be of particular advantage when considering wound infection, in particular mixed species biofilms. A number of biofilm disruptors exist which could help the clearance of a biofilm, whilst the bacteria within could be treated with multiple antibiotics at once in order to maximize the possibility of treatment. As his been discussed throughout this thesis there are a number bacteria that are resistant to antibiotics, and so a cocktail of bio-film disruptors and antibiotics could be released that would clear hard to treat infections. As such, a library of drug molecules come cross-linkers could be developed which would allow for the treatment of persistent infections with antibiotics of various classes. Potential candidates for such a scenario can be seen in figure 27.

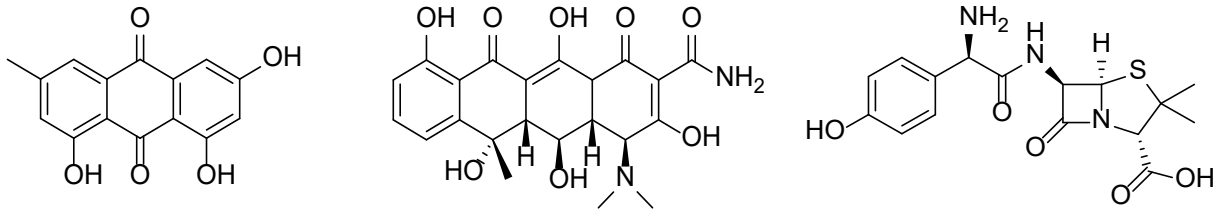

Emodin	**Oxytetracycline**	**Amoxicillin**
Antibiofilm agent – Binding sites phenols	Antibiotic – Binding sites phenols	Antibiotic – Binding sites phenol amine and acid

Figure 27 Potential additional therapeutics that could be co-delivered to treat wound infection using the bis-PBA acid PVA technique

Other gels and gel formulations could allow for new applications of the system. As previously discussed, cancer cells have a much higher levels of H_2O_2 than normal cells. A system such as this could potentially allow for an injectable hydrogel anti-cancer drug delivery system into tumours. The masked drugs would only activate in the presence of ROS, and the gel would degrade into harmless products as the drug is released, making the process highly bio-compatible, and increasing the pharmacokinetic profile of the drugs. Much like antibiotics,

anticancer drugs often feature a number of functionalities that would be suitable for the synthesis of the bis-PBA crosslinkers.

5.6.2 Theranostic Development

The purpose of the work within this thesis was for the development of a hydrogel system that could be used in a wound dressing and would able to detect and treat bacterial infection. A dressing that could do this without being removed, thus exposing the wound to the air, would help prevent reinfection.

A system that can both diagnose and treat a disease state is known as a theranostic system. Whilst in this instance we are tailoring our work toward infection, theranostics have been used extensively in the treatment of cancer.[33] These often involve the use of H_2O_2 triggered systems that are mainly used for imaging purposes due to an increase in fluorescence, although they can be tailored to release a drug.

Of the two PVA systems outlined in chapter 3 and chapters 4 and 5, the most suitable system to produce a theranostic system would be that in chapter 3, binding compounds with just a single PBA or boronic acid moiety. This expands the scope of potential molecules greatly, however would require a separate crosslinking method compared to the bis-PBA functionalised compounds of this chapter. This can be overcome by methods as discussed in chapter 3. Whilst this would give rise to the therapeutic aspect of a theranostic, it still does not contain a diagnostic method. There are numerous ways in which this could be incorporated, two of which will be outlined.

5.6.2.1 Incorporation of Bacterial Toxin Sensitive Vesicles

As previously discussed, bacteria secrete a number of different virulence factors, including toxins. One of these toxins, delta toxin produced by *S. aureus* amongst other pathogens, is used by the bacteria to disrupt phospholipid membranes aiding in its colonization of the host. This has been utilized by Thet *et al.* to create detection systems for bacteria, based around the use of phospholipid vesicles. The breakdown of the phospholipid vesicles, thus the presence of bacteria, can be detected through the release of a self-quenching fluorescent dye (*i.e.* fluorescein) or through electrochemical methods.[34, 35]

These vesicles form the basis of the '*Smart Wound'* technology developed, and can be suspended in a variety of hydrogels including CMC, agarose and PVA.[9]

If a PVA hydrogel were to be created in which a boronic acid or PBA functionalised drug were bound, and fluorescein filled vesicles were suspended in the hydrogel, there would be a colorimetric and fluorescent response to the presence of an infection. This obvious change in the wound dressing would act as an alert to a medical professional that an infection had occurred, and they could then apply H_2O_2 or CAP to the dressing to release the bound drug, clearing the infection. This system is represented schematically in figure 28.

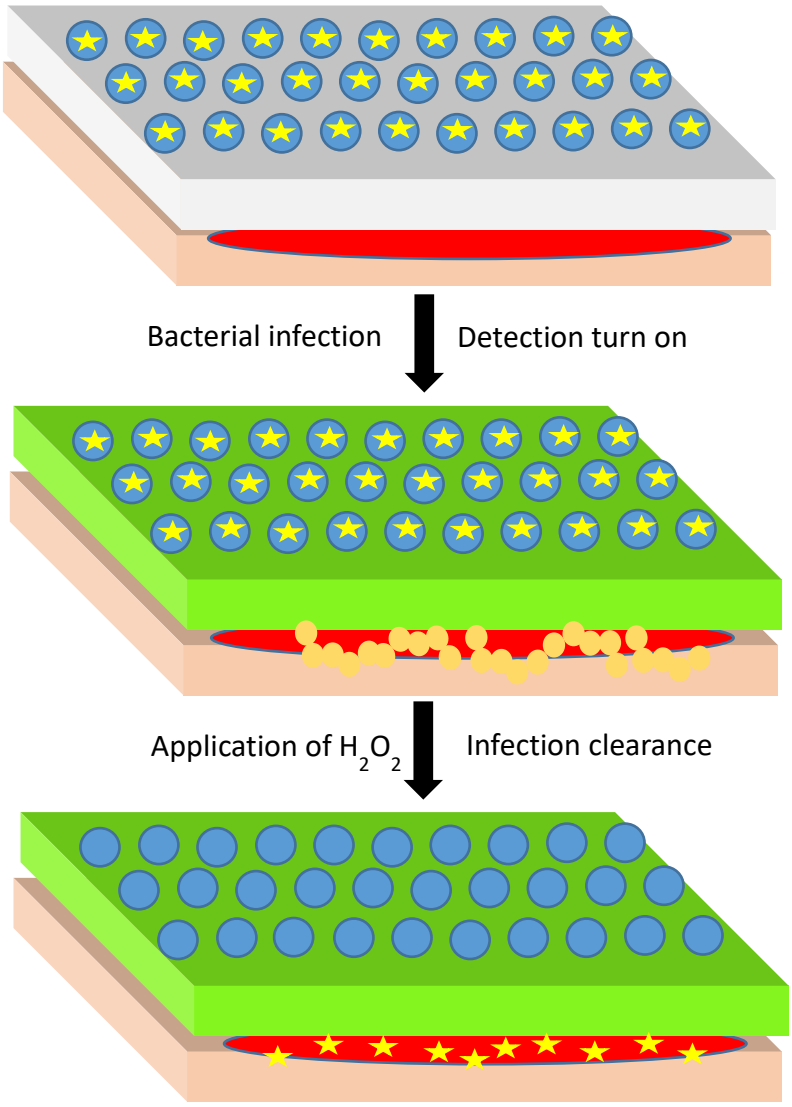

Figure 28 A schematic representation of a PVA wound dressing loaded with carboxyfluorescein filled vesicles, and with boronic acid bound ciprofloxacin in the gel matrix. On infection, the bacteria release toxins, breaking down the vesicles. This then releases carboxyfluorescein giving a colour change. This indicates an infection to the clinician, who would then apply topical H_2O_2 to release the bound antibiotic, clearing the infection

The use of the boronic acid/diol functionalisation could allow multiple therapeutic agents to be bound within the matrix. There is also the potential for modification of the phospholipid vesicles to give a more rapid response versus certain species and strains of bacteria, which is ongoing work within the Jenkins group.

5.6.2.2 Use of Pyroelectric Particles to Create an Automatic Wound Infection Warning and Drug Release

Pyroelectric particles are a subset of piezoelectric particles. In piezoelectric or pyroelectric particles or materials, mechanical or thermal energy is converted into chemical energy.[36] The formation of a dipole due to mechanical stress results in a collection of surface charges at each pole. Upon depolarization this electrochemical gradient can cause redox reactions with water, producing ROS such as ·OH and $\cdot O_2$.[37] This has led to interest in their use as a green methods of waste water treatment. Some more recent materials can produce H_2O_2, giving them the potential for incorporation into the previously discussed ROS sensitive triggered release systems.[38]

$Sr_{0.3}Ba_{0.7}TiO_3$ particles, produced by the Bowen group in the mechanical engineering department at the University of Bath, have been shown to both disinfect bacterial solutions as well as degrade organic dyes in solution. The temperature at which these particles depolarise is 35 °C, though this can be tuned by varying the ratios of Sr to Ba. The amount of organic dye decomposition, correlating to the amount of ROS, is dependent on the number of heating/cooling cycles. Similarly, with the inhibition of bacterial growth, more effective bacterial clearance is achieved with more cycles. In order to get sufficient production of ROS to achieve the inhibition of bacterial growth the particles need to be heated and cooled cycled 6 times. Whilst inherently there is ROS produced, it is clear that in a clinical scenario this would be an inefficient way of treating bacteria.

A healthy and normally healing wound has a temperature of around 32 - 33 °C, whilst an infected wound has a surface temperature of 37 - 38 °C.[39, 40] The temperature associated with the generation of ROS by the $SrBaTiO_3$ particles lies between these ranges, offering the possibility of an infection initiated trigger for a theranostic system. As the amount of ROS generated by a single cycle is insufficient for the killing of bacteria, this 'killing signal' requires amplification. A way of doing this would be to suspend the particles within a PVA matrix, to which is bound a boronic acid doped dye and a boronic acid doped drug. In order to ensure the biocompatibility of this system, cryo-crosslinking would be the optimum crosslinking methodology, preventing the need for any toxic crosslinking chemicals. This requires both the drug and the dye to be soluble in a solution of

aqueous PVA. Aqueous solubility of the original boronic pinacol ester compounds used can be improved by the conversion of the boronic ester to the boronic triflate, which in aqueous solution will convert to the boronic acid. Once bound to the PVA through this boronic acid, previously aqueous insoluble compounds can be dissolved, as proved with the AuFluor 483-Bpin™.

The different drug delivery and sensing systems developed, offer potential route to the development of novel medical materials. Their combination with other emerging medical technologies such as CAP and the 'smart wound' vesicles gives them potential for being developed further and being incorporated into theranostic systems. The full extent of the potential applications of these boronic acid soft materials is only just being realised, and it is my hope that modern medicine can benefit as a result of this research.

5.7 Bibliography

1. K. Ulbrich, K. Hola, V. Subr, A. Bakandritsos, J. Tucek and R. Zboril, *Chemical Reviews*, 2016, **116**, 5338-5431.
2. L. Zhang, D. Pornpattananangkul, C. M. J. Hu and C. M. Huang, *Current Medicinal Chemistry*, 2010, **17**, 585-594.
3. T. M. Allen and P. R. Cullis, *Science*, 2004, **303**, 1818-1822.
4. X. Q. Yi, J. Dai, Y. Y. Han, M. Xu, X. J. Zhang, S. J. Zhen, Z. J. Zhao, X. D. Lou and F. Xia, *Communications Biology*, 2018, **1**, 13.
5. S. Kumari, A. K. Badana, G. M. Mohan, G. Shailender and R. Malla, *Biomarker Insights*, 2018, **13**, 9.
6. M. S. Shim and Y. N. Xia, *Angewandte Chemie-International Edition*, 2013, **52**, 6926-6929.
7. S. Kane, ClinCalc Drugstats Database, (accessed 5/09/19, 2019).
8. H. C. Su, K. Ramkissoon, J. Doolittle, M. Clark, J. Khatun, A. Secrest, M. C. Wolfgang and M. C. Giddings, *Antimicrobial Agents and Chemotherapy*, 2010, **54**, 4626-4635.
9. N. T. Thet, D. R. Alves, J. E. Bean, S. Booth, J. Nzakizwanayo, A. E. R. Young, B. V. Jones and A. T. A. Jenkins, *Acs Applied Materials & Interfaces*, 2016, **8**, 14909-14919.
10. M. Lebel, R. P. Rapp, G. E. Stein, S. L. Barriere and G. L. Drusano, *Pharmacotherapy*, 1988, **8**, 3-33.
11. X. Tabary, N. Moreau, C. Dureuil and F. Legoffic, *Antimicrobial Agents and Chemotherapy*, 1987, **31**, 1925-1928.
12. D. C. Hooper, *Clinical Microbiology and Infection*, 1998, **4**, S15-S20.
13. S. Fardeau, A. Dassonville-Klimpt, N. Audic, A. Sasaki, M. Pillon, E. Baudrin, C. Mullie and P. Sonnet, *Bioorganic & Medicinal Chemistry*, 2014, **22**, 4049-4060.
14. S. M. Hamed, W. F. Elkhatib, H. A. El-Mahallawy, M. M. Helmy, M. S. Ashour and K. M. A. Aboshanab, *Scientific Reports*, 2018, **8**, 10.
15. E. Albornoz, N. Tijet, D. De Belder, S. Gomez, F. Martino, A. Corso, R. G. Melano and A. Petroni, *Antimicrobial Agents and Chemotherapy*, 2017, **61**, 8.
16. A. Robicsek, J. Strahilevitz, G. A. Jacoby, M. Macielag, D. Abbanat, C. H. Park, K. Bush and D. C. Hooper, *Nature Medicine*, 2006, **12**, 83-88.

17. K. Yamane, J. I. Wachino, S. Suzuki, K. Kimura, N. Shibata, H. Kato, K. Shibayama, T. Konda and Y. Arakawa, *Antimicrobial Agents and Chemotherapy*, 2007, **51**, 3354-3360.
18. D. van Elsland and J. Neefjes, *Embo Reports*, 2018, **19**, 11.
19. *IARC Monographs on the Evaluation of Carcinogenic Risks to Humans*, 2012, x + 475 pp.
20. P. Pisani, D. M. Parkin, N. Munoz and J. Ferlay, *Cancer Epidemiology Biomarkers & Prevention*, 1997, **6**, 387-400.
21. H. Moller, E. Heseltine and H. Vainio, *International Journal of Cancer*, 1995, **60**, 587-589.
22. J. Kullander, O. Forslund and J. Dillner, *Cancer Epidemiology Biomarkers & Prevention*, 2009, **18**, 472-478.
23. D. B. Longley, D. P. Harkin and P. G. Johnston, *Nature Reviews Cancer*, 2003, **3**, 330-338.
24. CLSI, Methods for Dilution Antimicrobial Susceptibility Tests for Bactera That Grow Aerobically, (accessed 15/01/2020, 2020).
25. G. S. Tillotson, *Journal of Medical Microbiology*, 1996, **44**, 320-324.
26. T. Idowu and F. Schweizer, *Antibiotics-Basel*, 2017, **6**, 24.
27. V. Patel, M. Kelleher and M. McGurk, *British Dental Journal*, 2010, **208**, 61-64.
28. F. Varanda, M. J. P. de Melo, A. I. Caco, R. Dohrn, F. A. Makrydaki, E. Voutsas, D. Tassios and I. M. Marrucho, *Industrial & Engineering Chemistry Research*, 2006, **45**, 6368-6374.
29. R. G. Wilkins and M. Unverdorben, *Advances in Skin & Wound Care*, 2013, **26**, 160-163.
30. H. F. Mi, D. Wang, Y. X. Xue, Z. Zhang, J. J. Niu, Y. Z. Hong, K. Drlica and X. L. Zhao, *Antimicrobial Agents and Chemotherapy*, 2016, **60**, 5054-5058.
31. D. H. Oh and D. L. Marshall, *International Journal of Food Microbiology*, 1993, **20**, 239-246.
32. A. F. Jerant, J. T. Johnson, C. D. Sheridan and T. J. Caffrey, *American Family Physician*, 2000, **62**, 357-368.
33. H. Kim, G. Kwak, K. Kim, H. Y. Yoon and I. C. Kwon, *Biomaterials*, 2019, **213**, 16.
34. N. T. Thet, S. H. Hong, S. Marshall, M. Laabei and A. T. A. Jenkins, *Biosensors & Bioelectronics*, 2013, **47**, 574-574.

35. N. T. Thet and A. T. A. Jenkins, *Electrochemistry Communications*, 2015, **59**, 104-108.
36. C. R. Bowen, J. Taylor, E. LeBoulbar, D. Zabek, A. Chauhan and R. Vaish, *Energy & Environmental Science*, 2014, **7**, 3836-3856.
37. A. Benke, E. Mehner, M. Rosenkranz, E. Dmitrieva, T. Leisegang, H. Stocker, W. Pompe and D. C. Meyer, *Journal of Physical Chemistry C*, 2015, **119**, 18278-18286.
38. K. F. Wang, D. K. Shao, L. Zhang, Y. Y. Zhou, H. P. Wang and W. Z. Wang, *Journal of Materials Chemistry A*, 2019, **7**, 20383-20389.
39. A. Chanmugam, D. Langemo, K. Thomason, J. Haan, E. A. Altenburger, A. Tippett, L. Henderson and T. A. Zortman, *Advances in Skin & Wound Care*, 2017, **30**, 406-414.
40. M. Fierheller and G. Sibbald, *Advances in Skin & Wound Care*, 2010, **23**, 369-378.

6 Synthetic Experimental

6.1 Chapter 2

***N*-(3-(4,4,5,5-tetramethyl-1,3,2-dioxaborolan-2yl)phenyl)methacrylamide (PBA monomer)**

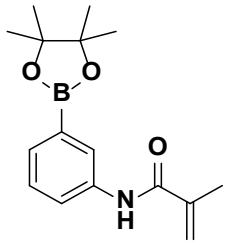

A solution of NEt_3 (0.49 g, 4.88 mmol) and methacryloyl chloride (0.51 g, 4.88 mmol) in DCM (4.0 mL) was added dropwise to a solution of 3-(4,4,5,5-tetramethyl-1,3,2-dioxaborolan-2-yl)aniline (1.00 g, 4.56 mmol) in DCM (60 mL) at 0 °C. The reaction mixture was stirred for 2 h and was allowed to warm to rt, which was then stirred for a further 30 min. It was ensured that the temperature did not rise above 30 °C in order to minimise the occurrence of side polymerisation products. The solution was then washed with H_2O (3 x 40 mL) and dried over $MgSO_4$. The organic solvent was removed under reduced pressure and the title compound yielded as an off white solid (1.25 g, 95 %). Mp 138 – 142 °C. ^{1}H NMR (δ; 300 MHz; DMSO-*d*$_6$) 7.98 (1H, dq, C*H*), 7.68 (1H, d, C*H*), 7.56 (1H, d, C*H*), 7.36 (1H, t, C*H*), 5.79 (1H, s, C*H*H), 5.44 (1H, s, CH*H*), 2.05 (3H, s, CH_3), 1.35 (12H, s, 4 x CH_3). ^{13}C NMR (δ; 75 MHz; DMSO-*d*$_6$) 166.54, 140.90, 137.32, 130.73, 128.74, 125.89, 123.23, 119.15, 84.14, 24.98, 18.85. FTIR (thin film) ν (cm^{-1}),; 1622, 1662, 2977, 3355. HRMS (FTMS): m/z calculated for $C_{16}H_{22}BNO_3$: requires 288.1768 for $[M-H]^+$, found 288.1795.

***N*-(1-hydroxy-1,3-dihydrobenzo[c][1,2]oxaborol-6-yl)methacrylamide (BOB monomer)**

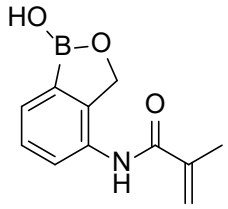

Methacryloyl chloride (1.32 mL, 13.42 mmol) was added dropwise to a solution of 6-Aminobenzoxaborale (1.00 g, 6.71 mmol) and $NaHCO_3$ (2.26 g, 26.84 mmol) in H_2O:THF (1:1, 40 mL) at 0 °C. The reaction was stirred for 2 h at 0 °C, then overnight at room temperature. The organic solvent was removed under reduced pressure and solid product obtained via extraction with EtOAc for 2 h. The organic layer was continuously washed with H_2O, sat. $NaHCO_3$ solution and brine. The organic layer was dried over $MgSO_4$ and the solvent removed under reduced pressure, yielding a pale brown solid (1.19 g, 82 %). Mp 167 - 170 °C. ^{1}H NMR (300 MHz, DMSO-d6): δ 9.81 (1H, NH, s), 9.19 (1H, s, O*H*), 8.07 (1H, d, C*H*, J = 1.6 Hz), 7.68 (1H, dd, C*H* , J^1 = 8.2, J^2 = 1.9 Hz), 7.35 (1H, d, C*H*, J = 8.2 Hz), 5.82 (1H, C*H*, s), 5.51 (1H, s, C*H*), 4.95 (2H, s, CH_2), 1.97 (3H, s, CH_3); ^{13}C NMR (75 MHz, DMSO-d6): δ 167.10, 149.34, 140.77, 138.12, 123.85, 122.60, 121.68, 120.20, 70.05, 18.46; FTIR ν (cm-1): 3276, 3086, 2973, 1655, 1214, 979. HRMS (ES) m/z calculated for $C_{11}H_{13}BNO_3$: [M+H]+ 218.0988, found 218.0993.

6.2 Chapter 3

4-(4,4,5,5-tetramethyl-1,3,2-dioxaborolan-2-yl)benzyl 1-cyclopropyl-6-fluoro-4-oxo-7-(piperazin-1-yl)-1,4-dihydroquinoline-3-carboxylate

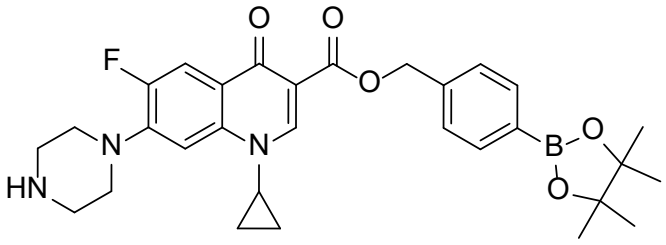

Ciprofloxacin (1.00 mmol, 331 mg) and Di-tert-butyldicarbonate (1.20 mmol 260 mg) were stirred in 5 mL of Dioxane. Triethylamine (1.20 mmol, 167 μL) was added. The reaction was stirred at room temperature for 4 hrs. The solvent was evaporated *in-vacuo* and the resulting powder was dissolved in Acetonitrile (8 mL). After stirring for 5 minutes 2-(4-bromomethyl-phenyl)-4,4,5,5-tetramethyl [1,3,2]dioxaborolane (1.20 mmol, 356 mg) and K_2CO_3 (1.20 mmol, 165 mg) were added. Following heating the mixture at reflux (90 °C) overnight. After cooling the solution down, solids were separated with a sintered glass funnel. The precipitate was washed with water (ca. 50 mL) followed by cyclohexane (20 mL) and dried under reduced pressure. The pale yellow powder was mixed with THF (5 mL) and 4N hydrochloric acid (0.5 mL). The reaction was stirred at rt for 24 hrs. Then the mixture was basified with an aqueous solution of $NaHCO_3$ and the solvent was removed *in-vacuo*. This was followed by a soxhlet extraction in diethylether. The resulting powder was dissolved in THF (2 mL) and TFA (1 mL) was added. After stirring at room temperature for 24h the solvent was removed *in-vacuo* yielding the title compound as an orange oil (47%). Mp 112 – 115 °C. 0^1H NMR (500 MHz, CD_3OD): δ 8.7 (1H, s C*H*), 7.98-7.90 (1H, C*H, m*), 7.78-7.70 (4H, m, C*H*), 4H), 7.57-7.32 (2H, m C*H*), 5.41 (2H, s, CH_2), 5.34 (1H, s, C*H*), 3.73-3.70 (2H, m, CH_2), 3.62-3.45 (4H, m, *CH₂*, 4H), 1.86 (1H, quin, CH_2, J = 1.8 Hz), 1.40-1.11 (17H, cycloprop, pinnacol, m). HRMS (ES) m/z calculated for $C_{30}H_{35}BFN_3O_5$ [M+H]+ 546.2690, found 546.2712.

2-(4-((5-chloro-2-(2,4-dichlorophenoxy)phenoxy)methyl)phenyl)-4,4,5,5-tetramethyl-1,3,2-dioxaborolane

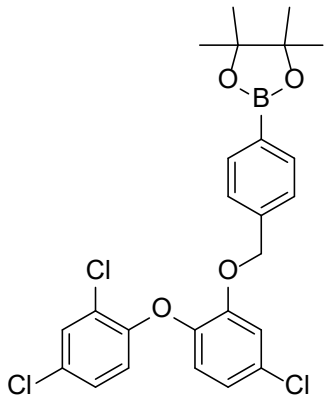

Triclosan (480 mg, 1.64 mmol) and potassium carbonate (909 mg, 6.57 mmol) were stirred at 55 °C in 3 mL anhydrous dimethylformamide for 2 hours. 2-(4-bromomethyl-phenyl)-4,4,5,5-tetramethyl [1,3,2]dioxaborolane (586 mg, 1.97 mmol) was added and stirred for 22 hours at 55 °C. The reaction mixture was dissolved in ethyl acetate (50 mL), washed with brine (3 x 50 mL) and dried with $MgSO_4$. Solvent was removed *in-vacuo*, yielding a white crystalline solid (501 mg, 60%) that was purified via silica chromatography: EtOAc:petroleum ether (5:95) Mp 130-131 °C.^{1}H NMR (500 MHz, $CDCl_3$): δH = 7.75 (2H, d, C*H*), 7.42 (1H, d, C*H*), 7.21 (2H C*H*, d), 7.08 (1H, dd, C*H*), 7.00 (1H, d, C*H*), 6.93 (1H, dd, C*H*), 6.96 (1H, d, C*H*), 6.65 (1H, d, C*H*), 5.07 (2H, s, CH_2), (12H, s, CH_3). ^{13}C NMR (157.5 MHz, DMSO-d_6): δC = 24.9, 70.2, 83.8, 115.5, 118.4, 121.7, 123.1, 123.9, 125.9, 126.1 126.6, 127.2, 128.7, 130.1, 134.8, 139.9, 142.7, 150.6, 152.6. HRMS (ES) m/z (MS (ESI) m/z) calculated for $C_{25}H_{24}Cl_3BO_4$: [M+H]+ 505.6212, found 505.5801.

6.3 Chapter 4

3',6'-Dibromo-3H-spiro[isobenzofuran-1,9'-xanthen]-3-one

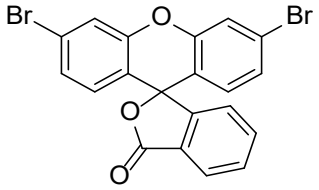

3-Bromophenol (3.66 g, 20.0 mmol) and pthalic anhydride (1.43 g, 10.0 mmol) were dissolved in methanesulfonic acid (10 mL). The reaction was stirred under reflux at 140 °C for 16 hours. The reaction was quenched with ice. Reaction mixture was extracted with EtOAc (3 x 30 mL) then washed with water and sat NaCl solution. Combined organic extracts were dried with $MgSO_4$ and the solvent was removed *in vacuo*. Crude product was purified by trituration in pet. ether yielding a dark grey solid (2.87 mmol, 6.3 mmol, 63%). Mp 289-290 °C. ^{1}H NMR (δ 500 MHz, $CDCl_3$); 8.04 (1H, d, C*H* J= 1.0 Hz); 7.66 (2H, m, C*H*); 7.49 (2H, d, J=1.9 Hz, C*H*), 7.19 (2H, dd, ^{1}J = 8.5 Hz, C*H* ^{2}J=1.9 Hz); 7.12 (1H, d, C*H,* ^{1}J = 7.5 Hz, C*H*); 6.70 (2H, d, C*H* J=7.5 Hz,). ^{13}C NMR (δ 125 MHz, $CDCl_3$); 168.87, 152.71, 151.05, 135.53, 130.12, 129.15, 127.37, 125.71, 125.34, 124.12, 123.58, 120.31, 117.85. FTIR (thin film) ν max ($cm^{-1)}$; 1760.91. HRMS (ES) m/z calculated for $C_{20}H_{10}Br_2O_3$ [M+H]+ 458.1061, found 458.1093.

3',6'-Bis(4,4,5,5-tetramethyl-1,3,2-dioxaborolan-2-yl)-3H-spiro[isobenzofuran-1,9'-xanthen]-3-one (PF-1)

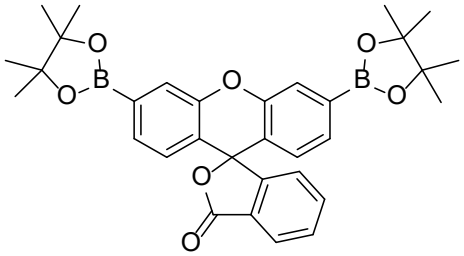

Dibromofluorescein (666 mg, 1.4 mmol), potassium acetate (1.30 g, 13.2 mmol), bis(pinacolato)diboron (1.33 g, 5.2 mmol) and $Pd(dppf)Cl_2$ (330 mg, 0.45 mmol) were dissolved in anhydrous degassed DMF (5 mL) under N_2 in a dried 100 mL round bottomed flask. The reaction stirred at 80 °C for 12 hours. The product was extracted thrice with EtOAc and the combined organic extracts were washed three times with brine. The organic fractions were combined and drired with $MgSO_4$. The crude product was isolated as a sticky brown solid. Compound was purified by column chromatography (10:90 EtOAc:Pet ether – 20:80 EtOAc:Pet Ether) yielding a pale pink solid (435 mg, 0.79 mmol, 58%). Pink colour was reduced when washed with Pet ether. Mp 239-241 °C. ^{1}H NMR (δ 500 MHz, $CDCl_3$); 8.03 (1H, m, C*H*); 7.73 (2H, s); 7.60 (2H, Q, *CH, J*=3.5 Hz); 7.43 (2H, dd, C*H* ^{1}J = 10 Hz, ^{2}J = 1.0. Hz); 7.06 (1H, m, C*H*); 6.86 (2H, d, C*H,* J = 8.0 Hz); 1.35 (24H, s, $(CH_3)_8$). ^{13}C NMR (δ 125 MHz, $CDCl_3$); 169.60, 154.00, 150.47, 135.08, 129.70, 129.30, 126.89, 125.44, 125.16, 123.56, 123.50, 121.29, 84.16, 24.71. FTIR (thin film) ν max ($cm^{-1)}$; 2980.90, 1762.19. HRMS (ES) m/z calculated for $C_{32}H_{34}B_2O_7$ [M+H]+ 552.2370, found 552.2256

3-7-Dibromo-10*H*-phenothiazine

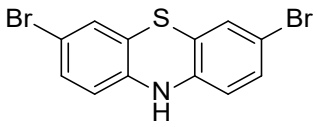

Phenothiazine (5.0 g, 25 mmol) was dissolved in AcOH (200 mL). Br_2 (3.3 mL, 128 mmol) was dissolved in AcOH (200ml), this Br_2 solution was added to the phenothiazine solution dropwise over 1 h. The reaction was then stirred overnight at room temperature. The reaction was then cooled to 0 °C and Na_2SO_3 (6.50 g, 51.5 mmol) was added. After stirring for one more hour KOH (4.5 g, 80.2 mmol) in H_2O (1 L) was added. The formed dark purple precipitate was isolated and recrystallized to yield the title compound as a green solid (6.60 g, 18.5 mmol, 74%). M.p. 191 – 193 °C; 1H NMR (500 MHz, DMSO-d6) δ 8.85 (1H, s, C*H*), 7.20 - 7.09 (4H m, C*H*), 6.58 (2H, d, C*H* J = 8.3 Hz); 13C NMR (125 MHz, DMSO-d6) δ 141.3, 130.7, 128.5, 118.6, 116.4, 113.1; I.R (thinfilm) ν max (cm-1): 3310.68; HRMS (ES) m/z calculated for $C_{12}H_7Br_2NS$, [M+H]+ 354.8666, found 354.8652

3,7-bis(4,4,5,5-tetramethyl-1,3,2-dioxaborolan-2-yl)-10H-phenothiazine (Purplement)

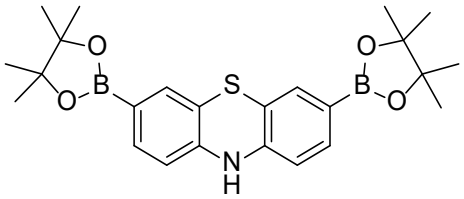

3-7-dibromo-10*H*-phenothiazine (1.00 g, 2.1 mmol), potassium acetate (1.95 g, 14.7 mmol), bis(pinacolato)diboron (2.00 g, 7.8 mmol) and Pd(dppf)Cl_2 (500 mg, 0.68 mmol) were dissolved in anhydrous degassed DMF (8 mL) under N_2 in a dried 100 mL round bottomed flask. The reaction stirred at 80 °C for 12 hours. The product was extracted thrice with EtOAc and the combined organic extracts were washed three times with brine. The organic fractions were combined and dried with $MgSO_4$. The crude product was isolated as a gummy brown solid. Compound was purified by recyrystalisation in DCM and MeOH yielding a yellow solid (407 mg, 0.90 mmol, 43%). Mp > 300 °C. ^{1}H NMR (500 MHz, d_6-DMSO) δ 8.94 (1H, s, N*H*), 7.23 (2H, dd, C*H* J = 1.3 Hz), 7.04 2H ,s, C*H*), 6.61 (2H, d, C*H J* = 10 Hz), 1.23 (24H, s, (CH_3)$_8$); ^{13}C NMR (125 MHz, d_6-DMSO) δ 145.3, 135.6, 133.8, 118.0, 115.3, 84.7, 25.6; HRMS (FTMS-NSI): m/z calculated for $C_{24}H_{31}B_2NO_4S$ requires 450.2305 for [M+H]+, found 450.2303

6.4 Chapter 5

4-(4,4,5,5-tetramethyl-1,3,2-dioxaborolan-2-yl)benzyl 1-cyclopropyl-6-fluoro-4-oxo-7-(4-(4-(4,4,5,5-tetramethyl-1,3,2-dioxaborolan-2-yl)benzyl)piperazin-1-yl)-1,4-dihydroquinoline-3-carboxylate

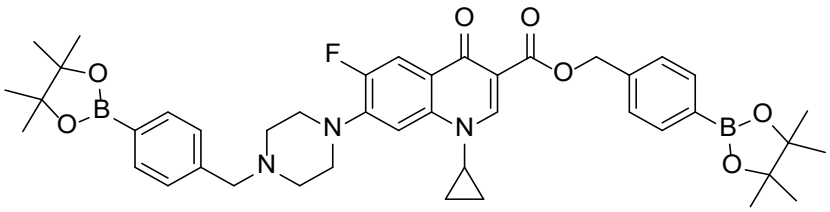

Ciprofloxacin (1.00 g, 2.73 mmol) was stirred with K_2CO_3 (1.54 g, 10.7 mmol) in MeCN (15 mL) at 100 °C for 90 minutes. 4-Bromomethylphenyl boronic acid pinnacol ester (3.41 g, 10.7 mmol) was added, and the reaction was stirred for 36 hours at 100 °C. The reaction mixture was extracted with EtOAc and washed twice with brine. The resulting pale green precipitate was filtered. The crude product was recrystallized in EtOAc yielding a white solid. (48 %). MP 267 – 270 °C. ^{1}H NMR (δ; 500 MHz: $CDCl_3$) 8.50 (1H, C*H, s*), 8.04 (1H, d, C*H*, ^1J = 13.2 Hz) 7.80 (4H, m, C*H*) 7.49 (2H, d, C*H*, ^1J = 8.1), 7.38 (2H, d, C*H*, ^1J = 7.5) 7.24 (1H, d, C*H*, ^1J = 7.0), 5.38 (2H, s, CH_2O) 3.62 (2H, s, CH_2N) 3.38 (1H, m, C*H*(CH_2)$_2$) 3.28 (4H, br, N(CH_2)$_2$) 2.67 (4H, br, N(CH_2)$_2$) 1.35 (12H, s, (CH_3)$_4$) 1.33 (12H, s, (CH_3)$_4$) 1.26 (2H, m, (CH_2)$_2$), 1.08 (2H, m, (CH_2)$_2$). ^{13}C NMR (δ; 125 MHz: $CDCl_3$) 173.05, 165.39, 154.42, 152.45, 148.18, 139.57, 137.97, 134.96, 134.85, 128.59, 127.09, 113.46, 113.28, 110.10, 104.73, 83.79, 83.75, 66.22, 52.79, 49.95, 34.46, 14.19, 8.12, 1.88. HRMS (FTMS): m/z calculated for $C_{43}H_{52}B_2FN_3O_7$: requires 764.4048 for $[M-H]^+$, found 764.4064

5-fluoro-1,3-bis(4-(4,4,5,5-tetramethyl-1,3,2-dioxaborolan-2-yl)benzyl)pyrimidine-2,4(1H,3H)-dione

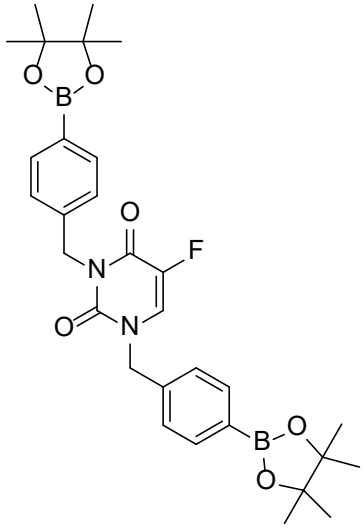

5-fluorouracil (1.00 g, 7.63 mmol) was stirred with K_2CO_3 (3 g, 21.7 mmol) in MeCN (15 mL) at 100 °C for 90 minutes. 4-Bromomethylphenyl boronic acid pinnacol ester (5.92 g, 20 mmol) was added, and the reaction was stirred for 36 hours at 80 °C. The reaction mixture was extracted with EtOAc and washed twice with brine. The resulting pale orange precipitate was filtered. The crude product was recrystallized in EtOAc yielding a white solid (87%). Mp 216 -220 °C. ^{1}H NMR (δ; 500 MHz: $CDCl_3$) 7.83 (2H, d, C*H*, ^1J = 8.1 Hz) 7.77 (2H, d, C*H,* ^1J = 8.1 Hz) 7.4 (2H, d, C*H*, ^1J = 8.1), 7.26 (2H, d, C*H*, ^1J = 21.0), 7.13 (1H, d, C*H*, ^1J = 5.2), 5.18 (2H, s, CH_2N) 4.90 (2H, s, CH_2N) 1.35 (12H, s, (CH_3)$_4$) 1.34 (12H, s, (CH_3)$_4$). ^{13}C NMR (δ; 125 MHz: $CDCl_3$) 157.16, 156.99, 141.09, 139.22, 139.03, 137.39, 135.60, 134.93, 128.30, 127.43, 125.97, 125.69, 84.02, 83.68, 52.26, 45.22, 24.85, 24.83. I.R (thinfilm) ν max (cm-1): 2978.05, 1717.01, 1658.69. $C_{43}H_{52}B_2FN_3O_7$: requires 562.2524 for $[M-H]^+$, found 562.2493

7 Appendix

7.1 Chapter 1

Appendix 1 Structure of glycopeptides mentioned in Figure, Teicoplanin and Chloreomycin

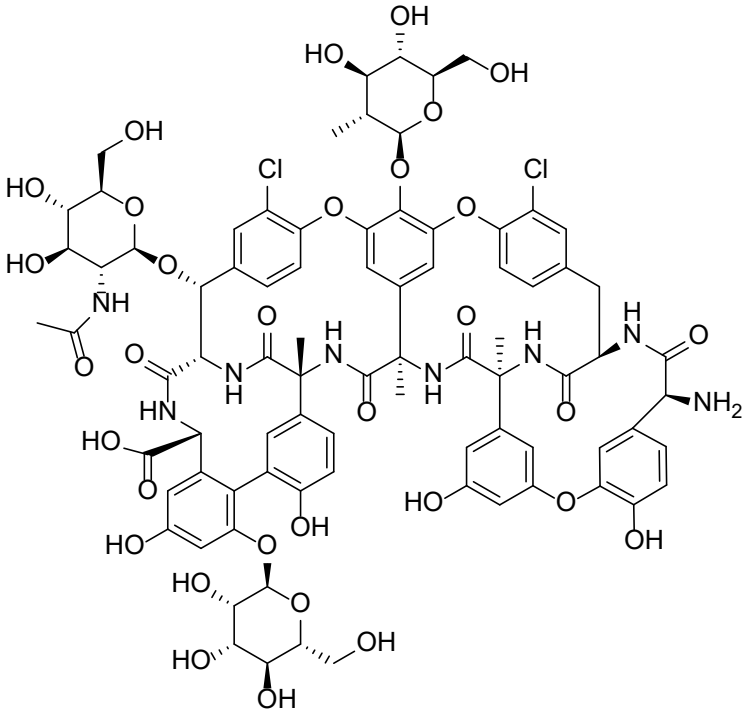

Teicoplanin

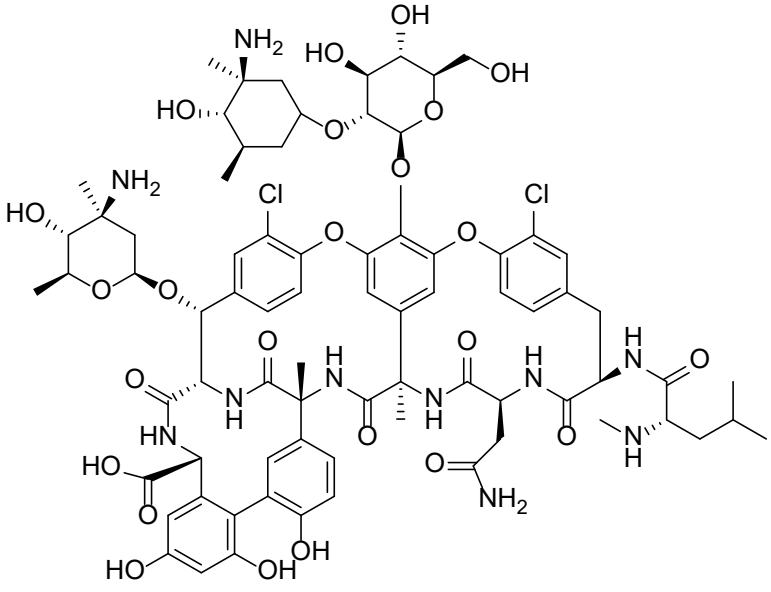

Chloroereomycin

7.2 Chapter 2

Appendix 1 – Acrylamide gel synthesis

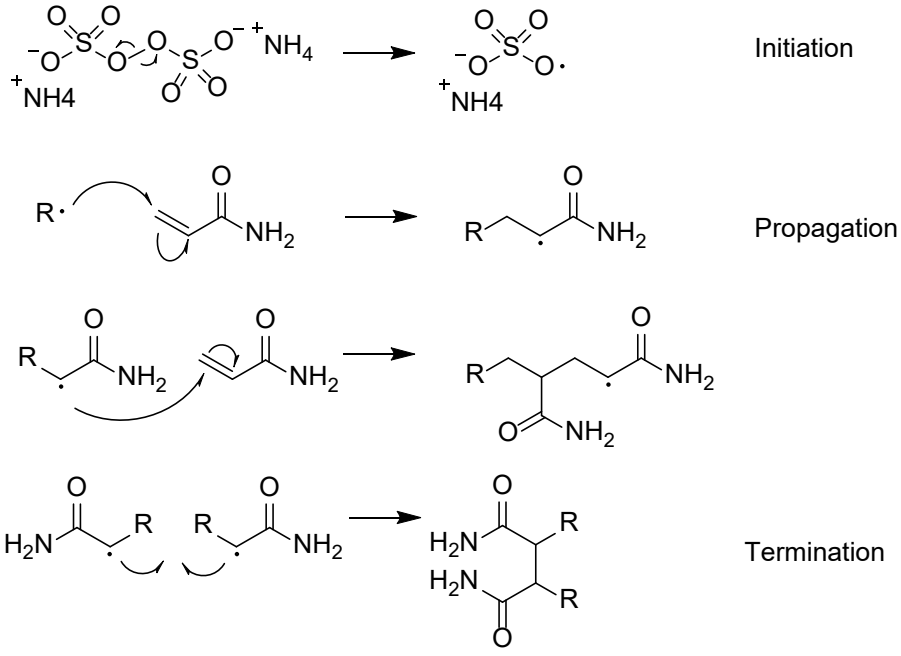

Appendix 2 – The Deep red colour of ARS solution

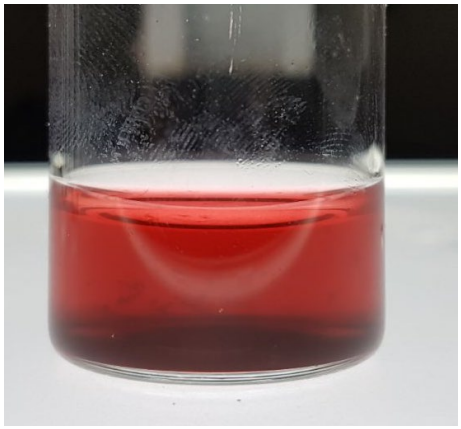

Appendix 3 - Determination of the Minimum Inhibitory Concentration (MIC) of Alizarin Red S (ARS) for (A) *Staphylococcus aureus* MRSA252, (B) *Staphylococcus aureus* H560, (C) *Pseudomonas aeruginosa* PAO1 and (D) *Escherichia coli* NCTC 10418. The MIC was above 125 µM (the maximum solubility of ARS) for all bacterial strains.

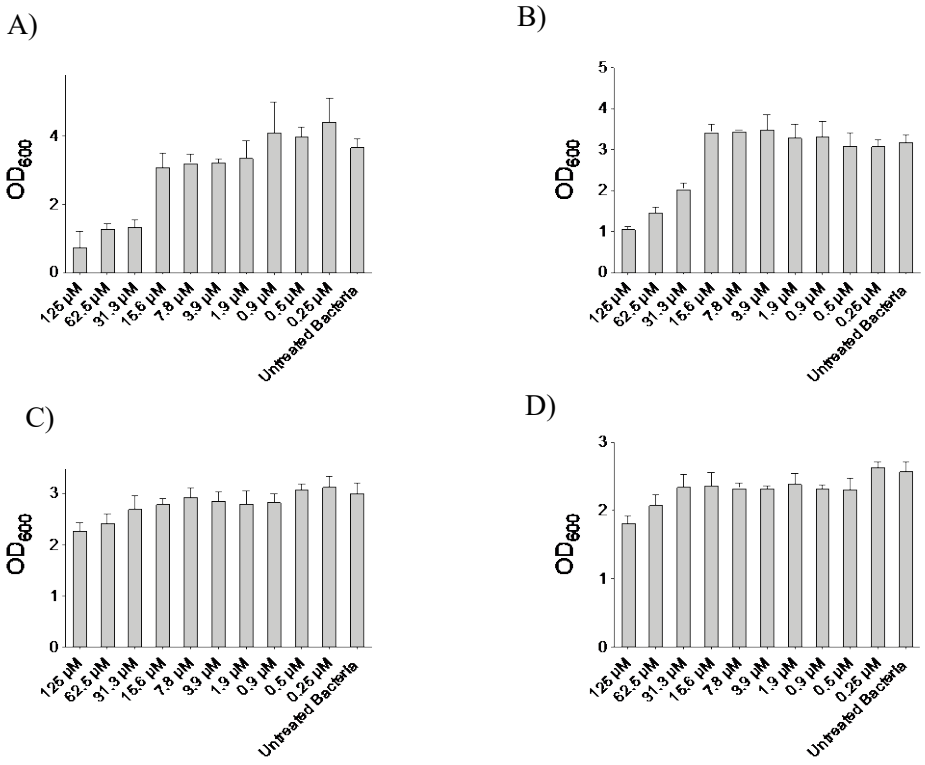

Appendix 3 – The effect of adding ARS at exponential phase on biofilm formation for (A) *S. aureus* MRSA252, (B) *S. aureus* H560, (C) *P. aeruginosa* PAO1 and (D) *Escherichia coli* NCTC 10418.

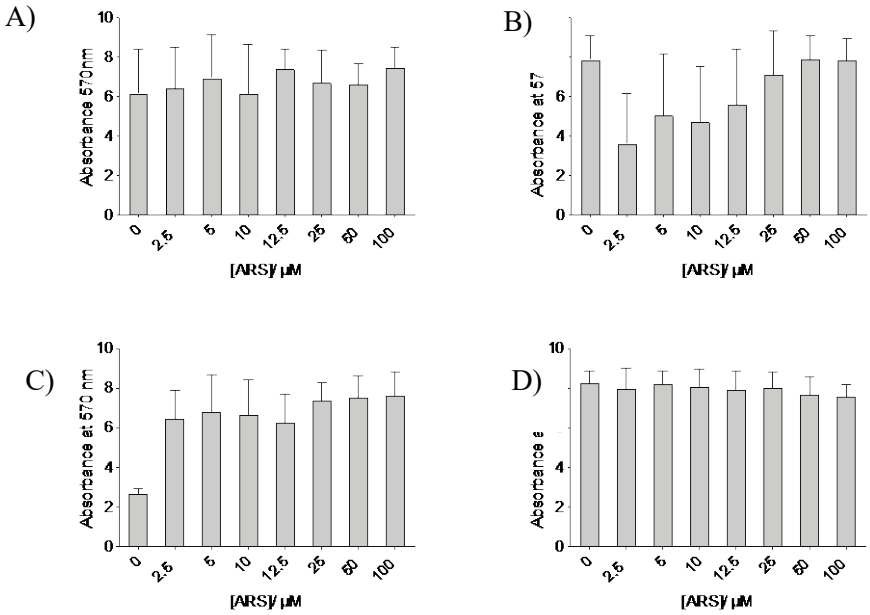

Appendix 4 – The effect of adding ARS at stationary phase on biofilm formation for (A) *S. aureus* MRSA252, (B) *S. aureus* H560, (C) *P. aeruginosa* PAO1 and (D) *Escherichia coli* NCTC 10418.

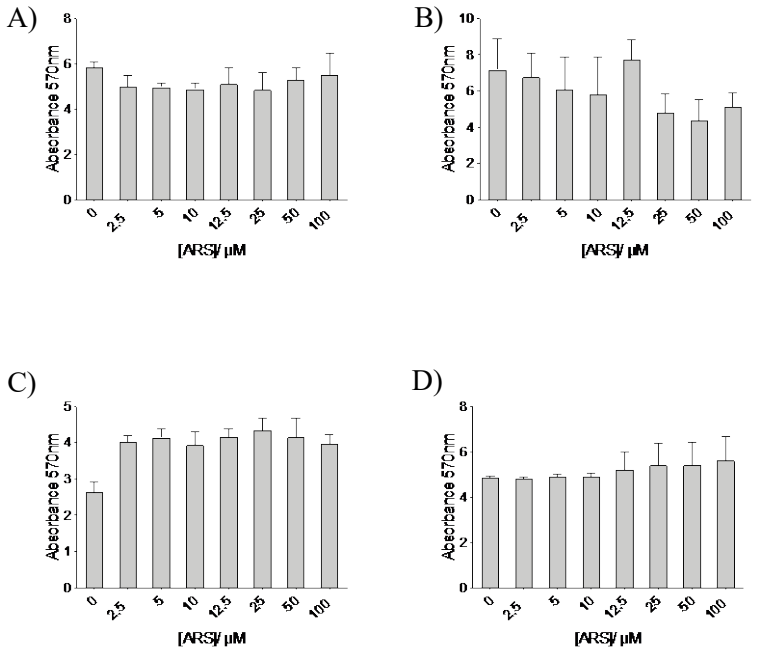

Appendix 5 – Bacteral growth curves for (A) *S. aureus* MRSA252, (B) *S. aureus* H560, (C) *P. aeruginosa* PAO1 and (D) *Escherichia coli* NCTC 10418.

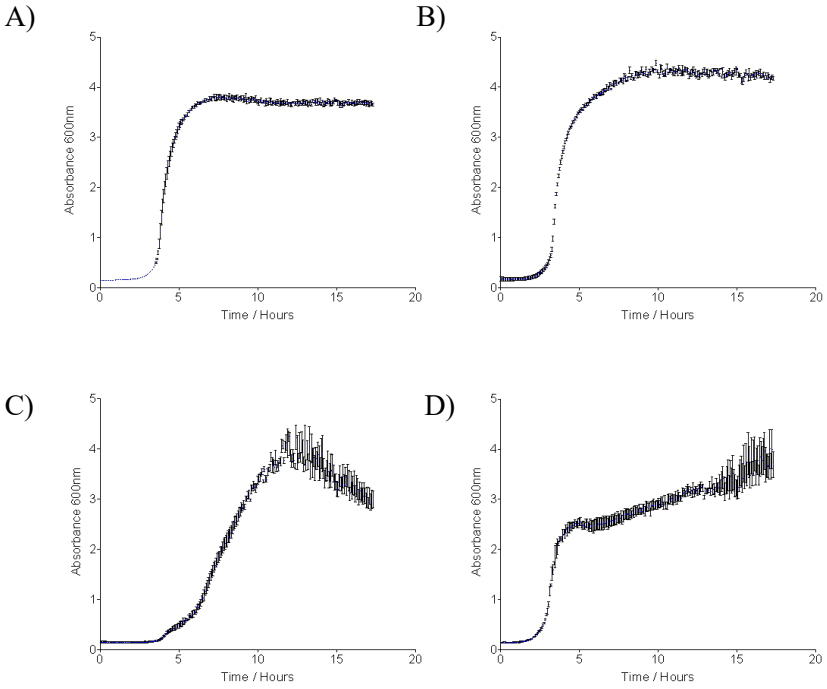

7.3 Chapter 4

Appendix 1 Gment gel stability in PBS as measured by UV-vis

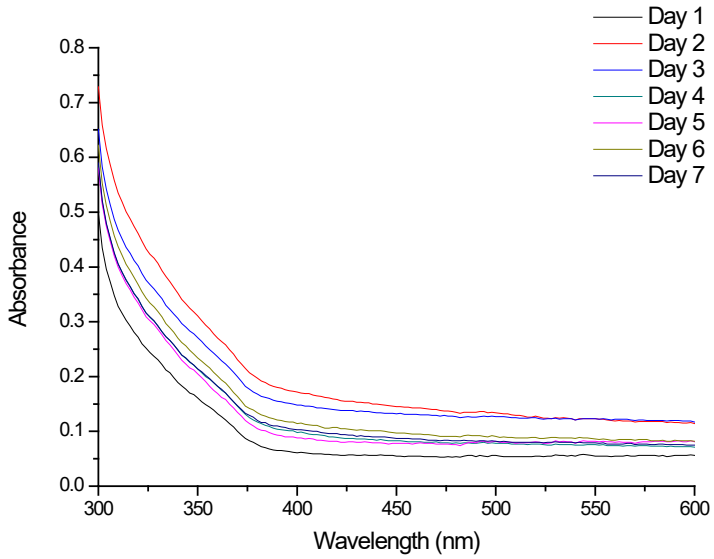

Appendix 2 – Pment gel stability in PBS as measured by UV-vis

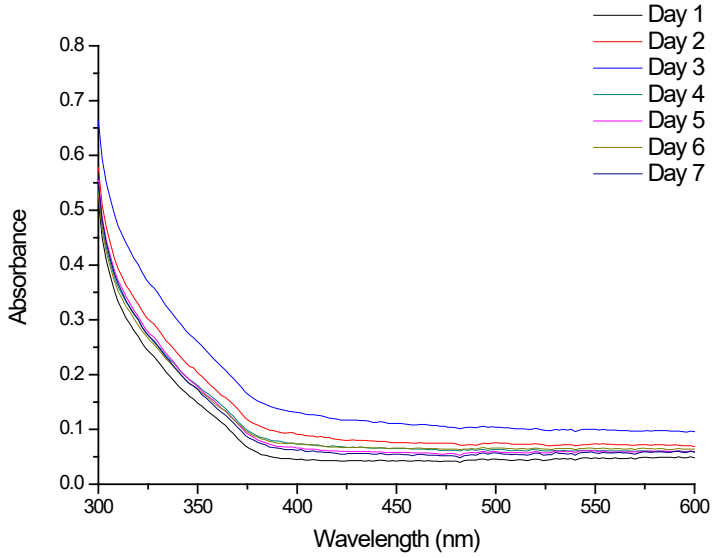

7.4 Chapter 5

Appendix 1 Increasing absorbance at 275 nm as ciprofloxacin is released from PVA due to exposure to H_2O_2

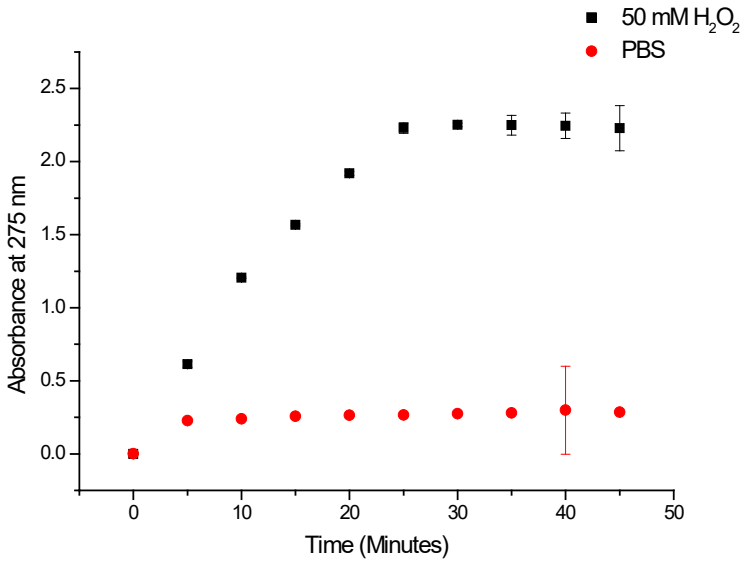

Appendix 2 Full data for CBPBA release

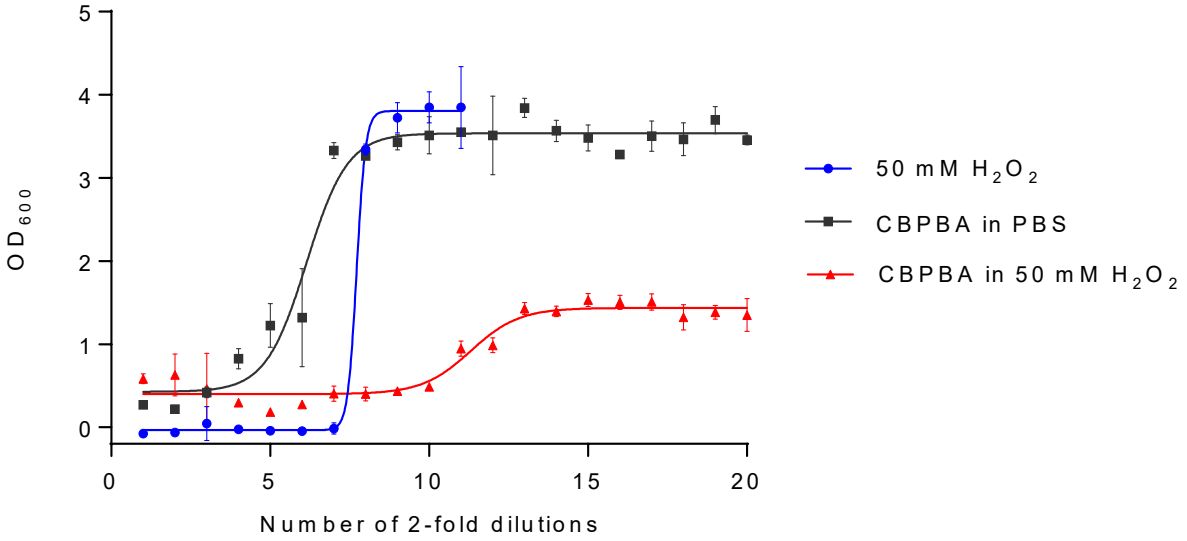

Optical density of *S. aureus* H560 upon exposure to 2-fold serially diluted: 50 mM H_2O_2, exudate from CBPBA hydrogels in PBS and exudate from CBPBA hydrogels in 50 mM H_2O_2. CBPBA hydrogels were incubated for 3 h at 25 °C in PBS/H_2O_2 before subsequent use. Optical density was measured at 600 nm after 18 h incubation at 37 °C. Error bars indicate standard deviation (n = 3)

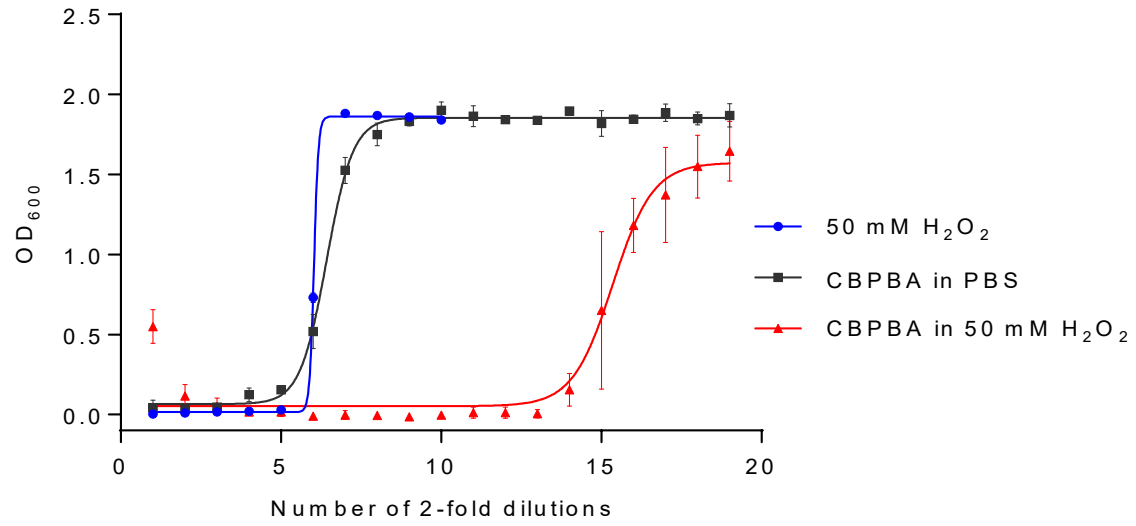

Optical density of *E. coli* NCTC 10418 upon exposure to 2-fold serially diluted: 50 mM H_2O_2, exudate from CBPBA hydrogels in PBS and exudate from CBPBA hydrogels in 50 mM H_2O_2. CBPBA hydrogels were incubated for 3 h at 25 °C in PBS/H_2O_2 before subsequent use. Optical density was measured at 600 nm after 18 h incubation at 37 °C. Error bars indicate standard deviation (n = 3)

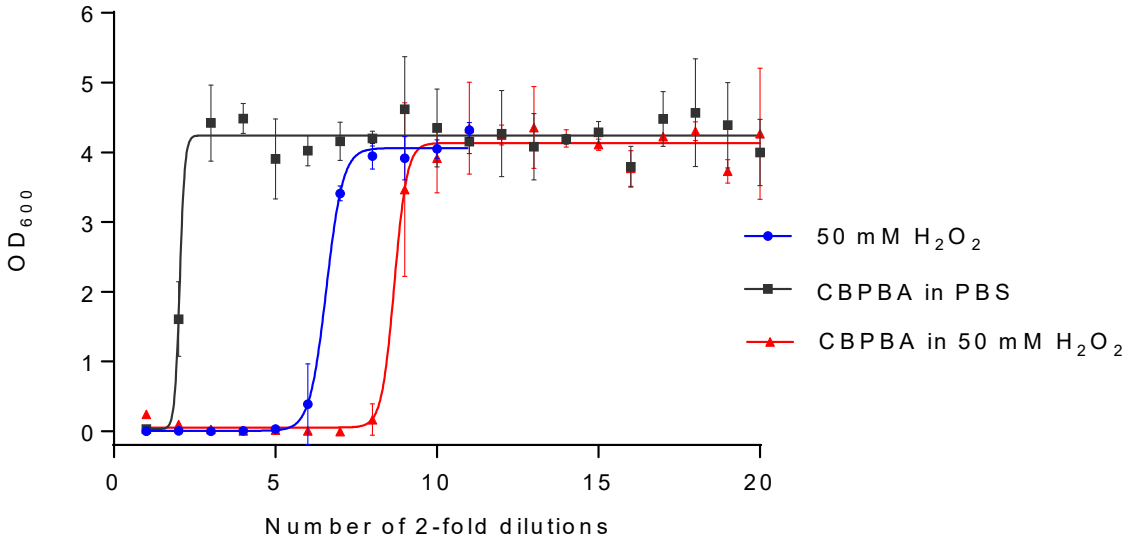

Optical density of *P. aeruginosa* PAO1 upon exposure to 2-fold serially diluted: 50 mM H_2O_2, exudate from CBPBA hydrogels in PBS and exudate from CBPBA hydrogels in 50 mM H_2O_2. CBPBA hydrogels were incubated for 3 h at 25 °C in PBS/H_2O_2 before subsequent use. Optical density was measured at 600 nm after 18 h incubation at 37 °C. Error bars indicate standard deviation (n = 3)

7.5 Published Manuscripts

Limiting *Pseudonmonas aeruginosa* Biofilm Formation Using Cold Atmospheric Plasma

Plasma Medicine, 8(3):269–277 (2018)

Limiting *Pseudomonas aeruginosa* Biofilm Formation Using Cold Atmospheric Pressure Plasma

Bethany L. Patenall,[a] Hollie Hathaway,[b] Adam C. Sedgwick,[a] Naing T. Thet,[a] George T. Williams,[a] Amber E. Young,[c] Sarah L. Allinson,[d] Robert D. Short,[b] & A. Toby A. Jenkins[a,*]

[a]Department of Chemistry, University of Bath, UK; [b]Department of Chemistry, Lancaster University, UK; [c]The Scar Free Foundation Centre for Children's Burns Research, The Bristol Royal Hospital for Children, Bristol, UK; [d]Division of Biomedical and Life Sciences, Lancaster University, Lancaster, UK

[*]Address all correspondence to: A. Toby A. Jenkins, Department of Chemistry, University of Bath, UK; Tel.: +441225386188; Fax: +44122538623, E-mail: A.T.A.Jenkins@bath.ac.uk

ABSTRACT: We investigate the ability to disrupt and limit growth biofilms of *Pseudomonas aeruginosa* using application of cold atmospheric pressure (CAP) plasma. The effect of the biofilm's exposure to a helium (CAP) jet was assessed at varying time points during biofilm maturation. Results showed that the amount of time during biofilm growth that CAP pressure was applied has a crucial role on the ability of biofilms to mature and recover after CAP exposure. Intervention during the early stages of biofilm formation (0–8 h) results in a 4–5-log reduction in viable bacterial cells (measured at 24 h of incubation) relative to untreated biofilms. However, CAP treatment of biofilm at 12 h and above only results in a 2-log reduction in viable cells. This has potentially important implications for future clinical application of CAP to treat infected wounds.

KEY WORDS: plasma, biofilm, *Pseudomonas aeruginosa*

I. INTRODUCTION

Owing to the increasing disparity between the rate of antimicrobial resistance and discovery of new antibiotics, interest has grown for the use of novel antimicrobial technologies. One such field of research surrounds the use of cold atmospheric pressure (CAP) plasma, often referred to as plasma medicine. CAP therapy has proven itself to be a promising alternative to traditional antimicrobial therapies, demonstrating its ability to inactivate a wide range of pathogens, including significantly drug-resistant isolates termed ESKAPE pathogens.[1,2] CAP therapy relies on delivery of a range of reactive oxygen and nitrogen species (RONS), including longer-lived species such as hydrogen peroxide (H_2O_2).[3–5] Already well documented are the effects of plasma-generated reactive species, including the ability to control both composition and delivery of such species according to the plasma parameters used.[6–9] As such, the versatility of CAP therapy has facilitated its use in a wide range of applications, including surface decontamination (both biotic and abiotic), equipment sterilization, microbial and spore inactivation, and cancer therapy.[10] Of particular relevance to this study is the application of CAP to wound healing. In addition to its proven antimicrobial effects, studies have shown that CAP

1947-5764/18/$35.00

therapy may further enhance wound healing (at appropriate doses) via stimulation of fibroblast/keratinocyte proliferation and migration or by its proangiogenic effects, thus making it an attractive alternative treatment option for wound infection.[8–12]

It is estimated that between 65% and 80% of all wound infections are biofilm associated.[13] Biofilm occurs when "free-living" planktonic cells adhere to a surface to form a dense community of biologically active, surface-bound microbes. Such bacterial communities are frequently encased in a polymeric layer comprised of proteins, glycoproteins, and polysaccharides, collectively known as the extracellular polysaccharide (EPS) matrix.[14] In addition to the protective nature of the EPS, it also confines the cells in close proximity to each other, facilitating the activation of quorum sensing networks via the secretion of specific signaling molecules. The subsequent alteration in gene expression may control production of extracellular virulence factors and regulate specific intracellular metabolic functions, both of which contribute to the enhanced resistance of biofilms to many forms of antibiotics.[15,16] Indeed, biofilm formation can increase the concentration of antimicrobial that is required by 100–1000 times, relative to planktonic cells.[17]

Pseudomonas aeruginosa is an opportunistic, Gram-negative bacterium that is responsible for 85% of all nosocomial infections. It is particularly prevalent in burns, causing 57% of all infections, and in cystic fibrosis, causing 30% patient mortality in ventilator-associated pneumonia.[18,19] *P. aeruginosa* uses multiple antimicrobial-resistance strategies (e.g., efflux pump–mediated resistance), exhibiting the highest levels of resistance to fluoroquinolones, ranging from 20% to 35%, and increasing each year according to epidemiological trends.[20] As a result of the increasing prevalence of biofilm-associated infection, there is a growing requirement within the scientific and medical community for the development of therapeutic treatment strategies aimed at limiting and ultimately eradicating bacterial biofilms. An important consideration in the development of such technologies surrounds the recalcitrant nature of many antimicrobials toward biofilms when compared to planktonic cells. This study reports on the ability of CAP treatment to effectively reduce formation of *P. aeruginosa* biofilms, potentially increasing susceptibility to conventional treatment strategies (such as antibiotics), which, if used in conjunction, may facilitate total infection clearance.

II. MATERIALS AND METHODS

A. Materials

We obtained *P. aeruginosa* strain PA01 from a strain collection belonging to the Biophysical Chemistry Research Group at the University of Bath, UK. Lysogeny broth (LB), LB agar, brain–heart infusion (BHI) agar, fetal calf serum (HyClone; GE Life Sciences; Pittsburgh, PA), and LIVE/DEAD™ BacLight™ bacterial viability kits were all purchased from ThermoFisher Scientific (Loughborough, UK). The polycarbonate membranes (19-mm diameter and 0.22-nm pore size) that we used to cultivate biofilms were purchased from Whatman (Kent, UK). Phosphate-buffered saline

(PBS), sodium chloride (NaCl), and peptone were all purchased from Sigma-Aldrich (Dorset, UK).

B. Bacteria and Growth Conditions

P. aeruginosa PA01 was taken from freezer stocks and grown on LB agar overnight at 37°C to obtain single colonies. Bacteria cultures were grown from single colonies overnight at 37°C with agitation (200 rpm) in LB, resulting in 10^9 colony forming units (CFU) per milliliter in final culture. Bacterial aliquots were stored at –80°C in LB supplemented with 15% (v/v) glycerol.

C. Bacterial Biofilm Formation

Polycarbonate membranes were positioned on BHI agar and sterilized with ultraviolet light for 10 min. We aliquoted 20 μL of wound fluid mimic (fetal calf serum mixed in equal volume with 0.85% NaCl [w/v] and 0.1% peptone [w/v]) onto membrane surfaces. Artificial wound fluid was added to the membranes before bacterial inoculation to more closely mimic the wound environment. The membranes were inoculated with 30 μL of overnight bacterial culture, diluted 1:1000 into fresh LB broth. Membranes were incubated statically for 24 h at 37°C. Following treatment and incubation, biofilms were stripped from the membranes into sterile PBS via sonication (2 × 15 min with 1 min vortex before and between sonication steps). The value of CFU/mL was then determined via serial dilution into sterile PBS and plating on LB agar to colony count.[21]

D. Plasma Treatment

The plasma source used in this study was a helium-driven plasma jet, as previously described.[22] Gas flow was fixed at 2 standard liters per min, and plasma was operated at 10 $kV_{peak-peak}$ and 25 kHz. We used a treatment distance of 5 mm between the end of the capillary tube and the surface of the bacterial biofilms ("contact mode"). The *P. aeruginosa* biofilms were all incubated for a total time of 24 h, removed from incubation at varying time points (0, 4, 8, 12, 20, and 24 h), and subjected to 5 min of plasma treatment before being reincubated for the remaining time (with the exception of the 24-h biofilms that were assessed immediately after treatment).

E. Scanning Electron Microscopy

Biofilms were fixed overnight in glutaraldehyde (1.5%) and paraformaldehyde (3%) in phosphate buffer (pH 7.3). Samples were rinsed with osmium tetroxide and dehydrated in ethanol/water mixtures at increasing concentrations. Biofilms were sputter coated with gold and imaged via scanning electron microscope (SEM) JEOL SEM6480LV (Tokyo, Japan), operated at 10 kV.

F. Live/Dead Staining and Confocal Microscopy

Biofilms were washed three times in PBS to remove planktonic bacteria. We prepared BacLight™ stains (consisting of two nucleic acid dyes of SYTO-9 and propidium iodide) according to manufacturer instructions. Each biofilm was immersed in 1.5 mL of stain mixture and incubated for 15 min in the dark. After staining, biofilms were rinsed once with PBS, fixed onto a microscope slide, and imaged using a confocal microscope to obtain Z-stacked images of the bacterial biofilms.

III. RESULTS AND DISCUSSION

The effect of plasma jet treatment of *P. aeruginosa* biofilms at varying time points during biofilm maturation is shown in Fig. 1. Relative to the untreated control, we found a significant reduction in the number of viable bacterial cells at each treatment intervention point, demonstrating a clear disruption in the formation of mature biofilms as a result of CAP exposure.

CAP treatment at 0 and 4 h produced a 5-log reduction in CFU/mL, reducing bacterial load below the clinically relevant value of 10^6 CFU/mL.[23,24] However, CAP treatment at later stages during biofilm maturation (12, 20, and 24 h) reduced CFU/mL values by only 1–2-log units. From these data, we notice a critical time frame for treatment intervention to limit bacterial proliferation within a biofilm. Although the exact

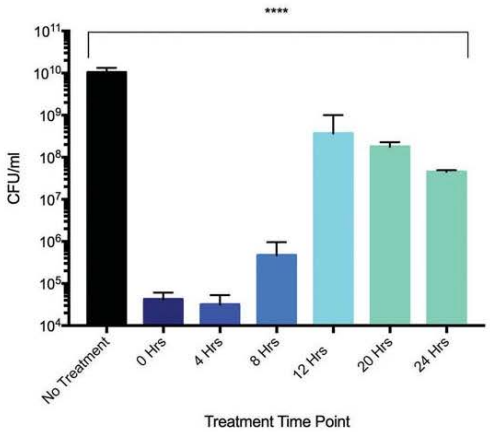

FIG. 1: Effect of treatment intervention time on bacterial viability after 24 h of incubation. CAP treatment was carried out as previously described at the time points shown ($p < 0.0001$; one-way analysis of variance with multiple comparisons)

reason for this is unclear at this point, a number of possible factors may play a part in the resistance of mature biofilms to plasma exposure, for example, EPS production and/or a change in bacterial genotype/phenotype within the biofilms. The difference in cell counts at the varying stages of intervention may indeed have a role in the susceptibility of bacteria to plasma treatment. However, owing to the fact that each biofilm is incubated for 24 h regardless of treatment time, the results suggest that not only does CAP treatment reduce the number of viable cells, it also prevents the recovery of biofilms into the mature state.

We carried out qualitative analysis of the biofilms before and after CAP treatment using SEM to look more closely and evaluate the effect of CAP exposure on a cellular level. Figure 2(A) shows an untreated *P. aeruginosa* biofilm grown for 24 h. The bacterial cells are present in high density, reflecting the high CFU/mL value calculated in the previous quantitative data (Fig. 1). The presence of the EPS matrix is clearly visible, holding the cells in close proximity to one another. Figure 2(B) shows a *P. aeruginosa* biofilm incubated for 24 h but treated with

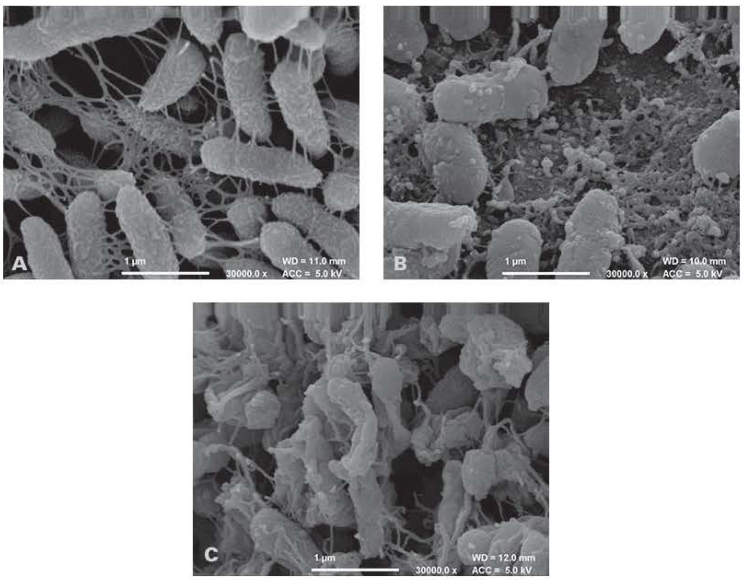

FIG. 2: SEM images of CAP-treated biofilms. (A) Untreated 24-h growth *P. aeruginosa* biofilm (control); (B) 24-h *P. aeruginosa* biofilm treated with CAP jet for 5 min at 8-h growth; (C) 24-h *P. aeruginosa* biofilm treated with CAP jet for 5 min at 12-h growth

CAP jet at 8 h of growth. Relative to Fig. 2(A), this shows a distinct reduction in bacterial cell density alongside an accumulation of cellular debris, likely the result of bacterial cell death during CAP treatment. There is also a clear reduction in the EPS matrix. Figure 2(C) shows a *P. aeruginosa* biofilm grown for 24 h, treated with the CAP jet at 12 h of growth. As expected from the quantitative data, we see a higher density of cells relative to the biofilms treated at 8 h. However, cell morphology suggests significant bacterial cell death and a clear disruption to the EPS relative to the untreated control [Fig. 2(A)]. Interestingly, despite the higher number of viable cells when treating the biofilms at 12 h relative to 8 h, the ability of the former to recover to full cell density as expected in a mature biofilm is reduced, potentially reflecting the disruption in both bacterial cells and EPS matrix, as shown in Fig. 2(C).

To further investigate the 3-log difference in CFU/mL between biofilms treated at 8 and 12 h, we carried out live/dead staining to assess difference in viable bacteria. Figure 3 shows the difference in cell density between biofilms treated at the two different intervention points. As expected from the previous quantitative and qualitative data, a significantly higher density of cells can be seen in the biofilms treated at 12 h [Fig. 3(B)]. Figure 3(A) shows a thin layer of healthy viable cells, likely the result of the 16-h post-treatment recovery period to which the biofilm was subjected, supporting the presentation of healthy cells in Fig. 2(B). Early treatment of the biofilms (8 h and less) provides adequate time for the recovery of viable bacterial cells (albeit not to the full cell density seen in untreated, mature biofilms during the same time period). However, in Fig. 3(B), we clearly find a larger proportion of dead bacteria, suggested by SEM [Fig. 2(C)]. The density of the bacterial biofilm provides an impenetrable layer of biological material that protects cells in the lower levels of the biofilm from the plasma jet action. Despite the ability of CAP treatment to cause significant cellular lysis, the protective nature of the more established biofilms shields the cells in the lower layers of the biofilm, thus retaining cell viability (Fig. 1) despite the presence of dead cells (Figs. 2 and 3).

IV. CONCLUSIONS

Using CAP therapy in a time-dependent manner is crucial for reducing the formation of mature *P. aeruginosa* biofilms. Although CAP therapy is able to cause significant bacterial cell death, the presence of both dead and living cells contained within an established biofilm offers protective effects relative to the cells in the lower layers of the biofilm, resulting in retention of viable cells. However, treating biofilms in the early stages of development (< 12 h) can significantly reduce bacterial loads to levels, wherein traditional treatment strategies may become effective. Using CAP therapy as a tool to limit biofilm formation may prove to be clinically advantageous by increasing the potential for immune system clearance without the need for pharmaceutical intervention. Furthermore, CAP treatment could be effectively used in tandem with antibiotics by disrupting biofilm formation, thus reducing the concentration of antimicrobial required. This technology

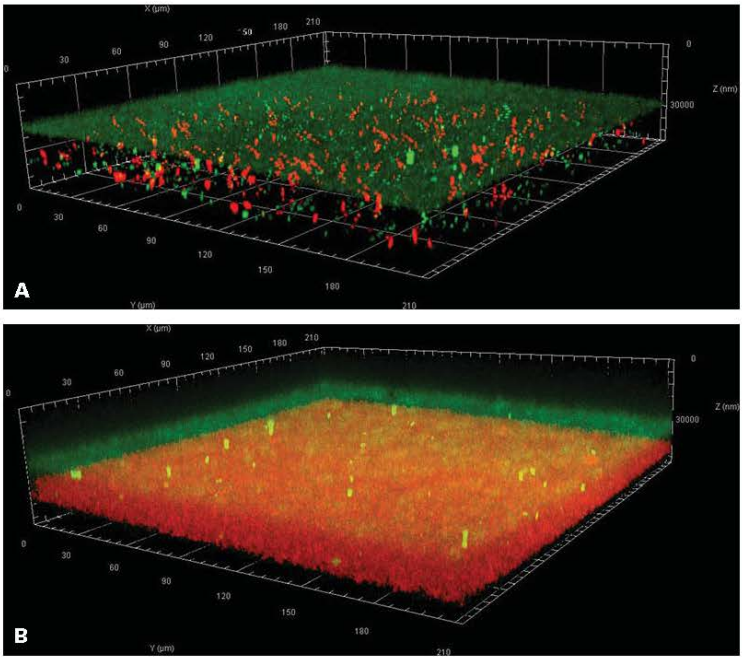

FIG. 3: BacLight™ live/dead staining of 24 h P. aeruginosa biofilms. (A) Treated with CAP jet for 5 min at 8 h growth; (B) treated with CAP jet for 5 min at 12 h growth. SYTO9 stains all cells Light Grey (LIVE) and PI only stains cells with damaged cytoplasmic membrane Dark Grey (DEAD). Images are inverted, representing the biofilms from the base of the membrane downwards.

therefore has the capacity to contribute to the global aim of decreased reliance on antibiotic use.

ACKNOWLEDGMENTS

The authors thank the Engineering and Physical Sciences Research Council (EPSRC) for Grant No. EP/R003556/1. B.L.P. thanks James Tudor and Alastair and Nathalie Watson for additional funding. G.T.W. is grateful to the EPSRC and Public Health England. A.T.A.J., A.C.S., and N.T.T. thank the EPSRC for funding smart-wound plasma (Grant

No. EP/R003939/1). We are grateful to the Microscopy and Analysis suite at the University of Bath, UK for assistance with SEM and confocal microscopy.

REFERENCES

1. Flynn PB, Higginbotham S, Alshraiedeh NaH, Gorman SP, Graham WG, Gilmore BF. Bactericidal efficacy of atmospheric pressure non-thermal plasma (APNTP) against the ESKAPE pathogens. Int J Antimicrob Agents. 2015;46(1):101–7.
2. Modic M, McLeod NP, Sutton JM, Walsh JL. Cold atmospheric pressure plasma elimination of clinically important single- and mixed-species biofilms. Int J Antimicrob Agents. 2017;49(3):375–8.
3. Fridman G, Friedman G, Alexander G, Shekhter A, Anatoly SB. Vasilets VN, Fridman A. Applied Plasma Medicine. Plasma Proc Polymers. 2008;5(6):503–33.
4. Alkawareek MY, Algwari QT, Laverty G, Gorman SP, Graham WG, O'Connell D, Gilmore BF. Eradication of Pseudomonas aeruginosa biofilms by atmospheric pressure non-thermal plasma. PLoS ONE. 2012;7(8):e44289.
5. Boxhammer V, Morfill GE, Jokipii JR, Shimizu T, Klämpfl T, Li Y-F, Köritzer J, Schlegel J, Zimmermann JL. Bactericidal action of cold atmospheric plasma in solution. New J Phys. 2012;14(11) 113042.
6. Gilmore BF, Flynn PB, O'Brien S, Hickok N, Freeman T, Bourke P. Cold plasmas for biofilm control: Opportunities and challenges. Trends Biotechnol. 2018;36(6):627–38.
7. Padrig BF, Brendan FG. Understanding plasma biofilm interactions for controlling infection and virulence. J Phys D Appl Phys. 2018;51(26):263001.
8. Haertel B, von Woedtke T, Weltmann K-D, Lindequist U. Non-thermal atmospheric-pressure plasma possible application in wound healing. Biomol Therapeut. 2014;22(6):477–90.
9. Mai-Prochnow A, Murphy AB, McLean KM, Kong MG, Ostrikov K. Atmospheric pressure plasmas: Infection control and bacterial responses. Int J Antimicrob Agents. 2014;43(6):508–17.
10. O'Connor N, Cahill O, Daniels S, Galvin S, Humphreys H. Cold atmospheric pressure plasma and decontamination. Can it contribute to preventing hospital-acquired infections? J Hosp Infect. 2014;88(2):59–65.
11. Xu GM, Shi XM, Cai JF, Chen SL, Li P, Yao CW, Chang ZS, Zhang GJ. Dual effects of atmospheric pressure plasma jet on skin wound healing of mice. Wound Repair Regen. 2015;23(6):878–84.
12. von Woedtke T, Metelmann H-R, Weltmann K-D. Clinical plasma medicine: State and perspectives of in vivo application of cold atmospheric plasma. Contrib Plasma Phys. 2014;54(2):104–17.
13. Percival SL, McCarty SM, Lipsky B. Biofilms and wounds: An overview of the evidence. Adv Wound Care (New Rochelle). 2015;4(7):373–81.
14. Olson ME, Ceri H, Morck DW, Buret AG, Read RR. Biofilm bacteria: Formation and comparative susceptibility to antibiotics. Can J Vet Res. 2002;66(2):86–92.
15. Stewart PS. Diffusion in biofilms. J Bacteriol. 2003;185(5):1485–91.
16. Heurlier K, Dénervaud V, Haas D. Impact of quorum sensing on fitness of Pseudomonas aeruginosa. Int J Med Microbiol. 2006;296(2):93–102.
17. Ceri H, Olson ME, Stremick C, Read RR, Morck D, Buret A. The Calgary biofilm device: New technology for rapid determination of antibiotic susceptibilities of bacterial biofilms. J Clin Microbiol. 1999;37(6):1771–6.
18. Morrison AJ, Wenzel RP. Epidemiology of infections due to Pseudomonas aeruginosa. Rev Infect Dis. 1984;6(Suppl. 3):S627–42.
19. Gellatly SL, Hancock REW. Pseudomonas aeruginosa: New insights into pathogenesis and host defenses. Pathogens Dis. 2013;67(3):159–73.
20. Livermore DM. Multiple mechanisms of antimicrobial resistance in Pseudomonas aeruginosa: Our worst nightmare? Clin Infect Diseases. 2002;34(5):634–40.
21. Thet NT, Wallace L, Wibaux A, Jenkins ATA. Development of a mixed-species biofilm model and its virulence implications in device related infections. J Biomed Mater Res Appl Biomater. 2018 Mar 8. doi: 10.1002/jbm.b.34103.

22. Szili EJ, Gaur N, Hong SH, Kurita H, Oh JS, Ito M, Mizuno A, Hatta A, Cowin AJ, Graves DB, Short RD. The assessment of cold atmospheric plasma treatment of DNA in synthetic models of tissue fluid, tissue and cells. J Phys D Appl Phys. 2017;50(27):274001-1–15.
23. Jacobs MR, Lazarus HM, Yomtovian RA. Relationship between bacterial load, species virulence, and transfusion reaction with transfusion of bacterially contaminated platelets. Clin Infect Dis. 2008;46(8):1214–20.
24. Opota O, Croxatto A, Prod'hom G, Greub G. Blood culture-based diagnosis of bacteraemia: State of the art. Clin Microbiol Infect. 2015;21(4):313–22.

ChemPubSoc Europe
DOI: 10.1002/open.201700193
Open Access ChemistryOPEN Communications

Dye Displacement Assay for Saccharides using Benzoxaborole Hydrogels

Emma V. Lampard,[a] Adam C. Sedgwick,*[a] Thitima Sombuttan,[b] George T. Williams,[a] Boontana Wannalerse,*[b, c] A. Toby A. Jenkins,[a] Steven D. Bull,[a] and Tony D. James*[a]

Dye displacement assays are a simple but effective method to determine the concentration of target analytes. Previously, we have shown that phenylboronic acid pinacol ester hydrogels (borogels) can be used to develop a boronic acid–Alizarin red S dye displacement assay for the determination of fructose (orange to red). In this work, benzoxaborole hydrogels (BOBgels) were developed, and these BOBgels demonstrated an enhanced apparent binding affinity towards monosaccharides, in particular towards glucose.

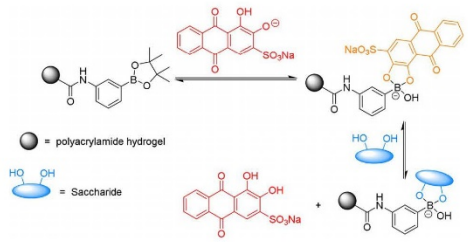

Scheme 1. Previously reported dye displacement assay utilizing an ARS-bound borogel for the determination of fructose concentration.

In dye displacement assays, the dye is reversibly bound to a specific receptor. The addition of a competitive analyte results in the displacement of the dye from the host, eliciting a response as an optical signal. These systems have several advantages over traditional sensing assays, which include a non-covalently bound dye, enabling the use of different dyes on the same receptor and the system works well in both aqueous and organic solvents. Owing to this, these systems have been elegantly employed by many research groups.[1–7]

Boronic acids have a well-known affinity to bind to 1,2- and 1,3-diols.[8,9] Therefore, boronic acids in combination with the (1,2-diol containing) dye Alizarin red S (ARS) have been developed into dye displacement assays for the detection of various analytes.[10–12] Previously, we developed an ARS–boronate hydrogel (borogel) displacement assay by utilizing the strong affinity of boronic acids towards saccharides (Scheme 1).[13] Prior to treatment with ARS, the borogel appeared colorless (including blank); however, the addition of ARS resulted in red (blank) and orange borogels. The visual color change of red to orange for ARS is indicative of its binding to boronic acids. It was then shown that the addition of fructose resulted in the displacement of the ARS dye, providing a measurable increase in absorbance at 513 nm in solution. Thereby resulting in a method for the determination of the concentration of saccharides in solution.

Despite boronic acids being regarded as one of the best receptors for the recognition of carbohydrates in water,[9] they have a number of limitations. These include the inability to bind non-reducing sugars and glycosides, which account for a large proportion of biologically important oligosaccharides. However, Dowlut and Hall reported that *ortho*-hydroxyalkyl arylboronic acids (benzoxaboroles) were capable of binding to glycosides.[14] Benzoxaboroles were also shown to bind to monosaccharides such as fructose and glucose with higher affinity compared to other boronic acids in neutral water, and also displayed an enhanced solubility profile.[14]

Therefore, in this research, we turned our attention to the development of borogels containing benzoxaboroles. To afford the benzoxaborole monomer (BOB), 2-formylphenylboronic acid was treated with $NaBH_4$, reducing the aldehyde functionality. The generated alcohol immediately underwent cyclization to form the oxaborole ring with the loss of a molecule of water. The BOB intermediate was subsequently treated with fuming nitric acid to afford 6-nitrobenzoxaborole in good yield (66%). 6-Nitrobenzoxaborole was then reduced by using hydrogenation conditions (Pd/C), giving 6-aminobenzoxaborole in good yield (78%). The methylacrylamide BOB monomer was prepared by the addition of methylacryloyl chloride to 6-aminobenzoxaborole in excellent yield (82%).

[a] E. V. Lampard, A. C. Sedgwick, G. T. Williams, Prof. A. T. A. Jenkins, Prof. S. D. Bull, Prof. T. D. James
Department of Chemistry, University of Bath
BA2 7AY Bath (UK)
E-mail: A.C.Sedgwick@bath.ac.uk
T.D.James@bath.ac.uk

[b] T. Sombuttan, Dr. B. Wannalerse
The Department of Chemistry
Faculty of Science, Kasetsart University
50 Ngam Wong Wan Road, Lat Yao, Chatuchak
Bangkok 10900 (Thailand)

[c] Dr. B. Wannalerse
The Center of Excellence for Innovation in Chemistry
Faculty of Science, Kasetsart University
50 Ngam Wong Wan Road, Lat Yao, Chatuchak
Bangkok 10900 (Thailand)
E-mail: fscibnw@ku.ac.th

Supporting Information and the ORCID identification number(s) for the author(s) of this article can be found under https://doi.org/10.1002/open.201700193.

With 6-methacryloylamino BOB monomer in hand, a series of polyacrylamide hydrogels were synthesized, consisting of water (60% w/w), acrylamide (38% w/w), methylene bisacrylamide (1% w/w), and either 6-methacryloylamino BOB monomer (1% w/w) or 3-methacyryloylamino phenylboronic acid pinacol ester monomer (PBA; 1% w/w). Blank gels were also prepared containing additional acrylamide in the place of the boronate compound (1% w/w) (Scheme 2).

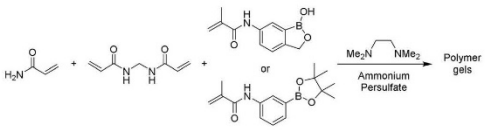

Scheme 2. Preparation of boronate ester hydrogels.

For qualitative purposes, treatment of the blank gel, borogel, and BOBgel with ARS solution (pH 7.3) resulted in red (blank) and orange (borogel and BOBgel) slabs. Gel slabs were then placed in PBS to wash out any non-specifically bound dye. The orange color of the borogels and BOBgels persisted after washing, whereas the blank gel was pale pink, owing to a small amount of non-specifically bound dye remaining (see the Supporting Information).

To obtain quantitative data, hydrogels were prepared in plastic disposable syringes, which provided a method that consistently produces an identically sized hydrogel. Further to this, the size of the polymer gels can easily be modified by increasing or decreasing the amount of polymer solution taken up into the syringe.

The hydrogel cylinders (0.1 g) were immersed in 2.0×10^{-4} M ARS solution [in phosphate buffer solution (PBS)]. As illustrated in Figure 1, the decrease in absorbance at 513 nm corresponds to the amount of dye uptake into the gel. After 5 h, both borogel and BOBgel were completely dye saturated with no further decrease in absorption at 513 nm. Similar to the gel slabs, both borogels and BOBgels appeared orange in color, whereas the blank gels were red.

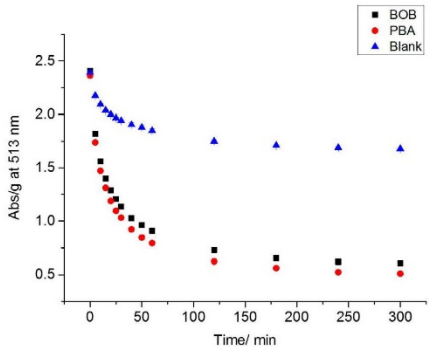

Figure 1. UV absorption (at 513 nm) measurements for dye (ARS) uptake per unit mass of gels versus time for smaller hydrogel cylinders in PBS solution (pH 7.3).

Each gel was then placed in PBS to wash out any non-boron-bound dye. As previously reported, there was no further increase in dye concentration in solution after 2 h (see the Supporting Information).

The PBS-washed hydrogels were then exposed to an increasing concentration of glucose (0–1 M). As shown in Figure 2, an increase in the addition of glucose led to the displacement of ARS from the borogel, leading to an increase in absorption at 513 nm. The largest amount of dye release was seen for the BOBgels, indicating a greater affinity for saccharides over the simple boronate receptor—borogel. Scheme 3 illustrates the dye displacement assay for the binding of a saccharide to BOB, displacing the ARS dye.

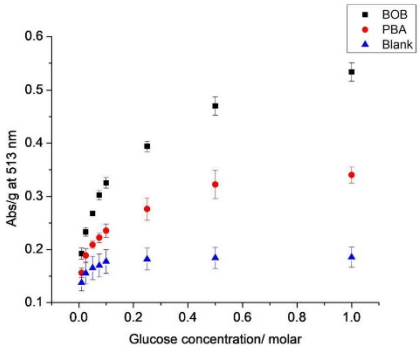

Figure 2. UV absorption (at 513 nm) measurements for glucose addition to ARS dye displacement assay for smaller hydrogel cylinders in PBS solution (pH 7.3).

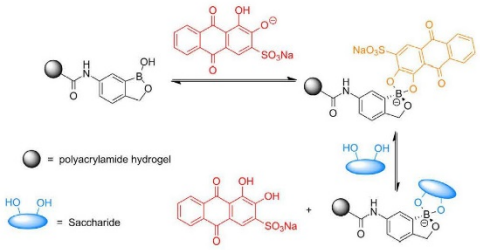

Scheme 3. An improved dye displacement assay utilizing an ARS-bound BOBgel for the determination of fructose concentration.

We then turned our attention to the addition of various saccharides to the borogels and BOBgels (Table 1). In comparison to glucose, a similar response was observed for galactose and mannose; however, both the borogels and BOBgels released considerably more dye when exposed to fructose. This is consistent with the saccharide binding stability constants reported for phenylboronic acid by Lorand and Edwards (fructose >

Table 1. Amount of dye released [abs g^{-1} at 513 nm] upon the addition of various saccharides (1 M).

Gel	Fructose	Galactose	Mannose	Glucose
BOB	0.94	0.53	0.59	0.53
PBA	0.82	0.40	0.41	0.34
blank	0.23	0.21	0.22	0.19

other saccharides).[15] Unfortunately, the addition of methyl α-D-glucopyranoside to both borogel and BOBgel resulted in no change in absorbance.

In summary, borogels and BOBgels have been prepared. Interestingly, BOBgels demonstrated an enhanced apparent binding affinity for all the monosaccharide sugars evaluated. With the greatest enhancement in binding being observed with D-glucose and the BOBgels, relative to borogels. We are currently exploring the utility of borogels and BOBgels for the detection of biologically important saccharides under a variety of conditions.

Experimental Section

General Methods

All starting materials and reagents were purchased from Sigma Aldrich, Alfa Aesar, Fluorochem, Acros Organics, or Apollo Scientific and used as received without any further purification. Unless otherwise stated, all solvents used were reagent grade and were used without distillation. Dry solvents were obtained from an Innovative Technology Inc. PS-400-7 solvent purification system. All water was distilled. PBS buffer solution (52.1 wt% MeOH) was prepared according to the literature.[16] Thin-layer chromatography was performed by using commercially available Macherey–Nagel aluminum-backed plates coated with a 0.20 mm layer of silica gel (60 Å) with fluorescent indicator UV254. These plates were visualized by using ultraviolet light with a wavelength of either 254 or 365 nm, or by staining the plates with vanillin or ninhydrin solution. Silica gel column chromatography was carried out by using Fisher or Sigma Aldrich 60 Å silica gel (35–70 μm).

Unless otherwise stated, all NMR spectra were obtained by using a Bruker Advance 300 with all spectra recorded in chloroform-*d* or [D_6]DMSO. ^{1}H NMR spectra were recorded at an operating frequency of 300 MHz, ^{11}B NMR spectra were recorded at an operating frequency of 96 MHz, and ^{13}C NMR spectra were recorded at an operating frequency of 75 MHz, with proton decoupling for all ^{13}C NMR spectra. High-resolution mass spectrometry (HRMS) results were typically acquired on an externally calibrated Bruker Daltonics microTOF time-of-flight mass spectrometer coupled to an electrospray source (ESI-TOF). All solvents used in fluorescence measurements were HPLC or fluorescence grade and the water was deionized. Further reprocessing of the data was carried in OriginPro 8.0 software. All pH measurements taken during fluorescence/absorption experiments were recorded on a Hanna Instruments HI 9321 microprocessor pH meter, which was routinely calibrated by using Fisher Chemicals standard buffer solutions (pH 4.0: phthalate; 7.0: phosphate; 10.0: borate). UV/Vis measurements were performed on a PerkinElmer Lambda 20 Spectrophotometer, utilizing a Starna silica (quartz) cuvette with a 10 mm path length (two faces polished). Further reprocessing of the data was carried out in OriginPro 8.0 software.

Synthesis of Hydrogel Monomers

Previously reported methacyryloylamino PBA was synthesized according to the literature reported procedure.[13]

See the Supporting Information for a full synthetic procedure of BOB monomer.

Acknowledgements

E.V.L. thanks the EPSRC Doctoral Training Centre in Sustainable Chemical Technologies: EP/G03768X/1 for a studentship. A.C.S would like to thank the EPSRC and the University of Bath for funding. G.T.W. would like to thank the EPSRC, Public Health England, and the University of Bath for funding. T.S. thanks the Development and Promotion of Science and Technology Talents Project (DPST) for a Royal Government of Thailand Scholarship. T.D.J wishes to thank the Royal Society for a Wolfson Research Merit Award. NMR characterization facilities were provided through the Chemical Characterization and Analysis Facility (CCAF) at the University of Bath (www.bath.ac.uk/ccaf). All data supporting this study are provided as supplementary information accompanying this paper.

Conflict of Interest

The authors declare no conflict of interest.

Keywords: boronic acids · colorimetric detection · dye displacement assays · glucose · saccharides

[1] B. T. Nguyen, E. V. Anslyn, *Coord. Chem. Rev.* **2006**, *250*, 3118–3127.
[2] M. A. Palacios, R. Nishiyabu, M. Marquez, P. Anzenbacher, *J. Am. Chem. Soc.* **2007**, *129*, 7538–7544.
[3] T. Minami, Y. L. Liu, A. Akdeniz, P. Koutnik, N. A. Esipenko, R. Nishiyabu, Y. Kubo, P. Anzenbacher, *J. Am. Chem. Soc.* **2014**, *136*, 11396–11401.
[4] D. G. Smith, I. L. Topolnicki, V. E. Zwicker, K. A. Jolliffe, E. J. New, *Analyst* **2017**, *142*, 3549–3563.
[5] X. J. Liu, D. G. Smith, K. A. Jolliffe, *Chem. Commun.* **2016**, *52*, 8463–8466.
[6] N. Busschaert, C. Caltagirone, W. Van Rossom, P. A. Gale, *Chem. Rev.* **2015**, *115*, 8038–8155.
[7] S. L. Wiskur, H. Ait-Haddou, J. J. Lavigne, E. V. Anslyn, *Acc. Chem. Res.* **2001**, *34*, 963–972.
[8] W. L. Zhai, X. L. Sun, T. D. James, J. S. Fossey, *Chem. Asian J.* **2015**, *10*, 1836–1848.
[9] X. L. Sun, T. D. James, *Chem. Rev.* **2015**, *115*, 8001–8037.
[10] Y. Kubo, T. Ishida, A. Kobayashi, T. D. James, *J. Mater. Chem.* **2005**, *15*, 2889–2895.
[11] X. L. Sun, M. L. Odyniec, A. C. Sedgwick, K. Lacina, S. Y. Xu, T. T. Qiang, S. D. Bull, F. Marken, T. D. James, *Org. Chem. Front.* **2017**, *4*, 1058–1062.
[12] X. L. Sun, K. Lacina, E. C. Ramsamy, S. E. Flower, J. S. Fossey, X. H. Qian, E. V. Anslyn, S. D. Bull, T. D. James, *Chem. Sci.* **2015**, *6*, 2963–2967.
[13] W. M. J. Ma, M. P. P. Morais, F. D'Hooge, J. M. H. van den Elsen, J. P. L. Cox, T. D. James, J. S. Fossey, *Chem. Commun.* **2009**, 532–534.
[14] M. Dowlut, D. G. Hall, *J. Am. Chem. Soc.* **2006**, *128*, 4226–4227.
[15] J. P. Lorand, J. O. Edwards, *J. Org. Chem.* **1959**, *24*, 769–774.
[16] D. D. Perrin, B. Dempsey, *Buffers for pH and Metal Ion Control*, Chapman and Hall, London, **1974**.

Received: December 5, 2017
Version of record online January 30, 2018

An ESIPT Probe for the Ratiometric Imaging of Peroxynitrite Facilitated by Binding to Aβ-Aggregates

JACS JOURNAL OF THE AMERICAN CHEMICAL SOCIETY
Article
Cite This: J. Am. Chem. Soc. 2018, 140, 14267−14271
pubs.acs.org/JACS

Adam C. Sedgwick,[†,∥,⊥] Wei-Tao Dou,[‡,⊥] Jin-Biao Jiao,[‡] Luling Wu,[†] George T. Williams,[†] A. Toby A. Jenkins,[†] Steven D. Bull,[†] Jonathan L. Sessler,[*,∥] Xiao-Peng He,[*,‡] and Tony D. James[*,†,§]

[†]Department of Chemistry, University of Bath, Bath BA2 7AY, U.K.

[‡]Key Laboratory for Advanced Materials and Joint International Research Laboratory of Precision Chemistry and Molecular Engineering, Feringa Nobel Prize Scientist Joint Research Center, School of Chemistry and Molecular Engineering, East China University of Science and Technology, 130 Meilong Rd., Shanghai 200237, China

[§]Department of Materials and Life Sciences, Faculty of Science and Technology, Sophia University, 7-1 Kioi-cho, Chiyoda-ku, Tokyo 102-8554, Japan

[∥]Department of Chemistry. University of Texas at Austin, 105 East 24th Street A5300, Austin, Texas 78712-1224, United States

Supporting Information

ABSTRACT: A series of 3-hydroxyflavone (**3-HF**) ESIPT (excited-state intramolecular proton transfer) boronate-based fluorescent probes have been developed for the detection of peroxynitrite ($ONOO^-$). The dyes are environmentally sensitive, and each probe exhibited a ratiometric response toward $ONOO^-$ in a micellar environment. The probes were used to image different aggregation states of amyloid-β (Aβ) in the presence of $ONOO^-$. The **3-HF-OMe** probe was found to produce a ratiometric response toward $ONOO^-$ when bound to Aβ aggregates, resulting in a novel host−guest ensemble, which adds insight into the development of other ESIPT-based probes for the simultaneous sensing of fibrous proteins/peptides and environmental ROS/RNS.

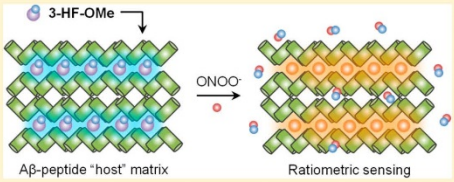

Alzheimer's disease (AD) is a common neurodegenerative disease that involves the progressive and gradual decline in cognitive functions. Self-associating amyloid-β peptides Aβ_{1-42} result in the buildup of amyloid-β (Aβ) plaques, which are one of the key factors for this cognitive decline.[1−3] The neurotoxicity of Aβ peptides is believed to alter calcium homeostasis, inducing the inflammatory response, and increase the formation of reactive oxygen and nitrogen species (ROS/RNS).[4] Furthermore, it has been shown that Aβ peptides can damage neurons by activating microglia, which generate peroxynitrite ($ONOO^-$).[5] $ONOO^-$ is an RNS known for its deleterious effects, causing irreversible damage to a range of biological targets such as lipids, proteins, and DNA.[6,7] In addition, higher levels of nitrated proteins are typically found in the neurons ($ONOO^-$ indicator) of AD victims.[8] As a result, a number of small molecule fluorescent probes have been developed for Aβ detection[9−12] or for $ONOO^-$ detection.[13−17] However, to date, no fluorescence-based probe has been developed that can simultaneously detect $ONOO^-$ while bound to an Aβ peptide. The development of such a probe would provide a powerful tool that might enhance the understanding of AD progression and could potentially be used to evaluate AD therapeutic strategies.

We have been particularly interested in developing small molecule fluorescence-based probes owing to their high sensitivity, selectivity, and high spatial and temporal resolution.[18−20] Here we report the use of 3-hydroxyflavones (**3-HFs**) as fluorescence-based reporters for the ratiometric detection of $ONOO^-$ when bound to Aβ aggregates (Scheme 1 and Figure 1).

3-HFs have been used extensively as fluorescent probes for the detection of a wide range of analytes.[21−25] The interest in such systems arises from the dual fluorescence emission ascribed to the normal (**N**) and photo tautomeric (**T***) forms that result from excited-state intramolecular proton transfer (ESIPT) (Scheme 1).[26] The ratio of the intensity of these two emission peaks is dependent on the surrounding environment of the molecule, especially the polarity of the solvent. We have previously shown (Scheme 1) that the ESIPT process can be blocked using a benzyl boronic ester protecting group.[27] The group can then be selectively removed by $ONOO^-$ resulting in a "turn-on" fluorescence-based probe suitable for the detection of $ONOO^-$. Our work and that of others has clearly demonstrated that $ONOO^-$ has a much greater reactivity

Received: August 7, 2018
Published: October 2, 2018

DOI: 10.1021/jacs.8b08457
J. Am. Chem. Soc. 2018, 140, 14267−14271

Scheme 1. ESIPT Fluorescent Probes[a]

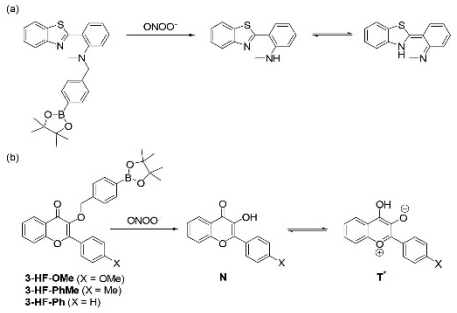

[a](a) Our previous work on boronate-based ESIPT fluorescent probes for peroxynitrite. (b) Boronate-based ESIPT fluorescent probes for peroxynitrite based on 3-hydroxyflavones (**3-HFs**) (X = OMe, Me, or H). Also shown are the normal (**N**) and phototautomeric (**T***) forms of the excited-state intramolecular proton transfer (ESIPT) process.

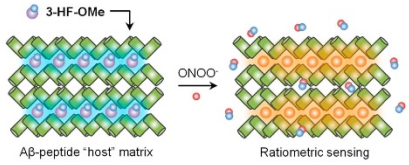

Figure 1. Schematic illustration of the proposed interactions of **3-HF** probes with amyloid-β (Aβ) aggregates and their use as a new host–guest system for the ratiometric sensing of peroxynitrite ($ONOO^-$). The **3-HF-OMe** "guest" molecules can associate with the hydrophobic cavity of a "host" matrix formed by Aβ peptide aggregation. This leads to an enhanced fluorescence of the **N** state of the ESIPT probe. Subsequent reaction of ONOO⁻ with the peptide-matrix-bound **3-HF-OMe** probe activates the **T*** fluorescence state of the ESIPT probe, thus enabling the ratiometric detection of RNS.

toward boronates than other oxidants, including ClO^- and H_2O_2.[13,28,29] Environmentally sensitive fluorescent dyes have been used to image amyloid-β plaques (Aβ), taking advantage of the presence of multiple β-sheets that entropically form hydrophobic pockets.[12] We believed the development of a **3-HF** $ONOO^-$ fluorescence-based probe could be used as a diagnostic tool for AD as it would provide information on the surrounding environment (hydrophilic or hydrophobic) and simultaneously detect $ONOO^-$.

Three benzyl boronic ester-protected **3-HF** fluorescence-based probes were developed (**3-HF-OMe**, **3-HF-PhMe**, and **3-HF-Ph**). The synthesis of **3-HF** fluorophores were achieved using a simple procedure developed by Ozturk et al.[26] Subsequently, their alcohol functionalities were alkylated with 2-(4-(bromomethyl)phenyl)-4,4,5,5-tetramethyl-1,3,2-dioxaborolane to afford the desired **3-HF** probes (**3-HF-OMe**, **3-HF-PhMe**, and **3-HF-Ph**).

First, we evaluated the fluorescence behavior of the **3-HF** probes in aqueous PBS (pH 7.4). The addition of $ONOO^-$ (10 μM) to each **3-HF** probe resulted in a decrease in **N** fluorescence emission intensity and no **T*** was observed (see Figures S1–S3 in the SI). It is known that micelles can create a hydrophobic microenvironment facilitating emission from the **T*** tautomer.[30] Therefore, the addition of $ONOO^-$ to the **3-HF** probes in the presence of CTAB (hexadecyltrimethylammonium bromide) (2 mM) led to a ratiometric fluorescence change with an increase in fluorescence intensity of the **T*** emission peak at 530 nm and a decrease in fluorescence emission at 425 nm (see Figures S4–S9). The LOD (limit of detection) for the probes with $ONOO^-$ are in the nanomolar range for **3-HF-OMe** (65.5 nM), **3-HF-PhMe** (21.0 nM), and **3-HF-Ph** (255.5 nM) (see Figure S10). We then evaluated the selectivity of the **3-HF** probes toward other ROS (see Figures S11–S19). The probes exhibited an excellent selectivity for $ONOO^-$ against most ROS. However, the addition of ClO^- (100 μM) led to the degradation of the probe as a fluorescence decrease of the **N** emission intensity and decrease of the initial **T*** fluorescence emission intensity was observed.[31] Of note, ClO^- is an important ROS that plays a vital role in immune defense systems due to its microbiocidal properties. It is produced enzymatically, through the reaction of H_2O_2 and chloride (Cl^-) catalyzed by myeloperoxidase.[29,32,33] Therefore, when $ONOO^-$ is present in cells the levels of ClO^- are expected to be low.

We then turned our attention toward the **3-HF** $ONOO^-$ fluorescence-based probes in the presence of oligomeric Aβ42 peptides. The Aβ42 peptide was purchased, used as provided, and was incubated in Tris-HCl buffer at room temperature at pH 8.0 for 2 h, 4 h, 8 h, 16 h, 1 d (24 h), 3 d (72 h), 5 d (120 h), and 7 d (168 h) in order to produce different Aβ42 aggregates.[34] The addition of the oligomeric (oligo) Aβ42 peptides and Aβ42 aggregates (aggr) to **3-HF-OMe** led to an increase in **N** fluorescence intensity (Figure 2). However, in the presence of Aβ42, for **3-HF-PhMe** and **3-HF-Ph** only a slight change in fluorescence intensity was observed with and without the addition of $ONOO^-$ (see Figures S20 and S21).

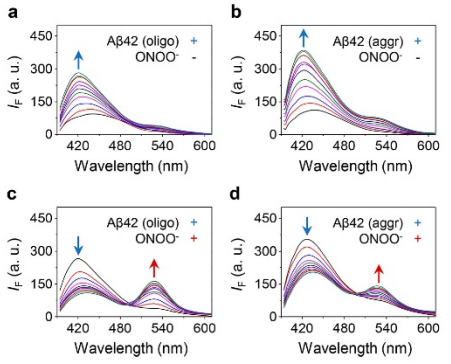

Figure 2. Fluorescence emission spectra of **3-HF-OMe** (5 μM) in the presence of (a) Aβ42 oligomers (blue arrow (I_{420}), represents an increase in fluorescence intensity, 0–50 μM, interval 5 μM), (b) Aβ42 aggregates (blue arrow (I_{420}), represents an increase in fluorescence intensity, 0–50 μM, interval 5 μM), (c) Aβ42 oligomers (50 μM) and then $ONOO^-$ (red arrow (I_{530}), represents an increase in fluorescence intensity, 0–10 μM, interval 1 μM), and (d) Aβ42 aggregates (50 μM) and then $ONOO^-$ (red arrow (I_{530}), represents an increase in fluorescence intensity, 0–10 μM, interval 1 μM). All measurements were carried out in Tris-HCl (0.01 M, pH 7.4) using an excitation wavelength of 365 nm.

DOI: 10.1021/jacs.8b08457
J. Am. Chem. Soc. 2018, 140, 14267–14271

Interestingly, with **3-HF-OMe** a larger increase in fluorescence intensity was observed for Aβ42 aggregates than the oligomeric Aβ42 peptides. This is believed to be due to a more "compact" matrix enhancing the hydrophobic pockets. We deduce that the stronger binding of **3-HF-OMe** with the Aβ42 peptides might be caused by the additional methoxyl group facilitating hydrogen bonding interactions within the aggregated peptide matrix. Moreover, the addition of $ONOO^-$ to **3-HF-OMe** in the Aβ42 "host matrix" (oligomeric and aggregates) led to a remarkable ratiometric change in fluorescence intensity (Figure 2). In addition, **3-HF-OMe** bound to oligomeric Aβ42 peptides was found to have a greater sensitivity toward $ONOO^-$. This is believed to be due to the compact matrix of the Aβ42 aggregate providing a protective barrier against $ONOO^-$.

To corroborate further the ratiometric response of our **3-HF-OMe**/Aβ hybrid system for $ONOO^-$, different aggregates of Aβ42 were used. First, we determined that the concentration-dependent **N** fluorescence increase of probe **3-HF-OMe** was gradually enhanced with Aβ aggregation (Figure S22). In contrast, the concentration-dependent **T*** fluorescence increase of the probe was gradually reduced at the same level of Aβ42 aggregation (Figure S23). Furthermore, plotting the ratio of the fluorescence intensity of the probe in the **N**-state (I_{420}) with that of the **T***-state (I_{530}) (Figure 3a) revealed

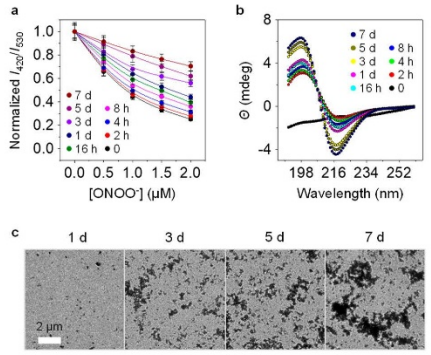

Figure 3. (a) Plot of the ratiometric change for **3-HF-OMe** (5 μM) with Aβ42 with different aggregation states (50 μM) as a function of $ONOO^-$ concentration. The Aβ42 aggregates were produced by incubating the peptide in Tris-HCl at room temperature (pH 8.0) for 2 h, 4 h, 8 h, 16 h, 1 d (24 h), 3 d (72 h), 5 d (120 h), and 7 d (168 h). All measurements were carried out in Tris-HCl (0.01 M, pH 7.4) with excitation at 365 nm. (b) Circular dichroism spectra of Aβ42 with different aggregation states. (c) Scanning electron microscopic images of Aβ42 with different aggregation states (note that when Aβ42 was aggregated for 2−16 h they are almost invisible in the images; therefore, only those with aggregation times exceeding 1 d are shown).

that the decreased ratiometric response of the probe/Aβ42 hybrid to $ONOO^-$ (at low concentrations 0−2.0 μM) is proportional to the aggregation state of Aβ42 determined by both circular dichroism spectroscopy (Figure 3b) and scanning electron microscopy (Figure 3c). Furthermore, the ratiometric response of the **3-HF-OMe**/Aβ hybrid system was shown to be independent of the concentration of **3-HF-OMe**. (Figures S24 and S25)

Using the titration data, we have also calculated the LODs for the different probe/Aβ42 hybrids with $ONOO^-$ (Figure S26). While the sensitivity of the hybrid system gradually decreases as Aβ aggregation increases, the LOD of our new host−guest system for $ONOO^-$ is in the nanomolar range (21.7 ± 1.2 nM to 106.9 ± 4.6 nM). We also measured the selectivity of the probe and the probe/Aβ42 hybrid for a range of other proteins and ROS/RNS, respectively. (Figures S27 and S28), the excellent selectivity supported the conclusion that the probe can detect Aβ and the probe/Aβ42 hybrid is a sensor for $ONOO^-$. Dynamic light scattering confirmed the association of **3-HF-OMe** with Aβ42 through the increased diameter of the latter species (Figure S29). In addition, the fluorescence quantum yield of **3-HF-OMe** was found to increase when bound to Aβ42 oligomers and aggregates (Figure S30).

To investigate the potential of the probe for real world applications, we used the brain of an AD-transgenic mouse for fluorescence imaging. We observed that the Aβ42 aggregates of the brain sections displayed the **N**-state fluorescence of **3-HF-OMe** (Figure 4a, blue channel), which accorded well with the

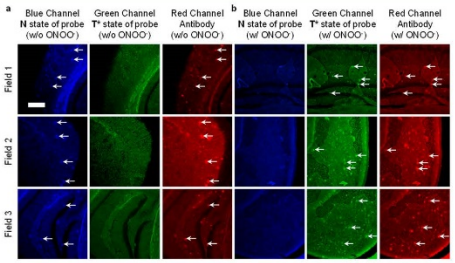

Figure 4. Fluorescence imaging of a brain section of a transgenic mouse treated with **3-HF-OMe** (20 μM) without (w/o) (a) and with (w/) (b) $ONOO^-$ (30 μM). The excitation/emission wavelengths for the blue (**N**-state fluorescence of **3-HF-OMe**), green (**T***-state fluorescence of **3-HF-OMe**), and red channel (anti-Aβ antibody) are 404/425−475, 404/500−550, and 561/640−730 nm, respectively. The white arrows indicate some representative, stained Aβ aggregates.

fluorescence of an anti-Aβ antibody (Figure 4a, red channel). Then, after treatment with $ONOO^-$ the fluorescence emission of the probe bound to the peptide aggregates of the brain section switched to the **T*** state (Figure 4b, green channel), which correlated well with the antibody fluorescence (Figure 4b, red channel). While the excitation and emission wavelengths of **3-HF-OMe** are not long enough for in vivo staining (ideally NIR is required),[35−37] our concept of using peptide aggregates as part of a naturally inspired host system for environmentally sensitive fluorescence-based probes provides the basis and motivation for the development of a new generation of ratiometric probes.

In summary, we have demonstrated that an ESIPT probe, **3-HF-OMe**, could be used to form a supramolecular hybrid with Aβ aggregates for the ratiometric detection of $ONOO^-$. Importantly, it has been reported that the concentration of $ONOO^-$ in the brain is ~300 nM,[4] which is above the LOD of the hybrid system. Our novel ESIPT probe/Aβ hybrid system

DOI: 10.1021/jacs.8b08457
J. Am. Chem. Soc. 2018, 140, 14267−14271

for ratiometric $ONOO^-$ sensing is unprecedented and will pave the way for the development of supramolecular peptide/probe hybrids for the simultaneous sensing of fibrous protein/peptides and oxidative state.

■ ASSOCIATED CONTENT

Supporting Information

The Supporting Information is available free of charge on the ACS Publications website at DOI: 10.1021/jacs.8b08457.

Preparation of ROS/RNS; fluorescence analysis; peroxynitrite addition to **3-HF** probes in aqueous solution and in CTAB−aqueous buffer; selectivity of **3-HF** probes with different ROS; fluorescence of **3-HF** probes in the presence of Aβ; experimental section, and NMR spectra (PDF)

■ AUTHOR INFORMATION

Corresponding Authors

*t.d.james@bath.ac.uk
*xphe@ecust.edu.cn
*Sessler@cm.utexas.edu

ORCID

Adam C. Sedgwick: 0000-0002-3132-2913
A. Toby A. Jenkins: 0000-0002-8981-3029
Steven D. Bull: 0000-0001-8244-5123
Jonathan L. Sessler: 0000-0002-9576-1325
Xiao-Peng He: 0000-0002-8736-3511
Tony D. James: 0000-0002-4095-2191

Author Contributions

⊥These authors contributed equally.

Notes

The authors declare no competing financial interest.

■ ACKNOWLEDGMENTS

We thank the EPSRC and the University of Bath for funding. A.C.S. and A.T.A.J. thank the EPSRC for funding (EP/R003939/1). T.D.J. wishes to thank the Royal Society for a Wolfson Research Merit Award and Sophia University for a visiting professorship. NMR characterisation facilities were provided through the Chemical Characterisation and Analysis Facility (CCAF) at the University of Bath (www.bath.ac.uk/ccaf). The EPSRC U.K. National Mass Spectrometry Facility at Swansea University is thanked for analyses. Hai-Hao Han and Jing−Jing Zhang are thanked for biological experiments. X.-P.H. thanks the National Natural Science Foundation of China (21788102, 21722801, and 21572058), the Programme of Introducing Talents of Discipline to Universities (B16017), and the Shanghai Rising-Star Program (16QA1401400) for support. J.L.S. thanks The Robert A. Welch Foundation (F-0018). He Tian is warmly thanked for his helpful advice. We would like to thank Lauren Gwynne for proof reading the manuscript.

■ REFERENCES

(1) Greenwald, J.; Riek, R. *Structure* **2010**, *18* (10), 1244−1260.
(2) Rojas-Gutierrez, E.; Munoz-Arenas, G.; Trevino, S.; Espinosa, B.; Chavez, R.; Rojas, K.; Flores, G.; Diaz, A.; Guevara, J. *Synapse* **2017**, *71*, e21990.
(3) Lambert, M. P.; Barlow, A. K.; Chromy, B. A.; Edwards, C.; Freed, R.; Liosatos, M.; Morgan, T. E.; Rozovsky, I.; Trommer, B.; Viola, K. L.; Wals, P.; Zhang, C.; Finch, C. E.; Krafft, G. A.; Klein, W. L. *Proc. Natl. Acad. Sci. U. S. A.* **1998**, *95* (11), 6448−6453.
(4) Malinski, T. *J. Alzheimer's Dis.* **2007**, *11* (2), 207−218.
(5) Boje, K. M.; Arora, P. K. *Brain Res.* **1992**, *587* (2), 250−256.
(6) Beckman, J. S.; Koppenol, W. H. *Am. J. Physiol. Cell Physiol.* **1996**, *271* (5), C1424−C1437.
(7) Pacher, P.; Beckman, J. S.; Liaudet, L. *Physiol. Rev.* **2007**, *87* (1), 315−424.
(8) Smith, M. A.; Richey Harris, P. L.; Sayre, L. M.; Beckman, J. S.; Perry, G. *J. Neurosci.* **1997**, *17* (8), 2653−2657.
(9) Yang, H. Y.; Zhang, J. J.; Zang, Y.; Zhang, H. Y.; Li, J.; Chen, G. R.; He, X. P. *Dyes Pigm.* **2017**, *136*, 224−228.
(10) Cui, M. C.; Ono, M.; Watanabe, H.; Kimura, H.; Liu, B. L.; Saji, H. *J. Am. Chem. Soc.* **2014**, *136* (9), 3388−3394.
(11) Kim, D.; Moon, H.; Baik, S. H.; Singha, S.; Jun, Y. W.; Wang, T.; Kim, K. H.; Park, B. S.; Jung, J.; Mook-Jung, I.; Ahn, K. H. *J. Am. Chem. Soc.* **2015**, *137* (21), 6781−6789.
(12) Ran, C. Z.; Xu, X. Y.; Raymond, S. B.; Ferrara, B. J.; Neal, K.; Bacskai, B. J.; Medarova, Z.; Moore, A. *J. Am. Chem. Soc.* **2009**, *131* (42), 15257−15261.
(13) Kim, J.; Park, J.; Lee, H.; Choi, Y.; Kim, Y. *Chem. Commun.* **2014**, *50* (66), 9353−9356.
(14) Sun, Z. N.; Wang, H. L.; Liu, F. Q.; Chen, Y.; Tam, P. K. H.; Yang, D. *Org. Lett.* **2009**, *11* (9), 1887−1890.
(15) Yu, F. B. A.; Li, P.; Li, G. Y.; Zhao, G. J.; Chu, T. S.; Han, K. *J. Am. Chem. Soc.* **2011**, *133* (29), 11030−11033.
(16) Li, X.; Tao, R.-R.; Hong, L.-J.; Cheng, J.; Jiang, Q.; Lu, Y.-M.; Liao, M.-H.; Ye, W.-F.; Lu, N.-N.; Han, F.; Hu, Y.-Z.; Hu, Y.-H. *J. Am. Chem. Soc.* **2015**, *137* (38), 12296−12303.
(17) Sun, X.; Xu, Q.; Kim, G.; Flower, S. E.; Lowe, J. P.; Yoon, J.; Fossey, J. S.; Qian, X.; Bull, S. D.; James, T. D. *Chem. Sci.* **2014**, *5* (9), 3368−3373.
(18) Sedgwick, A. C.; Han, H. H.; Gardiner, J. E.; Bull, S. D.; He, X. P.; James, T. D. *Chem. Sci.* **2018**, *9* (15), 3672−3676.
(19) Sedgwick, A. C.; Chapman, R. S. L.; Gardiner, J. E.; Peacock, L. R.; Kim, G.; Yoon, J.; Bull, S. D.; James, T. D. *Chem. Commun.* **2017**, *53* (75), 10441−10443.
(20) Sedgwick, A. C.; Gardiner, J. E.; Kim, G.; Yevglevskis, M.; Lloyd, M. D.; Jenkins, A. T. A.; Bull, S. D.; Yoon, J.; James, T. D. *Chem. Commun.* **2018**, *54* (38), 4786−4789.
(21) Hu, Q. H.; Zeng, F.; Yu, C. M.; Wu, S. Z. *Sens. Actuators, B* **2015**, *220*, 720−726.
(22) Liu, B.; Wang, J. F.; Zhang, G.; Bai, R. K.; Pang, Y. *ACS Appl. Mater. Interfaces* **2014**, *6* (6), 4402−4407.
(23) Liu, B.; Wang, H.; Wang, T. S.; Bao, Y. Y.; Du, F. F.; Tian, J.; Li, Q. B. A.; Bai, R. K. *Chem. Commun.* **2012**, *48* (23), 2867−2869.
(24) Shynkar, V. V.; Klymchenko, A. S.; Kunzelmann, C.; Duportail, G.; Muller, C. D.; Demchenko, A. P.; Freyssinet, J. M.; Mely, Y. *J. Am. Chem. Soc.* **2007**, *129* (7), 2187−2193.
(25) Klymchenko, A. S.; Shvadchak, V. V.; Yushchenko, D. A.; Jain, N.; Mely, Y. *J. Phys. Chem. B* **2008**, *112* (38), 12050−12055.
(26) Gunduz, S.; Goren, A. C.; Ozturk, T. *Org. Lett.* **2012**, *14* (6), 1576−1579.
(27) Sedgwick, A. C.; Sun, X. L.; Kim, G.; Yoon, J.; Bull, S. D.; James, T. D. *Chem. Commun.* **2016**, *52* (83), 12350−12352.
(28) Sedgwick, A. C.; Han, H. H.; Gardiner, J. E.; Bull, S. D.; He, X. P.; James, T. D. *Chem. Commun.* **2017**, *53* (95), 12822−12825.
(29) Sikora, A.; Zielonka, J.; Lopez, M.; Joseph, J.; Kalyanaraman, B. *Free Radical Biol. Med.* **2009**, *47* (10), 1401−1407.
(30) Sarker, N.; Das, K.; Das, S.; Datta, A.; Nath, D.; Bhattacharyya, K. *J. Phys. Chem.* **1995**, *99* (50), 17711−17714.
(31) Chakrabartty, S. K.; Kretschmer, H. O. *J. Chem. Soc., Perkin Trans. 1* **1974**, *0*, 222−228.
(32) van der Veen, B. S.; de Winther, M. P. J.; Heeringa, P. *Antioxid. Redox Signaling* **2009**, *11* (11), 2899−2937.
(33) Klebanoff, S. J. *J. Leukocyte Biol.* **2005**, *77* (5), 598−625.
(34) Ishida, Y.; Tanimoto, S.; Takahashi, D.; Toshima, K. *MedChemComm* **2010**, *1* (3), 212−215.

(35) Zhang, X.; Tian, Y.; Yuan, P.; Li, Y.; Yaseen, M. A.; Grutzendler, J.; Moore, A.; Ran, C. *Chem. Commun.* **2014**, *50*, 11550−11553.
(36) Zhang, X.; Tian, Y.; Zhang, C.; Tian, X.; Ross, A. W.; Moir, R. D.; Sun, H.; Tanzi, R. E.; Moore, A.; Ran, C. *Proc. Natl. Acad. Sci. U. S. A.* **2015**, *112*, 9734−9739.
(37) Chen, C.; Liang, Z.; Zhou, B.; Li, X.; Lui, C.; Ip, N. Y.; Qu, J. Y. *ACS Chem. Neurosci.* **2018**, 1.

DOI: 10.1021/jacs.8b08457
J. Am. Chem. Soc. 2018, 140, 14267−14271

Delivery and Quantification of Hydrogen Peroxide Generated via Cold Atmospheric Pressure Plasma Through Biological Material

IOP Publishing
Journal of Physics D: Applied Physics
J. Phys. D: Appl. Phys. **52** (2019) 505203 (8pp)
https://doi.org/10.1088/1361-6463/ab4539

Delivery and quantification of hydrogen peroxide generated via cold atmospheric pressure plasma through biological material

H J Hathaway[1], B L Patenall[2], N T Thet[2], A C Sedgwick[2], G T Williams[2], A T A Jenkins[2], S L Allinson[3] and R D Short[1]

[1] Department of Chemistry, Lancaster University, Lancaster, United Kingdom
[2] Department of Chemistry, University of Bath, Bath, United Kingdom
[3] Division of Biomedical and Life Sciences, Lancaster University, Lancaster, United Kingdom

E-mail: holliejanehathaway@gmail.com

Received 2 November 2018, revised 28 August 2019
Accepted for publication 17 September 2019
Published 9 October 2019

Abstract

The ability of plasma-generated hydrogen peroxide (H_2O_2) to traverse bacterial biofilms and the subsequent fate of the generated H_2O_2 has been investigated. An *in vitro* model, comprising a nanoporous membrane impregnated with artificial wound fluid and biofilms of varying maturity was treated with a helium-driven, cold atmospheric pressure plasma (CAP) jet. The concentration of H_2O_2 generated below the biofilms was quantified. The results showed that the plasma-generated H_2O_2 interacted significantly with the biofilm, thus exhibiting a reduction in concentration across the underlying nanoporous membrane. Biofilm maturity exhibited a significant effect on the penetration depth of H_2O_2, suggesting that well established, multilayer biofilms are likely to offer a shielding effect with respect to cells located in the lower layers of the biofilm, thus rendering them less susceptible to plasma disinfection. This may prove clinically significant in the plasma treatment of chronic, deep tissue infections such as diabetic and venous leg ulcers. Our results are discussed in the context of plasma-biofilm interactions, with respect to the fate of the longer lived reactive species generated by CAP, such as H_2O_2.

Keywords: plasma, biofilms, reactive species, cold plasma

Supplementary material for this article is available online

(Some figures may appear in colour only in the online journal)

1. Introduction

The ability to treat antibiotic resistant microorganisms has become paramount in the fight against bacterial infection owing to their ever-increasing prevalence. The apparent stagnation in antimicrobial drug development has fuelled urgent initiatives from a number of prominent healthcare organisations tailored towards treating and ultimately preventing such infections [1–3]. The extent of the current crisis is exemplified according to a predicted annual death toll of ten million by 2050 arising solely from drug resistant infections (surpassing that of cancer) [4]. In addition to antimicrobial resistance (both *de novo* and pre-existing), the ability of bacteria to form biofilms, (dense, multilayer communities of bacterial cells protected by an extracellular polymeric substance (EPS)), further encumbers effective disinfection owing to changes in the physiological state of the cells contained within. Notoriously difficult to treat, it is estimated that biofilms are associated with 65% of all bacterial infections, rising to 85% when considering chronic infections [5]. Biofilms are able to form on a multitude of surfaces; both biotic and abiotic, thus providing a significant reservoir of pathogenic microorganisms responsible for numerous human infections. Biofilms are reported to be involved in half of all hospital-acquired infections, which

the World Health Organisation estimates to affect 4.5 million people per annum in Europe, highlighting the significant challenge currently facing the global healthcare community [6, 7].

Wound infections, specifically chronic wound infections have a reported prevalence of 6% in the UK and account for at least 5.5% of the total NHS expenditure [8]. In the USA such non-healing wounds carry an annual cost of $25 billion and it has been estimated that 1%–2% of the population in developed countries will develop a chronic wound in their lifetime [9]. Wounds (venous, pressure, arterial and diabetic) are the leading cause of amputation, the latter being responsible for 70% of all lower limb amputations which occur globally every 30 seconds as a direct result of non-healing diabetic ulcers [10, 11]. The protective nature of the EPS along with the induction of various quorum sensing pathways and the subsequent alteration in gene expression, has rendered biofilms largely recalcitrant to common antimicrobial agents. Hence, the need for effective treatment strategies has become imperative in reducing both the social and economic burden of wound infection [12].

Cold atmospheric pressure plasma (CAP) has been proven to deliver a potent antimicrobial cocktail of reactive species able to successfully decontaminate numerous clinically relevant single- and mixed-species biofilms, including those associated with significant drug resistance; termed the 'ESKAPE' pathogens [13–15]. The composition and delivery of reactive species generated during CAP therapy, such as reactive oxygen and nitrogen species (RONS) may be controlled according to the plasma parameters employed, providing an attractive therapeutic treatment option currently undergoing significant investigation within the scientific community [16, 17]. Extensive discussion can be found in the literature surrounding the effects of the plasma source, the variation in operating conditions and the current progress and challenges facing CAP therapy in the control of microbial biofilms and wound infection [18–22]. The interaction of non-thermal plasma with biological material has been well documented in terms of bactericidal effects, phenotypic and genetic consequences (in both eukaryotic and prokaryotic cells) and with respect to plasma-activated liquids [23–25]. Studies have been conducted using tissue surrogates such as gelatin and agarose, alongside cellular mimics such as phospholipid vesicles to track plasma delivery of RONS [26–30]. Furthermore, the biofilm penetration depth of CAP-generated reactive species has been reported as a function of cell death and via computational modelling [31–33]. However, the direct quantification of longer-lived species, such as hydrogen peroxide (H_2O_2) has yet to be conducted through living biofilms. This study reports the effects of biofilm composition on the delivery of plasma-generated H_2O_2 across the cellular interface, thus confirming the ability of biologically active plasma-generated products to traverse bacterial biofilms according to biofilm density/maturity. The presence of H_2O_2, or lack thereof, may provide insight into the fate of the longer-lived species generated by CAP and the subsequent implications this may have for the safe and effective decontamination of chronic wounds.

2. Materials and methods

2.1. Materials

Tryptic soy broth (TSB), Tryptic soy agar (TSA), Luria-Bertani (LB) broth, phosphate buffered saline (PBS) tablets (pH 7.4), Brain heart infusion (BHI) agar, foetal calf serum (FCS) (HyClone), sodium chloride (NaCl), potassium iodide (KI), H_2O_2, peptone, poly (vinyl alcohol) (PVA) (M_W 14600–18600 g mol^{-1}), carboxymethyl cellulose (CMC) and agarose were all purchased from Sigma-Aldrich, UK. Biofilms were formed on sterile, nanoporous polycarbonate filter membranes (Whatman), 19 mm in diameter with an average pore size of 200 nm.

2.2. CAP jet

The plasma jet used consists of a single electrode configuration with a 150 mm glass capillary tube and a 15 mm external ring copper electrode operating at a distance of 40 mm from the end of the tube [30]. Helium was used as the carrier gas at a fixed flow rate of 0.6 standard litres per minute (SLPM). The jet was operated at an applied voltage of 10 kV_{p-p} and a frequency of 25 kHz. The distance from the end of the capillary tube to the surface of the substrate was 5 mm. The jet used predominantly produces H_2O_2 under the described operation parameters [28]. There is evidence that the initial interaction of the plasma with ambient air in the gas phase is the primary production site for H_2O_2 [34].

2.3. Quantification of H_2O_2

Potassium iodide (KI) was used to quantify H_2O_2 concentration in solution via the generation of a standard curve. 1M KI in deionised (DI) water was added to varying concentrations of H_2O_2 at a ratio of 1:1 and incubated at 25 °C for 30 min. Absorbance measurements were taken at 410 nm using a microplate reader (Spectrostar Omega, BMG Labtech) and used to produce a calibration curve (online supplementary information, figure 1 (stacks.iop.org/JPhysD/52/505203/mmedia)) [35]. For quantification of plasma-generated H_2O_2 in PBS, 350 μl of PBS was added to each well in a 96 well microtiter plate and treated for 0.5–5 min. 100 μl of the treated solution was then removed, added to 1 M KI (1:1 v/v) and incubated at 25 °C for 30 min. Absorbance measurements were taken as before and the concentration calculated using the calibration curve.

2.4. Bacterial strains and growth conditions

Methicillin-resistant *Staphylococcus aureus* (MRSA) 252 and *Pseudomonas aeruginosa* (*P. aeruginosa*) PA01 were sourced from a bacterial strain collection belonging to the Biophysical Research Group housed at the University of Bath, UK. Single colonies were cultured from freezer stocks (stored at −80 °C) on TSA or LB agar for MRSA 252 and PA01, respectively. Overnight cultures were grown from single colonies in TSB or LB liquid media for MRSA 252 and PA01, respectively. Cultures were incubated at 37°C with agitation (200 rpm)

for 18 h to achieve a cell density of 10^9 colony forming units (CFU) ml^{-1}.

2.5. Bacterial biofilm formation

Overnight cultures of MRSA 252 and PA01 were centrifuged at 10000 × g for 10 min, washed and resuspended in fresh PBS to an optical density of ~0.2 (~10^6 CFU ml^{-1}). White sterile polycarbonate filter membranes positioned on BHI agar were inoculated with 20 μl artificial wound fluid (FCS mixed in equal volume with 0.85% NaCl and 0.1% peptone) in order to better model the wound environment and components supporting bacterial growth and adhesion. 30 μl of bacterial subculture was added to the conditioned membranes. Membranes were UV sterilised for 10 min prior to bacterial inoculation. Plates were incubated at 32 °C for 8, 12 and 24 h [36].

2.6. Quantification of viable bacterial cells

Following incubation, biofilms were removed from the plates and transferred into 5 ml of PBS. The solutions were vortexed at 3000 rpm for 1 min and sonicated for 15 min. This process was repeated twice to ensure complete detachment of the bacterial cells from the membrane. Serial dilutions were carried out in PBS and plated on TSA or LB agar with subsequent incubation at 37 °C for 24 h to enumerate the number of viable bacteria.

2.7. CAP treatment of bacterial biofilms

Bacterial biofilms grown for 8, 12 and 24 h were placed atop 350 μl of PBS in a 96 well microtiter plate (full experimental set-up is shown in figure 2 of the supplementary information). Biofilms were plasma treated for 5 min, with manual movement of the jet around the circumference of the well similarly as *in vivo* wound treatments. Following plasma treatment, 100 μl of PBS was removed from each well and the concentration of H_2O_2 determined as before via correlation to the standard curve. In order to assess any time-dependent generation of H_2O_2 as a result of plasma treatment, additional 8 h biofilms were subject to plasma treatment followed by a further 4 h incubation *in situ* at 32 °C prior to H_2O_2 quantification. Separate experiments were undertaken to quantify the number of viable bacterial cells (post plasma treatment) as previously described. All experiments were conducted in triplicate for each bacterial species and each time point.

2.8. Temperature measurement of plasma jet

The temperature of the CAP jet and biofilm onto which the jet was directed was measured using a Xenics® GOBI-640-GigE thermal imaging camera. Plasma temperature was assessed when treating a PA01 biofilm grown for 24 h and placed atop 350 μl PBS in 96 well microtiter plate.

2.9. Topical application of H_2O_2

The effect of H_2O_2 on bacterial survival was investigated via topical application of H_2O_2 to 8, 12 and 24 h biofilms of both MRSA 252 and PA01. 100 μl of 550 μM H_2O_2 (the same concentration of H_2O_2 produced in solution by the plasma jet in 5 min) was applied to the surface of the biofilms. The concentration of H_2O_2 below the biofilms was quantified after 5 min, and after 4 h incubation at 32 °C as previously described.

2.10. Hydrogel formulation

PVA/CMC hydrogels were prepared by dissolving PVA (5% w/v) in DI water and heating to 97 °C with constant stirring to facilitate dissolution. The solution was supplemented with 0.5% w/v CMC, cast to a thickness of 1 mm and stored for 18 h at −20 °C to promote cryogenic gelation. Discs of gel were cut to a diameter of ~1 cm before being placed atop 350 μl PBS in a 96 well plate and subject to CAP treatment.

Agarose hydrogels were prepared by dissolving agarose (1.5% w/v) in DI water and heating to 90 °C. The solution was cooled, supplemented with 0.5 M KI and cast to a thickness of 1 cm. Biofilms were placed atop discs of gel (~17 mm in diameter) before treatment with the CAP jet.

3. Results

3.1. CAP generation of H_2O_2 in PBS

As previously reported, an increase in CAP exposure time results in a greater production of H_2O_2 [28]. The CAP jet used and the time dependent generation of H_2O_2 in PBS is shown in figure 1. The KI calibration curve used to calculate concentration is shown in figure 1 of the supplementary information.

3.2. Temperature measurement of plasma jet

Measurement of the temperature of the plasma jet in contact with a *P. aeruginosa* biofilm reached a maximum temperature of 34 °C (figure 2).

3.3. CAP treatment of bacterial biofilms

The effect of biofilm maturity on the transmission of plasma-generated H_2O_2 was first evaluated by calculating bacterial cell density of untreated biofilms at various time points, corresponding to biofilm incubation time. For comparative purposes, biofilms of Gram-positive MRSA 252 and Gram-negative *P. aeruginosa* PA01 were chosen as representative isolates commonly associated with chronic wound infection [37]. Further experiments were conducted evaluating the effect of CAP treatment on cell density as a function of biofilm maturity as shown in figure 3. A scanning electron micrograph of a 24 h biofilm is shown in the supplementary information (figure 3) in order to highlight the density of the bacterial matrix.

Owing to the high bacterial cell densities in the biofilms used in this study, it is not unexpected that the application of CAP fails to reduce the density of the mature biofilms. Plasma treatment of 8 h biofilms reduces the cell density but does not necessarily provide a clinically significant reduction in biomass with viable cell count remaining arguably high post

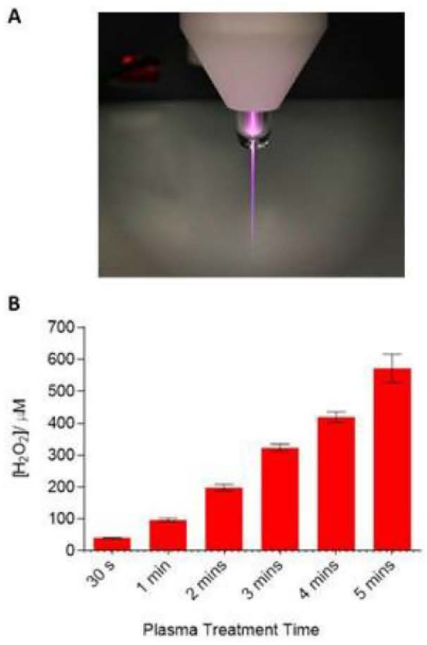

Figure 1. (A) CAP jet used in this study. (B) Generation of H_2O_2 in PBS as a function of plasma treatment time. Means and standard deviations from three independent replicates are presented.

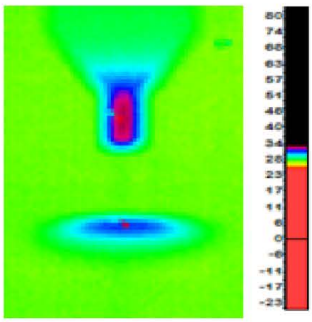

Figure 2. Temperature of plasma jet (top colour spot) showing a temperature gradient within the capillary tube and biofilm temperature at point of plasma contact (5 mm gap distance, image captured after 5 min, scale bar corresponds to temperature in °C).

treatment. Previous studies have focused on the recovery of biofilms post CAP treatement as a function of biofilm maturity [38]. Additional studies have been reported in which CAP therapy is able to significantly reduce or even eliminate bacterial biofilms (albeit often when treating biofilms with a lower bioburden), however this study concerns the fate of CAP-generated RONS as opposed to their biological effect [39, 40]. Therefore high density biofilms indicative of chronic infection

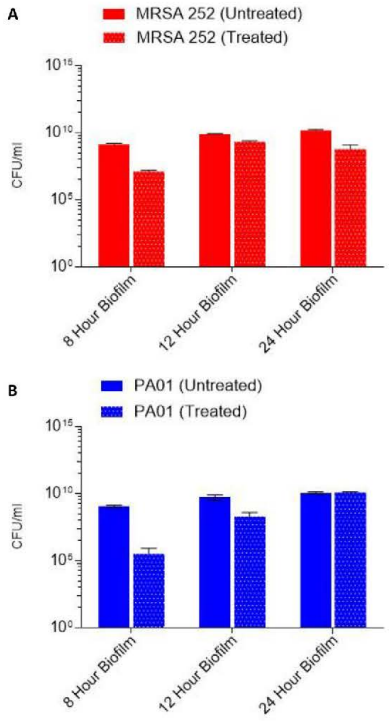

Figure 3. Effect of 5 min CAP treatment on cell density (CFU/ml) of *P. aeruginosa* PA01 (A) and MRSA 252 (B) biofilms at varying maturities relative to untreated control biofilms. Means and standard deviations from three biological replicates are presented.

were chosen as the cellular interface over which to monitor H_2O_2 formation.

Prior to establishing the concentration of H_2O_2 able to traverse the cellular interface, it was necessary to evaluate transmission across the polycarbonate membrane on which the biofilms were grown. Plasma treatment through the nanoporous membrane for 5 min resulted in a 33% reduction in H_2O_2 concentration in the PBS below the membrane (relative to direct treatment of PBS), as shown in figure 4. This was taken into account in subsequent experiments by the introduction of a transmission factor (TF) of 0.67 to account for the interference of the membrane.

Considering the TF, the presence of AWF on the membranes (included as a pre-treatment prior to bacterial inoculation) was also investigated. Membranes were pre-treated with a conditioning layer of AWF and incubated at 37 °C for 8, 12 or 24 h (in-keeping with subsequent biofilm growth conditions) to establish any interference from the conditioning layer over time. The concentration of H_2O_2 generated in the PBS below the membrane impregnated with AWF was comparable to the membrane only (data shown in figure 4), regardless of incubation time as summarised in table 1. Results illustrate

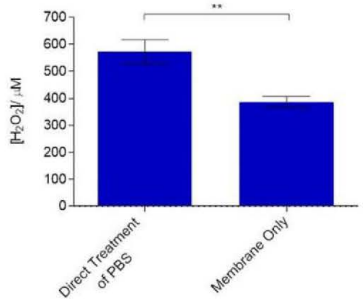

Figure 4. Effect of the polycarbonate membrane (a function of the experimental protocol) on the generation of H_2O_2 in PBS after 5 min, showing a significant reduction in H_2O_2 concentration. Means and standard deviations from three independent replicates are presented and have been analysed using an unpaired t test: ** $p = 0.0029$.

Table 1. Concentration of H_2O_2 generated across polycarbonate membranes inoculated with AWF following incubation for various time periods (taking into account the TF). Means and standard deviations from three biological replicates are presented and have been analysed using a one-way ANOVA with multiple comparisons.

Incubation time h^{-1}	$[H_2O_2]/TF/\mu M$
8	374.9 ± 40.4
12	520.5 ± 13.1
24	400.2 ± 96.8

no statistical significance with respect to H_2O_2 concentration as a result of the inclusion of AWF or the incubation period. This suggests little measurable interference of the AWF on the transmission of H_2O_2 across the interface.

However, figure 5 shows the presence of bacterial biofilms (of all maturities) to have a significant effect on the transmission of H_2O_2 relative to the membrane + AWF only. Biofilms grown for 8 h, corresponding to approximately 10^9 CFU ml^{-1}, reduced the concentration of H_2O_2 by approximately half, whereas biofilms approaching 10^{10} CFU ml^{-1} almost entirely prevented the detection of H_2O_2. The results show a significant difference in H_2O_2 concentration when comparing 8 h biofilms of both MRSA and *P. aeruginosa* to the corresponding 12 and 24 h biofilms, which may be as a direct result of the observed difference in bacterial cell death (seen in figure 3) when comparing 8 h biofilms to more mature biofilms. There is no significant difference observed between the 12 and 24 h biofilms of either MRSA or *P. aeruginosa*; likewise, there is no difference in H_2O_2 concentration between the bacterial species at each time point.

In order to investigate time-dependent formation and/or diffusion of plasma-generated H_2O_2, PVA/CMC hydrogels were used as a model system prior to commencing biofilm analysis. The gels were placed atop wells containing PBS and treated with the CAP jet for 5 min. The concentration of H_2O_2 in the PBS was then determined immediately (0 h incubation) and following incubation at 32 °C (skin temperature) for 1–8 h (figure 6) [41]. In this case, the incubation period

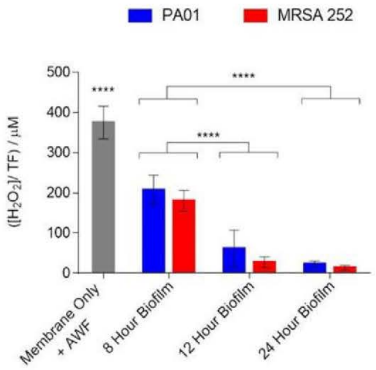

Figure 5. Effect of biofilm composition on the generation of H_2O_2 in PBS below the interface as a function of biofilm maturity. Means and standard deviations from three biological replicates are presented and have been analysed using a two-way ANOVA with multiple comparisons: **** $p < 0.0001$.

facilitated the formation of H_2O_2 in a time dependent manner over the course of 8 h, reaching a maximum concentration within ~4 h.

However, this trend was not seen when subjecting 8 h biofilms to the same incubation conditions. Conversely, the concentration of H_2O_2 was lower for both MRSA and *P. aeruginosa* post incubation (figure 7). Previous studies have indicated the role of catalase in protecting biofilms from the effects of hydrogen peroxide by catalysing its decomposition into oxygen and water [42, 43]. Both *S. aureus* and *P. aeruginosa* are catalase-positive, which could explain the results seen in figure 7 using biofilms that had been incubated for 4 h post CAP treatment. Further experimental studies will aim to address this point in the future.

3.4. Visualisation of H_2O_2 formation

Qualitative assessment of H_2O_2 formation (both immediately and over time) was undertaken using agarose gels containing KI. The hydrogel reservoir was able to indicate the formation and diffusion of CAP-generated H_2O_2 through bacterial biofilms via a distinctive colour change upon the liberation of iodine. Biofilms were placed on the surface of the gels and subjected to CAP treatment. The gels were then imaged immediately following exposure, before being incubated for 4 h at 32 °C, after which the biofilms were removed and the gels imaged once more. In agreement with previous quantitative data, no colour change was observed within the gels during CAP treatment of 24 h biofilms, whereas an immediate colour change was observed with 8 h biofilms of both bacterial species (supplementary figures 5 and 6). However, when treating biofilms grown for 12 h, MRSA biofilms facilitated a greater degree of iodine release within the agarose gels relative to *P. aeruginosa* biofilms grown for the same length of time. Figure 8 shows the colour change within the gels immediately post exposure (A) and (B) and after 4 h incubation (C) and (D).

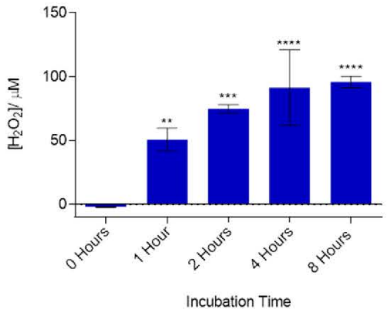

Figure 6. Effect of incubation time on H_2O_2 concentration in PBS post CAP treatment of PVA/CMC hydrogels. Means and standard deviations from three independent replicates are presented and have been analysed using a one-way ANOVA with multiple comparisons: **** $p < 0.0001$, *** $p < 0.001$, ** $p < 0.0001$. Statistical significance is reported with respect to the concentration of H_2O_2 detected immediately post exposure (0 h).

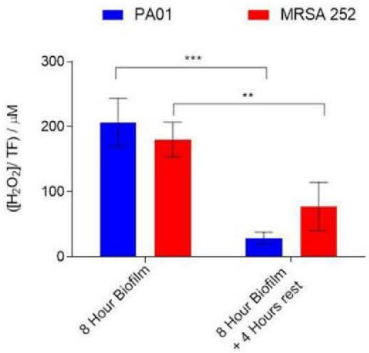

Figure 7. Effect of incubation time on H_2O_2 concentration in PBS post CAP treatment of 8 h biofilms. Means and standard deviations from three biological replicates are presented and have been analysed using a two-way ANOVA with multiple comparisons: *** $p < 0.001$, ** $p < 0.0001$.

This result contrasts with the quantitative data, which indicates very little H_2O_2 generated across the 12 h biofilms of both MRSA and *P. aeruginosa* into PBS (figure 5). Indeed, within the range of the experimental error the concentration of H_2O_2 below the biofilms is effectively equal for both species. However, in the case of biofilms placed atop a hydrogel surface there is a negligible colour change in the gel supporting the *P. aeruginosa* biofilms, whereas there is a clear colour change for the MRSA biofilms (albeit this change is small when compared to the 'membrane only' control). This discrepancy may be due to a number of factors; the delivery reservoir (PBS versus a gel matrix) is likely to affect the diffusion of reactive species and the uniformity of the biofilms may vary (they are matured by time as opposed to thickness and therefore there will undoubtedly be some variation). The behaviour of the biofilms when placed atop a liquid or solid

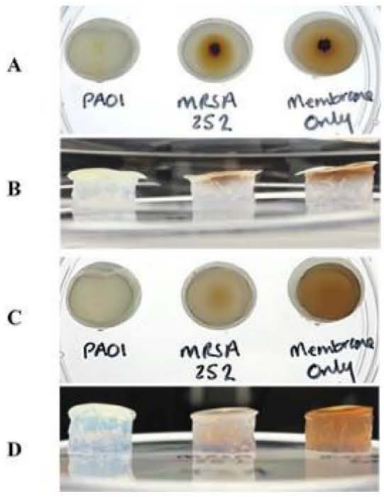

Figure 8. 12 h biofilms of MRSA 252 and *P. aeruginosa* PA01 placed atop agarose gels containing KI and subject to CAP treatment imaged immediately post treatment (A) and (B) and after 4 h incubation at 32 °C (C) and (D), compared to the uninoculated nanoporous membrane pre-treated with AWF.

interface may change and/or there may be a change in the H_2O_2 catalysis under these conditions. Such considerations when designing experimental protocols for the analysis of CAP therapy should be carefully rationalised and investigated with respect to the intended application in order to more accurately predict and measure the possible outcomes.

3.5. Topical application of H_2O_2

Owing to the multitude of different processes occurring during CAP treatment which go beyond the direct operating parameters (to include gas mixing with atmospheric gases and mixing at the solution interface), it is challenging to provide a representative control for the analysis of plasma-generated species across biological interfaces [44]. Consequently, we have focused solely on H_2O_2 transmission (as this is the major long-lived species generated by the jet described). H_2O_2 at the same concentration as generated by the CAP jet in 5 min was topically applied to *P. aeruginosa* and MRSA biofilms determine equivalency between plasma-assisted penetration and topical therapy. Whilst it is difficult to compare the results directly, topically applied H_2O_2 was unable to traverse biofilms of all maturities indicated by the absence of any quantifiable concentration of H_2O_2 in the PBS reservoir below. This was confirmed immediately after the 5 min exposure time and following a subsequent 4 h incubation at 32 °C. This result suggests that plasma-generated H_2O_2 (and possibly other CAP-generated RONS), are better able to penetrate bacterial biofilms than topical application of the same chemical species. Again, this is likely a result of the additional processes occurring, including continuous gas flow as a driving force

into the biofilms, localised heating and/or synergistic effects from other plasma-generated RONS.

4. Discussion and conclusions

The bioburden of the mature biofilms used in this study is arguably much higher than seen in some other studies. However, healthy skin is reportedly permanently colonised with 10^3–10^4 microorganisms per cm^2 skin (rising to 10^6 in moist areas), as part of a healthy skin microflora [45]. Therefore, dense biofilms with high microbial cell counts were used to represent the exponential proliferation of opportunistic pathogens associated with untreated chronic infection. In this study the use of CAP is intended as a therapeutic treatment as opposed to a preventative measure (whereby treatment may commence at lower cell densities than those often considered indicative of progressive infection).

In contrast to other studies, this work describes the effect of bacterial biofilms on the fate of plasma-generated products rather than any direct cellular effects of CAP therapy on the biofilms—an important consideration in the future clinical application of cold plasma. This investigation highlights the ability of plasma-generated reactive species to traverse live biofilms, remaining active despite interaction with the bacterial species present. This is observed up to cell densities of 10^9 CFU ml^{-1}, above which the concentration of longer lived species is significantly reduced when evaluated across the interface of the biofilm. Determining the exact mechanism of cellular interaction with plasma-generated H_2O_2 is ongoing. Owing to the complexity in determining the exact pathway of plasma-generated H_2O_2 with respect to both the gas phase and the liquid interface, there are a number of considerations to take into account such as direct interaction of biofilm components (including catalase) with plasma-generated H_2O_2, alongside the transport and any subsequent reactions with additional plasma-generated RONS [46, 47]. Nonetheless, the ability of high density bacterial biofilms to influence the transmission of such species may have implications for the application of CAP therapy in the treatment of chronic infection, whereby high bacterial loads may be readily encountered. In the context of deep-seated infections, the ability to deliver RONS directly into the infected tissues may vary with different device designs or may in fact be a ubiquitous challenge associated with CAP therapy. This should be established with the intention of improving RONS delivery and penetration in order to successfully apply this technology to highly contaminated wounds. Alongside ensuring the efficacy of CAP therapy via adequate penetration and delivery of plasma-generated reactive species, the effects of such species on other cellular entities cannot be underestimated. Ultimately, for the succesful therapeutic treatement of infection, a balance must be established between efficacious elimination of pathogenic organisms and implementaion of adequate controls for the protection of the surrounding host tissue.

Further research will focus on establishing the effect of catalase on the lifetime and bioavaliability of plasma-generated H_2O_2, the effect of CAP-induced bacterial cell death on the transmission of H_2O_2 and any protective effects offered by bacterial biofilms with respect to surrounding host tissues. Additional research will also aim to investigate the formation and transmission of other reactive species such as O_2^-, ·OH, $·HO_2$, to determine additional transportation mechanisms of plasma-generated RONS with respect to the material interface (biotic or abiotic).

Acknowledgments

The authors would like to thank the EPSRC for Grant EP/R003556/1. B Patenall would like to thank James Tudor and Mr and Mrs Watson for additional funding. G Williams would also like to thank Public Health England.

ORCID iDs

H J Hathaway https://orcid.org/0000-0002-0026-3340

References

[1] 2017 Innovative medicines initiative: ND4BB new drugs for bad bugs (https://doi.org/10.2879/113970)
[2] CDC 2015 US national action plan for the combating antibiotic-resistant bacteria
[3] World Health Organisation 2015 Global action plan on antimicrobial resistance
[4] O'Neill J 2016 Tackling drug-resistant infections globally: final report and recommendations *AMR Rev.*
[5] Jamal M, Ahmad W, Andleeb S, Jalil F, Imran M, Nawaz M A, Hussain T, Ali M, Rafiq M and Kamil M A 2018 Bacterial biofilm and associated infections *J. Chin. Med. Assoc.* **81** 7–11
[6] Herman-Bausier P and Dufrene Y F 2018 Force matters in hospital-acquired infections *Science* **359** 1464–5
[7] Flanagan M E, Welsh C A, Kiess C, Hoke S and Doebbeling B N 2011 A national collaborative for reducing health careassociated infections: current initiatives, challenges, and opportunities *Am. J. Infect. Control* **39** 685–9
[8] Phillips C J, Humphreys I, Fletcher J, Harding K, Chamberlain G and Macey S 2016 Estimating the costs associated with the management of patients with chronic wounds using linked routine data *Int. Wound J.* **13** 1193–7
[9] Gottrup F 2004 A specialized wound-healing center concept: importance of a multidisciplinary department structure and surgical treatment facilities in the treatment of chronic wounds *Am. J. Surg.* **187** 38S–43
[10] Robson M C and Barbul A 2006 Clinical treatment guidelines *Wound Rep. Reg.* **14** 645–711
[11] Jarbrink K, Ni G, Sonnergren H, Schmidtchen A, Pang C, Bajpai R and Car J 2017 The humanistic and economic burden of chronic wounds: a protocol for a systematic review *Systemat. Rev.* **6** 7
[12] Omar A, Wright J B, Schultz G, Burrell R and Nadworny P 2017 Microbial biofilms and chronic wounds *Microorganisms* **5** 15
[13] Modic M, McLeod N P, Sutton J M and Walsh J L 2017 Cold atmospheric pressure plasma elimination of clinically important single- and mixed-species biofilms *Int. J. Antimicrob. Agents* **49** 375–8
[14] Mai-Prochnow A, Clauson M, Hong J M and Murphy A B 2016 Gram positive and gram negative bacteria differ in their sensitivity to cold plasma *Sci. Rep.* **6** 11
[15] Flynn P B, Higginbotham S, Alshraiedeh N H, Gorman S P, Graham W G and Gilmore B F 2015 Bactericidal efficacy

of atmospheric pressure non-thermal plasma (APNTP) against the ESKAPE pathogens *Int. J. Antimicrob. Agents* **46** 101–7
[16] Laroussi M, Lu X and Keidar M 2017 Perspective: The physics, diagnostics, and applications of atmospheric pressure low temperature plasma sources used in plasma medicine *J. Appl. Phys.* **122** 020901
[17] Lu X, Naidis G V, Laroussi M, Reuter S, Graves D B and Ostrikov K 2016 Reactive species in non-equilibrium atmospheric-pressure plasmas: generation, transport, and biological effects *Phys. Rep. Rev.* **630** 1–84
[18] O'Connor N, Cahill O, Daniels S, Galvin S and Humphreys H 2014 Cold atmospheric pressure plasma and decontamination. Can it contribute to preventing hospital-acquired infections? *J. Hosp. Infect.* **88** 59–65
[19] Mai-Prochnow A, Murphy A B, McLean K M, Kong M G and Ostrikov K 2014 Atmospheric pressure plasmas: infection control and bacterial responses *Int. J. Antimicrob. Agents* **43** 508–17
[20] Gilmore B F, Flynn P B, O'Brien S, Hickok N, Freeman T and Bourke P 2018 Cold plasmas for biofilm control: opportunities and challenges *Trends Biotechnol.* **36** 627–38
[21] Flynn P B and Gilmore B F 2018 Understanding plasma biofilm interactions for controlling infection and virulence *J. Phys. D: Appl. Phys.* **51** 263001
[22] Haertel B, von Woedtke T, Weltmann K D and Lindequist U 2014 Non-thermal atmospheric-pressure plasma possible application in wound healing *Biomol. Therapeut.* **22** 477–90
[23] Rödder K, Gandhirajan R, von Woedtke T and Bekeschus S 2018 Where do ROS go? Oxidation cascades in melanoma exposed to cold physical plasma *Clin. Plasma Med.* **9** 29
[24] Boehm D, Heslin C, Cullen P J and Bourke P 2016 Cytotoxic and mutagenic potential of solutions exposed to cold atmospheric plasma *Sci. Rep.* **6** 21464
[25] Oh J S *et al* 2016 How plasma induced oxidation, oxygenation, and de-oxygenation influences viability of skin cells *Appl. Phys. Lett.* **109** 203701
[26] Szili E J, Hong S H, Oh J S, Gaur N and Short R D 2018 Tracking the penetration of plasma reactive species in tissue models *Trends Biotechnol.* **36** 594–602
[27] Marshall S E, Jenkins A T A, Al-Bataineh S A, Short R D, Hong S H, Thet N T, Oh J S, Bradley J W and Szili E J 2013 Studying the cytolytic activity of gas plasma with self-signalling phospholipid vesicles dispersed within a gelatin matrix *J. Phys. D: Appl. Phys.* **46** 185401
[28] Oh J S, Szili E J, Gaur N, Hong S H, Furuta H, Kurita H, Mizuno A, Hatta A and Short R D 2016 How to assess the plasma delivery of RONS into tissue fluid and tissue *J. Phys. D: Appl. Phys.* **49** 304005
[29] Szili E J, Bradley J W and Short R D 2014 A 'tissue model' to study the plasma delivery of reactive oxygen species *J. Phys. D: Appl. Phys.* **47** 152002
[30] Szili E J *et al* 2017 The assessment of cold atmospheric plasma treatment of DNA in synthetic models of tissue fluid, tissue and cells *J. Phys. D: Appl. Phys.* **50** 274001
[31] Chen C, Liu D X, Liu Z C, Yang A J, Chen H L, Shama G and Kong M G 2014 A model of plasma-biofilm and plasma-tissue interactions at ambient pressure *Plasma Chem. Plasma Process.* **34** 403–41
[32] Xiong Z, Du T, Lu X, Cao Y and Pan Y 2011 How deep can plasma penetrate into a biofilm? *Appl. Phys. Lett.* **98** 225103
[33] Pei X, Lu X, Liu J, Liu D, Yang Y, Ostrikov K, Chu P K and Pan Y 2012 Inactivation of a 25.5 μm enterococcus faecalis biofilm by a room-temperature, battery-operated, handheld air plasma jet *J. Phys. D: Appl. Phys.* **45** 165205
[34] Gorbanev Y, O'Connell D and Chechik V 2016 Non-thermal plasma in contact with water: the origin of species *Chemistry* A **22** 3496
[35] Junglee S, Urban L, Sallanon H and Lopez-Lauri F 2014 Optimized assay for hydrogen peroxide determination in plant tissue using potassium iodide *Am. J. Anal. Chem.* **05** 730
[36] Thet N T, Wallace L, Wibaux A, Boote N and Jenkins A T A 2018 Development of a mixed-species biofilm model and its virulence implications in device related infections *J. Biomed. Mater. Res.* B **107** 129–37
[37] Bowler P G, Duerden B I and Armstrong D G 2001 Wound microbiology and associated approaches to wound management *Clin. Microbiol. Rev.* **14** 244
[38] Patenall B L, Hathaway H, Sedgwick A C, Thet N T, Williams G T, Young A E, Allinson S L, Short R D and Jenkins A T A 2018 Limiting *Pseudomonas aeruginosa* biofilm formation using cold atmospheric pressure plasma *Plasma Med.* **8** 269–77
[39] Ziuzina D, Boehm D, Patil S, Cullen P J and Bourke P 2015 Cold plasma inactivation of bacterial biofilms and reduction of quorum sensing regulated virulence factors *PLoS One* **10** 0138209
[40] Alkawareek M Y, Algwari Q T, Laverty G, Gorman S P, Graham W G, O'Connell D and Gilmore B F 2012 Eradication of *Pseudomonas aeruginosa* biofilms by atmospheric pressure non-thermal plasma *PLoS One* **7** 44289
[41] Fierheller M and Sibbald G 2010 A clinical investigation into the relationship between increased periwound skin temperature and local wound infection in patients with chronic leg ulcers *Adv. Skin Wound Care* **23** 369–78
[42] Stewart S P, Roe F, Rayner J, Elkins J G, Lewandowski Z, Ochsner U A and Hassett D J 2000 Effect of catalase on hydrogen peroxide penetration into *Pseudomonas aeruginosa* biofilms *Appl. Environ. Microbiol.* **66** 836–8
[43] Ochieng' Olwal C, Oyieng' Ang'ienda P and Otieno Ochiel D 2019 Alternative sigma factor B (σ^B) and catalase enzyme contribute to *Staphylococcus epidermidis* biofilm's tolerance against physico-chemical disinfection *Sci. Rep.* **9** 5355
[44] Girard F *et al* 2018 Correlations between gaseous and liquid phase chemistries induced by cold atmospheric plasmas in a physiological buffer *Phys. Chem. Chem. Phys.* **20** 9198–210
[45] Greene J N 1996 The microbiology of colonization, including techniques for assessing and measuring colonization *Infect. Control Hosp. Epidemiol.* **17** 114–8
[46] Bruggeman P and Schram D C 2010 On OH production in water containing atmospheric pressure plasmas *Plasma Sources Sci. Technol.* **19** 045025
[47] Liu J, He B, Chen Q, Li J, Xiong Q, Yue G, Zhang X, Yang S, Liu H and Liu Q H 2016 Direct synthesis of hydrogen peroxide from plasma-water interactions *Sci. Rep.* **5** 38454

A Boronic Acid-based Fluorescent Hydrogel for Monosaccharide Detection

Front. Chem. Sci. Eng.
https://doi.org/10.1007/s11705-019-1812-5

COMMUNICATION

A boronic acid-based fluorescent hydrogel for monosaccharide detection

Suying Xu[1,2], Adam C. Sedgwick[2,3], Souad A. Elfeky[2,4,5,6], Wenbo Chen[2,4,7], Ashley S. Jones[2], George T. Williams[2], A. Toby A. Jenkins[2], Steven D. Bull[2], John S. Fossey (✉)[4], Tony D. James (✉)[2]

1 Department of Biochemistry, Faculty of Science, Beijing University of Chemical Technology, Beijing 100029, China
2 Department of Chemistry, University of Bath, Bath BA2 7AY, UK
3 Department of Chemistry, University of Texas at Austin, TX 78712-1224, USA
4 School of Chemistry, University of Birmingham, Birmingham B15 2TT, UK
5 National Institute of Laser Enhanced Sciences, Cairo University, Giza 12613, Egypt
6 Higher Institute for Optics Technology, Sheraton, Cairo 17361, Egypt
7 Shanghai Key Laboratory of Materials Protection and Advanced Materials in Electric Power, Shanghai University of Electric Power, Shanghai 200090, China

Abstract A boronic acid-based anthracene fluorescent probe was functionalised with an acrylamide unit to incorporate into a hydrogel system for monosaccharide detection. In solution, the fluorescent probe displayed a strong fluorescence turn-on response upon exposure to fructose, and an expected trend in apparent binding constants, as judged by a fluorescence response where D-fructose > D-galactose > D-mannose > D-glucose. The hydrogel incorporating the boronic acid monomer demonstrated the ability to detect monosaccharides by fluorescence with the same overall trend as the monomer in solution with the addition of D-fructose resulting in a 10-fold enhancement ($\leqslant$0.25 mol/L).

1 Introduction

Monosaccharides are among the basic building blocks of life and play an essential role in the function of several physiological processes, including metabolism and cellular recognition [1]. The monosaccharide glucose serves as the main form of energy for tissues and cells [2]. Due to their biological importance, there has been extensive effort in the development of methods and techniques for monosaccharide detection [3–4].

Lorand and Edwards reported the ability of boronic acids to form complexes with 1,2- and 1,3- diols. In addition it was discovered that D-fructose formed a 1:1 fructose-boronic acid complex and D-glucose formed a 1:2 glucose-boronic acid complex [5]. The strength of the boronic acid binding to monosaccharides is determined by the orientation and relative position of hydroxyl groups. In aqueous solution fructose predominates in the furanose form with a *syn*-periplanar pair of hydroxyl groups resulting in a strong binding constant with boronic acids [4]. As a result, a number of aryl boronic acid-based sensors have been developed for the detection of monosaccharides which exploit the difference in binding stoichiometry and inherent binding affinity to achieve either D-fructose or D-glucose selectivity [4,6–8]. More specifically, in 1994, James et al. developed an anthracene-containing mono boronic acid derivative as a photoinduced electron transfer (PET) fluorescence probe for the detection of fructose (Fig. 1) [9]. In this system, it was discovered that *ortho*-aminomethylphenylboronic acid functionality facilitated the detection of fructose in neutral aqueous solution. This pioneering work has led to the development of other *ortho*-aminomethylphenylboronic acid-containing fluorescence sensors improving selectivity, increasing excitation/emission profile and binding affinities [10–12]. While there was never any doubt that the *ortho*-aminomethylphenylboronic acid group was important to improve saccharide binding at neutral pH the mechanism of action had been under debate for a number of years [13–15]. Recently, the debate was concluded and the fluorescence enhancement on saccharide binding is caused by modulation of internal conversion resulting in different levels of quenching. Initially, before saccharide binding the free $-B(OH)_2$ groups quench the fluorescence by internal

Received October 10, 2018; accepted January 6, 2019

E-mails: j.s.fossey@bham.ac.uk (Fossey J S);
T.D.James@bath.ac.uk (James T D)

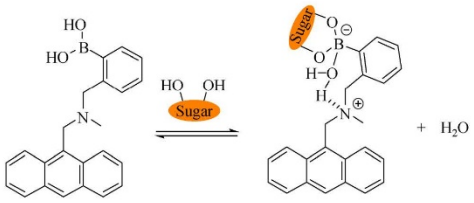

Fig. 1 Shinkai et al. anthracene-based boronic acid PET fluorescence probe for the detection of fructose

conversion, then when saccharides bind the $-B(OR)_2$ groups formed have reduced internal conversion and less quenching resulting in an enhanced fluorescence [16].

The saccharide-binding properties of aryl boronic acid derivatives have been exploited as recognition motifs across a number of different domains including polymer hydrogels [6,17,18]. Hydrogels are three dimensionally cross-linked hydrophilic polymers, with a high (~90 wt-%) water content [19]. The modification of hydrogels to contain boronic-acid binding motifs enables the physical properties of the hydrogel to be reversibly modulated through exposure to saccharide-containing stimuli, i.e., glucose responsivity [20–23]. Co-authors of this report have developed stimuli responsive hydrogels and fluorescent sensors [24–30], and as a result, we were motivated to translate a Shinkai-like anthracene-containing boronic acid sensor unit into a hydrogel sensor by linking to an acrylamide functionality, thus generating a fluorescence-on sensor hydrogel for monosaccharide detection.

2 Results and discussion

Whilst solution-based fluorescent sensors offer a significant advantage in terms of binding-kinetics over analogous heterogenous sensors [31]. Heterogenous immobilisation of a fluorescent sensor is preferential as it avoids contamination of the sensor in a practical situtation, i.e., *in vivo* [32,33]. The near-solvated nature of a hydrogel is thus an attractive alternative as they offer heterogeneity without the disadvantages associated with a solution-based system. By integrating the Shinkai et al. anthracene PET fluorescent probe into a hydrogel, we hoped to develop a fluorescence responsive boronic acid hydrogel, which could eliminate the need for an additional competitive optical reporter [33]. The desired boronic acid monomer **AM-5** is shown below in Fig. 2.

AM-5 was synthesised over five steps (Scheme 1). In brief, 1,6-hexanediamine was mono-Boc protected through the dropwise addition of di-*tert*-butyl dicarbonate ($(Boc)_2O$) to an excess of 1,6-hexanediamine, which afforded *tert*-butyl (6-aminohexyl)carbamate (**1**) in 74% yield. To attach the desired anthracene fluorophore, **1** was stirred with anthracene-9-carbaldehyde at room temperature overnight to form an imine intermediate. $NaBH_4$ was then added portion-wise to produce the desired secondary amine *tert*-butyl (6-((anthracen-9-ylmethyl)amino)hexyl) carbamate (**2**) in reasonable yield (48%). Compound **2** was subsequently alkylated with 2-bromomethylphenylboronic acid pinacol ester to afford **3** in good yield (89%). Compound **3** was then Boc-deprotected using trifluoroacetic acid, which also resulted in the partial hydrolysis of the boronate ester to form boronic acid **4**, this intermediate was taken onto the next step without purification. Methacryloyl chloride was then used to afford **AM-5**, which was confirmed by mass spectrometry. Compound **AM-5** proved difficult to characterise by NMR techniques and exhibited a broad and complex ^1H NMR due to the formation of "oligomeric boronic acid anhydrides" [34–35].

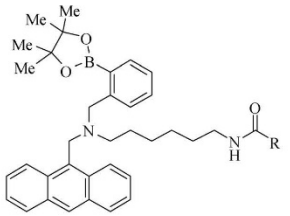

R = O^{t}Bu (**3**), C(=CH_2)CH_3 (**A-M5**)

Fig. 2 Anthracene-based fluorescent monomer (**A-M5**) for the development of a hydrogel for the detection of monosacharides

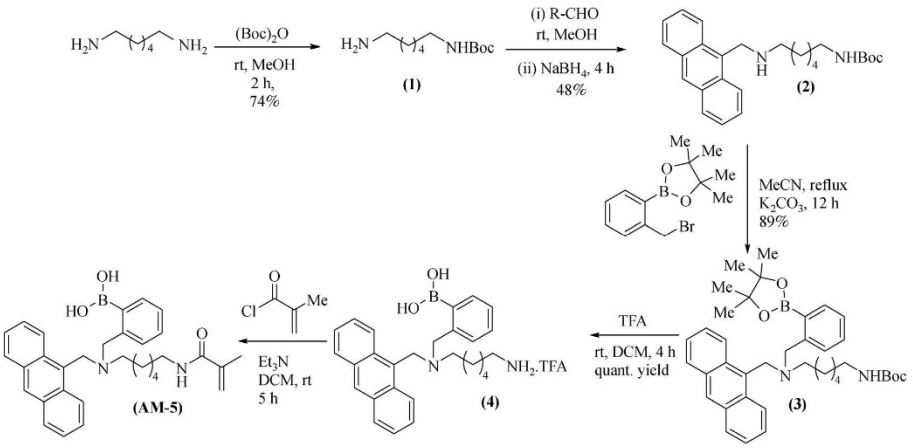

Scheme 1 Synthesis of boronic acid fluorescent probes **3** and **AM-5**

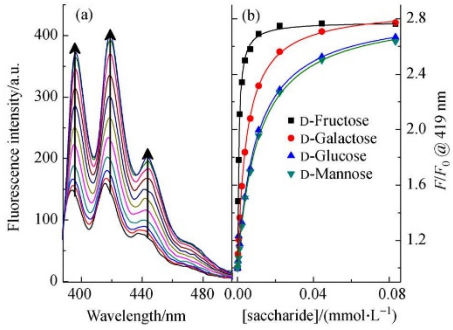

Fig. 3 (a) Fluorescent spectral changes of **3** (0.6 μmol/L) with different concentrations of D-fructose in pH 8.21 aqueous methanolic buffer solution (52.1 wt-% methanol (KCl, 10 mmol/L; KH_2PO_4, 2.73 mmol/L and Na_2HPO_4, 2.78 mmol/L)); (b) Fluorescence intensity changes (F/F_0) at 419 nm *versus* increasing saccharide concentration. λ_{ex} – 370 nm

With **3** in hand, the fluorescence properties and responses to a panel of monosaccharides were evaluated to demonstrate its sensing ability before incorporation into a hydrogel. As shown in Fig. 3(b), **3** was more sensitive towards fructose over other monosaccharides (as expected) and the binding stability constants between mono-boronic acids and saccharides followed: D-fructose > D-galactose > D-mannose > D-glucose (Table S1, cf. Electronic Supplementary Material (ESM)). From these results, we turned our attention towards the incorporation of **3** into a hydrogel.

Hydrogels containing **AM-5** were formed by co-polymerisation of acrylamide and methylene bisacrylamide in water through free radical polymerisation using ammonium persulfate (APS) and tetramethylethylenediamine (TMEDA) (cf. ESM for full detailed procedure). For the evaluation of the fluorescence response of the hydrogel towards different monosaccharides, each hydrogel was placed into a monosaccharide solution for 2 h (Note: 2 h was chosen since at this time point no further increase in fluorescence intensity was observed after addition of monosaccharides).

Acrylamide-based hydrogels consisting of **AM-5** were exposed to increasing concentrations of fructose and a significant fluorescence enhancement was observed (~16-fold) as shown in Fig. 4, the selectivity order for

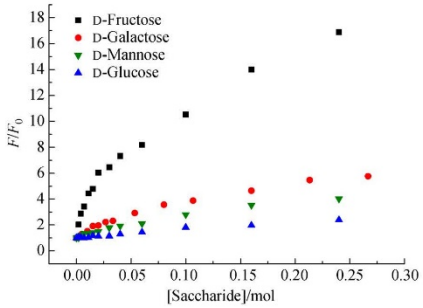

Fig. 4 Fluorescence intensity ratios of **AM-5** (F/F_0) at 409 nm *versus* monosaccharide concentration in a (1:1) 0.1 mol/L KH_2PO_4/0.1 mol/L NaOH, pH 8.00 buffer solution and λ_{ex} = 370 nm

the detection of monosaccharides was consistent with the solution titration data of **3** (Fig. 2, Table S1 and Table S2), D-fructose > D-galactose > D-mannose > D-glucose. However, the observed binding constants for each monosaccharide were much lower than in the solution phase, which is believed to be due to the binding event being a diffusion-based process ((1381.7±41.80) *versus* (52.6±5.3) dm^3/mol for D-fructose). The response towards D-glucose in the hydrogel was too low for the binding constant to be determined.

3 Conclusions

A fluorescent monosaccharide responsive hydrogel was developed by functionalising the proven *ortho*-aminomethylphenylboronic acid anthracene PET sensor with an acrylamide unit to incorporate into a hydrogel backbone. The boronic acid-containing hydrogel produced a significant fluorescent enhancement (~16 fold) with the addition of fructose and the binding stability constants followed the well-established order for binding between mono-boronic acids and saccharides: D-fructose > D-galactose > D-mannose > D-glucose.

Acknowledgements The University of Bath are thanked for support. ACS thanks the EPSRC for a PhD studentship. TDJ and JSF are grateful for the support of the EPSRC and DTI (DT/F00267X/1). Preliminary results of this project stemmed from another project pump-primed by the University of Bath Enterprise Development Fund (EDF award to investigators including JSF, ATAJ and TDJ). TDJ wishes to thank the Royal Society for a Wolfson Research Merit Award. JSF and WC thanks the Leverhulme Trust for support (F00094BC). JSF thanks the JDRF (2-SRA-2016-267-A-N) for support. Spectroscopy facilities were provided through the Material and Chemical Characterisation Facility (MC2) at the University of Bath. The investigators are grateful to the CASE consortium for providing knowledge transfer and networking opportunities [36,37].

Electronic Supplementary Material Supplementary material is available in the online version of this article at https://doi.org/10.1007/s11705-019-1812-5 and is accessible for authorized users.

References

1. Levine R. Monosaccharides in health and disease. Annual Review of Nutrition, 1986, 6(1): 211–224
2. Mergenthaler P, Lindauer U, Dienel G A, Meisel A. Sugar for the brain: The role of glucose in physiological and pathological brain function. Trends in Neurosciences, 2013, 36(10): 587–597
3. Pickup J C, Hussain F, Evans N D, Rolinski O J, Birch D J S. Fluorescence-based glucose sensors. Biosensors & Bioelectronics, 2005, 20(12): 2555–2565
4. Wu X, Li Z, Chen X X, Fossey J S, James T D, Jiang Y B. Selective sensing of saccharides using simple boronic acids and their aggregates. Chemical Society Reviews, 2013, 42(20): 8032–8048
5. Lorand J P, Edwards J O. Polyol complex and structure of the benzene boronate ion. Journal of Organic Chemistry, 1959, 24(6): 769–774
6. Sun X, James T D. Glucose sensing in supramolecular chemistry. Chemical Reviews, 2015, 115(15): 8001–8037
7. Huang Y J, Ouyang W J, Wu X, Li Z, Fossey J S, James T D, Jiang Y B. Glucose sensing via aggregation and the use of "knock-out" binding to improve selectivity. Journal of the American Chemical Society, 2013, 135(5): 1700–1703
8. Cao H S, Heagy M D. Fluorescent chemosensors for carbohydrates: A decade's worth of bright spies for saccharides in review. Journal of Fluorescence, 2004, 14(5): 569–584
9. James T D, Sandanayake K, Shinkai S. Novel photoinduced

electron-transfer sensor for saccharides based on the interaction of boronic acid and amine. Journal of the Chemical Society. Chemical Communications, 1994, 0(4): 477 478
10. Zhang X T, Liu G J, Ning Z W, Xing G W. Boronic acid-based chemical sensors for saccharides. Carbohydrate Research, 2017, 452: 129 148
11. James T D, Sandanayake K R A S, Shinkai S. A glucose-selective molecular fluorescence sensor. Angewvandte Chemie International Edition, 1994, 33: 2207 2209
12. James T D, Sandanayake K R A S, Iguchi R, Shinkai S. Novel saccharide-photoinduced electron transfer sensors based on the interaction of boronic acid and amine. Journal of the American Chemical Society, 1995, 117(35): 8982 8987
13. Franzen S, Ni W, Wang B. Study of the mechanism of electron-transfer quenching by boron–nitrogen adducts in fluorescent sensors. Journal of Physical Chemistry B, 2003, 107(47): 12942 12948
14. Ni W, Kaur G, Springsteen G, Wang B, Franzen S. Regulating the fluorescence intensity of an anthracene boronic acid system: A B N bond or a hydrolysis mechanism? Bioorganic Chemistry, 2004, 32 (6): 571 581
15. Chapin B M, Metola P, Vankayala S L, Woodcock H L, Mooibroek T J, Lynch V M, Larkin J D, Anslyn E V. Disaggregation is a mechanism for emission turn-on of ortho-aminomethylphenylboronic acid-based saccharide sensors. Journal of the American Chemical Society, 2017, 139(15): 5568 5578
16. Sun X, James T D, Anslyn E V. Arresting "loose bolt" internal conversion from $-B(OH)_2$ groups is the mechanism for emission turn-on in ortho-aminomethylphenylboronic acid-based saccharide sensors. Journal of the American Chemical Society, 2018, 140(6): 2348 2354
17. Zhao L, Huang Q W, Liu Y, Wang Q, Wang L Y, Xiao S S, Bi F, Ding J X. Boronic acid as glucose-sensitive agent regulates drug delivery for diabetes treatment. Materials, 2017, 10 (2): 170
18. Guan Y, Zhang Y J. Boronic acid-containing hydrogels: Synthesis and their applications. Chemical Society Reviews, 2013, 42(20): 8106 8121
19. Ahmed E M. Hydrogel: Preparation, characterization, and applications: A review. Journal of Advanced Research, 2015, 6(2): 105 121
20. Li Y Y, Zhou S Q. A simple method to fabricate fluorescent glucose sensor based on dye-complexed microgels. Sensors and Actuators. B, Chemical, 2013, 177: 792 799
21. Matsumoto A, Tanaka M, Matsumoto H, Ochi K, Moro-oka Y, Kuwata H, Yamada H, Shirakawa I, Miyazawa T, Ishii H. Synthetic "smart gel" provides glucose-responsive insulin delivery in diabetic mice. Science Advances, 2017, 3, eaaq0723
22. Matsumoto A, Kataoka K, Miyahara Y. New directions in the design of phenylboronate-functionalized polymers for diagnostic and therapeutic applications. Polymer Journal, 2014, 46(8): 483 491
23. Sanjoh M, Miyahara Y, Kataoka K, Matsumoto A. Phenylboronic acids-based diagnostic and therapeutic applications. Analytical Sciences, 2014, 30(1): 111 117
24. Sedgwick A C, Chapman R S L, Gardiner J E, Peacock L R, Kim G, Yoon J, Bull S D, James T D. A bodipy based hydroxylamine sensor. Chemical Communications, 2017, 53(75): 10441 10443
25. Sedgwick A C, Sun X L, Kim G, Yoon J, Bull S D, James T D. Boronate based fluorescence (ESIPT) probe for peroxynitrite. Chemical Communications, 2016, 52(83): 12350 12352
26. Sun X L, Odyniec M L, Sedgwick A C, Lacina K, Xu S Y, Qiang T T, Bull S D, Marken F, James T D. Reaction-based indicator displacement assay (RIA) for the colorimetric and fluorometric detection of hydrogen peroxide. Organic Chemistry Frontiers: An International Journal of Organic Chemistry, 2017, 4(6): 1058 1062
27. Sedgwick A C, Han H H, Gardiner J E, Bull S D, He X P, James T D. Long-wavelength fluorescent boronate probes for the detection and intracellular imaging of peroxynitrite. Chemical Communications, 2017, 53(95): 12822 12825
28. Wu D, Sedgwick A C, Gunnlaugsson T, Akkaya E U, Yoon J, James T D. Fluorescent chemosensors: The past, present and future. Chemical Society Reviews, 2017, 46(23): 7105 7123
29. Sedgwick A C, Han H H, Gardiner J E, Bull S D, He X P, James T D. The development of a novel AND logic based fluorescence probe for the detection of peroxynitrite and GSH. Chemical Science (Cambridge), 2018, 9(15): 3672 3676
30. Lampard E V, Sedgwick A C, Sombuttan T, Williams G T, Wannalerse B, Jenkins A T A, Bull S D, James T D. Dye displacement assay for saccharides using benzoxaborole hydrogels. ChemistryOpen, 2018, 7(3): 266 268
31. Kreisig T, Hoffmann R, Zuchner T. Homogeneous fluorescence-based immunoassay detects antigens within 90 seconds. Analytical Chemistry, 2011, 83(11): 4281 4287
32. Grabchev I, Qian X H, Xiao Y, Zhang R. Novel heterogeneous PET fluorescent sensors selective for transition metal ions or protons: Polymers regularly labelled with naphthalimide. New Journal of Chemistry, 2002, 26(7): 920 925
33. Basabe-Desmonts L, Reinhoudt D N, Crego-Calama M. Design of fluorescent materials for chemical sensing. Chemical Society Reviews, 2007, 36(6): 993 1017
34. Li M, Liu Z J, Wang H C, Sedgwick A C, Gardiner J E, Bull S D, Xiao H N, James T D. Dual-function cellulose composites for fluorescence detection and removal of fluoride. Dyes and Pigments, 2018, 149: 669 675
35. Hall D G. Boronic acids: Preparation and applications in organic synthesis, medicine and materials.Weinheim: Wiley-VCH Verlag GmbH & Co. KGaA, 2005, 1 550
36. Fossey J S, Brittain W D G. The CASE 2014 symposium: Catalysis and sensing for our environment, Xiamen 7th–9th November 2014. Organic Chemistry Frontiers: An International Journal of Organic Chemistry, 2015, 2(2): 101 105
37. Payne D T, Fossey J S, Elmes R B P. Catalysis and Sensing for our Environment (CASE2015) and the Supramolecular Chemistry Ireland Meeting (SCI 2015): Dublin and Maynooth, Ireland. 8th–11th July. Supramolecular Chemistry, 2016, 28(11-12): 921 931

Long Wavelength TCF-Based Fluorescent Probe for the Detection of Alkaline Phosphotase in Live Cells

frontiers in Chemistry

ORIGINAL RESEARCH
published: 30 April 2019
doi: 10.3389/fchem.2019.00255

Long Wavelength TCF-Based Fluorescent Probe for the Detection of Alkaline Phosphatase in Live Cells

Lauren Gwynne[1], Adam C. Sedgwick[2], Jordan E. Gardiner[1], George T. Williams[1], Gyoungmi Kim[3], John P. Lowe[1], Jean-Yves Maillard[4], A. Toby A. Jenkins[1], Steven D. Bull[1]*, Jonathan L. Sessler[2]*, Juyoung Yoon[3]* and Tony D. James[1]**

[1] Department of Chemistry, University of Bath, Bath, United Kingdom, [2] Department of Chemistry, University of Texas at Austin, Austin, TX, United States, [3] Department of Chemistry and Nano Science, Ewha Womans University, Seoul, South Korea, [4] Cardiff School of Pharmacy and Pharmaceutical Sciences, Cardiff University, Cardiff, United Kingdom

OPEN ACCESS

Edited by:
Leyong Wang,
Nanjing University, China

Reviewed by:
Ruibing Wang,
University of Macau, China
Huaqiang Zeng,
Institute of Bioengineering and Nanotechnology (A*STAR), Singapore

***Correspondence:**
A. Toby A. Jenkins
a.t.a.jenkins@bath.ac.uk
Steven D. Bull
s.d.bull@bath.ac.uk
Jonathan L. Sessler
sessler@cm.utexas.edu
Juyoung Yoon
jyoon@ewha.ac.k
Tony D. James
t.d.james@bath.ac.uk

Specialty section:
This article was submitted to Supramolecular Chemistry, a section of the journal Frontiers in Chemistry

Received: 02 January 2019
Accepted: 01 April 2019
Published: 30 April 2019

Citation:
Gwynne L, Sedgwick AC, Gardiner JE, Williams GT, Kim G, Lowe JP, Maillard J-Y, Jenkins ATA, Bull SD, Sessler JL, Yoon J and James TD (2019) Long Wavelength TCF-Based Fluorescent Probe for the Detection of Alkaline Phosphatase in Live Cells. Front. Chem. 7:255. doi: 10.3389/fchem.2019.00255

A long wavelength TCF-based fluorescent probe (**TCF-ALP**) was developed for the detection of alkaline phosphatase (ALP). ALP-mediated hydrolysis of the phosphate group of **TCF-ALP** resulted in a significant fluorescence "turn on" (58-fold), which was accompanied by a colorimetric response from yellow to purple. **TCF-ALP** was cell-permeable, which allowed it to be used to image ALP in HeLa cells. Upon addition of bone morphogenic protein 2, **TCF-ALP** proved capable of imaging endogenously stimulated ALP in myogenic murine C2C12 cells. Overall, TCF-ALP offers promise as an effective fluorescent/colorimetric probe for evaluating phosphatase activity in clinical assays or live cell systems.

Keywords: reaction-based fluorescent probe, alkaline phosphatase, cell imaging, fluorescence, colorimetric

INTRODUCTION

Alkaline phosphatase (ALP) is an ubiquitous enzyme found in the majority of human tissues, where it catalyses the dephosphorylation of various substrates such as nucleic acids, proteins, and other small molecules (Coleman, 1992; Millán, 2006). ALP also plays an important role in signal transduction and regulation of intracellular processes (cell growth, apoptosis, and signal transduction pathways) (Julien et al., 2011). Abnormal levels of ALP in serum are an indicator of several diseases including bone disease (Garnero and Delmas, 1993), liver dysfunction (Rosen et al., 2016), breast and prostatic cancer (Ritzke et al., 1998; Wymenga et al., 2001), and diabetes (Tibi et al., 1988). As a result, ALP is regarded as a key biomarker in medical diagnosis (Coleman, 1992; Ooi et al., 2007). Therefore, it is important to develop a fast, reliable, and selective detection system for monitoring ALP activity that is amenable to clinical diagnostics.

There have been numerous approaches to determine ALP levels, including colorimetric (Yang et al., 2016; Hu et al., 2017), chemiluminescent (Jiang and Wang, 2012), electrochemical (Zhang L. et al., 2015), surface-enhanced Raman methods (Ruan et al., 2006), and fluorescence (Cao et al., 2016; Fan et al., 2016). Our group has been particularly interested in the development of fluorescent probes for the detection of biologically relevant analytes (Sedgwick et al., 2017a,b, 2018a,b; Wu et al., 2017; Zhang et al., 2019). Fluorescence has many advantages over other methods owing to its simplicity and high sensitivity/selectivity, providing rapid, non-invasive, real-time detection (Wu et al., 2017). Whilst there have been many fluorophores developed for assaying ALP activity such as organic dyes (Zhang H. et al., 2015; Zhao et al., 2017), conjugated polymers (Li et al., 2014), inorganic semiconductor dots (Qian et al., 2015), and noble metal clusters (Sun et al., 2014), most require

high probe concentrations and crucially rely on short wavelength emission, thus limiting their applicability in biological systems. Therefore, ALP probes that operate at long wavelengths are required to allow for deeper tissue penetration and to avoid cell-based autofluorescence (Liu et al., 2017; Tan et al., 2017; Zhang et al., 2017).

RESULTS AND DISCUSSION

Chemistry

Here we report a TCF-based fluorescent probe that allows for the detection of ALP and/or acid phosphatase (ACP). As shown in **Scheme 1**, this probe (**TCF-ALP**) is based on the conjugation of 2-dicyanomethylene-3-cyano-4,5,5-trimethyl-2,5-dihydrofuran (**TCF**) to an electron-donating phenol moiety, a phosphorylated phenol; this affords an internal charge transfer (ICT) donor-π-acceptor (D-π-A) system whose fluorescence properties vary dramatically following ALP-mediated phosphate group cleavage (Gopalan et al., 2004; Liao et al., 2006; Bouffard et al., 2008; Lord et al., 2008; Jin et al., 2010; Sedgwick et al., 2017b; Teng et al., 2018). **TCF-ALP** was synthesized in four steps with an overall yield of 27% (**Scheme 2**). In brief, 3-hydroxy-3-methyl-2-butanone, malononitrile, and NaOEt were heated at reflux in EtOH for 1 h and then cooled. The resultant precipitate **TCF** (**1**) was then added to a mixture of piperidine (cat.) and 4-hydroxybenzaldehyde in EtOH, which was subsequently heated to 100°C by microwave irradiation to afford intermediate **2** (**TCF-OH**). Intermediate **2** was then treated with diethylchlorophosphate, DMAP (cat.) and NEt_3 in THF to give the phosphonate ester **3**. Hydrolysis using trimethylsilyl iodide in dichloromethane (DCM) afforded **TCF-ALP** as a crystalline solid (After trituration with Et_2O).

Spectroscopic Studies of TCF-ALP

UV-Vis and fluorescence spectroscopic titrations of **TCF-ALP** were performed in 50 mM Tris-HCl buffer in the absence and presence of ALP from porcine kidney. In the absence of ALP, **TCF-ALP** was found to have no UV absorption features above ~550 nm; however, upon addition of ALP a bathochromic shift in the UV absorption maximum was observed (from 440 to 580 nm), which was accompanied by a change in color from yellow to purple (**Figure S1**). ALP-mediated hydrolysis of **TCF-ALP** to form the highly fluorescent phenol (**2**), was confirmed by ^{31}P NMR studies and HRMS (see **Figures S1–S4**). The effect of pH on the rate of ALP mediated hydrolysis of **TCF-ALP** was evaluated. It was found that incubation with 0.8 U/mL of ALP at pH 9.2 resulted in the largest fluorescence response (**Figure S5**). Consequently, all *in vitro* experiments to determine ALP activity were carried out in 50 mM Tris-HCl buffer at pH 9.2.

The kinetics of ALP toward **TCF-ALP** were determined via fluorescence spectroscopy (**Figures S6, S7**), with the resultant fluorescence data analyzed using the Michaelis-Menten equation (**Figure S8**). This revealed a K_m of 35.81 ± 2.63 μM and a V_{max} of 3029 ± 157.3 min^{-1} for hydrolysis of **TCF-ALP** by ALP at pH 9.2 (see **Supplementary Material** for details). **TCF-ALP** was then incubated with various concentrations of ALP (0.0–0.2 U/mL) for 15 min to evaluate its ability to monitor ALP activity. As shown in **Figure 1**, a significant fluorescence response was observed in the presence of ALP (58-fold) with a limit of detection (LOD) calculated as 0.12 mU/mL (**Figure S9**). This sensitivity is comparable to other fluorescent probes found in the literature (**Table S3**). Although serum alkaline phosphatase levels vary with age in normal individuals (Kattwinkel et al., 1973), it is widely accepted that serum ALP levels in healthy adults lies between 39 and 117 U/mL (Saif et al., 2005; Sahran et al., 2018). This suggests that **TCF-ALP** is capable of detecting ALP in human serum, and therefore could be used in clinical assays.

Inhibition studies were carried out in the presence of sodium orthovanadate (Na_3VO_4), which is known to be a strong inhibitor of ALP activity. Addition of Na_3VO_4 resulted in a decrease in the fluorescence response in the **TCF-ALP** hydrolysis assay (see **Figure S10**) (Swarup et al., 1982). These inhibition studies enabled an IC_{50} of 6.23 μM to be calculated (**Figure S11**), which is similar in value to other ALP substrates that have been reported in the literature (Zhang H. et al., 2015; Tan et al., 2017).

The selectivity of **TCF-ALP** toward other biologically relevant enzymes (at their optimal pH values) was then determined (**Figure 2** and **Figure S12**), with **TCF-ALP** displaying high substrate selectivity for ALP over other common hydrolytic enzymes (e.g., trypsin, porcine liver esterase) or non-specific binding proteins [e.g., bovine serum albumin (BSA)]. Interestingly, **TCF-ALP** produced a fluorescence response when treated with ACP. The detection of this enzyme is of significance since it is a tumor biomarker for metastatic prostate cancer (Makarov et al., 2009). Normal levels of ACP

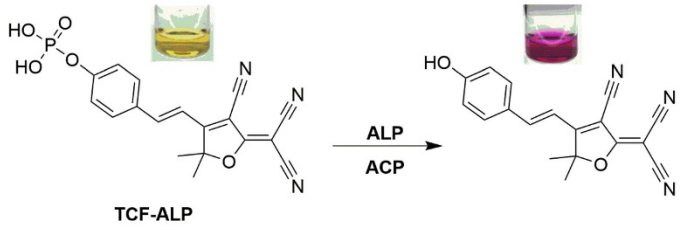

TCF-ALP

SCHEME 1 | A TCF-based fluorescence probe (**TCF-ALP**) for the detection of alkaline phosphatase.

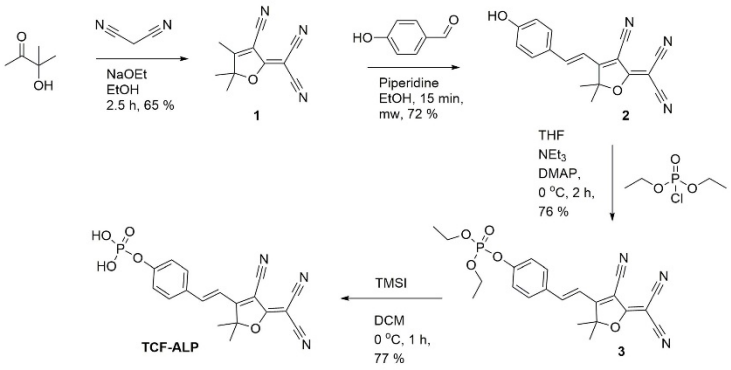

SCHEME 2 | Synthesis of TCF-ALP.

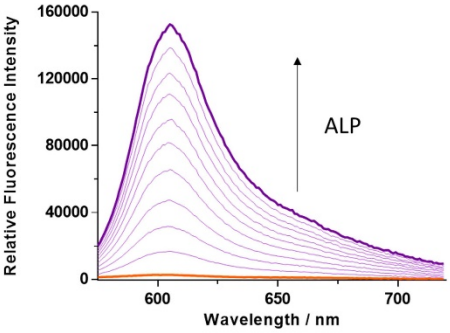

FIGURE 1 | Fluorescence spectra of **TCF-ALP** (10 μM) produced via the addition of alkaline phosphatase (ALP; 0–0.2 U/mL) in 50 mM Tris-HCl buffer, pH = 9.2 at 25°C. λ_{ex} = 542 (bandwidth 15) nm. All measurements were made 15 min after the addition of ALP.

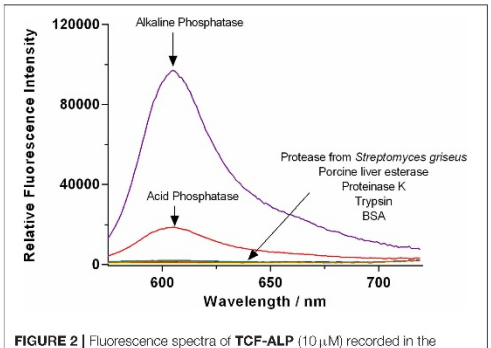

FIGURE 2 | Fluorescence spectra of **TCF-ALP** (10 μM) recorded in the presence of trypsin (0.8 BAEE U/mL), porcine liver esterase, protease from *Streptomyces griseus*, proteinase K, bovine serum albumin (0.1 mg/mL), acid phosphatase (50 mM Tris-HCl, pH = 5.0), and alkaline phosphatase (50 mM Tris-HCl, pH = 9.2). All enzymes were standardized to 0.8 U/mL in Tris-HCl buffer pH 7.1 unless otherwise stated. λ_{ex} = 542 (bandwidth 15) nm/ λ_{em} = 606 nm. Fluorescence measurements were made 30 min after adding the enzyme in question.

in serum range from 3.0 to 4.7 U/mL, and elevated ACP levels can be indicative of a variety of other diseases (Bull et al., 2002). Furthermore, **TCF-ALP** proved capable of detecting ACP (25-fold fluorescence enhancement) and ALP (38-fold enhancement) at a physiological pH of 7.1 (**Figures S13, S14**). Kinetic determination of ALP and ACP toward **TCF-ALP** at pH 7.1 was conducted, and the resultant K_m and V_{max} were compared (see **Supplementary Material 3.1** and **Figures S15–S18**). It was found that ALP has a smaller K_m value in comparison to ACP (0.38 ± 0.042 μM and 99.22 ± 13.16 μM, respectively) and a lower V_{max} (208 ± 3.81 min^{-1} and 1962 ± 223.6 min^{-1}, respectively). Hence, ALP has higher affinity toward **TCF-ALP** compared to ACP, thus **TCF-ALP** is more selective toward ALP at physiological pH.

According to current standards, determination of ALP and ACP is undertaken at the phosphatase's optimum pH. For example, the Centers for Disease Control and Prevention (CDC) procedure for ALP determination is carried out in 2-amino-2-methyl-1-propanol (AMP) buffer at pH 10.3 [Centers For Disease Control Prevention (CDC), 2012]. This is in accordance with other literature sources (Di Lorenzo et al., 1991; Radio et al., 2006; Pandurangan and Kim, 2015; Guo et al., 2018). Likewise, ACP determination is carried out at pH 4–6 (Li et al., 1984; Boivin and Galand, 1986; Myers and Widlanski, 1993). Following these observations, further studies were conducted to determine selectivity at pH 5.0 and 9.2 (**Figures S19–S22**). Results showed

that **TCF-ALP** acts selectivity toward ACP at acidic pH, and ALP at alkaline pH. Therefore, **TCF-ALP** can be used to selectively detect ALP/ACP in clinical assays, or live cell systems (provided the buffer solution is optimal for the phosphatase under study).

Imaging of ALP in Living Cells

Prior to exploring whether **TCF-ALP** could be used to image ALP activity levels in live cells, the cytotoxicity of **TCF-ALP** was assessed using a MTT assay (**Figure S23**). Negligible cell toxicity was observed for **TCF-ALP** concentrations between 0 and 5 μM, and cell viability was only slightly reduced (91%) when incubated with 10 μM **TCF-ALP**, indicating good biocompatibility.

TCF-ALP proved cell permeable to HeLa cells that express ALP and provided a clear "turn on" response (**Figure 3**). In contrast, pre-treatment of HeLa cells with Na_3VO_4 (5 mM) prior to incubation with **TCF-ALP** resulted in minimal "turn on." This was taken as evidence that the increase in **TCF-ALP** fluorescence levels seen for HeLa cells in the absence of Na_3VO_4 is due to ALP activity. We thus conclude **TCF-ALP** is a probe that allows for the selective cellular imaging of ALP activity.

Bone morphogenetic protein 2 (BMP-2) is capable of inducing osteoblast differentiation into a variety of cell types (Guo et al., 2014; Wang et al., 2015) via pathways that result in increased ALP mRNA expression, leading to increased ALP activity (Kim et al., 2004). Treatment of myogenic murine C2C12 cells with **TCF-ALP** resulted in a low fluorescence intensity (low ALP levels) being observed (**Figure 4**); however, pre-treatment of these cells with BMP-2 (300 ng/mL, 3 days) resulted in a significant increase in **TCF-ALP**-derived fluorescence intensity (high ALP levels). Once again, pre-incubation with Na_3VO_4 (5 mM) led to no fluorescence response being observed in the cells treated with

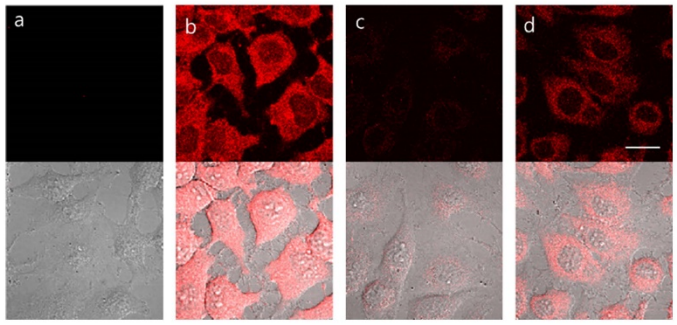

FIGURE 3 | HeLa cells incubated under the following conditions: **(a)** No treatment. **(b) TCF-ALP** (10 μM, 30 min). **(c)** Pre-treated with Na_3VO_4 (5 mM, 30 min), followed by the addition of **TCF-ALP** (10 μM, 30 min). **(d)** Pretreated with Na_3VO_4 (0.5 mM, 30 min) and **TCF-ALP** (10 μM, 30 min). Cells were washed with DPBS before their fluorescence images were acquired using a confocal microscope. Top half: fluorescence images, bottom half: fluorescence images merged with its corresponding DIC image. Ex. 559 nm/em. 575–675 nm. Scale bar: 20 μm. DIC, differential interference contrast.

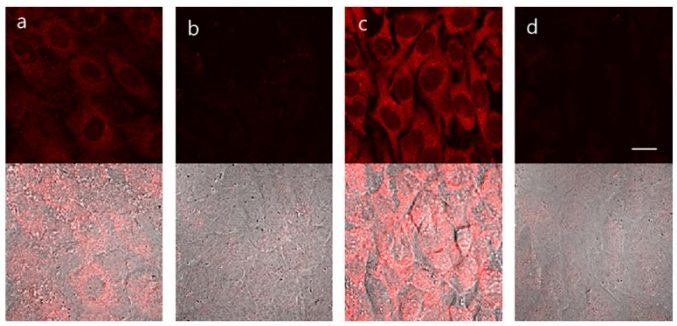

FIGURE 4 | TCF-ALP in C2C12 cells. C2C12 cells were treated with 300 ng/mL BMP-2 for 3 days and then pretreated with 5 mM levamisole for 30 min and stained with 10 μM **TCF-ALP** for 30 min. After washing with DPBS, fluorescence images were acquired by confocal microscopy. **(a)** only **TCF-ALP**, **(b)** levamisole + **TCF-ALP**, **(c)** BMP-2 + **TCF-ALP (d)** BMP-2 + levamisole + **TCF-ALP**. Top: fluorescence images, bottom: merged with DIC image. Ex. 559 nm/em. 575–675 nm. Scale bar: 20 μm. DIC, differential interference contrast.

TCF-ALP (with or without BMP-2). This provided support for the notion that **TCF-ALP** is capable of imaging endogenous ALP activity induced by BMP-2.

CONCLUSIONS

In summary, a long wavelength TCF-based fluorescent probe (**TCF-ALP**) has been prepared with the goal of detecting ALP activity. ALP Hydrolysis of the phosphate group of **TCF-ALP** resulted in a significant "turn on" fluorescence response (58-fold) within 15 min. These spectroscopic changes were accompanied by a colorimetric change from yellow to purple. This enables **TCF-ALP** to be used as a simple assay for the evaluation of ALP activity. Further analysis revealed that **TCF-ALP** could also be used as a probe for detecting ACP activity. **TCF-ALP** was shown to be cell permeable, enabling its use as a fluorescent probe for monitoring ALP levels in HeLa cells. **TCF-ALP** also proved capable of imaging endogenously stimulated ALP produced in myogenic murine C2C12 cells through the addition of bone morphogenetic protein 2. We thus suggest that **TCF-ALP** offers promise as a tool for measuring ALP and ACP activity levels in clinical assays or in live cell systems.

AUTHOR CONTRIBUTIONS

LG and AS carried out synthetic and spectroscopic experiments and co-wrote the manuscript with TJ and JS. JG and GW carried out background experiments. GK carried out cellular imaging experiments. JL carried out the ^{31}P NMR titrations. J-YM and AJ are supervisors of LG and GW. SB, JY, JS, and TJ all conceived the idea and helped with the manuscript.

FUNDING

This work was supported in part by grant MR/N0137941/1 for the GW4 BIOMED DTP, awarded to the Universities of Bath, Bristol, Cardiff and Exeter from the Medical Research Council (MRC)/UKRI We would also like to thank the EPSRC (EP/R003939/1) and the University of Bath and Public Health England for funding. AS and JS thank The Robert A. Welch Foundation (F-0018).

ACKNOWLEDGMENTS

TJ wishes to thank the Royal Society for a Wolfson Research Merit Award. The EPSRC UK National Mass Spectrometry Facility at Swansea University is thanked for mass analyses.

SUPPLEMENTARY MATERIAL

The Supplementary Material for this article can be found online at: https://www.frontiersin.org/articles/10.3389/fchem.2019.00255/full#supplementary-material

REFERENCES

Boivin, P., and Galand, C. (1986). The human red cell acid phosphatase is a phosphotyrosine protein phosphatase which dephosphorylates the membrane protein band 3. *Biochem. Biophys. Res. Commun.* 134, 557–564. doi: 10.1016/S0006-291X(86)80456-9

Bouffard, J., Kim, Y., Swager, T. M., Weissleder, R., and Hilderbrand, S. A. (2008). A highly selective fluorescent probe for thiol bioimaging. *Org. Lett.* 10, 37–40. doi: 10.1021/ol702539v

Bull, H., Murray, P. G., Thomas, D., Fraser, A. M., and Nelson, P. N. (2002). Acid phosphatases. *J. Clin. Pathol. Mol. Pathol.* 55, 65–72. doi: 10.1136/mp.55.2.65

Cao, F.-Y., Long, Y., Wang, S.-B., Li, B., Fan, J.-X., Zeng, X., et al. (2016). Fluorescence light-up aie probe for monitoring cellular alkaline phosphatase activity and detecting osteogenic differentiation. *J. Mater. Chem. B* 4, 4534–4541. doi: 10.1039/C6TB00828C

Centers For Disease Control and Prevention (CDC) (2012). *Alkaline Phosphatase (ALP) in Refigerated Serum: NHANES 2011-2012.* Available online at: https://wwwn.cdc.gov/nchs/data/nhanes/2011-2012/labmethods/biopro_g_met_alkaline_phosphatase.pdf (accessed January 29, 2019).

Coleman, J. E. (1992). Structure and mechanism of alkaline phosphatase. *Annu. Rev. Biophys. Biomol. Struct.* 21, 441–483. doi: 10.1146/annurev.bb.21.060192.002301

Di Lorenzo, D., Albertini, A., and Zava, D. (1991). Progestin regulation of alkaline phosphatase in the human breast cancer cell line T47D. *Cancer Res.* 51, 4470–4475.

Fan, C., Luo, S., and Qi, H. (2016). A ratiometric fluorescent probe for alkaline phosphatase via regulation of excited-state intramolecular proton transfer. *Luminescence* 31, 423–427. doi: 10.1002/bio.2977

Garnero, P., and Delmas, P. D. (1993). Assessment of the serum levels of bone alkaline phosphatase with a new immunoradiometric assay in patients with metabolic bone disease. *J. Clin. Endocrinol. Metab.* 77, 1046–1053.

Gopalan, P., Katz, H. E., Mcgee, D. J., Erben, C., Zielinski, T., Bousquet, D., et al. (2004). Star-shaped azo-based dipolar chromophores: design, synthesis, matrix compatibility, and electro-optic activity. *J. Am. Chem. Soc.* 126, 1741–1747. doi: 10.1021/ja039768k

Guo, F. J., Jiang, R., Xiong, Z., Xia, F., Li, M., Chen, L., et al. (2014). Ire1a constitutes a negative feedback loop with bmp2 and acts as a novel mediator in modulating osteogenic differentiation. *Cell Death Dis.* 5:e1239. doi: 10.1038/cddis.2014.194

Guo, J., Gao, M., Song, Y., Lin, L., Zhao, K., Tian, T., et al. (2018). An allosteric-probe for detection of alkaline phosphatase activity and its application in immunoassay. *Front. Chem.* 6:618. doi: 10.3389/fchem.2018.00618

Hu, Q., Zhou, B., Dang, P., Li, L., Kong, J., and Zhang, X. (2017). Facile colorimetric assay of alkaline phosphatase activity using fe (ii)-phenanthroline reporter. *Chim. Acta* 950, 170–177. doi: 10.1016/j.aca.2016.11.012

Jiang, H., and Wang, X. (2012). Alkaline phosphatase-responsive anodic electrochemiluminescence of cdse nanoparticles. *Anal. Chem.* 84, 6986–6993. doi: 10.1021/ac300983t

Jin, Y., Tian, Y., Zhang, W., Jang, S. H., Jen, A. K. Y., and Meldrum, D. R. (2010). Tracking bacterial infection of macrophages using a novel red-emission ph sensor. *Anal. Bioanal. Chem.* 398, 1375–1384. doi: 10.1007/s00216-010-4060-6

Julien, S. G., Dubé, N., Hardy, S., and Tremblay, M. L. (2011). Inside the human cancer tyrosine phosphatome. *Nat. Rev. Cancer* 11, 35–49. doi: 10.1038/nrc2980

Kattwinkel, J., Taussig, L. M., Statland, B. E., and Verter, J. I. (1973). The effects of age on alkaline phosphatase and other serologic liver function tests in normal subjects and patients with cystic fibrosis. *J. Pediatr.* 82, 234–242.

Kim, Y. J., Lee, M. H., Wozney, J. M., Cho, J. Y., and Ryoo, H. M. (2004). Bone morphogenetic protein-2-induced alkaline phosphatase expression is stimulated by dlx5 and repressed by msx2. *J. Biol. Chem.* 279, 50773–80. doi: 10.1074/jbc.M404145200

Li, H. C., Chernoff, J., Chen, L. B., and Kirschonbaum, A. (1984). A phosphotyrosyl-protein phosphatase activity associated with acid phosphatase from human prostate gland. *Eur. J. Biochem.* 138, 45–51. doi: 10.1111/j.1432-1033.1984.tb07879.x

Li, Y., Li, Y., Wang, X., and Su, X. (2014). A label-free conjugated polymer-based fluorescence assay for the determination of adenosine triphosphate and alkaline phosphatase. *N. J. Chem.* 38, 4574–4579. doi: 10.1039/C4NJ00935E

Liao, Y., Bhattacharjee, S., Firestone, K. A., Eichinger, B. E., Paranji, R., Anderson, C. A., et al. (2006). Antiparallel-aligned neutral-ground-state and zwitterionic chromophores as a nonlinear optical material. *J. Am. Chem. Soc.* 128, 6847–6853. doi: 10.1021/ja057903i

Liu, H. W., Hu, X. X., Zhu, L., Li, K., Rong, Q., Yuan, L., et al. (2017). *In vivo* imaging of alkaline phosphatase in tumor-bearing mouse model by a promising near-infrared fluorescent probe. *Talanta* 175, 421–426. doi: 10.1016/j.talanta.2017.04.081

Lord, S. J., Conley, N. R., Lee, H. L. D., Samuel, R., Liu, N., Twieg, R. J., et al. (2008). A photoactivatable push– pull fluorophore for single-molecule imaging in live cells. *J. Am. Chem. Soc.* 130, 9204–9205. doi: 10.1021/ja802883k

Makarov, D. V., Loeb, S., Getzenberg, R. H., and Partin, A. W. (2009). Biomarkers for prostate cancer. *Ann. Rev. Med.* 60, 139–151. doi: 10.1146/annurev.med.60.042307.110714

Millán, J. L. (2006). Alkaline phosphatases. *Purinergic Signal.* 2, 335–41. doi: 10.1002/3527608060

Myers, J. K., and Widlanski, T. S. (1993). Mechanism-based inactivation of prostatic acid phosphatase. *Science* 262, 1451–1453. doi: 10.1126/science.8248785

Ooi, K., Shiraki, K., Morishita, Y., and Nobori, T. (2007). High-molecular intestinal alkaline phosphatase in chronic liver diseases. *J. Clin. Lab. Anal.* 21, 133–139. doi: 10.1002/jcla.20178

Pandurangan, M., and Kim, D. H. (2015). ZnO nanoparticles augment ALT, AST, ALP, and LDH expressions in C2C12 cells. *Saudi. J. Biol. Sci.* 22, 679–684. doi: 10.1016/j.sjbs.2015.03.013

Qian, Z., Chai, L., Tang, C., Huang, Y., Chen, J., and Feng, H. (2015). Carbon quantum dots-based recyclable real-time fluorescence assay for alkaline phosphatase with adenosine triphosphate as substrate. *Anal. Chem.* 87, 2966–2973. doi: 10.1021/ac504519b

Radio, N. M., Doctor, J. S., and Witt-Enderby, P. A. (2006). Melatonin enhances alkaline phosphatase activity in differentiating human adult mesenchymal stem cells grown in osteogenic medium via MT2 melatonin receptors and the MEK/ERK (1/2) signaling cascade. *J. Pineal Res.* 40, 332–342. doi: 10.1111/j.1600-079X.2006.00318.x

Ritzke, C., Stieber, P., Untch, M., Nagel, D., Eiermann, W., and Fateh-Moghadam, A. (1998). Alkaline phosphatase isoenzymes in detection and follow up of breast cancer metastases. *Anticancer Res.* 18, 1243–1249.

Rosen, E., Sabel, A. L., Brinton, J. T., Catanach, B., Gaudiani, J. L., and Mehler, P. S. (2016). Liver dysfunction in patients with severe anorexia nervosa. *Int. J. Eat. Disord.* 49, 151–158. doi: 10.1002/eat.22436

Ruan, C., Wang, W., and Gu, B. (2006). Detection of alkaline phosphatase using surface-enhanced raman spectroscopy. *Anal. Chem.* 78, 3379–3384. doi: 10.1021/ac0522106

Sahran, Y., Sofian, A., and Saad, A. (2018). Pre-treatment serum lactate dehydrogenase (LDH) and serum alkaline phosphatase (ALP) as prognostic factors in patients with osteosarcoma. *J Cancer. Prev. Curr. Res.* 9, 58–63. doi: 10.15406/jcpcr.2018.09.00320

Saif, M. W., Alexander, D., and Wicox, C. M. (2005). Serum alkaline phosphatase level as a prognostic tool in colorectal cancer: a study of 105 patients. *J. Appl. Res.* 5, 88–95.

Sedgwick, A. C., Chapman, R. S. L., Gardiner, J. E., Peacock, L. R., Kim, G., Yoon, J., et al. (2017a). A bodipy based hydroxylamine sensor. *Chem. Commun.* 53, 10441–10443. doi: 10.1039/C7CC05872A

Sedgwick, A. C., Gardiner, J. E., Kim, G., Yevglevskis, M., Lloyd, M. D., Jenkins, A. T. A., et al. (2018a). Long-wavelength tcf-based fluorescence probes for the detection and intracellular imaging of biological thiols. *Chem. Commun.* 54, 4786–4789. doi: 10.1039/C8CC01661E

Sedgwick, A. C., Han, H. H., Gardiner, J. E., Bull, S. D., He, X. P., and James, T. D. (2017b). Long-wavelength fluorescent boronate probes for the detection and intracellular imaging of peroxynitrite. *Chem. Commun.* 53, 12822–12825. doi: 10.1039/C7CC07845E

Sedgwick, A. C., Han, H. H., Gardiner, J. E., Bull, S. D., He, X. P., and James, T. D. (2018b). The development of a novel and logic based fluorescence probe for the detection of peroxynitrite and gsh. *Chem. Sci.* 9, 3672–3676. doi: 10.1039/C8SC00733K

Sun, J., Yang, F., Zhao, D., and Yang, X. (2014). Highly sensitive real-time assay of inorganic pyrophosphatase activity based on the fluorescent gold nanoclusters. *Anal. Chem.* 86, 7883–7889. doi: 10.1021/ac501814u

Swarup, G., Cohen, S., and Garbers, D. L. (1982). Inhibition of membrane phosphotyrosyl-protein phosphatase activity by vanadate. *Biochem. Biophys. Res. Commun.* 107, 1104–1109. doi: 10.1016/0006-291X(82)90635-0

Tan, Y., Zhang, L., Man, K. H., Peltier, R., Chen, G., Zhang, H., et al. (2017). Reaction-based off–on near-infrared fluorescent probe for imaging alkaline phosphatase activity in living cells and mice. *ACS Appl. Mater. Interfaces* 9, 6796–6803. doi: 10.1021/acsami.6b14176

Teng, X., Tian, M., Zhang, J., Tang, L., and Xin, J. (2018). A tcf-based colorimetric and fluorescent probe for palladium detection in an aqueous solution. *Tetrahedron Lett.* 59, 2804–2808. doi: 10.1016/j.tetlet.2018.06.016

Tibi, L., Collier, A., Patrick, A. W., Clarke, B. F., and Smith, A. F. (1988). Plasma alkaline phosphatase isoenzymes in diabetes mellitus. *Clin. Chim. Acta* 177, 147–155. doi: 10.1016/0009-8981(88)90136-2

Wang, G., Zhang, X., Yu, B., and Ren, K. (2015). Gliotoxin potentiates osteoblast differentiation by inhibiting nuclear factor-κb signaling. *Ren. Mol. Med. Rep.* 12, 877–884. doi: 10.3892/mmr.2015.3524

Wu, D., Sedgwick, A. C., Gunnlaugsson, T., Akkaya, E. U., Yoon, J., and James, T. D. (2017). Fluorescent chemosensors: the past, present and future. *Chem. Soc. Rev.* 46, 7105–7123. doi: 10.1039/C7CS00240H

Wymenga, L. F., Boomsma, J. H., Groenier, K., Piers, D. A., and Mensink, H. J. (2001). Routine bone scans in patients with prostate cancer related to serum prostate-specific antigen and alkaline phosphatase. *BJU Int.* 88, 226–230. doi: 10.1046/j.1464-410x.2001.02275.x

Yang, J., Zheng, L., Wang, Y., Li, W., Zhang, J., Gu, J., et al. (2016). Guanine-rich dna-based peroxidase mimetics for colorimetric assays of alkaline phosphatase. *Biosens. Bioelectron.* 77, 549–556. doi: 10.1016/j.bios.2015.10.003

Zhang, H., Xiao, P., Wong, Y. T., Shen, W., Chhabra, M., Peltier, R., et al. (2017). Construction of an alkaline phosphatase-specific two-photon probe and its imaging application in living cells and tissues. *Biomaterials* 140, 220–229. doi: 10.1016/j.biomaterials.2017.06.032

Zhang, H., Xu, C., Liu, J., Li, X., Guo, L., and Li, X. (2015). An enzyme-activatable probe with a self-immolative linker for rapid and sensitive alkaline phosphatase detection and cell imaging through a cascade reaction. *Chem. Commun.* 51, 7031–7034. doi: 10.1039/C5CC01005E

Zhang, J., Chai, X., He, X. P., Kim, H. J., Yoon, J., and Tian, H. (2019). Fluorogenic probes for disease-relevant enzymes. *Chem. Soc. Rev.* 48, 683–722. doi: 10.1039/C7CS00907K

Zhang, L., Hou, T., Li, H., and Li, F. (2015). A highly sensitive homogeneous electrochemical assay for alkaline phosphatase activity based on single molecular beacon-initiated t7 exonuclease-mediated signal amplification. *Analyst* 140, 4030–4036. doi: 10.1039/C5AN00516G

Zhao, L., Xie, S., Song, X., Wei, J., Zhang, Z., and Li, X. (2017). Ratiometric fluorescent response of electrospun fibrous strips for real-time sensing of alkaline phosphatase in serum. *Biosens. Bioelectron.* 91, 217–224. doi: 10.1016/j.bios.2016.12.025

Conflict of Interest Statement: The authors declare that the research was conducted in the absence of any commercial or financial relationships that could be construed as a potential conflict of interest.

Reaction-based Indicatior Displacement Assay (RIA) for the Development of a Triggered Release System Capable of Biofilm Inhibition

ChemComm

COMMUNICATION

View Article Online
View Journal | View Issue

Cite this: *Chem. Commun.*, 2019, 55, 15129

Received 3rd October 2019,
Accepted 5th November 2019

DOI: 10.1039/c9cc07759f

rsc.li/chemcomm

Reaction-based indicator displacement assay (RIA) for the development of a triggered release system capable of biofilm inhibition†

Bethany L. Patenall, ‡[a] George T. Williams‡, [a] Lauren Gwynne, [a] Liam J. Stephens, [a] Emma V. Lampard, [a] Hollie J. Hathaway, [b] Naing T. Thet,[a] Amber E. Young, [c] Mark J. Sutton, [d] Robert D. Short, [b] Steven D. Bull, [a] Tony D. James, *[a] Adam C. Sedgwick *[e] and A. Toby A. Jenkins *[a]

Here, a reaction-based indicator displacement hydrogel assay (RIA) was developed for the detection of hydrogen peroxide (H_2O_2) *via* the oxidative release of the optical reporter Alizarin Red S (ARS). In the presence of H_2O_2, the RIA system displayed potent biofilm inhibition for Methicillin-resistant *Staphylococcus aureus* (MRSA), as shown through an *in vitro* assay quantifying antimicrobial efficacy. This work demonstrated the potential of H_2O_2-responsive hydrogels containing a covalently bound diol-based drug for controlled drug release.

Dye displacement assays exploit the chemoselective reactivity of certain chemical moieties and the reversible binding of dye molecules to a specific receptor.[1] Such chemistry has begun to find widespread use with marked enhancement over traditional sensing assays.[1–8] More complex systems containing multiple dyes also offer new paradigms for microarray development.[9] Not surprisingly, dye displacement assays have been elegantly employed by a number of research groups. These constructs often rely on boronic acid systems as the receptor (host) subunit with a 1,2- and 1,3-diol guest.[10]

Previously our group has developed boronate-based hydrogel systems as dye displacement assays (borogel) for monosaccharide detection.[11,12] As shown in Scheme 1, the commercially available 1,2-diol dye Alizarin Red S (ARS) was shown to successfully bind to the boronate hydrogel and result in a colour change from red to orange. Upon the addition of a monosaccharide, the competitive displacement of ARS was observed with concomitant observation of an increase in absorption at 513 nm in solution (ARS wavelength).

Aryl boronic acids/boronate esters are well known to undergo hydrogen peroxide (H_2O_2)-mediated oxidation to form the corresponding phenol.[13] This unique synthetic transformation has been exploited in organic synthesis and fluorescence sensing.[13] We thus envisaged that modification of the previously developed ARS hydrogel bound indicator displacement assay (IDA) would yield a multimodal detection platform for the

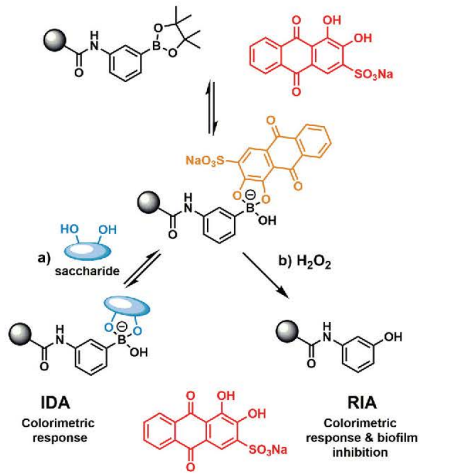

Scheme 1 (a) Previously developed hydrogel bound dye displacement assay (IDA) for the detection of monosaccharides.[11,12] (b) Present work – the development of a hydrogel bound reaction-based indicator displacement (RIA) assay for the detection of H_2O_2 and for the inhibition of MRSA biofilm formation.

[a] *Department of Chemistry, University of Bath, Bath, BA2 7AY, UK. E-mail: t.d.james@bath.ac.uk, A.T.A.Jenkins@bath.ac.uk*
[b] *Department of Chemistry, Lancaster University, UK*
[c] *The Scar Free Foundation Centre for Children's Burns Research, The Bristol Royal Hospital for Children, Bristol, UK*
[d] *Public Health England, Porton Down, Salisbury, Wiltshire SP4 0JG, UK*
[e] *Department of Chemistry, University of Texas at Austin, 105 East 24th Street A5300, Austin, Texas 78712-1224, USA. E-mail: a.c.sedgwick@utexas.edu*

† Electronic supplementary information (ESI) available. See DOI: 10.1039/c9cc07759f

‡ Equal contribution.

detection of H_2O_2 with attendant antimicrobial activity (Scheme 1).[14–16] Here, we report the construction of a covalently incorporated ARS polyacrylamide hydrogel that undergoes oxidative activation in the presence of H_2O_2 to release ARS and afford a reaction-based indicator displacement assay (RIA).[15] *In vitro* antibacterial assays with Methicillin-resistant *Staphylococcus aureus* (MRSA) indicated significant activity against biofilm formation for the combination of ARS and H_2O_2.[17,18]

In brief, phenylboronic acid (**PBA**) and benzoxaborole (**BOB**) acrylamide monomers were synthesised as previously reported.[11,12] Polyacrylamide hydrogels were synthesised using water (60% w/w), acrylamide (38% w/w), methylene bisacrylamide (1% w/w), and **BOB** (1% w/w) or **PBA** (1% w/w). For qualitative purposes, hydrogel slabs containing **BOB** and **PBA** were immersed in 2.5×10^{-4} M ARS (PBS solution). Covalent incorporation was qualitatively measured *via* the observed colour change from red to orange, as measured against a blank hydrogel (Fig. S1 and S2, ESI†). For quantitative purposes, hydrogel cylinders (0.1 g) were immersed in a 2.5×10^{-4} M ARS solution (1 mL) and the UV-Vis absorption at 513 nm was measured over time. As shown in Fig. S3 and S4 (ESI†), a decrease in absorbance at 513 nm was observed, which corresponded to ARS uptake into the gel. After approximately 5 h, both **PBA** and **BOB** gels were saturated with ARS, which was indicated by no further decrease in absorption at 513 nm. Each gel was then placed into a solution of PBS (1 mL) to wash out any unbound ARS, which was shown by an increase in absorption at 513 nm (Fig. S5 and S6, ESI†). No further increase in absorption was observed after 3 h, which indicated the full release of any unbound ARS from each gel.

The prepared gels were then used to evaluate the response towards H_2O_2. Each gel (**PBA** and **BOB**) was placed into a solution of PBS (1 mL) and then exposed to various concentrations of H_2O_2 (0–4 mM). As shown in Fig. 1 and 2, increasing

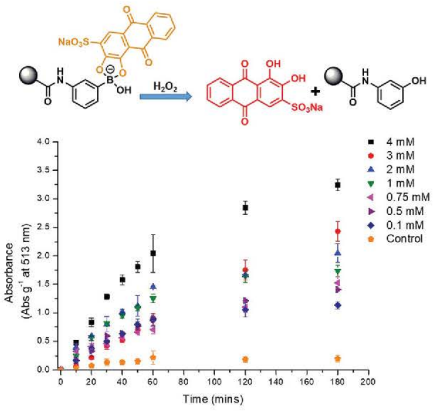

Fig. 1 UV-Vis absorption per gram of **PBA** upon addition of various concentrations of H_2O_2 (0–4 mM) in PBS (pH 7.4, PBS = 0.01 M) over time (minutes). Absorbance was measured at 513 nm at 25 °C. Error bars indicate standard deviation (n = 3).

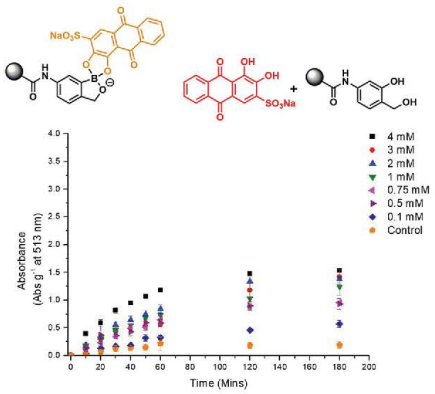

Fig. 2 UV-Vis absorption per gram of **BOB** upon addition of various concentrations of H_2O_2 (0–4 mM) in PBS (pH 7.4, PBS = 0.01 M) over time (minutes). Absorbance was measured at 513 nm at 25 °C. Error bars indicate standard deviation (n = 3).

the concentration of H_2O_2 led to an increased release of ARS from the borogels, as seen in the higher absorption at 513 nm. Interestingly, the greatest sensitivity and ARS release was observed for the **PBA**-based gels, indicative of a greater reactivity towards H_2O_2 over the **BOB**-based gels (see Fig. S7 and S8, ESI†). This change in sensitivity is rationalised as the **BOB** moiety displays an enhanced binding affinity towards 1,2-diols due to an adjacent alkyl alcohol coordinating to the boron atom.[12,19] Therefore, we believe the adjacent methyl alcohol retards oxidation of ARS bound-boronic acid by H_2O_2.

Recent efforts by Lee and co-workers have demonstrated that alizarin (10 μg mL^{-1}) is an effective inhibitor of biofilm formation for three *Staphylococcus aureus* (*S. aureus*) strains and one *Staphylococcus epidermidis* strain.[20,21] Biofilms are complex bacterial communities that can facilitate antibiotic resistance and impair wound healing.[22] Hence, the development of new systems that can effectively treat or inhibit biofilm formation are highly desirable.

H_2O_2 is a commonly used disinfectant and antiseptic in wound care. Therefore, we explored the potential of this system in the development of a H_2O_2-responsive hydrogel for the triggered release of ARS for biofilm inhibition against the three key stages of bacterial growth: lag, exponential and stationary. Due to the **PBA**-based gel displaying the greatest sensitivity towards H_2O_2 over **BOB**-based gels (see Fig. S7 and S8, ESI†), only **PBA** gels were evaluated for biofilm inhibition. Control studies showed that the minimum inhibitory concentration (MIC) of H_2O_2 was 3.5–7 mM for *Staphylococcus aureus* (*S. aureus*) H560 and MRSA252, 0.8–1.6 mM for *Pseudomonas aeruginosa* PAO1 (*P. aeruginosa* PAO1) and 3–6 mM for *Escherichia coli* NCTC 10418 (*E. coli* NCTC 10418). Unfortunately, due to poor solubility, no MIC was determined for ARS against all the bacterial strains used in this study (see Fig. S9–S11, ESI†).[23–25]

ARS was able to inhibit biofilm formation for *S. aureus* MRSA252 and *S. aureus* H560 at 100 μM when added during

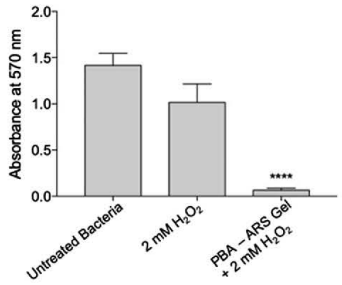

Fig. 3 Biofilm inhibition of *S. aureus* MRSA252 when treated with 2 mM H_2O_2 and solution containing released ARS from ARS-**PBA**-based gel using 2 mM H_2O_2 (3 h incubation). Experiments were repeated using three biological replicates, and error bars indicate standard deviation. Statistical significance of biofilm inhibition was assessed by performing a one-way ANOVA using GraphPad 7.0. ****$p \leq 0.001$ relative to untreated control.

the lag phase of growth (0 h), similar to other reports in the literature for Alizarin.[21] However, ARS was unsuccessful in the inhibition of *P. aeruginosa* PAO1 and *E. coli* NCTC 10418 biofilms at concentrations below 100 μM (see Fig. S14–S16, ESI†). Additionally, H_2O_2 inhibited biofilm formation, albeit at much higher concentrations, prevents growth at 5 mM for *S. aureus* MRSA252 and *S. aureus* H560, 10 mM for *E. coli* NCTC 10418, and 100 mM for *P. aeruginosa* PAO1 (see Fig. S17–S19, ESI†). H_2O_2 (2 mM) with ARS (50 μM) acted synergistically, effecting biofilm inhibition of *S. aureus* MRSA252 when added during the lag phase (Fig. S20, ESI†). Unfortunately, this combination was unable to inhibit biofilm formation at all other growth phases for each bacterial strain (Fig. S21 and S22, ESI†).

We next turned our attention towards the ability of the **PBA**-ARS hydrogel system to inhibit MRSA biofilm formation. Initial control experiments were carried out. **PBA**-ARS gel incubated in PBS solution for 3 h was shown to result in no biofilm inhibition, which indicates the requirement of H_2O_2 for ARS release and no off-target gel toxicity (Fig. S23, ESI†). Control "blank" acrylamide gels were subsequently tested to evaluate the requirement of the boronic acid units for the H_2O_2-mediated release of ARS. Following the usual ARS-loading protocol (see ESI†), acrylamide gels loaded with ARS (ARS uptake through passive diffusion – see Fig. S2, ESI†) were treated with H_2O_2. No biofilm inhibition was observed, which illustrated the requirements of the boronic acid units for H_2O_2-mediated release of ARS from the hydrogel (Fig. S24, ESI†). To capitalize upon the H_2O_2-mediated release of ARS from the boronic acid containing polyacrylamide hydrogel, **PBA**-based gels (0.1 g comprising of 2.5×10^{-4} M ARS) were incubated with H_2O_2 (2 mM) for 3 h to achieve maxiumum ARS release (*cf.* Fig. 1). The resultant ARS release was then applied to *S. aureus* MRSA252 at the lag phase. Remarkably, this resulted in complete biofilm inhibition (Fig. 3) thus demonstrating the potential of the **PBA**-based gels as a "smart" wound dressing.

In summary, we have developed a multimodal reaction-based indicator displacement (RIA) hydrogel assay for the detection of H_2O_2 with concomitant release of ARS for antimicrobial application. The greatest reactivity towards H_2O_2 was observed for the **PBA**-based gel compared to the **BOB**-based gel, attributed to attenuated reactivity of the cyclic **BOB**-boronate ester. In addition, the antimicrobial efficacy of each assay component was evaluated with the aim of developing a "triggered release" antimicrobial hydrogel. ARS was discovered to be a potent biofilm inhibitor in combination with hydrogen peroxide against *S. aureus* MRSA252, with the ARS loaded **PBA**-based gel successfully inhibiting biofilm formation. These results lead us to suggest that **PBA**-based gels, in combination with an early bacterial detection system for a MRSA biomarker, might find use as a "smart" wound dressing capable of preventing MRSA biofilm formation.[26]

The authors would like to thank the EPSRC for grant EP/R003556/1. BLP would also like thank James Tudor and Mr and Mrs Watson for additional funding. GTW would like to thank the EPSRC and Public Health England. ACS, ATAJ and NTT wish to thank the EPSRC for funding on Smartwound plasma – EP/R003939/1. TDJ wishes to thank the Royal Society for a Wolfson Research Merit Award. We would like to thank James T. Brewster II at Harvard college for helpful discussions and suggestions to improve the manuscript.

Conflicts of interest

No conflicts of interest.

Notes and references

1 B. T. Nguyen and E. V. Anslyn, *Coord. Chem. Rev.*, 2006, **250**, 3118–3127.
2 A. M. Piatek, Y. J. Bomble, S. L. Wiskur and E. V. Anslyn, *J. Am. Chem. Soc.*, 2004, **126**, 6072–6077.
3 D. Leung, J. F. Folmer-Andersen, V. M. Lynch and E. V. Anslyn, *J. Am. Chem. Soc.*, 2008, **130**, 12318–12327.
4 B. T. Nguyen, S. L. Wiskur and E. V. Anslyn, *Org. Lett.*, 2004, **6**, 2499–2501.
5 V. Janowski and K. Severin, *Chem. Commun.*, 2011, **47**, 8521–8523.
6 J. H. Zhang, S. Umemoto and K. Nakatani, *J. Am. Chem. Soc.*, 2010, **132**, 3660–3661.
7 T. Minami, Y. L. Liu, A. Akdeniz, P. Koutnik, N. A. Esipenko, R. Nishiyabu, Y. Kubo and P. Anzenbacher, *J. Am. Chem. Soc.*, 2014, **136**, 11396–11401.
8 S. Comby, S. A. Tuck, L. K. Truman, O. Kotova and T. Gunnlaugsson, *Inorg. Chem.*, 2012, **51**, 10158–10168.
9 Y. Sasaki, Z. J. Zhang and T. Minami, *Front. Chem.*, 2019, 7, 150, DOI: 10.3389/fchem.2019.00049.
10 X. Wu, Z. Li, X. X. Chen, J. S. Fossey, T. D. James and Y. B. Jiang, *Chem. Soc. Rev.*, 2013, **42**, 8032–8048.
11 W. M. J. Ma, M. P. P. Morais, F. D'Hooge, J. M. H. van den Elsen, J. P. L. Cox, T. D. James and J. S. Fossey, *Chem. Commun.*, 2009, 532–534.
12 E. V. Lampard, A. C. Sedgwick, T. Sombuttan, G. T. Williams, B. Wannalerse, A. T. A. Jenkins, S. D. Bull and T. D. James, *ChemistryOpen*, 2018, 7, 266–268.
13 J. Chan, S. C. Dodani and C. J. Chang, *Nat. Chem.*, 2012, **4**, 973–984.
14 A. Romieu, *Org. Biomol. Chem.*, 2015, **13**, 1294–1306.
15 X. L. Sun, M. L. Odyniec, A. C. Sedgwick, K. Lacina, S. Y. Xu, T. T. Qiang, S. D. Bull, F. Marken and T. D. James, *Org. Chem. Front.*, 2017, **4**, 1058–1062.
16 X. L. Sun, K. Lacina, E. C. Ramsamy, S. E. Flower, J. S. Fossey, X. H. Qian, E. V. Anslyn, S. D. Bull and T. D. James, *Chem. Sci.*, 2015, **6**, 2963–2967.
17 C. H. Ren, L. P. Chu, F. Huang, L. J. Yang, H. R. Fan, J. F. Liu and C. H. Yang, *RSC Adv.*, 2017, 7, 1313–1317.

18 F. Liu, L. B. Bai, H. L. Zhang, H. Z. Song, L. D. Hu, Y. G. Wu and X. W. Ba, *ACS Appl. Mater. Interfaces*, 2017, **9**, 31626–31633.
19 M. Dowlut and D. G. Hall, *J. Am. Chem. Soc.*, 2006, **128**, 4226–4227.
20 J. H. Lee, Y. G. Kim, S. Y. Ryu and J. Lee, *Sci. Rep.*, 2016, **6**, 19267, DOI: 10.1038/srep19267.
21 R. K. Manoharan, J. H. Lee, Y. G. Kim and J. Lee, *Front. Cell. Infect. Microbiol.*, 2017, **7**, 447, DOI: 10.3389/fcimb.2017.00447.
22 C. W. Hall and T. F. Mah, *FEMS Microbiol. Rev.*, 2017, **41**, 276–301.
23 G. Zhu, Q. Wang, S. Lu and Y. Niu, *Med. Princ. Pract.*, 2017, **26**, 301–308.
24 G. McDonnell and A. D. Russell, *Clin. Microbiol. Rev.*, 2001, **14**, 227–228.
25 Y. Yamada, T. Mokudai, K. Nakamura, E. Hayashi, Y. Kawana, T. Kanno, K. Sasaki and Y. Niwano, *J. Toxicol. Sci.*, 2012, **37**, 1091.
26 N. T. Thet, D. R. Alves, J. E. Bean, S. Booth, J. Nzakizwanayo, A. E. R. Young, B. V. Jones and A. T. A. Jenkins, *ACS Appl. Mater. Interfaces*, 2016, **8**, 14909–14919.

7.6 Unpublished Manuscripts

Boronate Ester Crosslinked PVA hydrogels for the H_2O_2 Triggered Delivery of Small Molecules

COMMUNICATION

Boronate ester cross-linked PVA hydrogels for the H_2O_2 triggered delivery of small molecules

ceived 00th June 2019,
Accepted 00th Month 20xx

DOI: 10.1039/x0xx00000x

George T. Williams,[a,†] Adam C. Sedgwick,[a,b,†] Lauren Gwynne,[a] Lloyd C. Murfin,[a] Jordan E. Gardiner,[a] James T. Brewster II,[b] Simon E. Lewis, Tony D. James,*[,a] A. Toby A. Jenkins,*[,a] and Jonathan L. Sessler*[b]

A new set of PVA hydrogels were formed utilising boronate ester fluorescent probes, *PT-1* and *PF-1*, as covalent crosslinkers. The inherent reactivity of the boronate functionalities present within these constructs allowed for an H_2O_2 responsive release with concomitant activation of the fluorescent dye. In addition to displaying a colorimetric and fluorescent response towards H_2O_2, the complete dissolution of each hydrogel was observed. These studies demonstrated the utility of boronate functionalities to covalenty cross-link new PVA-based "smart" material systems, allowing for the controlled release of pro-drug molecules.

Hydrogen peroxide (H_2O_2) finds common use as a topical antimicrobial agent for the cleaning of wounds and prevention of bacterial infection.[1, 2] The ease-of-use, low cost, and availability of H_2O_2 has thus made it a point of focus in the material sciences with potential for commercialisation.[3-7] Functionalised hydrogels have generated widespread interest as so-called intelligent devices, wherein a specific stimulus can yield a macroscopic change to the self-supporting material. Such constructs offer promise in the area of drug delivery and design of "smart" wound dressings.[6] Within this paradigm, hydrogel materials have been engineered to deliver bioactive agents with a controlled release allowing for passive wound treatment.[3, 8] These efforts represent a marked step forward, but rely on the non-covalent incorporation of bioactive agents within hydrogel. This loose association can result in unwanted drug leaching.

Next generation systems comprised of a pro-drug covalently linked to the hydrogel may address these issues by providing a higher local dose and sustained release of the bioactive molecule.[9] Lastly, the removal of a wound dressing often results in the damage to the healing tissue thus a material that simply dissolves in the presence of a stimulus is highly desirable.[10]

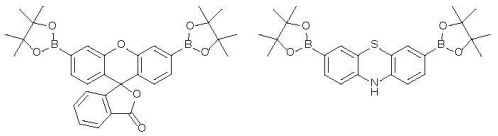

Figure 1. Chemical structures of the H_2O_2-responsive fluorescent dyes, ***PF-1*** and ***PT-1*** and ***Greenment***, utilized to cross-link the PVA hydrogel to form ***Gment*** and ***Pment*** hydrogels respectively

Boronic acids and boronate esters have found widespread application in material-based applications due to their ability to react with 1,2- and 1,3-diols, anions, and undergo oxidative transformation in the presence of H_2O_2 affording the corresponding phenol functionality.[11-14] Here, we report the preparation of a H_2O_2-responsive PVA hydrogel covalently cross-linked with boronate ester H_2O_2-responsive fluorescent probes, ***PF-1*** and ***PT-1*** (Figure 1). The resultant constructs greenment (***Gment***) and purplement (***Pment***), displayed excellent stability under aqueous conditions with no discernible fluorophore leaching (See ESI – Figure SX).

Upon exposure to H_2O_2, both ***PF-1*** and ***PT-1*** in aqueous solution are oxidised to theirs corresponding fluorophore, fluorescein and thionol respectively.[15, 16] This oxidation process is accompanied by a colorimetric responsive and an increase in the fluorescence emission (See ESI - scheme S1). With this information in hand, we evaluated the ability of both ***PF-1*** and ***PT-1*** to form the H_2O_2-responsive PVA-boronate hydrogels (Scheme 1).

[a] *Department of Chemistry, University of Bath, Bath, BA2 7AY, UK. Email: t.d.james@bath.ac.uk, a.t.a.jenkins@bath.ac.uk*
[b] Department of Chemistry. University of Texas at Austin, 105 E 24th street A5300, Austin, TX 78712-1224, United States. Email: sessler@cm.utexas.edu
† These authors contributed equally.
Electronic Supplementary Information (ESI) available: [details of any supplementary information available should be included here]. See DOI: 10.1039/x0xx00000x

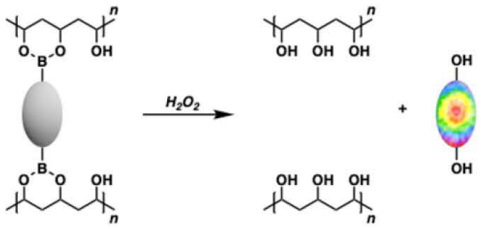

Scheme 1. Cartoon representation showing the boronate pro-fluorophore encapsulated within a PVA hydrogel being activated by H_2O_2 to release the active fluorophore.

PF-1 was prepared following literature procedures.[15] Briefly, ***PT-1*** was synthesized through the dibromination of commercially available phenothiazine (**1**) using Br_2 (5 equiv.) in acetic acid at room temperature, giving the desired product in 74% yield. Subsequent Suzuki-Miyaura borylation using potassium acetate, bis(pinacolato)diboron, and $Pd(dppf)Cl_2$ afforded ***PT-1*** in 43% yield after recrystallization (Scheme S1).

Next, the ***Gment*** and ***Pment*** PVA-hydrogels were prepared by mixing a solution of either ***PF-1*** or ***PT-1*** (100 mM) in dimethyl sulfoxide (DMSO) with 10% w/v PVA (13 – 23 kDa) in DMSO,and heated to induce gelation followed by heating at 60 °C overnight in an oven. The resultant gels were washed with petroleum ether to remove the displaced pinacol, and water to remove excess DMSO. These self-supporting gels proved robust in air and in aqueous solution, and were stored in PBS until used.

The ability of each ***Gment*** or ***Pment*** PVA hydrogel to release the corresponding dye in the presence of H_2O_2 was then evaluated. This was achieved by submerging the chosen hydrogel (200 ± 10 mg) in solutions containing varied concentrations of H_2O_2. As shown in figures 2 and 3, exposure of ***Gment*** or ***Pment*** gels to H_2O_2 (0 – 1 mM) led to a dose-dependent increase in fluorescence intensity after 40 min incubation.

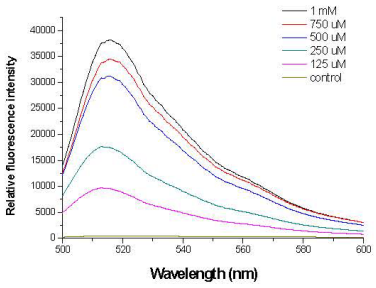

Figure 2 – Fluorescence spectra of the supernatant of ***Gment*** gels exposed to various concentrations of H_2O_2 (0 – 1 mM) in PBS, pH 7.4 after 40 mins. λex = 472 – 16 nm

As shown in Figure 3, ***Pment*** PVA hydrogels exposed to various concentrations of H_2O_2 (0 – 1 mM) also led to a dose-dependent increase in fluorescence intensity after 5 min incubation at emission maxima of 605 nm.

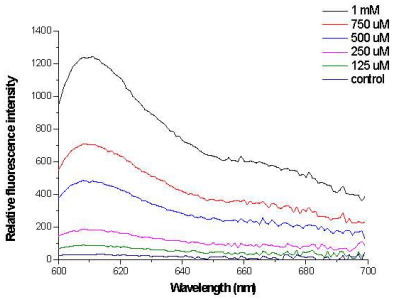

Figure 3 – Fluorescence spectra of the supernatant of ***Pment*** gels exposed to various concentrations of H_2O_2 (0 – 1 mM) in PBS, pH 7.4 after 40 mins. λex = 570 – 16 nm

The colorimetric nature of the boronate ester fluorophore cross-linked PVA systems was tested by placing the hydrogels (200 mg ± 10 mg) in an aqueous solution of H_2O_2 (1 mL, 100 mM). Aliquots (100 µL) were taken at 30, 60, and 90 minutes and subjected to UV-Vis spectroscopic analysis (see ESI figure XXX). As shown in Figure 4, a remarkable change in colour was observed from colourless to green (**A**) and purple (**B**) with an increase in the absorption intensity at 495 nm and 595 nm for ***Gment*** and ***Pment***, respectively (see ESI XXX).

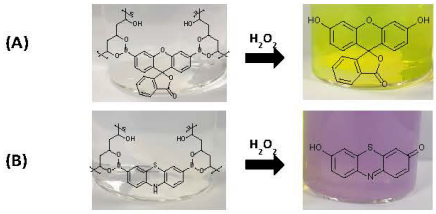

Figure 4 – Colour change in the gel and the supernatant of ***Gment*** and ***Pment*** hydrogels on addition of 1 mM of H_2O_2 in PBS, pH 7.4 after 90 mins.

Notably, subjecting the hydrogels to high concentrations of H_2O_2 (100 mM) resulted in complete dissolution of the hydrogels into solution after 30 minutes, demonstrating potentially utility as a smart material for wound dressing, as can be seen in ESI FIG XXX.

Conclusion

In conclusion, we have reported the synthesis of a new fluorescent dye, ***PT-1***, and developed a boronate ester containing PVA hydrogel that is covalently linked via boronate ester masked fluorophores. Exposure of the initially colourless and non-fluorescent systems to a

solution of H_2O_2, even at low concentrations (1 mM), allowed for the controlled release and activation of the encapsulated fluorophore. Such systems may thus demonstrate applicability in the controlled drug delivery of boronic acid pro-drugs through topical administration of H_2O_2, with potential application in injectable polymer cancer treatments.

Acknowledgments

The authors would like to thank the EPSRC for grant EP/ R003556/1. GTW would like to thank the EPSRC and Public Health England. LCM thanks the EPSRC for DTP Ph.D. funding. ACS and ATAJ wish to thank the EPSRC for funding on smart-wound plasma – EP/R003939/1. TDJ wishes to thank the Royal Society for a Wolfson Research Merit Award. We would like to thank James T. Brewster II at Harvard college for helpful discussions and suggestions to improve the manuscript.

Conflicts of interest

There are no conflicts to declare.

Notes and references

1. G. Zhu, Q. Wang, S. Lu and Y. Niu, in *Med Princ Pract*, 2017, vol. 26, pp. 301-308.
2. E. Linley, S. P. Denyer, G. McDonnell, C. Simons and J. Y. Maillard, *J. Antimicrob. Chemother.*, 2012, **67**, 1589-1596.
3. Y. Lee, K. H. Choi, K. M. Park, J. M. Lee, B. J. Park and K. D. Park, *Acs Applied Materials & Interfaces*, 2017, **9**, 16891-16900.
4. C. H. Ren, L. P. Chu, F. Huang, L. J. Yang, H. R. Fan, J. F. Liu and C. H. Yang, *Rsc Advances*, 2017, **7**, 1313-1317.
5. D. Huber, G. Tegl, A. Mensah, B. Beer, M. Baumann, N. Borth, C. Sygmund, R. Ludwig and G. M. Guebitz, *Acs Applied Materials & Interfaces*, 2017, **9**, 15307-15316.
6. K. R. Yang, Q. Han, B. P. Chen, Y. H. Zheng, K. S. Zhang, Q. Li and J. C. Wang, *International Journal of Nanomedicine*, 2018, **13**, 2217-2263.
7. H. Chen, Y. Y. Jin, J. J. Wang, Y. Q. Wang, W. Y. Jiang, H. D. Dai, S. Y. Pang, L. Lei, J. Ji and B. L. Wang, *Nanoscale*, 2018, **10**, 20946-20962.
8. D. E. Fullenkamp, J. G. Rivera, Y. K. Gong, K. H. A. Lau, L. H. He, R. Varshney and P. B. Messersmith, *Biomaterials*, 2012, **33**, 3783-3791.
9. S. Akkad and C. J. Serpell, *Macromol. Rapid Commun.*, 2018, **39**.
10. H. Matsumura, N. Ahmatjan, Y. Ida, R. Imai and K. Wanatabe, *International Wound Journal*, 2013, **10**, 291-294.
11. X. Wu, Z. Li, X. X. Chen, J. S. Fossey, T. D. James and Y. B. Jiang, *Chemical Society Reviews*, 2013, **42**, 8032-8048.
12. X. L. Sun, M. L. Odyniec, A. C. Sedgwick, K. Lacina, S. Y. Xu, T. T. Qiang, S. D. Bull, F. Marken and T. D. James, *Organic Chemistry Frontiers*, 2017, **4**, 1058-1062.
13. E. V. Lampard, A. C. Sedgwick, T. Sombuttan, G. T. Williams, B. Wannalerse, A. T. A. Jenkins, S. D. Bull and T. D. James, *Chemistryopen*, 2018, **7**, 266-268.
14. C. M. Lopez-Alled, A. Sanchez-Fernandez, K. J. Edler, A. C. Sedgwick, S. D. Bull, C. L. McMullin, G. Kociok-Kohn, T. D. James, J. Wenk and S. E. Lewis, *Chemical Communications*, 2017, **53**, 12580-12583.
15. E. W. Miller, A. E. Albers, A. Pralle, E. Y. Isacoff and C. J. Chang, *Journal of the American Chemical Society*, 2005, **127**, 16652-16659.
16. S. Granick and L. Michaelis, *Journal of the American Chemical Society*, 1947, **69**, 2983-2986.